University of Southampton

Faculty of Medicine

Clinical and Experimental Sciences

Nitrosomonas eutropha D23 – an *in vitro* evaluation of its metabolic phenotype and evidence for its bioactivity

by

Diogo Gonçalves da Silva

ORCID ID 0000-0001-7430-3034

Thesis for the degree of Doctor of Philosophy

September 2019

University of Southampton

Abstract

Faculty of Medicine

Clinical and Experimental Sciences

Thesis for the degree of Doctor of Philosophy

Nitrosomonas eutropha D23 – an *in vitro* evaluation of its metabolic phenotype and evidence for its bioactivity

by

Diogo Gonçalves da Silva

Contemporary lifestyle and hygienic behaviours have led to cutaneous microbial imbalances, including the loss of ammonia-oxidising bacteria (AOB) from the human skin. Ubiquitous in soil, AOB perform the nitritation step within the global nitrogen cycle. Their sole source of energy originates from the oxidation of ammonia (NH_3) to nitrite (NO_2^-), a reaction during which also nitric oxide (NO) is produced. Although believed to have been a constituent of the normal skin microbiome in the past, their role when present on the skin remains unknown. Topical application of *Nitrosomonas eutropha* D23 (AO+ Mist, MotherDirt™, AOBiome LLC) has been proposed to restore absent AOB on the skin. It may also serve as a biological tool to modulate the bioavailability of NO and its metabolites via oxidation of NH_3 present in sweat. There is limited information on the metabolic phenotype available, and often this is inferred from the model organism, *Nitrosomonas europaea*. It was hypothesised that the metabolic products NO and/or NO_2^- produced by *N. eutropha* D23 are of sufficient quantities to elicit *in vitro* and/or *in vivo* bioactivity. Experiments were carried out using an array of analytical instrumentation. The biochemical assessment was carried out in pure, live cultures of *N. eutropha* D23, and revealed the ability of energy-starved *N. eutropha* D23 to produce high levels of NO_2^- over time, immediately upon addition of substrate. The production of NO by *N. eutropha* D23 was quantified by gas-phase chemiluminescence in dependence of temperature, pH, concentration of substrate, and bacterial density. Maximal *in vitro* production of NO was observed at 25 mmol L^{-1} NH_4^+, at pH 8, and at 37-40 °C. Despite the apparent low yields of NO (fentomoles per *N. eutropha* D23 cell), these were found to be of sufficient quantities to trigger dispersal of *Pseudomonas aeruginosa* (PAO1) biofilms. NO was found to be the principal agent underpinning the reduction in *P. aeruginosa* biofilm biomass, and this effect was dependent on live *N. eutropha* D23. Furthermore, significant reductions in biofilm biomass were also demonstrated for the majority of clinical isolates of *P. aeruginosa* tested. Further biological activity of *N. eutropha* D23 was explored in healthy human volunteers, who applied the commercial product of these bacteria on the skin for 14 days. Although the study was underpowered and only exploratory, local and systemic changes were observed upon application of *N. eutropha* D23 (e.g. trans-epidermal water loss, blood pressure). Unexpectedly, circulatory NO_2^- concentrations were not found to be elevated. Instead, biomarker analysis in plasma samples suggested the existence of a potential oxidation process. This was indicated by a slight increase in oxidative stress markers, a decrease in total free thiols, and a generalised decrease in circulatory free thiols in the majority of participants, including reduced glutathione and cysteine. This systemic signature warrants further investigations in order to mechanistically characterise the action of *N. eutropha* D23 on the skin, which may ultimately offer opportunities for its medicinal use beyond the treatment of inflammatory skin diseases.

Table of Contents

List of Tables

List of Figures

Research Thesis: Declaration of Authorship

Print name:	Diogo Gonçalves da Silva
Title of thesis:	*Nitrosomonas eutropha* D23 – an *in vitro* evaluation of its metabolic phenotype and evidence for its bioactivity

I declare that this thesis and the work presented in it are my own and has been generated by me as the result of my own original research.

I confirm that:

1. This work was done wholly or mainly while in candidature for a research degree at this University;
2. Where any part of this thesis has previously been submitted for a degree or any other qualification at this University or any other institution, this has been clearly stated;
3. Where I have consulted the published work of others, this is always clearly attributed;
4. Where I have quoted from the work of others, the source is always given. With the exception of such quotations, this thesis is entirely my own work;
5. I have acknowledged all main sources of help;
6. Where the thesis is based on work done by myself jointly with others, I have made clear exactly what was done by others and what I have contributed myself;
7. None of this work has been published before submission.

Signature: Date:

Acknowledgements

This PhD project would have not be possible without the inimitable support of a large number of individuals. First and foremost, I would like to thank my primary supervisor, Professor Martin Feelisch, for his direction and guidance throughout my time here. He has moulded me to become a better thinker and a more poised individual. I would also like to thank Professors Michael Ardern-Jones and Jeremy Webb for being my secondary supervisors, and providing their input in their respective expertise and in helping me construct a piece of work that hopefully everyone can be pleased with. I am keenly aware that there were many suitable candidates for this particular project initially, and I am very thankful that I was given this superb opportunity.

I am grateful to AOBiome for financially supporting this PhD project and continuing to support my development as a post-doctoral Research Fellow. Without such monetary sources for years, I would not be where I am today.

In completing this PhD project, I have also been fortunate enough to work across two campuses, Highfield and Southampton General Hospital where I have met many different individuals whom surely I will never forget. From the Life Sciences, I would like to acknowledge Dr Raymond Allan, Bhavik Barochia, Priscila Vitola, Dr Yuming Cai, and Dr Odel Soren for all the help and teaching, and for making my biofilm days in the Microbiology laboratory both fruitful and highly enjoyable.

From the Southampton General Hospital, I would first like to thank transient members who have come and gone but their impact has never ceased, including Blanka Stelmaszczuk for training me on instrumentation when I first arrived, Saman Naghibi for listening and keeping me company when I first started; Dr Ina Roman for your sarcastic nature; Thomas Sutton for informing me more about mass spectrometry during our lab meetings; both Chris Petticrew and Mia Meiss for their candour and the stimulating conversations; Dr Andrew Cumpstey for his ‘it’ll be fine’ attitude; Jey Jeyapala for his positive outlook and perpetual smile despite any obstacles; Adam Tod for your naiveté which made my last months working on my PhD quite entertaining, Dr Jaimie Oldham for coffee-time, generousness and just being your genuine-self. To some of our visiting collaborators including the Groningen girls specifically Marion Bulthuis and Anne Koning whose can-do attitudes were admirable.

To the students I have had the opportunity to work with on my own project including Anson Chan and Gloria Zechmeister-Machhart. I truly hope that your experiences in our laboratory have stimulated your interest in science. For the people I have had the

pleasure of working with for many years including Magdalena Minnion and Laurie Lau for helping me with the analysis of samples for my last chapter; Monika Mikus-Lelinska for your constant laugh and positive attitude regardless what is happening around, and for the lovely birthday present; Rfeef Alyami for your enthusiasm, sharing findings of your research project with me and the true meaning of “I’m zero”, but overall the friendly company we shared as research students.

Lastly, Dr. Bernadette O. Fernandez, to whom I am mostly grateful since the very start of my time in Southampton, for her genuine personality and altruism, who was always available to help and guide me (well, everybody) in the laboratory, and for keeping a constant interest in my project. I certainly learnt a lot from you, and had the most amazing and fun times sharing silly conversations with you in the laboratory and in the office. Thanks for being an important pillar during my time here!

All these experiences in Southampton and memories would not be possible were it not for the encouragement of some members of my last team in Portugal, especially Ana Sofia Oliveira, Magda Santos and Inês Baptista, who dared me to go further, and seek adventures in the UK.

To my medical “cousins”, Manuel Garcês Gonçalves, Inês Mónica, Verónica Guiomar, Ana Cristina Martins, the “Abrantes” Joana Pereira and João Abrantes, and Pedro Maneira Sousa. Thank you for the encouragement you gave me before moving to the UK, and thanks for the starter pack (touristic guide of the UK, English tea and a crown). Thank you for being always so available to listen to my concerns and worries. Many thanks to Manuel, in particular, for having his house in Lisbon always open and ready for when I arrived from the airport. We might be all far away apart, but always in touch.

To my precious and dearest friends in Southampton for your open ears, sagacious words, gentle demeanour, and overall mentoring. All together you have been my family here, have seen me through (and continue to see me through) my most demanding years thus far and raise me up when hope was obscured. For this shining light in my path and the laughter we have shared, I am forever grateful. These are memories.

Finally, to my dearest family. My mom Maria, my father Manuel, and my sister Marisa. I thank you for raising me to be the person that I am today, and for allowing me to leave far from home to live these irreplaceable experiences, and for always looking out for me and my welfare. I would not be here without all of you.

Abbreviations

16S rRNA	16S ribosomal ribonucleic acid
AMO	Ammonia monooxygenase
AOA	Ammonia-oxidising archaea
AOB	Ammonia-oxidising bacteria
ATP	Adenosine 5'-triphosphate
CFU	Colony-forming units
cGMP	Guanosine 3, 5-cyclic monophosphate
CLD	Chemiluminescence detection
cNOS	Constitutively-expressed nitric oxide synthase
CPTIO	carboxy-PTIO
CV	Crystal violet
DAF-2	4,5-Diaminofluorescein
DAF-2T	4,5-Diaminofluorescein triazole
DMSO	Dimethyl sulfoxide
DNA	Deoxyribonucleic acid
eNOS	Endothelial nitric oxide synthase
EPS	Extracellular polymeric substance
HAO	Hydroxylamine oxidoreductase
iNOS	Inducible nitric oxide synthase
K_a	Acidity constant
L-Arg	L-arginine
L-Cit	L-citrulline
M9	Modified M9 minimal medium
metHb	Methaemoglobin
NED	*N*-(1-naphthyl)ethylenediamine
nNOS	Neuronal nitric oxide reductase
NO	Nitric oxide
NOB	Nitrite-oxidising bacteria
NONOates	Diazeniumdiolates
NOS	Nitric oxide synthase
NOx	Nitrite and nitrate
OD	Optical density
oxyHB	Oxyhaemoglobin
PB	Phosphate buffer pH 6.8
PBS	Phosphate-buffered saline
PROLI/NO	Proline NONOate
RNOS	Reactive nitrogen and oxygen species
ROS	Reactive oxygen species
RSNO	S-nitrosothiols
RXNO	Total nitroso species
sGC	Cytosolic guanylate ciclase
SULF	Sulphanilamide
UVA	Ultraviolet light A

Chemical Compendium

C	Carbon
Ca^{2+}	Calcium ion
Cl^{-}	Chloride ion
CO_2	Carbon dioxide
CO_3^{2-}	Carbonate
Fe_2^{+}	Ferrous iron
Fe_3^{+}	Ferric iron
H_2	Hydrogen
HCO_3^{-}	Bicarbonate
HNO_2	Nitrous acid
N	Nitrogen
N_2	Dinitrogen
N_2O	Dinitrogen oxide
N_2O_3	Dinitrogen trioxide
N_2O_4	Dinitrogen tetroxide
NH_2Cl	Monochloroamine
NH_2OH	Hydroxylamine
NH_3	Ammonia
NH_4^{+}	Ammonium
NO	Nitric oxide
NO_2	Nitrogen dioxide
NO_2^{-}	Nitrite
NO_2^{*}	Dinitrogen oxide (excited state)
NO_3^{-}	Nitrate
O_2	Dioxygen
O_2^{-}	Superoxide anion
O_3	Ozone
OCl^{-}	Hypochlorite
$ONOO^{-}$	Peroxynitrite
ONOOH	Peroxynitrous acid
SO_4^{2-}	Sulphate ion

Chapter 1

General Introduction

Chapter 1: Introduction

The following chapter provides the general background, a description of important concepts and an overview of relevant literature that support this doctoral thesis. Moreover, it defines the overall hypothesis that was tested and addresses the aims of the project.

1.1 Biogeochemical nitrogen cycle

Nitrogen (N) is a redox-active atom and one of the most abundant chemical elements found in Nature, representing nearly 80% of the composition of the Earth's atmosphere, as dinitrogen gas (N_2) (Hirsch and Mauchline, 2015). It is a pivotal element, as it forms the backbone of important macromolecules, including proteins and deoxyribonucleic acid (DNA), crucial for the development and maintenance of biological systems; moreover, it is present in small molecules with important roles in biology, such as nitric oxide (NO). Despite the abundance of N_2, the majority of living organisms cannot source their N demands directly from this molecule, and are therefore dependent on the biogeochemical N cycle, which transforms N_2 into bioavailable compounds by a series of redox reactions (i.e. oxidation and reduction reactions), mainly carried out by microorganisms (van de Leemput *et al.*, 2011; Hirsch and Mauchline, 2015; Stein and Klotz, 2016).

This cycle (Figure 1.1 below) is composed of a series of sequential steps, each one with its own particular properties and players. For the context of this project, an overview of important N-transforming reactions and their nomenclature occurring during the biogeochemical N cycle is worth-mentioning. Classically, the cycle can be dissected into fixation, nitrification, and denitrification reactions (Hirsch and Mauchline, 2015; Stein and Klotz, 2016). The fixation process entails formation of ammonium/ammonia (NH_4^+/NH_3) by reduction of N_2, either by direct action of nitrogen-fixing bacteria or via dissimilatory nitrite/nitrate (NO_2^-, NO_3^-) reduction to NH_4^+/NH_3. The nitrification step is accomplished by two distinct and consecutive oxidation processes, namely nitritation (NH_3 is first oxidised to NO_2^-) and nitratation (NO_2^- is oxidised to NO_3^-), carried out by separate groups of specialised microorganisms, as presented in the following section.

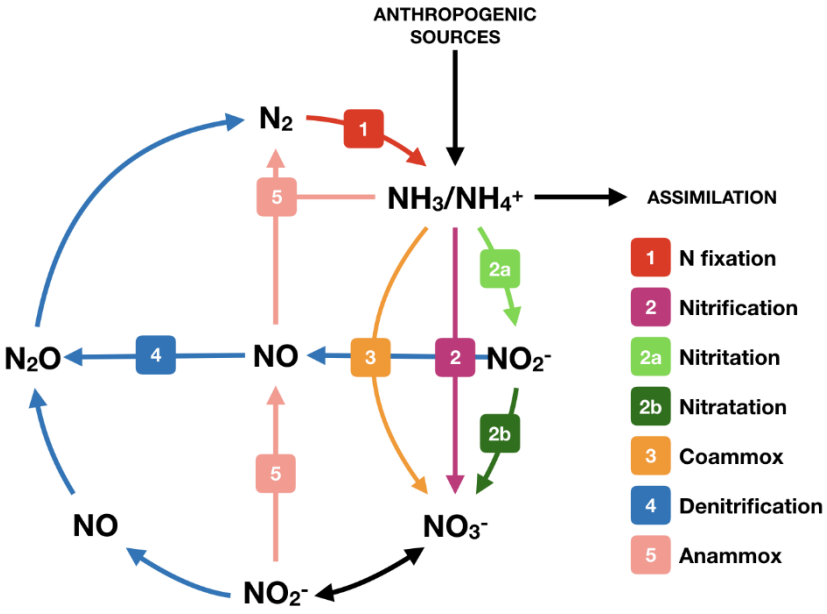

Figure 1.1 Overview of the nitrogen-transforming reactions occurring during the biogeochemical nitrogen cycle. Adapted from Hirsch & Mauchline (2015) and Stein & Klotz (2016).

Denitrification closes the cycle, with reduction of N-containing molecules leading to the liberation of N_2 back into the atmosphere. Recently, the discovery of the anaerobic NH_4^+ oxidation (anammox) pathway has led to its integration into this cycle, which also generates N_2 via conversion of NH_4^+ and NO_2^- molecules under complete anoxia.

1.1.1 Microorganisms

Microbial activity is crucial for maintaining the reactions within the cycle, and each of the afore-mentioned steps in the N cycle are known to be performed by different microorganisms, mainly prokaryotes. Some examples include species of *Rhizobium* and *Azobacter*, which provide plants with fixed forms of N, as well as cyanobacteria (Hirsch and Mauchline, 2015).

The nitrification step is performed by two different groups of microorganisms, such as ammonia-oxidising bacteria (AOB) and ammonia-oxidising archaea (AOA) (Könneke *et al.*, 2005; Schleper and Nicol, 2010; Prosser and Nicol, 2012), which perform nitritation reactions (i.e. formation of NO_2^- from NH_3); and nitrite-oxidising bacteria (NOB), that rely on NO_2^- generated by the former to proceed with nitritation reactions (i.e. formation of NO_3^- from NO_2^-). While it is widely accepted that these two oxidation processes are carried out by separate microbial entities, recent evidence (Daims *et al.*, 2015; van Kessel *et al.*,

2015) of complete ammonia oxidation (comammox, step 3 in Figure 1.1) by single organisms within the *Nitrospira* genus has reshaped the nitrification step.

Overall, incorporation of N into ecosystems by formation of bioavailable molecules like NH_4^+/NH_3 and NO_3^- and its recycling is possible through the N cycle, for which microorganisms play a vital role. The particular group of AOB is of ecological importance for its role in maintaining the rate-limiting nitritation step (Kowalchuk and Stephen, 2001), by oxidising the most reduced form of inorganic N (NH_3/NH_4^+, with an oxidation state of -3 on the N atom) to NO_2^- (with an oxidation state of +3 in the N atom), producing other important intermediates along the process.

1.2 Ammonia-oxidising bacteria

1.2.1 Phylogeny and ecology

AOB have been under the spotlight ever since early reports carried out by Warington and Winograsky (Dworkin, 2012; Monteiro, Séneca and Magalhães, 2014) which established historical landmarks on soil microbiology, including the elucidation of nitrification as a two-step, microbial-driven process; the isolation of the first ammonia-oxidising bacterium; and the establishment of chemolithoautrophy as a mode of life for this bacterial group (Arp and Bottomley, 2006; Monteiro, Séneca and Magalhães, 2014). In the early 1900s, Winogradsky (Dworkin, 2012; Monteiro, Séneca and Magalhães, 2014) isolated *Nitrosomonas europaea*. Since then, this particular species has been the model AOB organism for studying the biochemistry, physiology and ecology of the particular group of ammonia-oxidisers.

AOB comprise a group of aerobic, gram-negative prokaryotes belonging to the *Proteobacteria* phylum. Based on phylogenetic analysis (Head *et al.*, 1993), species of AOB are currently assigned into two major classes (Kowalchuk and Stephen, 2001; Wang *et al.*, 2014). The Betaproteobacteria class agglomerates the genera *Nitrosomonas* (which includes *Nitrosococcus mobilis*) and *Nitrospira*, as the most abundant and widely spread genera in the environment (Mendum, Sockett and Hirsch, 1999); while *Nitrosococcus oceani* and *Nitrosoccocus halophilus* are species assigned to the Gammaproteobacteria class (Koops *et al.*, 1991; Kowalchuk and Stephen, 2001; Koops and Pommerening-Röser, 2001). Currently, *N. europaea* ATCC 19718*, Nitrosomonas eutropha* C91, *Nitrosomonas ureae* Nm10 , *Nitrosomonas communis* Nm2, and *Nitrosospira multiformis* ATCC 25196 are examples of AOB species whose full genomes have been sequenced (Chain *et al.*, 2003; Stein *et al.*, 2007; Norton *et al.*, 2008; Kozlowski, Kits and Stein, 2016b, 2016a).

Due to their role in the biogeochemical N cycle, AOB are ubiquitously present in several habitats, including, but not restricted to soil, freshwater, marine sediments, and sludge (Lees, 1952; Kowalchuk and Stephen, 2001; Güven and Schmidt, 2009a; Dai *et al.*, 2015).

1.2.2 Chemolithoautrophy

AOB are chemolithoautotrophs, i.e. they obtain energy through oxidation of inorganic compounds, relying on the oxidation of NH_3 to NO_2^-, as the only source of energy and reducing equivalents for carbon (C) fixation (via the Calvin-Benson-Bassham cycle) (Lees, 1952; Koops *et al.*, 1991; Arp and Stein, 2003). Although a mode of lithoheterotrophy has been shown for *N. europaea* (Hommes et al. 2003) by its ability to use other carbon sources (e.g. pyruvate and fructose) to support its growth in the presence of NH_3, it is widely accepted that AOB are obligate chemolithoautotrophs regarding their energy-generation system, which is uniquely dependent on the oxidation of NH_3 to generate reductant power to fix carbon. Inorganic C sources include carbon dioxide (CO_2), which is in equilibrium with carbonate (CO_3^{2-}) and bicarbonate (HCO_3^-) and are usually added to well-defined mineral media to support growth of these bacteria in laboratory settings (Lewis and Pramer, 1958; Wallace and Nicholas, 1969; Sato *et al.*, 1985).

Despite sharing identical core features, for instance, the NH_3 oxidation and C fixation pathways, the physiological characteristics differ among species of AOB. Factors such as NH_3, temperature and pH requirements, urease activity, as well as salt tolerance are examples that may dictate their ecological niche and metabolic activities, for which some species are well-suited to thrive on as compared to others. *N. europaea* and *N. eutropha* cluster phylogenetically together (cluster 7), and can be found in NH_3-rich environments, whereas, for instance, *Nitrosomonas marina* and *Nitrosomonas aestuarii* are likely to be found in marine niches due to their high salinity tolerance. *N. europaea* and *N. eutropha* have high affinity for NH_3, but are not able to source NH_3 via enzymatic degradation of urea, as opposed to urease-positive AOB species, such as *Nitrosomonas oligotropha*, *Nitrosomonas ureae* and *Nitrosomonas nitrosa*, as well as some marine AOB species (Koops *et al.*, 1991; Koops and Pommerening-Röser, 2001).

1.2.3 Ammonia metabolism pathway

It is widely accepted that the pathway leading to the formation of NO_2^- by AOB proceeds mainly through a dioxygen (O_2)-dependent NH_3 metabolic route (termed “classical” in this thesis), even though a dinitrogen tetroxide (N_2O_4)-dependent pathway has been described, and may occur under anaerobic conditions (not discussed in this thesis).

The classical pathway (Figure 1.2 below) has been known to occur through a two-step enzymatic processes, involving the formation of hydroxylamine (NH_2OH) as a chemical intermediate (Hofman and Lees, 1953; Lisa Y Juliette, Hyman and Arp, 1993; Arp and Stein, 2003). Suzuki et al. (1974) demonstrated that NH_3 (gas) is the true substrate for oxidation, rather than the NH_4^+ (ion), using *N. europaea* as a model. Due to the chemical equilibrium between both species, NH_4^+ salts (usually sulphate or chloride, SO_4^{2-} and Cl^-, respectively) are added to support the growth of AOB in liquid growth media, in laboratory settings.

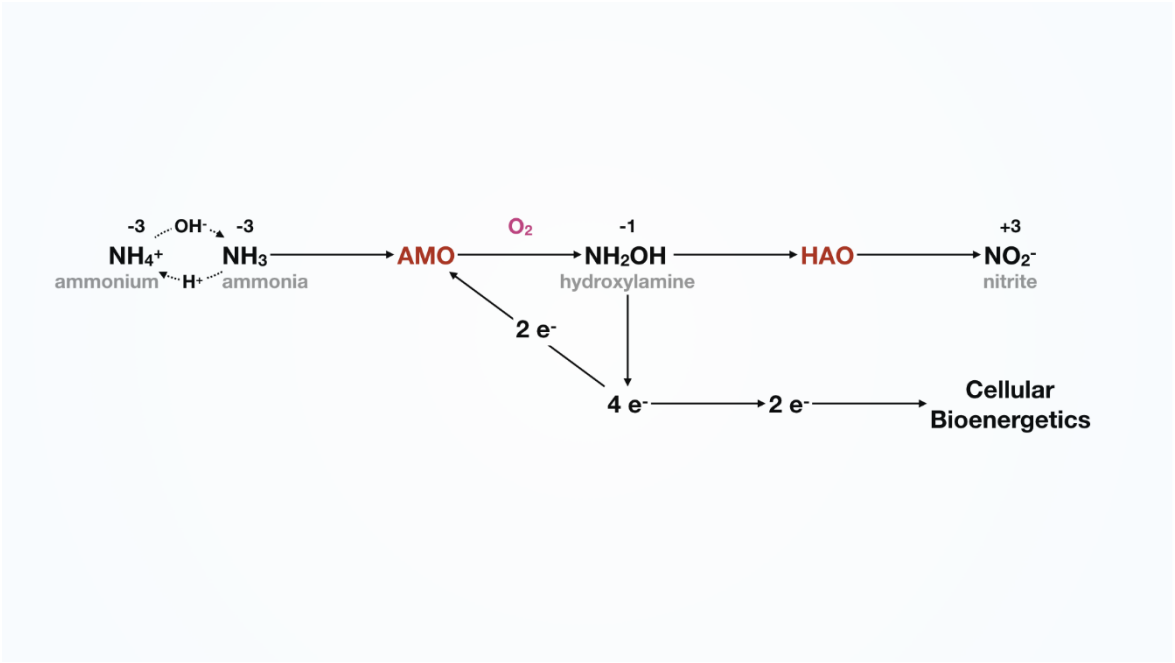

Figure 1.2 Classical pathway for aerobic ammonia oxidation by ammonia-oxidising bacteria. Ammonia monooxygenase (AMO) and hydroxylamine oxidoreductase (HAO) are the two enzymes responsible for the complete oxidation of NH_3 to NO_2^-.

In this pathway, NH_3 is first oxidised to NH_2OH, by the copper-containing, membrane-bound ammonia monooxygenase (AMO) using O_2 as an electron donor, and the process continues with this intermediate being ultimately oxidised to NO_2^-, through the periplasmic hydroxylamine oxidoreductase (HAO) (Kowalchuk and Stephen, 2001; Arp and Stein, 2003; Hatzenpichler, 2012). Despite this last process yielding four electrons, only two are diverted to supply the cell's biomass and to generate a proton gradient, while the remaining two electrons are required to continuously allow substrate oxidation by AMO. Along with NO_2^- formation (the main metabolic product of NH_3 oxidation), other N-containing species are also released (Figure 1.3 below), such as nitric oxide (NO) and nitrous oxide (N_2O) (Hooper and Terry, 1979).

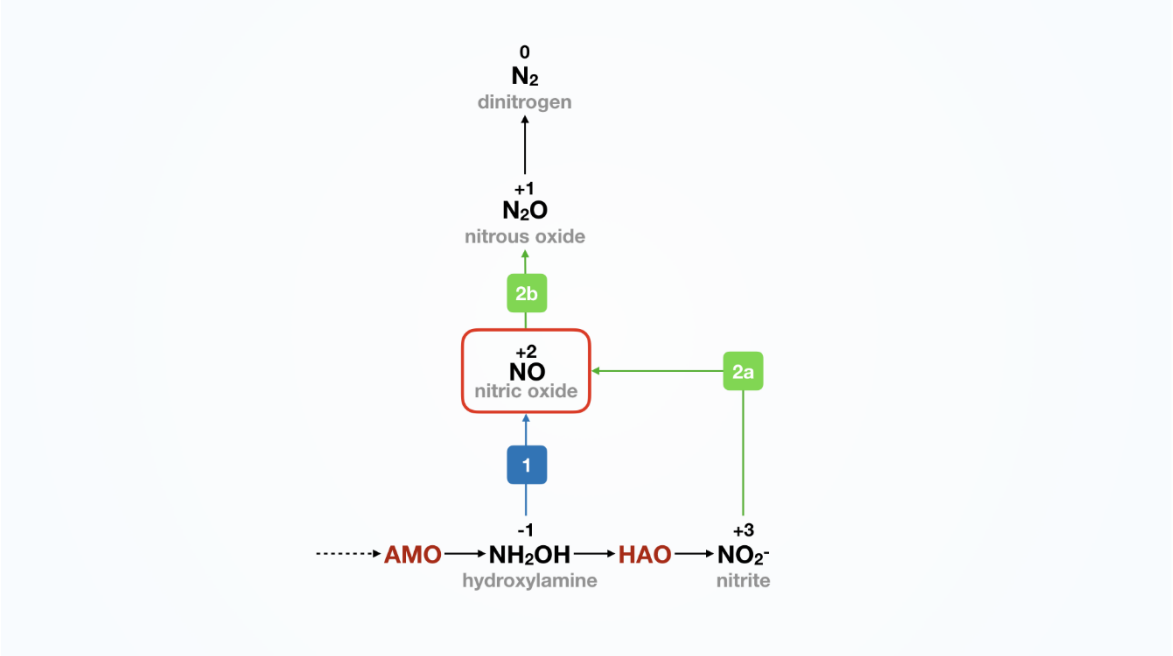

Figure 1.3 Generation of NO and N_2O during aerobic ammonia oxidation by ammonia-oxidising bacteria. NO may derive either from the incomplete oxidation of NH_2OH (step 1), or through the nitrifier-denitrification pathway; this latter mediated by the enzymes nitrite (step 2a) and nitric oxide (step 2b) reductases.

Although processes are poorly understood and not fully characterised, the formation of NO is known to occur through two distinct pathways, connected to the main metabolic route of NH_3 oxidation. This molecule may derive as a by-product during oxidation of the chemical intermediate NH_2OH (step 1 in Figure 1.3), or via enzymatic reduction of NO_2^-, in a process termed nitrifier denitrification, which occurs under O_2-limiting and anaerobic conditions. Nitrite- and nitric oxide-reductases mediate this process (as represented by steps 2a and 2b in Figure 1.3, respectively) (Hooper and Terry, 1979). Although recently discovered, the nitrifier-denitrification pathway has already been suggested as a protective mechanism against toxic accumulation of NO_2^- (Arp and Stein, 2003; Hatzenpichler, 2012; Medinets *et al.*, 2015).

Most of the available literature has focused its attention on the aforementioned nitrogen oxides (e.g. NO and N_2O) produced by AOB due to their role in the greenhouse effect (Feelisch and Martin, 1995; Conrad, 1996; Peng *et al.*, 2014; Stieglmeier *et al.*, 2014). For instance, it is known that NO_2^- and NO_3^- are dominant precursors for environmental NO under aerobic and anaerobic processes, respectively, identifying NH_4^+ as the principal source of NO under aerobic conditions (Medinets *et al.*, 2015). Microbial activity is thus one of the most important sources of environmental NO.

This pathway has been considered as the canonical route for NH_3 oxidation in AOB for a long time. However, recent perspectives on the matter have been made available that challenge the current understanding of the pathway of NH_3 oxidation, albeit in an integrative fashion. In simple terms, NO is regarded as an important intermediate in the oxidation of NH_3 to NO_2^-, rather than a by-product of this process.

Evidence on this matter is scarce, but fundamental. Zart et al. (2000) provided initial evidence for a potential role of NO for NH_3 oxidation in AOB, by demonstrating that oxidation of NH_3 is inhibited upon removal of NO from actively-nitrifying *N. eutropha* cells. Inhibition was assessed based on nitrification and ammonia oxidation rates, as compared to control cultures. Furthermore, this inhibition occurred independently of the three different methods used for removing NO; namely, by intense aeration of the cultures, by using an NO-binding chemical or by making use of biological NO-detoxifying systems (*Pseudomonas* PS88).

More recently, the role of NO in the pathway has been revisited by Caranto & Lancaster (2017). The authors proposed NO as a mandatory intermediate in the NH_3 oxidation pathway, and the direct product formed by HAO, rather than NO_2^-, using purified HAO enzyme from *N. europaea*. Based on the intriguing findings of this study that need further verification in whole AOB organisms, it has been hypothesised that this pathway proceeds through a three-step oxidation process, instead of the canonical two-step pathway, which

entails formation of NH_2OH and NO as mandatory intermediates, and further oxidation of NO to NO_2^- by yet an unidentified nitric oxide oxidoreductase enzyme. An integrated view of the aerobic NH_3 oxidation pathway with the current evidence of a central role of NO in this process is depicted in Figure 1.4.

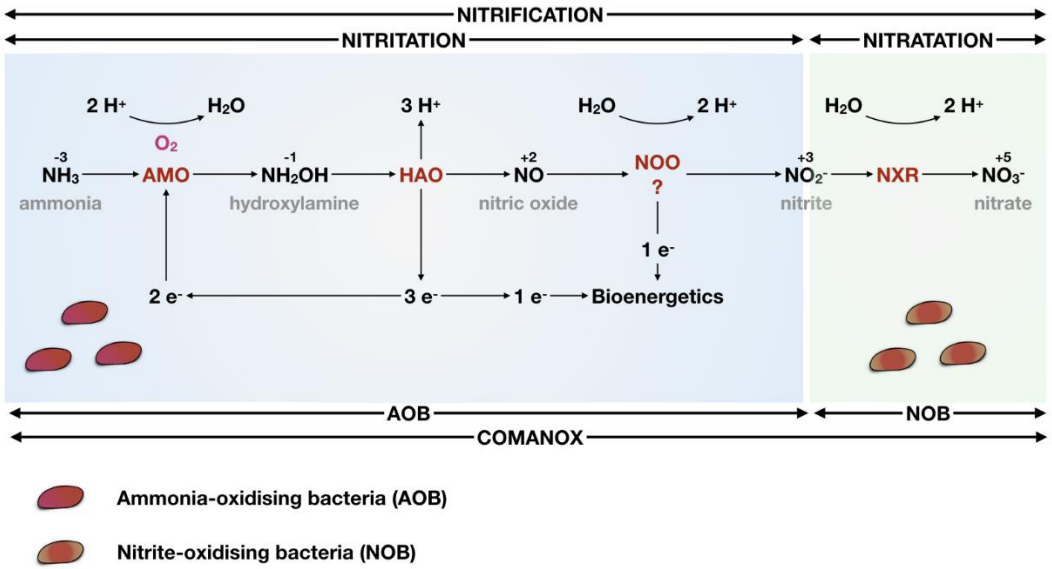

Figure 1.4 Current mechanistic view of the aerobic ammonia oxidation pathway by ammonia oxidisers. NOO: nitric oxide oxidoreductase; NXR: nitrite oxidoreductase. Adapted from Stein (2019) and Caranto & Lancaster (2017).

By fully understanding the NH_3 oxidation pathway by AOB, strategies to mitigate excessive microbial production of NO may be envisaged for environmental reasons, for instance (Aneja, Schlesinger and Erisman, 2008). Despite the deleterious effects of NO in the atmosphere, this small molecule also exhibits beneficial properties in mammalian biology. The following sections aim to review the fundamental characteristics of NO chemistry that are considered to be of relevance in biological systems (e.g. human) to help better understand the versatile actions of this molecule (protective, regulatory and deleterious) (Wink and Mitchell, 1998), as well as the known pathways underlying the generation of NO and NO-derived nitrogen oxides (e.g. NO_2^- and NO_3^-) in the human body.

1.3 Nitric oxide

1.3.1 General description

NO and related gaseous N oxides have ever been known as atmospheric toxic pollutants, for which anthropogenic action has continuously exerted its action (Monteny, Bannink and Chadwick, 2006; Aneja, Schlesinger and Erisman, 2008; Rockström *et al.*, 2009; Spiertz, 2010). Despite its deleterious actions, NO exhibits wide and important functions in mammalian biology (Szaciłowski, Chmura and Stasicka, 2005; Bryan and Grisham, 2007; Hetrick and Schoenfisch, 2009; Gupta *et al.*, 2011; Csonka *et al.*, 2015), whose appreciation and spectrum of action has grown substantially ever since its discovery as an important effector molecule in the cardiovascular system (Moncada, Palmer and Higgs, 1991; Moncada and Higgs, 1995). Its action is currently known to be diverse across organic systems, and examples include its action as an antimicrobial agent, either by direct microbicidal action on pathogens or via stimulation of host immunity, and its participation in inflammation processes, either as pro- or anti-inflammatory agent (Feelisch and Martin, 1995; Daniela, Thomas and Kolb-Bachofen, 1998; Bogdan, 2001; Schairer *et al.*, 2012).

Due to its unconventional properties for an endogenous signalling agent, NO was honoured to be chosen as “The Molecule of the Year” by Science, in early 1990s (Koshland, 1992). In the same decade, Robert F. Furchgott, Louis J. Ignarro, and Ferid Murad were awarded the Nobel Prize in Physiology or Medicine (1998) for their contribution in this field, for which the simultaneous work of Salvador Moncada contributed to the discovery of the vasodilatory properties of NO, and the elucidation of the mechanisms underlying its endogenous generation through oxidation of L-arginine (Palmer, Ashton and Moncada, 1988; Yetik-Anacak and Catravas, 2006).

Chemically, NO is a small, diatomic gas molecule with a stoke radius of about 3-4 Å (Fang, 1997). It is also a free radical (NO$^{\bullet}$) due to the existence of an unpaired electron (Figure 1.5 below). Due to its size, along with its solubility in water and lipids and high diffusion rate (Cals-Grierson and Ormerod, 2004; Heller, 2009; Csonka *et al*., 2015), NO is capable of freely crossing cell membranes, without the involvement of specialised transport systems (Loscalzo and Welch, 1995; Feelisch, 2008; Schairer *et al.*, 2012).

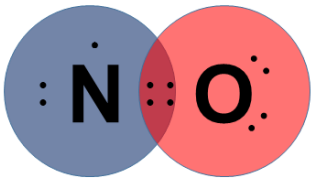

Figure 1.5 Lewis dot representation of nitric oxide.

Despite its radical nature, NO is a strikingly stable molecule due to its low tendency to dimerise and low oxidant and reductant capacities (Fukuto *et al*., 2012; Heinrich *et al.*, 2013). However, NO is a short-lived species in biological systems (Lancaster, 1994; Bryan and Grisham, 2007), due to its reactivity towards other biomolecules/targets of NO, such as O_2, other free radicals (e.g. superoxide), metalloproteins (e.g. soluble guanylate cyclase, heme moieties) and thiols (Wink *et al.*, 2002; Szaciłowski, Chmura and Stasicka, 2005; Hetrick and Schoenfisch, 2009). The downstream effects of NO in human biology are largely determined by the activity of its formation and consumption, its unique chemistry, and the overall redox status of the biological target (Wink and Mitchell, 1998).

1.3.2 Endogenous sources of nitric oxide

NO is synthesised by a plethora of cells with distinct functions in the human body, ranging from immunity (e.g. dendritic cells, natural killer cells, mast cells, monocytes, microglia, Kupffer cells, eosinophils and neutrophils) to tissue support and maintenance (e.g. keratinocytes, melanocytes, fibroblasts and endothelial cells) (Bruch-Gerharz, Ruzicka and Kolb-Bachofen, 1998; Schairer *et al.*, 2012). Figure 1.6 below summaries the processes that lead to the formation of NO in humans, which can be dependent or independent on enzymatic action.

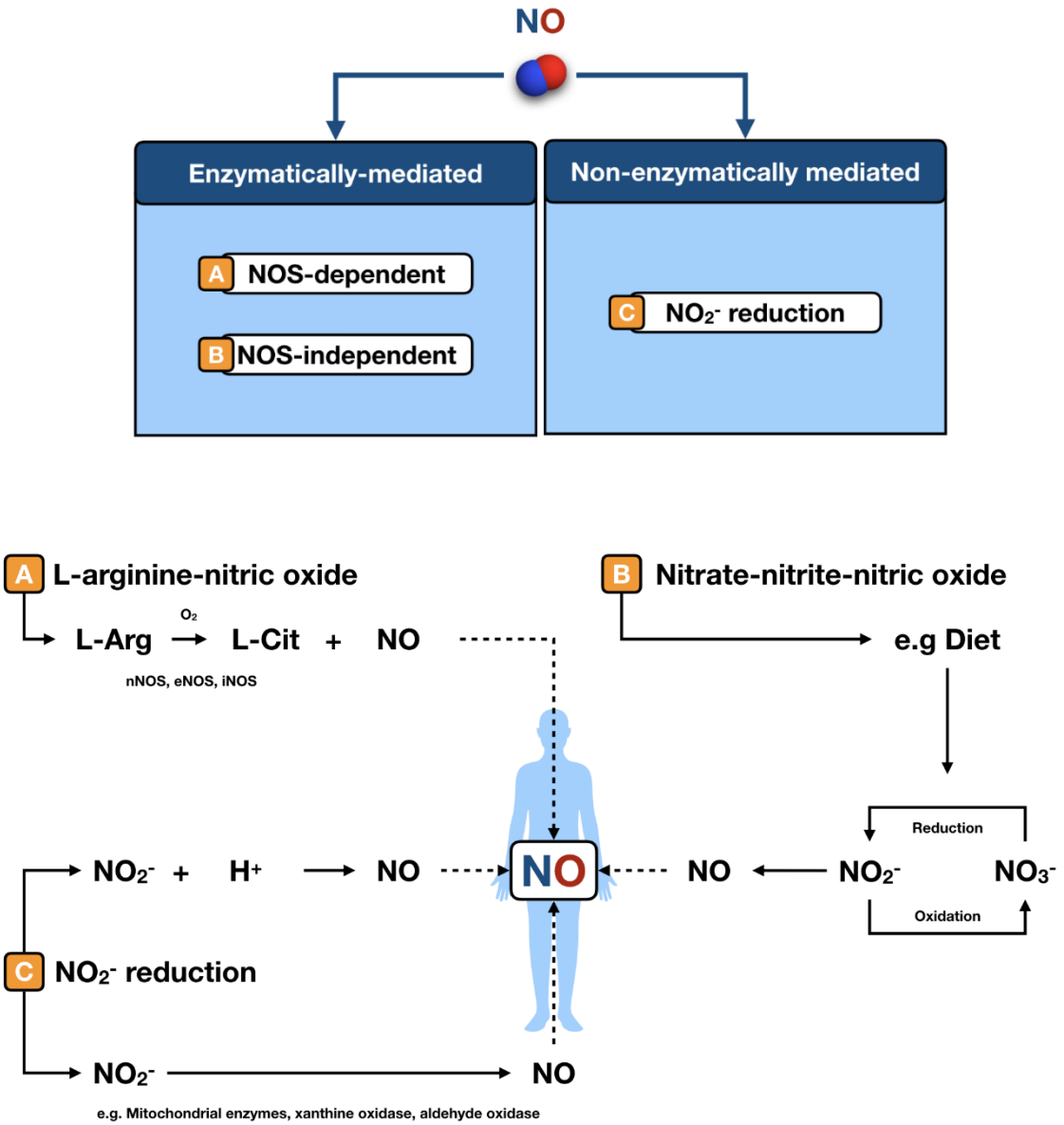

Figure 1.6 Mechanisms for nitric oxide generation (enzymatically and non-enzymatically mediated). The pathways that can contribute towards the NO pool include (A) the aerobic oxidation of L-arginine (L-Arg) to L-citruline (L-Cit) by nitric oxide synthases (nNOS, eNOS, and iNOS); (B) the contribution of NO_3^- from dietary sources; and (C) reduction of NO_2^- to NO by enzymatic action or chemically, under acidic conditions. Adapted from Lundberg *et al*. (2008) and Shiva (2013).

1.3.2.1 The L-arginine-nitric oxide pathway

NO can be produced endogenously by the L-arginine-nitric oxide pathway (Figure 1.6, pathway A), which entails a two-step oxidation of the amino acid L-arginine (L-Arg) to L-citrulline (L-Cit). This process is catalysed by nitric oxide synthases (NOS), which are produced by virtually all cell types and tissues (Weitzberg, Hezel and Lundberg, 2010). Different NOS isoforms are described, of which neuronal (nNOS, NOS1), inducible (iNOS, NOS2), and endothelial (eNOS, NOS3) are known (Moncada and Higgs, 1993; Brüne, Messmer and Sandau, 1995; Feelisch, 2008; Förstermann and Sessa, 2012).

All NOS isoforms are homodimers belonging to the family of monooxygenases, all containing a reductase and oxygenase protein domains (Szaciłowski, Chmura and Stasicka, 2005) in each monomer, requiring flavin mono- and di-nucleotide, tetrahydrobiopterin and reduced nicotinamide adenine dinucleotide phosphate, as co-factors (Cals-Grierson and Ormerod, 2004; Szaciłowski, Chmura and Stasicka, 2005; Förstermann and Sessa, 2012).

NOS differ in terms of their physiological regulation (i.e. constitutive or induced expression), magnitude of action (i.e. concentrations of NO achieved), duration of NO release and enzyme compartmentalization (Kiechle and Malinski, 1993; Daniela, Thomas and Kolb-Bachofen, 1998; Szaciłowski, Chmura and Stasicka, 2005; Schairer *et al.*, 2012). While nNOS and eNOS are both constitutively expressed (cNOS) in neural and vascular systems (Szaciłowski, Chmura and Stasicka, 2005), iNOS can be expressed upon a challenge by virtually every cell type (Szaciłowski, Chmura and Stasicka, 2005).

iNOS expression is triggered by molecules involved in inflammation and infection, such as bacterial lipopolysaccharide, interleukin-1β, tumour necrosis factor-α and interferon (Kiechle and Malinski, 1993). cNOS activity requires calcium (Ca^{2+})-calmodulin to produce low, basal concentrations (<1 μM) of NO (Thomas *et al.*, 2008). In contrast, iNOS do not require calmodulin activity and give rise to higher concentrations (~thousand-fold increase) of NO when expressed, often prolonged in time (from hours to days) (Brüne, Messmer and Sandau, 1995; Schairer *et al.*, 2012).

1.3.2.2 The nitrate-nitrite-nitric oxide pathway

NO can also derive from NOS-independent mechanisms, such as the reduction of NO_2^- by ubiquitous enzymes with reductase function, or through reduction of either endogenous or diet-sourced NO_2^- and NO_3^-, through the nitrate-nitrite-nitric oxide pathway (Lundberg, Weitzberg and Gladwin, 2008; Lundberg *et al.*, 2009; Lundberg, Gladwin and Weitzberg, 2015). This pathway may be of physiological relevance when NOS activity is impaired

(e.g. lack of O_2 or their co-factors), where reduction of these oxyanions may act as a source of biologically-active NO

Reduction of NO_3^- to NO_2^- is also achieved through action of bacterial nitrate reductases, commonly found in the upper parts of the gastrointestinal system (Duncan *et al.*, 1995; Lundberg, Weitzberg and Gladwin, 2008; Weitzberg, Hezel and Lundberg, 2010). Circulating NO_2^- can be further reduced to NO via xanthine and aldehyde oxidases, as well as mitochondrial enzymes (pathways B and C in Figure 1.6), which are known to have nitrite reductase activity (Lundberg, Weitzberg and Gladwin, 2008). In an enzyme-independent process, abiotic reduction of NO_2^- to NO (pathway C in Figure 1.6) occurs in chemically acidic environments, such as those seen in the stomach or during acidosis.

In summary, this pathway can be of pivotal importance as it constitutes a route for NO formation and delivery to biological tissues (e.g. cardiac and liver tissues), which is orchestrated in a NOS-independent fashion, and particularly relevant under ischemic conditions, for instance (Feelisch *et al.*, 2008; Li *et al*., 2008), during which provision of NO allows for regulation of blood flow, cell signalling and energetics (Feelisch, 2008; Lundberg, Weitzberg and Gladwin, 2008; Weitzberg, Hezel and Lundberg, 2010).

1.3.3 Chemical biology of nitric oxide

A non-extensive list of known biological outcomes derived from the action of NO in the human system is presented in Table 1.1 below. The versatility of NO allows its actions to be conveniently divided into the following categories: protective, regulatory, and deleterious (Wink & Mitchell 1998). Rather than an in-depth dedication to each of these actions, an overview of the chemistry of NO relevant to human biology is given in the following section, which helps to better understand the effects elicited by NO in human biology.

Table 1.1 Biological effects mediated by nitric oxide. Adapted from Wink & Mitchell (1998) and Szaciłowski et al. (2005).

Protective	*Regulatory*	*Deleterious*
Antioxidant	Vascular tone	Enzyme inhibition
Antihypertensive	Cellular adhesion	DNA damage
Antitumor activity	Vascular permeability	Lipid peroxidation
Antimicrobial activity	Neurotransmission	Antioxidant depletion
Free radical scavenging	Memory and learning	Septic shock
	Tissue oxygenation	Reperfusion injury
	Hepatic metabolism	
	Penile erection	
	Bronchodilation	
	Immune surveillance	

The above-presented outcomes can also be seen as directly- or indirectly-mediated through NO, as summarised in Figure 1.7 below, whose concentration and chemistry will mainly influence the downstream effects of NO in the human system.

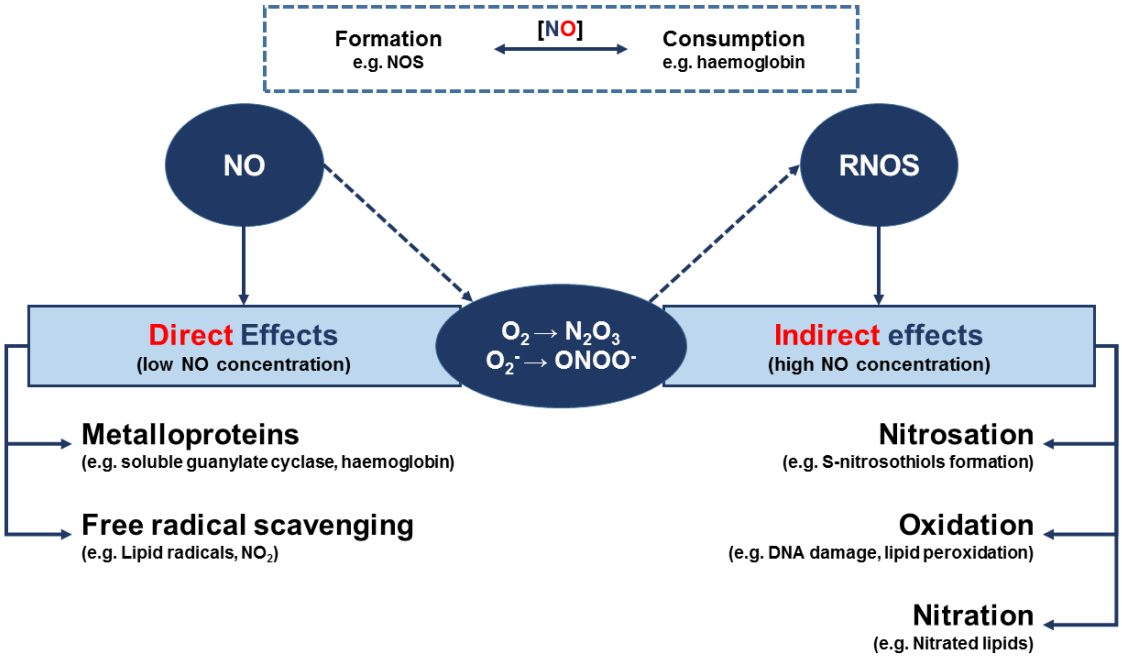

Figure 1.7 Schematic summary of the chemical biology of nitric oxide. The downstream effects can be mediated directly through NO, or indirectly through action of reactive nitrogen and oxygen species (RNOS). Adapted from Wink & Mitchell (1998) and Feelisch (2008).

The concentration of NO in human blood is a regulated process controlled by its constitutive formation by cNOS, and by mechanisms of its consumption. Under basal conditions, i.e. under constitutive production of NO, small amounts of NO (pmol) are mainly responsible for its function as a signalling molecule and antioxidant by direct interaction with other biomolecules, in particular, metal-containing proteins and other free radicals, respectively. At these small quantities, NO assume mainly protective and regulatory roles in cardiovascular (e.g. vasodilation and blood pressure control) and neuronal physiologies (e.g. memory formation and learning) (*Haynes et al*., 1993; Moncada and Higgs, 1993; Hawkins, 1996; Susswein *et al.*, 2004; Szaciłowski, Chmura and Stasicka, 2005; Shabeeh *et al*., 2013, 2017) for instance.

The most remarkable example of NO-mediated cell signalling occurs via activation of cytosolic guanylate (or guanylyl) cyclase (sGC), a metal-containing enzyme (Murad, 1994). Activation of sGC by formation of iron-nitrosyl (Fe-NO) complexes leads to cellular signal transduction, with formation of the second messenger guanosine 3, 5-cyclic monophosphate (cGMP) and activation of a cascade of phosphorylating events (Moncada and Higgs, 1993) that ultimately lead to relaxation of the smooth muscle, for instance. This signalling pathway shows the importance of NO to cardiovascular physiology as a paracrine mediator, whose production by endothelial cells leads to vasodilation, allowing maintenance of vascular tone and permeability, as well as tissue oxygenation. NO also interacts with heme moieties. In blood tissue, NO is oxidised to NO_3^- by its direct interaction with heme from ferrous (Fe^{2+})-haemoglobin (oxyhaemoglobin, oxyHb), in a coupled co-oxidation process that leads to the formation of ferric (Fe^{3+})-haemoglobin (methaemoglobin, metHb).

The NO autoxidation reaction with O_2 is fundamental to understand both a mechanism for NO regulation and the generation of higher N oxides, namely NO_2^- (Thomas *et al*., 2008). O_2 is an indispensable molecule for human biology, as it represents the final electron acceptor in the electron transport chain during cellular aerobic respiration, which ultimately leads to the generation of cellular energy in the form of adenosine triphosphate (ATP). Hence, dissolved O_2 is inevitable, which upon reaction with NO leads to the formation of reactive nitrogen and oxygen species (RNOS), such as the radical nitrogen dioxide (NO_2, equation 1.1 below) and dinitrogen trioxide (N_2O_3, equation 1.2 below) (Bonner and Stedman, 1996; Wink, Beckman and Ford, 1996; Wink and Mitchell, 1998), both more reactive than NO itself.

(1.1) $2\,NO + O_2 \rightarrow 2NO_2$

(1.2) $NO_2 + NO \leftrightharpoons N_2O_3$

In aqueous solutions, NO_2 reacts with NO to form N_2O_3. NO_2^- is the final product of the autoxidation of NO in aerobic, aqueous solutions, which is formed upon hydrolysis of N_2O_3 to nitrous acid (HNO_2), and final dissociation of the latter species (equation 1.3).

(1.3) $N_2O_3 + H_2O \rightarrow 2\,HNO_2 \leftrightharpoons 2\,H^+ + 2\,NO_2^-$

As a powerful nitrosative agent derived from the oxidation of NO under aerobic conditions, N_2O_3 participates in *in vivo* nitrosative reactions with other biomolecules (Fukuto *et al.*, 2012), for instance, thiols. These are molecules containing the sulfhydryl group SH, and are commonly represented as R-SH (R=organic), which upon nitrosation by N_2O_3 (via NO^+) form S-nitrosothiols ultimately (RSNO, equation 1.4 below), such as S-nitrosoalbumin and S-nitrosoglutathione (Stamler, Jaraki, *et al.*, 1992; Stamler, Simon, *et al.*, 1992; Gaston *et al.*, 1993).

(1.4) $R-SH + N_2O_3 \rightarrow RS-NO + NO_2^- + H^+$

Although their chemistry is not thoroughly presented in this thesis, it is worth mentioning the ability of these molecules to transport and deliver NO upon decomposition of RSNO (for instance, after exposure to light), or donate it to other thiols via transnitrosation (Heinrich *et al.*, 2013). Nitrosative chemistry thus conserves NO chemistry and contributes towards its endocrine action, under physiological conditions.

Besides NO_2, NO can also react with other radical species, such as reactive oxygen species (ROS), which are constitutively formed as a result of mitochondrial respiration. From these, the reaction of NO with superoxide anion (O_2^-) is of great relevance not only because it constitutes a pathway for NO consumption, but also because it is responsible for the generation of peroxynitrite ($ONOO^-$, equation 1.5 below), which undergoes

isomerisation to NO_3^- upon protonation to peroxynitrous acid (ONOOH) in physiological conditions.

(1.5) $$NO + O_2^- \rightarrow OONO^-$$

(1.6) $$ONOO^- + H^+ \leftrightharpoons ONOOH$$

(1.7) $$ONOOH \rightarrow NO_3^- + H^+$$

The afore-mentioned processes (i.e. nitrosation and ROS scavenging) readily occur under physiological conditions, and NO plays protective and regulatory roles (see examples in Table 1.1). However, when present at high quantities (nmoles), for instance, due to sustained production by iNOS or due to failure of mechanisms for regulating its concentration, NO may indirectly exert damaging actions for the host, largely mediated by RNOS (e.g. NO_2, N_2O_3, $ONOO^-$). These may include excessive nitrosative and oxidative reactions, which can lead to indiscriminate modification of other biomolecules, and thus alter their function, where deleterious effects may include modification of lipid components in cellular membranes due to increased lipid peroxidation, profound changes in DNA, as well as disturbances in energy metabolism by inhibition of mitochondrial electron transport chain (Wink and Mitchell, 1998; Win*k et al*., 2002).

In summary, the multifaceted and somewhat paradoxical roles that NO exhibits in human biology are largely dependent on its complex biochemistry, and its interplay with other biomolecules within its vicinity.

1.3.4 Translational approaches based on nitric oxide

The discovery of the important actions of NO and the role that the NO/cGMP signalling pathway plays in cardiovascular physiology is likely one of the most contemporary landmarks that allowed the development and commercialisation of pharmacological interventions capable of modifying the bioavailability of NO. Examples include currently available oral phosphodiesterase inhibitors used for the management of erectile dysfunction, of which sildenafil (Viagra®, Pfizer) is the lead molecule (Burnett, 2005; Davies, 2015).

Outside the cardiovascular system, therapies based on direct administration of inhaled NO are proposed for the treatment of pulmonary hypertension, for instance (Krasuski *et al*., 2000; Weinberger *et al*., 2001); however, its usage is limited by its dependence on

specialised staff to handle and safely administer NO to patients. The development of molecules with NO-donor properties may overcome potential drawbacks of inhaled NO by allowing safe administration and delivery of NO in a controlled fashion. Examples of these molecules include metal nitrosyls, RSNO, organic NO_2^- and NO_3^-, as well as diazeniumdiolates (NONOates) (Carpenter and Schoenfisch, 2012).

Ex vivo and *in vivo* evidence for the utility of NO-based therapies have been provided in the context of clinically-relevant pulmonary infections. For instance, Howlin et al. (2018) demonstrates *in vitro* efficacy of the metal-nitrosyl sodium nitroprusside in dispersing biofilms of *Pseudomonas aeruginosa*, an opportunistic bacterium that can colonise the lung epithelia of patients with cystic fibrosis, in which antimicrobial therapies are often ineffective. The results of this study show that NO can act synergistically with antimicrobial drugs, by triggering the dispersion of bacterial biofilms and potentiate the action of antibiotics. These findings were corroborated *in vivo* in a double-blind, controlled clinical trial with cystic fibrosis patients, in which administration of a low dosage of gaseous NO not only led to a decrease in *P. aeruginosa* aggregates, but also proved itself as a safe adjunctive therapeutic.

The human skin comes across as an attractive and useful platform for percutaneous generation of NO. Unlike other systems where direct application of gaseous NO may be practical, cutaneous generation of this molecule can be accomplished through several ways, for example by topical generation of exogenous NO, abiotic reduction of NO_2^-, or stimulation of NO release from photolabile dermal stores (e.g. RSNO) (Seabra *et al.*, 2004; Mowbray *et al*., 2009; Oplander *et al*., 2009; Weller, 2017; Monaghan *et al*., 2018). Evidence is provided in the following section regarding the development and application of these technologies as examples for delivering NO, at a cutaneous level.

1.3.5 Applications of nitric oxide on the human skin

Besides the contribution of the constitutive production of NO by dermal cells and resident immune cells on the skin (Bruch-Gerharz, Ruzicka and Kolb-Bachofen, 1998), it has been demonstrated that the nitrogen oxides NO_2^- and NO_3^- are sources of NO at the surface of the skin, and they are contributors for the bioavailable pool of NO on the skin. Weller et al. (1996) provided evidence for a NOS-independent mechanism of generation of NO on the outer layer of the skin of healthy human volunteers. The authors elegantly show measurable basal levels of NO on the surface of the human skin (hand and arm), and that its levels rise upon acidification of the human skin by topical application of acidic buffer. An identical trend is described after cutaneous application of NO_2^-, with levels of NO increasing in an NO_2^--concentration dependent manner, and independently of the skin microflora. Lastly, the authors show that sweat NO_3^- (mean concentration reported of

39.7±4.3 μmol L^{-1}) is the source of NO, due to its reduction to NO_2^- by the cutaneous microbial ecosystem present at the surface of the skin. These findings show therefore the importance of the oxyanions NO_2^- and NO_3^- as human sweat constituents, and a role for the resident microbial community on the surface of the skin as responsible for generating surface NO_2^-.

Biomedical technologies for generation and/or delivery of NO on the surface of the skin have been explored *in vivo* and in animal models, mainly in the context of microbial infections due to the known properties of NO as an antimicrobial agent, or for wound healing effects (Shabani *et al*., 1996; Fang, 1997; Luo and Chen, 2005; Weller and Finnen, 2006; Ghaffari *et al*., 2007; Hetrick *et al*., 2008; Weller, 2009; Li and Lee, 2010; Sulemankhil *et al*., 2012; Orman and Brynildsen, 2016). Weller et al. (1998) have provided *in vivo* evidence of the feasibility of a NO_2^--containing topical formulation as an NO-generating system for the treatment of Athlete's foot, for which mechanism of action is presumably based on the generation of NO by abiotic reduction of exogenously-applied NO_2^-, on the acidic skin surface.

Based on an identical principle, Jones et al. (2010) proposed an adhesive, permeable patch for the generation of NO on the skin, containing probiotic *Lactobacillus*, carbon source and NO_2^-, and provides *in vitro* evidence for its antibacterial and antifungal properties. In this technology, NO is formed through NO_2^- reduction due to the acidification of the patch microenvironment, upon formation of lactate by the probiotic bacteria. The concentrations of NO formed were enough to elicit bacterial and fungal cell deaths in clinically-relevant pathogens, such as *Staphylococcus aureus*, *P. aeruginosa*, *Acinetobacter baumannii*, *Escherichia coli, Trichophyton rubrum*, and *Trichophyton mentagrophytes*. While innovative for its ergonomic design and its ability to generate effective concentrations of NO, its release seems prone to patch-to-patch variability that may affect reproducibility of releasing controlled doses of NO.

In vivo feasibility of this probiotic patch is demonstrated by Jones et al. (2012), who reports decreased microbial burden and potentiation of wound closure in patch-treated rabbit models with an infected wound (*Staphylococcus aureus*) as compared to non-treated ones, and as observed from morphometric analysis of wounds. Moreover, safety was ensured as no significant differences in metHb formation of NO metabolites were seen in serum samples collected from treated animals. No evidence in humans has been provided for this technology. The effect of NO on potentiating wound closure has also been reported by Weller & Finnen (2006), who demonstrated the benefits of acidified NO_2^- in accelerating the closure of wounds in healthy and diabetic mice.

The attractiveness of the integumentary system for the development of NO-based technologies relies on the fact that locally-generated NO or its metabolites also have the ability to elicit systemic effects, regardless of whether they originate from dermal stores, or from exogenous sources. Blood pressure-lowering effects have been described by Oplander et al. (2009), after whole body exposure of healthy human volunteers to ultra-violet (UVA) light. The proposed mechanism of action is based on photo-induced release of NO from skin stores, with an increase in the circulating plasma levels of NO_2^- and total nitroso species (RXNO, which includes RSNO and other nitroso species); the latter parameter correlated well with the decreased blood pressure observed in UVA-irradiated volunteers. Similar findings are also reported by Liu et al. (2014), who report a decrease in mean arterial blood pressure in normotensive volunteers exposed to two erythemal UVA doses. Independently from UVA radiation, Oplander et al. (2012) report identical effects, which were achieved with a topical application of acidified NO_2^--containing liniments.

In summary, several approaches are described that aim to modify the bioavailability of NO on the surface of the skin, whose effects can be mediated locally (e.g. antimicrobial effects) or systemically (e.g. changes in blood pressure). Alternative approaches to abiotic generation of NO at the skin's interface may involve the use of microorganisms. Topical application of AOB has emerged as a viable cutaneous approach for restoring the microbial flora of the human skin, and as a biological tool for modifying the bioavailability of NO and its metabolites on the skin. AOBiome LLC is a company based in the United States of America, which has engineered the naturally-occurring, non-pathogenic ammonia-oxidising bacterium *Nitrosomonas eutropha* D23 (AO+ Mist™, MotherDirt™, AOBiome LLC), intended for topical administration as a spray formulation.

1.4 Hypothesis

It has been hypothesised that contemporary and urban lifestyles have led to the loss of AOB on the human skin (Whitlock and Feelisch, 2009). The underlying reasons may include the following: less exposure to soil, particularly for human beings inhabiting outside rural areas and thus decreasing the likelihood of cutaneous colonisation by AOB; and the overuse of cleaning agents, as well as intensive hygienic procedures (Whitlock and Feelisch, 2009; Scharschmidt and Fischbach, 2013; Barin, Tobias and Peterson, 2015; McCoy and Köller, 2015).

AOB have been placed as a constituent of the skin microflora of a non-Westernised, hunter-gatherer population (Clemen*te et al*., 2015), and were found in the gut of Ötzi the Tyrolean Iceman from the Copper Age (ca 3370-3100 BC) (Lugli *et al.*, 2017; Wierer *et al.*, 2018). The impact of modern personal hygiene products on the human skin has been assessed by Bouslimani et al. (2015), who demonstrated that exogenous molecules derived from hygienic and beauty products alters the chemical composition of the human skin, potentially influencing the metabolic crosstalk between the host and its microbial cutaneous ecosystem.

Although *N. eutropha* D23 is commercially available and currently used in clinical trials for treatment of skin inflammatory conditions, evidence for its metabolic activity is scarce (Gryllos, Vajrala, *et al*, 2014). Its mechanism of action is unknown, but NO and/or NO_2^- are presumably involved. Local generation and delivery of these metabolites by *N. eutropha* D23 on the skin is based on the production of these molecules by the bacteria upon oxidation of NH_3/NH_4^+ (substrate) present on the skin (as a sweat constituent, emanated through the skin, or as a breakdown product of urea) (Czarnowski *et al.*, 1992; Alvear-Ordenes *et al.*, 2005; Nose *et al.*, 2005; Schmidt *et al.*, 2013). I therefore hypothesised that the metabolic products NO and/or NO_2^- produced by *N. eutropha* D23 are of sufficient quantities to elicit *in vitro* and/or *in vivo* bioactivity. Specifically, bioactivity was evaluated using pathogenic biofilms as a tool, as well as a small cohort of healthy human volunteers. In order to test this hypothesis fully, initial *in vitro* biochemical assessment of the metabolic phenotype exhibited by axenic cultures of *N. eutropha* D23 was imperative.

1.5 Thesis outline

The overall aims for this doctoral thesis are outlined below, and divided into three major results chapters (Chapters 3 to 5). The aims described below and specific objectives within each aim are listed in the respective chapters.

- **Chapter 2** (Materials and methods) introduces the methodology that was followed for this doctoral project. Independent methodologies are used for detection and quantification of bacterial metabolites;
- **Chapter 3** (Biochemical characterisation of *Nitrosomonas eutropha* D23) aims to confirm the expected biochemical characteristics for *N. eutropha* D23, based on the known biochemistry and physiology of AOB. It mainly introduces the metabolic phenotype of this strain of AOB, and provides evidence for the production of NO and other metabolites, as well as factors influencing their production (e.g. temperature, pH, cell density and concentration of substrate);
- **Chapter 4** (Bioactivity towards *Pseudomonas aeruginosa* biofilms) aims to verify whether the amounts of NO and/or NO_2^- can elicit *in vitro* effects, using *Pseudomonas aeruginosa* biofilm models as an assessment tool, by co-culturing with *N. eutropha* D23. It also demonstrates bioactivity towards clinical isolates of *P. aeruginosa*, obtained from the lung epithelia of patients with cystic fibrosis;
- **Chapter 5** (Signature profile of *Nitrosomonas eutropha* D23 at a human systemic level) presents exploratory results of a short-time topical application of *N. eutropha* D23, in a small cohort of healthy human volunteers, at local and systemic marker levels. Specific methodology is included in this Chapter;
- **Chapter 6** (Conclusions) provides an overall discussion of the findings presented in this research thesis, the conclusions and a personal reflection.

Chapter 2

Materials and Methods

Chapter 2: Materials and Methods

2.1 Chemicals and buffer components

In the preparation of all solutions, Milli-Q water was used at 18.2 MΩ cm^{-1} (Merck Millipore). When appropriate, solutions were sterilised by means of filter sterilisation (0.22-μm pore size, Merck Millipore), or autoclaving (15 min, at 121 ºC). Table 2.1 lists general chemical components used throughout this thesis, their sources and chemical purity as reported by the manufacturers.

Phosphate buffers used throughout this thesis were as follow: $MgCl_2$-supplemented phosphate buffer (50 mmol L^{-1} Na_2HPO_4, 2 mmol L^{-1} $MgCl_2$, pH 7.6; hereinafter referred to as storage medium) was used for washing, storage of bacterial cells, dilution medium and vehicle for activity assays; phosphate-buffered saline (PBS, pH 7.3) was prepared according to manufacturer's instructions (Oxoid), and it was mainly used for washing steps during biofilm experiments; and phosphate buffer (PB, pH 6.8) was used exclusively for NH_2OH analysis.

For batch-grown *N. eutropha* D23, the composition of the growth medium (ATCC® medium 2265) has been described by Vajrala et al. (2010) and it is summarised in Table 2.2. For its preparation, three different components were prepared and filter-sterilised separately before being combined together. A stock solution of NH_4^+, provided as $(NH_4)_2SO_4$, was prepared in Milli-Q water (Millipore) and filter sterilised through a 0.22-µm filter. This solution was stored at 4°C and was used to incubate *N. eutropha* D23, at established NH_4^+ concentrations, by diluting from the stock into appropriate buffer/vehicle.

Table 2.1 List of general components used for this thesis, their sources and purity. Commercial kits are excluded from this list, and are mentioned in the future sections as appropriate.

Component	Source	Purity
4,5-diaminofluorescein	Abcam	≥ 95.0%
4,5-diaminofluorescein triazole	Abcam	≥ 95.0%
$CaCl_2.2H_2O$	Sigma-Aldrich	≥99.0%
Trichloroacetic acid	Sigma-Aldrich	≥99.0%
CPTIO (K^+ salt)	Sigma-Aldrich	≥ 98.0%
Crystal violet	Sigma-Aldrich	1%
$CuSO_4.5H_2O$	Sigma-Aldrich	≥ 98.0%
D-(+)-glucose	Sigma-Aldrich	≥ 99.5%
Dimethyl sulfoxide	Fisher Scientific	≥ 99.0%
EDTA pH 8.0	Invitrogen	-
$FeSO_4.7H_2O$	Sigma-Aldrich	≥ 99.0%
Glycerol	Sigma-Aldrich	≥ 99.5%
HCl	Sigma-Aldrich	36.5-38.0%
Human haemoglobin	Sigma-Aldrich	-
I_2	Sigma-Aldrich	≥ 99.9%
KH_2PO_4	Sigma-Aldrich	≥ 99.0%
KI	Sigma-Aldrich	≥ 99.0%
Malondialdehyde	Sigma-Aldrich	≥ 96.0%
$MgCl_2.6H_2O$	Sigma-Aldrich	≥ 99.0%
$MgSO_4.7H_2O$	Sigma-Aldrich	≥ 99.5%
Na_2CO_3	Sigma-Aldrich	≥ 99.5%
Na_2HPO_4	Sigma-Aldrich	≥ 99.0%
NaCl	Sigma-Aldrich	≥ 99.5%
NaH_2PO_4	Sigma-Aldrich	≥ 99.0%
NaOH	Sigma-Aldrich	≥ 98.0%
N-(1-Naphthyl)ethylenediamine	Sigma-Aldrich	≥ 98.0%
$NH_4(SO_4)_2$	Sigma-Aldrich	≥ 99.0%
NH_4Cl	Sigma-Aldrich	≥ 99.5%
Sulphanilamide	Sigma-Aldrich	≥ 99.0%
2,4,6-Tris(2-pyridyl)-*s*-triazine	Sigma-Aldrich	≥ 98.0%

Table 2.2 Composition of the growth medium used for batch-wise growth of *N. eutropha* D23.

Component		Final composition (~ 1.5 L)
1	Substrate and salt elements (1.2 L)	4.95 g $(NH_4)_2SO_4$ (50 mmol L^{-1} NH_4^+) 0.62 g KH_2PO_4 0.27 g $MgSO_4.7H_2O$ 0.04 g $CaCl_2.2H_2O$ 0.5 mL $FeSO_4.7H_2O$ (in 50 mmol L^{-1} EDTA pH 7.0) 0.2 mg $CuSO_4.5H_2O$
2	Buffer components (0.3 L)	8.2 g KH_2PO_4 0.7 g NaH_2PO_4
3	Carbon source (0.012 L)	0.6 g Na_2CO_3

Modified M9 minimal medium (M9 medium) was prepared either directly from the commercial source (Formedium), at pH 7.0, or using an in-house version, whenever adjustments in the concentration of NH_4^+ were needed. Its overall composition is summarised in Table 2.3 below.

Table 2.3 Standard composition of modified M9 minimal medium (M9 medium).

Component	Final concentration
Na_2HPO_4	48 mmol L^{-1}
KH_2PO_4	22 mmol L^{-1}
NH_4Cl	19 mmol L^{-1}
NaCl	9 mmol L^{-1}
$MgSO_4$	2 mmol L^{-1}
$CaCl_2$	100 μmol L^{-1}
Glucose	20 mmol L^{-1}

2.2 Microorganisms and culture conditions

2.2.1 Preparation of *N. eutropha* D23 cell suspensions from commercial source

N. eutropha (strain D23, ATCC accession number PTA-121157, Whitlock et al. 2015) were recovered from the AO+ Mist™ (Mother Dirt™, AOBiome LLC) commercial product within a biosafety cabinet, and transferred to sterile containers, which were subjected to centrifugation at 16,100 *g*, for 15 min, at 4 °C. Supernatant was discarded and bacterial pellets were washed three times, being ultimately re-suspended in storage medium at desired optical densities (OD, λ = 600 nm). Heat-killed *N. eutropha* D23 were prepared by subjecting aliquots of this suspension to controlled heat inactivation, at 60 ºC for 2 h. Live and dead bacterial pellets were kept in sterile light-impermeable containers at 4 ºC, until further use. For co-culture models with other bacterial species, *N. eutropha* D23 were washed and stored in PBS.

2.2.2 Batch-wise growth of *N. eutropha* D23 collected from commercial source

For the study of activity and/or growth of *N. eutropha* D23, bacteria collected as described in section 2.2.1 above were inoculated in appropriate recipients containing growth medium (Table 2.2), at desired inocula densities. Growth was allowed to occur in the dark, with no agitation, and at 31 °C. For experiments carried out by growing *N. eutropha* D23 in the laboratory, growth and metabolic activity were assessed through monitoring of several parameters, such as measurement of pH, NH_4^+, NOx, NH_2OH biomass (protein), optical density (OD), and intracellular bioenergetics. Details for the measurement of these parameters are described in section 2.4.

2.2.3 *N. eutropha* D23 collected from chemostat cultures

Chemostat-grown cultures of *N. eutropha* D23 were prepared at Oregon State University (Corvallis, United States of America), and sent over to the University of Southampton for metabolic assessment, through AOBiome LLC.

These chemostat cultures were prepared by optimising growth of *N. eutropha* D23 for continuous cultivation, in a mini-bioreactor (Applikon Biotechnology), containing 1 L of *N. eutropha* D23 growth medium (Table 2.2), in order to achieve reproducible biomass yields. Bacterial cells were harvested from continuous cultivation at different days (7, 81, 85, and 90 days after inoculation), washed in storage medium, and stored at 4 °C protected from light. Cell harvests were shipped to Southampton by air, using a cold-chain courier service as required, and kept in the fridge until further analysis.

2.2.4 *Pseudomonas aeruginosa* planktonic growth conditions

For biofilm experiments, cultures of *P. aeruginosa* (wild-type and clinical isolates, see Table 2.4 below) were propagated in 10 mL of lysogeny broth (overnight culture) from a cryogenic stock, according to standardised procedures (LaBauve and Wargo, 2012), at 200 rev min^{-1}, at 37ºC for 16-20 hours (late exponential phase).

Table 2.4 *Pseudomonas aeruginosa* strains used in this thesis.

Strain	Description	Source
PAO1	Laboratory, wild-type strain	University of Washington
PA08	Clinical isolate	Sputum samples[a]
PA10	Clinical isolate	Sputum samples[a]
PA15	Clinical isolate	Sputum samples[a]
PA20	Clinical isolate	Sputum samples[a]
PA21	Clinical isolate	Sputum samples[a]
PA26	Clinical isolate	Sputum samples[a]
PA30	Clinical isolate	Sputum samples[a]
PA37	Clinical isolate	Sputum samples[a]
PA39	Clinical isolate	Sputum samples[a]
PA44	Clinical isolate	Sputum samples[a]
PA49	Clinical isolate	Sputum samples[a]
PA55	Clinical isolate	Sputum samples[a]
PA56	Clinical isolate	Sputum samples[a]
PA57	Clinical isolate	Sputum samples[a]
PA58	Clinical isolate	Sputum samples[a]
PA66	Clinical isolate	Sputum samples[a]
PA68	Clinical isolate	Sputum samples[a]

[a] Sputum samples collected from 72 patients with cystic fibrosis (median age at informed consent: 21 years, range 17-62). UK NHS Research Ethics Reference 08/H0502/126.

2.2.5 *Pseudomonas aeruginosa* biofilm growth conditions

The following methodology is based on the work of Barraud et al. (2006), and it is schematically summarised in Figure 2.2 for ease of understanding. An overnight culture of *P. aeruginosa* grown as described in section 2.2.4 above was diluted to an OD ~ 0.01, which corresponds to ~10^6 colony-forming units (CFU), in freshly-prepared M9 medium. Aliquots of this bacterial suspension (100 μL) were inoculated in sterile, flat-bottomed 96-well microtiter plates (Nunc Microwell™, Thermo Scientific), and the biofilm was allowed to grow on the surface of a transfer-peg lid (Nunc™ Immuno TSP lids, Thermo Scientific), at 37 °C for 16-20 h, without shaking and under a humidified atmosphere. Transfer-peg lids with adherent *P. aeruginosa* biofilm were carefully washed twice with sterile PBS, before use in co-culture with *N. eutropha* D23.

2.2.6 Co-culture of biofilms with *N. eutropha* D23

For co-culture, microtiter plates (Nunc Microwell™, Thermo Scientific) were prepared by mixing M9 medium with either an equal volume of *N. eutropha* D23 suspension (co-culture wells) or an equal volume of PBS (control wells), to a final volume of 150 μL per well. The microtiter plates were covered by transfer-peg lids containing confluent *P. aeruginosa*

biofilms on the pegs. Different co-culture duration periods were studied (4, 6, and 8 h), but in all iterations, co-culture plates were kept at 37 °C, without shaking, and under a humidified atmosphere. Unless stated otherwise, for each 96-well microtiter plate (i.e. one technical replicate), 5 to 10 identical biological replicates were run for each experimental condition assayed.

2.2.7 Readout of dispersal outcomes

2.2.7.1 Crystal violet determination (biofilm biomass)

After co-culture, transfer-peg lids were washed twice with sterile PBS to remove planktonic *P. aeruginosa* and *N. eutropha* D23, followed by heat fixation for 1 h, at 60 °C. Afterwards, the remaining biofilm mass adherent on the pegs was stained with 0.1% (*w/v*) crystal violet (CV) for 15 min, and excess stain was removed by at least 3 successive washing steps with sterile H_2O. Transfer-peg lids were allowed to dry overnight before extracting the stain from the biofilm by immersion of the transfer-peg lids in glacial acetic acid (130 µL). The concentration of crystal violet in the acidic extract was then quantified by measuring the absorbance at 584 nm using a microplate reader (FLUOstar OPTIMA, BMG Labtech).

2.2.7.2 Colony-forming units

In some iterations, the contents from the co-culture plates were aspirated from each well and pooled into 1.5-mL microcentrifuge tubes (Fisherbrand) for counting of the colony-forming units (CFU). These samples were serially diluted in PBS and spot-plated onto cetrimide agar plates (cetrimide agar supplemented with 10 mL glycerol L^{-1}). Agar plates were incubated for 16-20 h, at 37 °C and CFU were calculated according to the following equation: CFU mL^{-1} = (number of colonies x dilution factor) / aliquot volume.

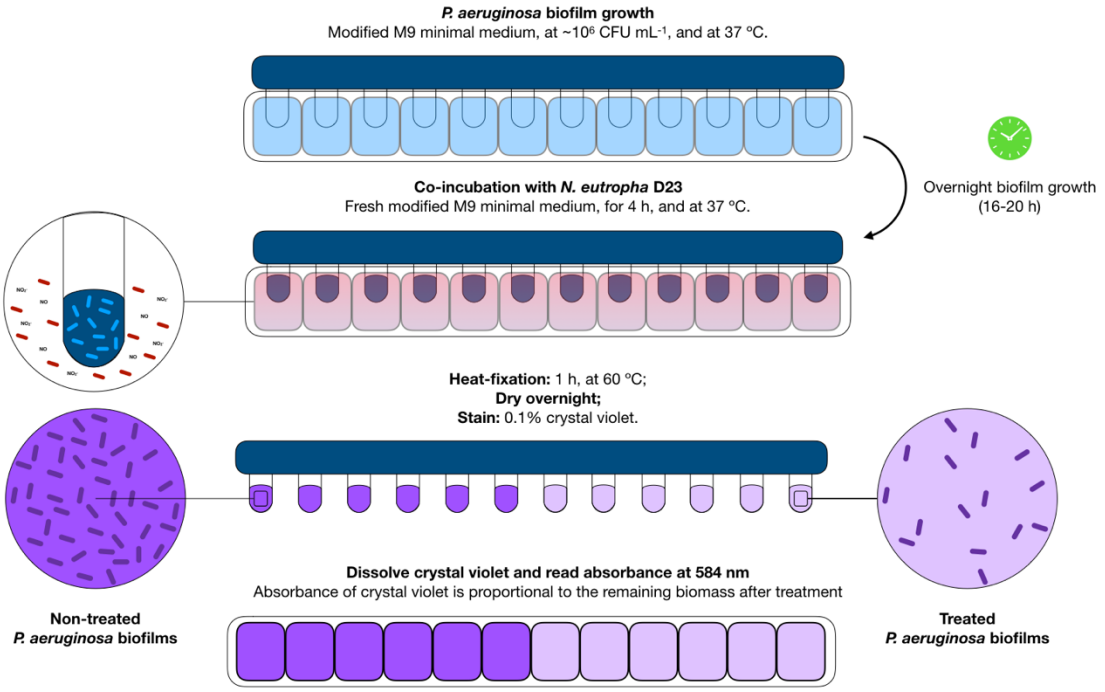

Figure 2.1 Experimental workflow used for growth of *P. aeruginosa* (section 2.2.5), including co-culture step with *N. eutropha* D23 (section 2.2.6), and outcome determination (2.2.7), based on crystal violet determination.

2.2.7.3 Confocal laser scanning microscopy

P. aeruginosa biofilms were prepared for imaging according to the experimental protocol described by Cai (2018). Overnight cultures of *P. aeruginosa* were diluted to an OD ~ 0.01 in freshly-prepared M9 medium, as previously described. An aliquot (3 mL) of this bacterial suspension was inoculated in poly-D-lysine-coated, glass-bottomed petri dishes (P35G-1.5-14-C, ⌀ 35 and 14 mm for dish and coverslip, MatTek Corporation), and incubated at 37 °C, under gentle orbital shaking (50 rpm). Formation of *P. aeruginosa* lasted 3 days, with spent media changed every 24 h, by pipetting it out and replacing with freshly-prepared M9 medium. Before imaging, bacteria attached onto the coverslip were washed thrice with 0.85 % (w/v) NaCl, followed by staining with propidium iodide (dead cells) and SYTO9® (live cells) for 20 min in the dark, according to the manufacturer's instructions (LIVE/DEAD® BacLight Bacterial Viability Kit, Invitrogen®). Excess stain was removed by washing with 0.85 % (w/v) NaCl. To avoid desiccation of *P. aeruginosa* biofilms from laser heating during image acquisition, 1 mL of 80% glycerol was carefully added to the surface of the coverslip, just moments before imaging.

For each MatTek petri dish, 3 to 4 random areas were selected for capturing image stacks, using 488 and 561 nm lasers for excitation of SYTO9® (excitation 485 nm, emission 498 nm) and propidium iodide (excitation 535 nm, emission 617 nm), respectively, using a confocal laser microscope (SP8, Leica Microsystems). Image stacks were analysed by COMSTAT 2.0 *(*Heydorn *et al*., 2000; Vorregaard, 2008) for biomass and surface coverage measurements, under the open-source software ImageJ.

2.2.8 Nitrite production by different harvests of *N. eutropha* D23

To assess NO_2^- formation by *N. eutropha* D23, cells were incubated in storage medium (pH 7.6), at 200 mmol L^{-1} NH_4^+ and monitoring of NO_2^- was done every 5 min, over a period of 1 h. All incubations were performed under aerated conditions, in a final volume of 12 mL, at 31± 0.2°C, with a cell density of ~10^7 *N. eutropha* D23 cells mL^{-1}, and agitated at 20 rpm. NO_2^- was measured by ion chromatography, as described in the metabolite analysis section.

2.2.9 Production of nitrite and ammonium consumption by *N. eutropha* D23 for co-culture experiments

Cell suspensions of *N. eutropha* were inoculated in 96-well microtiter plates (Nunc™ Microwell™, Thermo Scientific), with M9 medium at 1:1 ratio. Heat-inactivated *N. eutropha* D23 were incorporated as a negative control. M9 medium without bacteria was incorporated as a background control. Two technical replicas were assayed in parallel,

each containing two biological replicas. Hourly time-points from an 8-hour overall incubation were taken, collecting and pooling the contents from the wells into 1.5-mL microcentrifuge tubes (Fisherbrand). Samples were immediately centrifuged at 15,000g, at 4ºC for 15 minutes. Supernatants were then collected into fresh tubes and frozen in dry ice, until further analysis for NOx and NH_4^+ measurements.

2.3 Metabolite analysis

2.3.1 Ammonium (NH_4^+)

NH_4^+ was quantified by the indophenol blue method (Berthelot's reaction), as described by Baethgen & Alley (1989), in an 96-well microplate format for high-throughput analysis. The chemical reactions involved in this method are depicted in Figure 2.2 below.

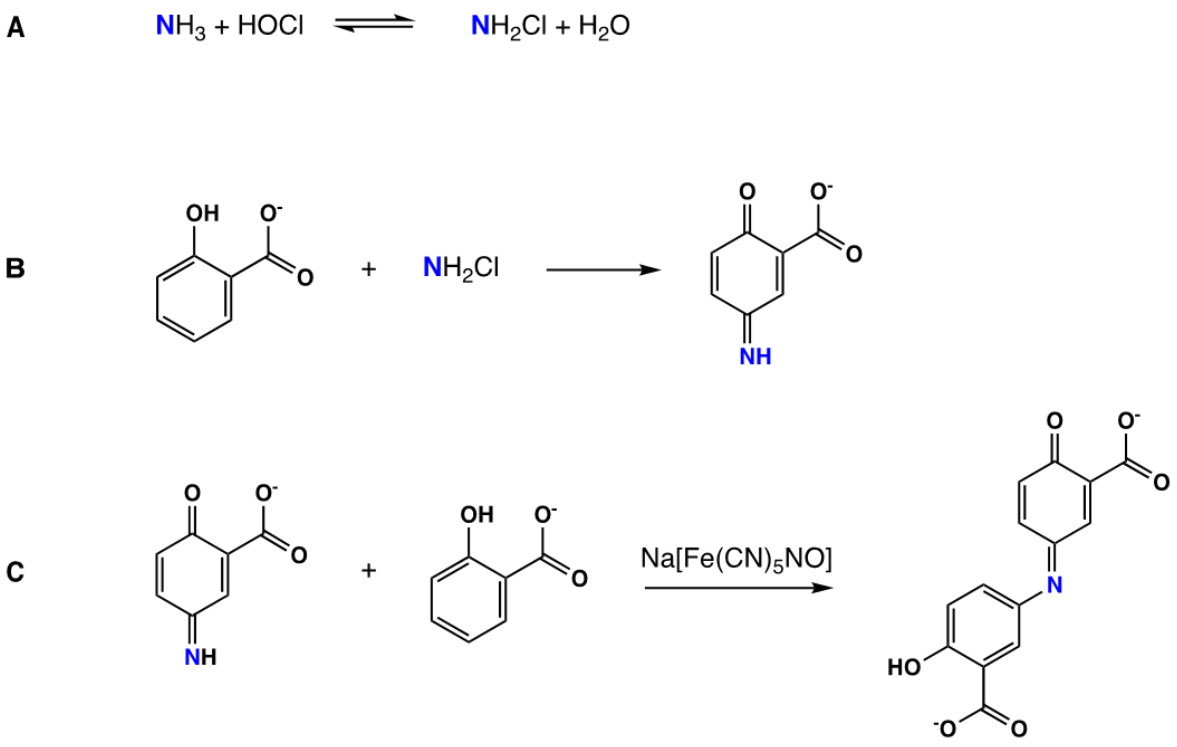

Figure 2.2 Chemical reactions for the Berthelot method employed for ammonia measurement. Adapted from Cogan et al. (2014).

Briefly, NH_3 reacts with hypochlorite (OCl^-) in alkaline conditions (pH 12) to form monochloroamine (NH_2Cl) (Figure 2.2, A), which then reacts with salicylate to form 5-aminosalicylate (Figure 2.2, B). In the presence of sodium nitroprusside as a catalyst, the

latter compound is further oxidised to form an indophenol complex (Figure 2.2, C), whose absorbance is proportional to the amount of NH_3 present in solution (C*ogan et al.*, 2014).

For this method, the salicylate-containing solution (phenolic solution) is composed of 425 mmol L^{-1} sodium salicylate, 200 mmol L^{-1} of trisodium citrate and sodium tartrate, and sodium nitroprusside. The hypochlorite-containing solution (referred as oxidising solution) was prepared freshly, by dilution of 10% NaHClO in 6 g L^{-1} NaOH (2% v/v OCl in NaOH). Samples (80 μL) for NH_4^+ measurement were placed in flat-bottomed 96-well microtiter plates (Nunc™ Microwell™, Thermo Scientific), followed by sequential addition of equivolumes (60 μL) of oxidising and phenolic solutions. Plates were incubated for 45 min at room temperature, protected from light, and absorbance values were recorded at 650 nm. NH_4^+ concentrations were interpolated from a calibration curve (examples presented in Figure B.1, in Appendix B), using $(NH_4)_2SO_4$ as standard.

2.3.2 Nitrite (NO_2^-)

For the measurement of NO_2^-, colorimetric and chromatographic-based methods were used.

2.3.2.1 Diazotization assay

NO_2^- was quantified by the classical diazotization assay (or Griess assay), adapted for 96-well microtiter plates, as described by Miranda et al. (2001). Samples were centrifuged at 16,100 *g* and culture supernatants were transferred to a 96-well microtiter plate (Nunc Microwell™, Thermo Scientific) containing storage medium, and incubated successively with 2 % (w/v) sulphanilamide (SULF, prepared in 5% v/v HCl) and 0.1 % (w/v) *N*-1(1-naphthyl)ethylenediamine (NED), by mixing equal volumes of these two reagents with sample, at a final proportion of 1:0.5 (v/v, sample:reagents), in a total volume of 300 µL. Plates were incubated at room temperature for 10 min, and absorbance values of the chromophore were read at λ = 540 nm. NO_2^- concentrations were interpolated from a calibration curve, using $NaNO_2$ as standards (acceptable linearity $R^2 \geq 0.99$).

2.3.2.2 Liquid chromatography

For the majority of the experiments requiring high-throughput sample analysis, NO_2^- was quantified by ion chromatography (IC) and high-performance liquid chromatography (HPLC).

For IC analysis (Dionex ICS-5000$^+$, Thermo Fisher), NO_2^- was determined through its chromatographic separation using an AS16-4 column (2x250 mm, Dionex™ IonPac AS16), kept at 35 °C, using isocratic elution with KOH (25 mmol L^{-1}) for a 12-min run time,

at a flow rate of 0.380 mL min^{-1}. Ion suppression (Dionex™ ERS™ 2mm, set to 24 mA, Thermo Fisher) enabled electrolyte separation using conductivity and UV-Vis detectors (set to 220 nm), connected in series. NO_2^- concentrations were estimated after integration of peak areas and interpolation from a calibration curve, using $NaNO_2$ as standards. Authentic anion standards (Dionex™ Combined Seven Anion Standard II, Thermo Fisher) were also incorporated in between runs for quality control check of the system.

For HPLC analysis, NO_2^- was determined after chromatographic separation and post-column Griess diazotization (ENO-20 Analyzer; Eicom, Japan), as described by Bryan et al. (2004).

2.3.3 Nitrate (NO_3^-)

For NO_3^- analysis, chromatography-based methods were used as essentially described in section 2.4.2.2 above, as both HPLC and IC systems allow simultaneous determination of both oxyanions. Using HPLC, NO_3^- was determined through its online reduction to NO_2^- and post-column derivatization by Griess diazotization reaction, using a dedicated NOx analysis system (ENO-20, Eicom, Japan).

2.3.4 Nitric oxide (NO)

Four different analytical techniques differing in principle of detection (Feelisch and Stamler, 1996) were employed to monitor and quantify NO production from *N. eutropha* D23.

2.3.4.1 Ozone-based chemiluminescence for detection of nitric oxide

The most sensitive of the methodologies employed detects NO in the gas phase using ozone-based chemiluminescence, which allows the measurement of NO from aerobic ammonia oxidation by *N. eutropha* D23 in real-time. The system herein used was similar to the one described by Feelisch et al. (2002) and Pinder et al. (2008), and it is depicted in Figure 2.3 (page 49).

A normoxic incubation environment was maintained inside a reaction vessel (Figure 2.3, A-B) using medical-grade compressed air (99.999%, BOC) as a purge gas which served to transfer NO from the reaction solution into the gas phase and further to the chemiluminescence detector (CLD, model 88y, operating in NO measurement mode; Ecophysics). A scrubbing bottle (Figure 2.3, C) containing 1 mol L^{-1} NaOH was positioned in-between the gas outlet of the reaction vessel and the inlet of the CLD (Figure 2.3, D), acting as a trapping solution for acid fumes and higher nitrogen oxides. The diameter of the sample tube restrictor ensured a constant flow rate of 300 mL min^{-1}.

A pressure gauge situated immediately before the sample line inlet allowed to continuously monitor and adjust the purge gas flow by means of a needle valve, as necessary, to maintain pressure neutrality; short, narrow-bore connection lines in conjunction with a high flow rate enabled rapid sample gas transfer, allowing aerobic measurements with minimal loss of analyte due to autoxidation. For all real-time recordings of NO production, *N. eutropha* D23 and substrate (NH_4^+) were injected via gas-tight Hamilon syringes into the reaction vessel, which was filled with storage medium and kept at a desired temperature (±0.1 °C) by means of a circulating water bath (LT ecocool™ 100, Grant). Reactions were started by addition of cells after recording of baseline values for at least 2 min. Recording frequency was set at 4 Hz, and peaks were integrated over a 20-minute incubation using PowerChrom® (eDAQ Pty Ltd, Australia). Peaks were integrated and absolute amounts of NO were interpolated from a calibration curve obtained by chemical reduction of NO_2^- standards, using a KI/I_2 reaction mixture (45 mmol L^{-1} KI and 10 mmol L^{-1} I_2) in glacial acetic acid, as also described by Feelisch et al. (2002). For that, 25 µL aliquots of NO_2^- standards (from 7.5 to 60 µmol L^{-1}) were injected via gas-tight Hamilton syringes to a previously-purged KI/I_2 reaction mixture, at 60ºC.

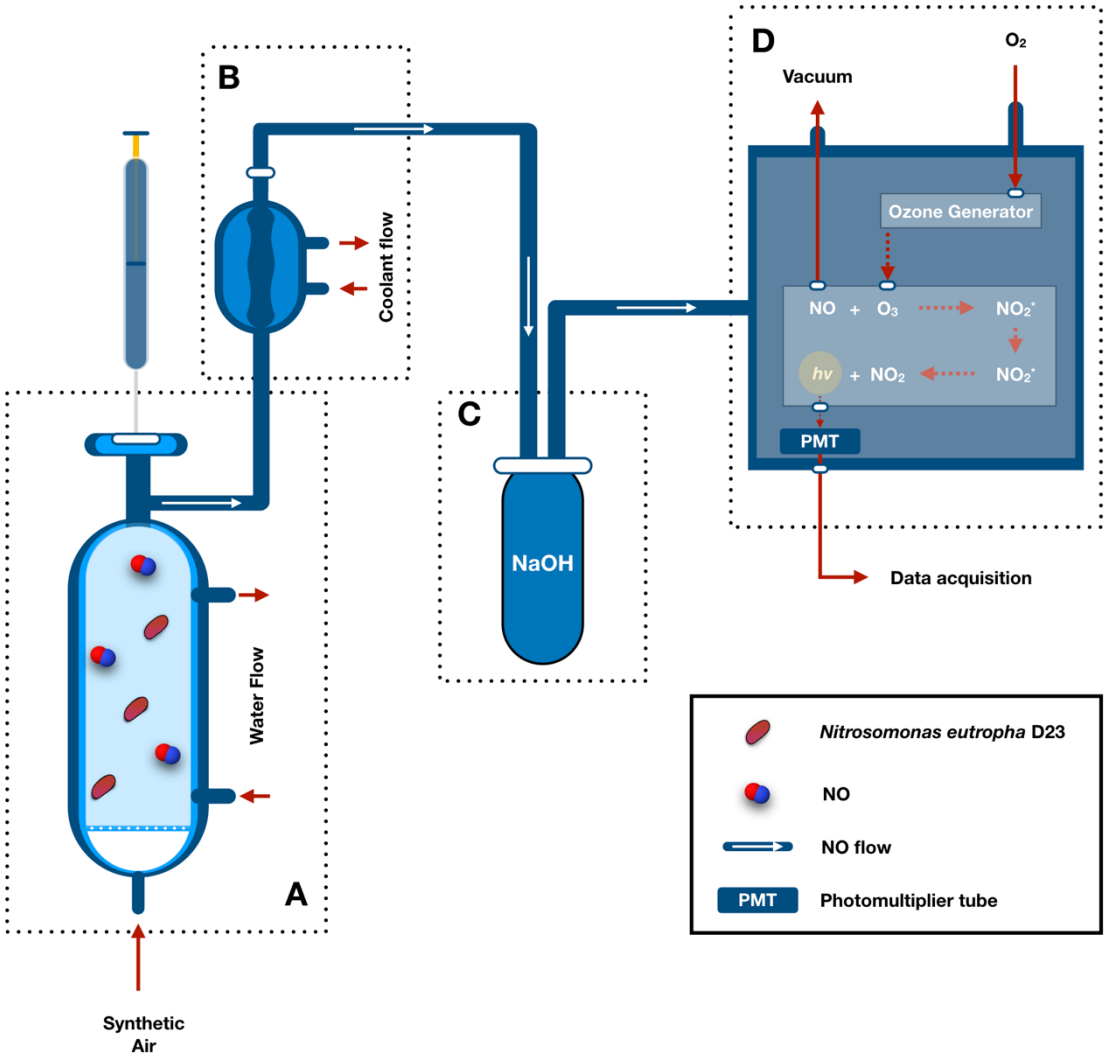

Figure 2.3 Schematic representation of the apparatus used for gas-phase chemiluminescence measurement of NO. A: reaction vessel, containing *N. eutropha* D23 and bacterial-derived NO; B: cooling piece; C: scrubbing bottle, containing 1 mol L^{-1} NaOH, D: chemiluminescence detector.

2.3.4.2 Fluorescence detection of nitric oxide

Production of NO from varying *N. eutropha* D23 cell densities was also determined through spectrofluorimetry. The principle of detection is based on the nitrosation of 4,5-diaminofluorescein (DAF-2) by nitrifying cells, and detection of its triazole derivative (DAF-2T). Stock solutions of DAF-2 and DAF-2T were prepared in argon-purged dimethyl sulfoxide. Only a limited set of conditions was used to monitor NO production fluorimetrically, namely different bacterial densities in M9 medium, at 37 °C.

Aliquots of *N. eutropha* D23 suspensions (75 µL) were inoculated in flat-bottomed, opaque 96-well microtiter plates (Nunc F96 MicroWell™, Thermo Fisher). Then, same volume of M9 medium containing 2.8 µmol L^{-1} DAF-2 was dispensed into the wells. The concentration of DAF-2 employed here ensured optimal signal-to-noise ratio, as determined by previous optimisation procedures. Without further delay, microplates were placed in the microplate reader (SpectraMax M5, Molecular Devices) and incubated at 37 °C. The sensitivity of the photomultiplier tube was set to high, and readings were taken every 30 min, over a window period of 300 min. Excitation and emission wavelengths for the detection of DAF-2T were set at 495 and 515 nm, respectively. Cell-free M9 medium and live *N. eutropha* D23 in the presence of CPTIO were incorporated as controls.

2.3.4.3 Oxyhaemoglobin capture assay

Fresh stock solutions of oxyhaemoglobin (oxyHb) were prepared according to protocols described by Feelisch et al. (1996). Their concentrations and characteristic UV-Vis spectral features were checked prior to any experiment as a quality control procedure, and kept on ice until use. A representative full spectrum is presented in Chapter 3. Production of NO from *N. eutropha* D23 at different substrate concentrations (1, 10, and 25 mmol L^{-1}) in M9 medium was assessed spectrophotometrically, using the OxyHb capture assay, essentially as described by Feelisch et al. (1996). Data acquisition started immediately after addition of *N. eutropha* D23 cells to a 1-cm quartz cuvette containing M9 medium, oxyHb (18.5 µmol L^{-1}), and NH_4^+ at the desired concentration. Cell suspensions were kept at 37±0.02 °C under gentle continuous stirring (500 rpm) inside the spectrophotometer (Cary 60 UV-Vis, Agilent Technologies, with t2 peltier-type cuvette holder and TC1 temperature controller, QuantumNorthwest). Full UV-Vis spectra were recorded between 300 and 600 nm min^{-1} in cycle mode (30 cycles, 2 min each), with the spectrophotometer set to acquisition at 600 nm min^{-1}, at 1 nm resolution. Differential spectra were computed using the Cary Win-UV software (Agilent Technologies) by deriving difference spectra by subtraction of sequential spectra during the NO/oxyHb co-oxidation reaction from the initial oxyHb spectrum.

2.3.4.4 Amperometric detection of nitric oxide

Detection and quantification of NO from *N. eutropha* D23 cells were done using a 7-µm carbon fibre NO sensor (ISO-NOP007, World Precision Instruments Inc.) connected to an NO meter (ISO-NO Mark II, World Precision Instruments). A poise voltage of +865.5 mV was applied to the probe, and recordings were collected at a rate of 0.5 Hz, in the 10 nA range. Prior to any registration, the probe was allowed to polarise overnight and calibrated using PROLI/NO. *N. eutropha* D23-derived NO tracings were acquired by incubating the bacteria in storage medium in a thermostatted acrylic reaction chamber (total volume of 3 mL), under gentle stirring (40-50 rpm). Incubations lasted for 10-20 min, at 37 °C.

2.3.5 Hydroxylamine (NH_2OH)

NH_2OH was measured using a colourimetric method as described by Arnelle & Stamler (1995), in a 96-well microtiter plate format. This assay is based on the condensation of 8-hydroxyquinoline with NH_2OH, which under oxidative conditions and at high temperatures, forms the chromophore indooxine. Briefly, an aliquot of samples (40 µL) for NH_2OH measurement was placed in 0.5-mL plastic tubes (Fisherbrand®), already containing 40 µL of PB (pH 6.8), followed by immediate addition of 25 µL of trichloroacetic acid (12%, w/v). To each tube, 40 µL of 8-hydroxyquinolinol (1% in 100% ethyl alcohol) and Na_2CO_3 (1 mol L^{-1}) were added sequentially and without delay. Tubes were vortexed for 10 minutes, and placed on floating boats in a water bath containing water at 100 °C. Formation of indooxine occurred at high temperatures for 1 minute, after which tubes were taken out and allowed to return to room temperature (~ 10 min). An aliquot (130 µL) from each tube was taken and placed in a microtiter plate for measuring absorbance at 710 nm. A parallel calibration curve was performed, using varying concentrations of NH_2OH (µmol L^{-1}), prepared from dilution of a stock solution. Stock solution was prepared immediately before sample measurement, due to the decomposition of NH_2OH over time in solution.

2.3.6 Bacterial biomass and adenosine 5'-triphosphate measurements

Biomass and intracellular concentration of ATP were quantified after cell lysis after subjecting the bacterial suspensions (in storage medium) to 3 cycles of slow freeze (-20 °C) and thaw (room temperature).

Total bacterial biomass (ng mL^{-1}) was quantified using Pierce™ BCA Protein Assay Kit (ThermoFisher Scientific), according to the manufacturer's instructions. The protein concentration from the bacterial suspensions was calculated by interpolation from a calibration curve (0-250 µg mL^{-1}, working range: 5-250 µg mL^{-1}), using bovine serum albumin (BSA, Pierce ™ Bovine Serum Albumin Standard Ampules 2 mg mL^{-1},

ThermoFisher Scientific) as protein standard. An example of a calibration curve is presented in Figure B11 (panel A), in Appendix B.

The intracellular levels of ATP (nmol L^{-1}) were measured using a luciferin-luciferase bioluminescence-based assay (ATP Determination Kit, Invitrogen®) in a 96-well microtiter plate format, according to the manufacturer's instructions. The ATP levels were calculated by interpolation from a calibration curve (0-1000 nmol L^{-1}), using ATP as a standard. An exemplary calibration curve is presented in Figure B14, in Appendix B.

2.4 Data presentation and statistical analysis

All data sets and statistical analysis were generated using GraphPad Prism® (v7, GraphPad Software, Inc., La Jolla, CA, USA). Statistical difference was evaluated using one-way analysis of variance (one-way ANOVA) and two-way ANOVA when comparing multiple groups, applying Sidak's and Tukey's correction methods for multiple comparisons, respectively. Results were considered significant for $p<0.05$.

Biofilm dispersal was calculated by taking the difference between mean absorbance values (OD_{584}) of *P. aeruginosa* biofilm biomass in co-culture with *N. eutropha* D23, and mean values of control. This difference was normalised to the mean value of the control, and presented ultimately as percentage. For co-culture experiments, a minimum of 5-10 biological replicates were collected and used to calculate mean absorbance values for CV and respective standard deviation. Statistical difference was evaluated using unpaired *t*-test, with either Holm-Sidak or Dunnett's correction method for multiple comparisons, or one-way analysis of variance (ANOVA). Results were considered significant for $p<0.05$. Numerical datasets used for the preparation of the figures presented in this Chapter 4 are available in Appendix C.

Chapter 3

Biochemical characterisation of *Nitrosomonas eutropha D23*

Chapter 3: Biochemical characterisation of *Nitrosomonas eutropha* D23

3.1 Overview

In 1890, Sergei Winograsky described the concept of “chemolithotropy” by isolating in the laboratory for the first time a species of ammonia-oxidising bacteria (AOB), *Nitrosomonas*, which provided a basis for the understanding of the nitrification step within the biogeochemical nitrogen cycle (Dworkin, 2012). Since then, AOB have been extensively studied in the context of microbial ecology and soil microbiology, mainly due to their role in the environment and to their contribution to the greenhouse effect (Feelisch and Martin, 1995; Conr*ad, 1996; Peng et al.*, 2014; Stieglmeier *et al.*, 2014; Medinets *et al*., 2015). Due to their N-transforming capabilities, AOB have been explored for a wide range of applications, for instance, from bioremediation (Law *et al.*, 2012; Zhao *et al.*, 2013) to integrative forms of life support systems for long-term human space missions (Hendrickx *et al.*, 2006; Farges *et al.*, 2012).

More recently, a strain of AOB is being offered as a strategy to restore those bacteria that are now mostly absent from the human microbiome, at least in individuals of the modern society due to intensive hygiene practices (Whitlock and Feelisch, 2009). Evidence suggest that this group of bacteria are constituents of the skin microflora of humans living non-urban lifestyles (Clemente *et al*., 2015), and once colonised the gut of ancient human hosts (Lugli *et al.*, 2017).

The ammonia-oxidiser *N. eutropha* D23 (AO+ Mist™, Mother Dirt™, AOBiome LLC; figure A.1 in Appendix A) is currently available for topical application in humans, and ongoing clinical trials have been carried out in the context of acne, atopic dermatitis/eczema, and rosacea (all completed Phase 2-3). Intranasal application of these bacteria have also been explored as a therapeutic adjuvant for allergic rhinitis, hypertension and migraine (Phase 1-2). Currently, pre-clinical studies are ongoing for pulmonary and gut studies.

In mouse models, *N. eutropha* D23 was found to enhance wound closure, potentially due to the production of NO (Gryllos, Ghosh, *et al*, 2014). Observations that *N. eutropha* D23 may exert bioactivity when applied to the human skin have been made available, and their effects include a systemic response. In a randomised, double-blinded clinical trial, Peter et al. (2017) recently described the effect of application of *N. eutropha* D23 in normotensive individuals (n=9 per treatment group), who enrolled for a facial acne vulgaris clinical trial. Besides safety of *N.* eutropha D23, the authors reported a significant, dose-dependent

(three *N. eutropha* D23 cell densities) decrease in the diastolic blood pressure of these individuals, as compared to placebo (vehicle), and suggested the effects are mediated via NO and NO_2^- formation on the skin.

Despite the outcome when applied to the human skin as mentioned above, the mechanism of action of *N. eutropha* D23 is yet poorly understood, but thought to entail production of NO and/or NO_2^- by *N. eutropha* D23, via consumption of NH_3/NH_4^+ from human skin (e.g. sweat). However, evidence for generation of the afore-mentioned nitrogen oxides is limited (Gryllos, Vajrala, *et al.*, 2014), and its formation is often inferred from the knowledge of other ammonia-oxidisers, such as *N. europaea*.

3.2 Aims

This chapter aims to introduce the general metabolic phenotype of a particular strain of AOB, *N. eutropha* D23, for which information in the literature is scarce. The wide range of the methodologies used herein comprised state-of-the-art analytical instrumentation less explored for bacterial metabolism studies (e.g. gas-phase chemiluminescence). Here, I present experimental conditions that allow monitoring of metabolites production from *N. eutropha* D23, and their quantitative assessment, including NO and NO_2^-.

The aims and specific objectives are as follows:

Aim 1 – To confirm expected characteristics for *N. eutropha* D23, based on the general physiology of ammonia-oxidisers.

A.1. To evaluate overall viability of *N. eutropha* D23 contained in the commercial product by simultaneous monitoring of growth and metabolic activities;
A.2. To use diverse analytical instrumentation and to select accepted methodologies to be used throughout to characterise the metabolic phenotype of *N. eutropha* D23;

Aim 2 – To select the source of *N. eutropha* D23 to be used for characterisation of their metabolic phenotype and for comparison of their metabolic performance.

A.3. To evaluate the feasibility of using batch- and chemostat-grown, as well as energy-starved *N. eutropha* D23 cells, and to select the bacterial population used for metabolic characterisation.

Aim 3 – To provide evidence for NO production by *N. eutropha* D23.

A.4. To use gas-phase chemiluminescence to study formation of NO by *N. eutropha* D23, and to determine how factors can affect its production;
A.5. To confirm or to validate production of NO using independent methodologies.

Aim 4 – To explore potential stress responses of *N. eutropha* D23.

A.1. To evaluate response mechanisms by *N. eutropha* D23 to stressors, including an NO scavenger and a nitrification inhibitor;
A.2. To explore the potential role for NO in whole cells of *N. eutropha* D23.

3.3 Initial metabolic insights into batch-grown *N. eutropha* D23

3.3.1 Substrate oxidation and main product formation

Even though “ammonia” (or NH_3) is the substrate for AMO (Suzuki, Dular and Kwok, 1974), the term “ammonium” (or NH_4^+) will be adapted throughout this thesis when referring to the substrate for oxidation by *N. eutropha* D23, as it entails both ionised (NH_4^+) and unionised (NH_3) species.

N. eutropha D23 were initially collected from the commercial source (AO+ Mist™) and inoculated in growth medium (Table 2.2, page 57). Growth was followed for 4 days, under conditions of no stirring, at 31 °C, in the dark. Representative results are shown in Figure 3.1 below.

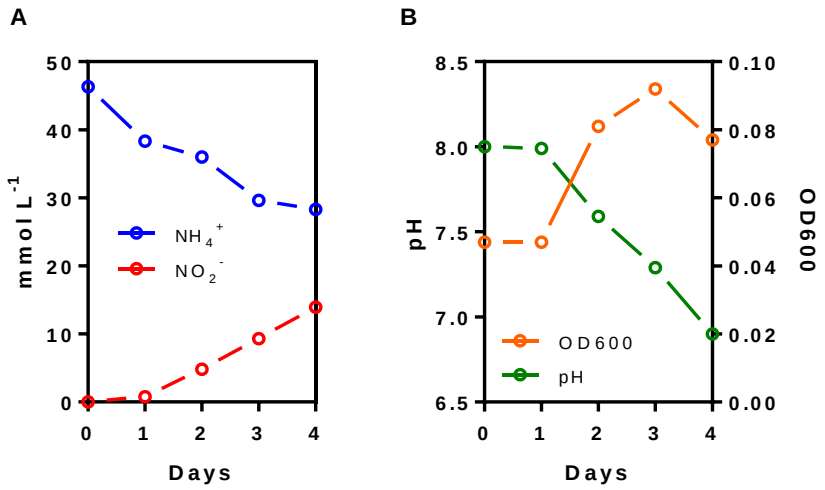

Figure 3.1 Growth of *N. eutropha* D23 under laboratory settings over time. Cells were collected from the commercial product, and inoculated in growth medium. Activity and growth were monitored simultaneously, with measurements of (A) NO_2^- production and NH_4^+ consumption, as well as (B) pH and optical density (biomass). Representative data from a single experiment (n=1) is presented.

As observed on panel A (Figure 3.1), *N. eutropha* D23 consumed NH_4^+ to NO_2^- from the start of the growth period considered, whose metabolic activity became particularly evident after the first day of growth. Overall, the variation in the concentration of substrate and product seemed to occur at nearly constant rates of consumption and production, throughout the growth period considered. At the end of the growth period, NO_2^- was produced at a final concentration of 13.9 mmol L^{-1}, for a consumption of around 18.1 mmol L^{-1} NH_4^+, with simultaneous acidification of the growth medium (panel B). This metabolic activity was associated with growth of *N. eutropha* D23, as seen by the increase in optical density (panel B, Figure 3.1) which is related to the increase in bacterial biomass; also evident after the initial 24 h of incubation.

This experiment was repeated to assess reproducibility of batch-grown *N. eutropha* D23. Cells were harvested from a different batch of the commercial product, inoculated in growth medium and subjected to the same experimental conditions as described above. The results are shown in Figure 3.2 below.

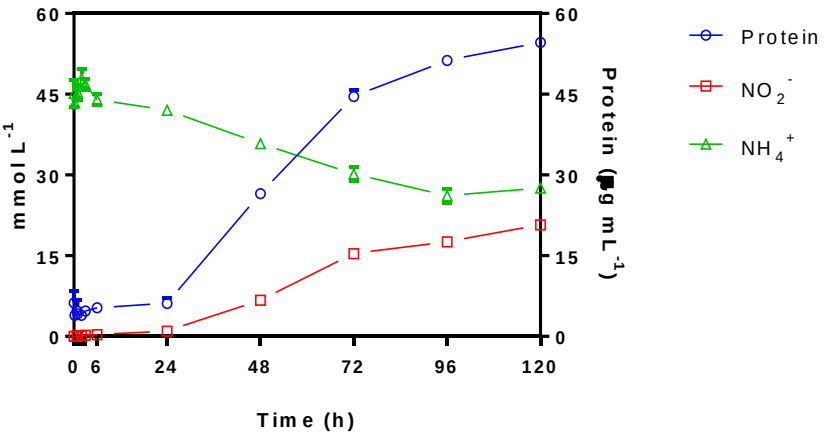

Figure 3.2 Growth and metabolic activity of *N. eutropha* D23, during 5 days. NH_4^+ and NO_2^- (mmol L^{-1}) are shown on the left y-axis, whereas protein values are shown on the right y-axis. Data points are presented as mean±SD (n=3).

Metabolite and biomass measurements were carried out initially at short intervals, during the first 6 h of growth, and later at time points 24, 48, 72, 96, and 120 h (5 days). Due to the increasing number of samples per replicate, NO_2^- concentrations were quantified using HPLC as an alternative analytical tool for this experiment.

As observed, growth and activity of *N. eutropha* D23 seemed highly reproducible, as compared to the first pilot growth. Overall, trends of consumption of NH_4^+ and production of NO_2^- were similar to those shown in Figure 3.1, with continuous increase in bacterial biomass (as evaluated by protein measurements in the growth medium). At the end of the growth period considered, *N. eutropha* D23 grew up to 54.61±0.53 µg mL^{-1} in biomass, with production of 20.74±0.22 mmol L^{-1} net NO_2^-, and consumption of 17.59±2.96 mmol L^{-1} NH_4^+.

Besides measurement of NH_4^+, NO_2^- and biomass, additional parameters were also evaluated during growth of *N. eutropha* D23, such as pH and intracellular levels of ATP. The results for these measurements are shown in Figure 3.3 below, and match those of the previous figure.

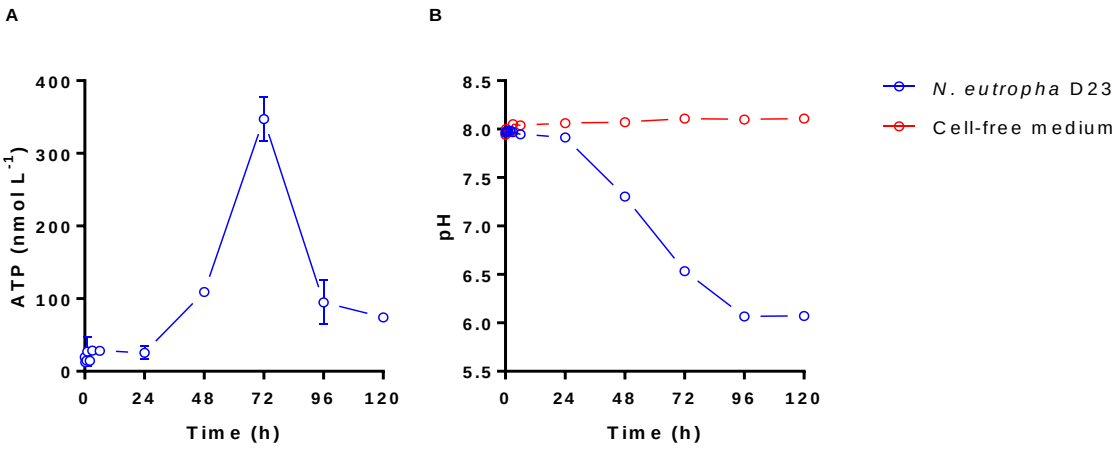

Figure 3.3 Growth and metabolic activity of *N. eutropha* D23, during 5 days. (A) Intracellular levels of ATP (n=3), (B) acidification of the growth medium during growth (n=2-3). Data is presented as mean±SD.

An overall increase in the intracellular pool of ATP was observed for the growth of *N. eutropha* D23; an observation especially evident between 24 and 72 h of growth, with mean levels of 26.6±8.9 and 347.1±30.7 nmol L^{-1} ATP, respectively. After 72 h, the intracellular levels of this metabolite decreased abruptly to 74.16±3.49 nmol L^{-1} ATP. In parallel with metabolic and growth activities, the pH of the growth medium changed from 7.96±0.02 (0 h) to 6.07±0.04 (120 h). The rate of medium acidification increased after the initial 24 h of growth, with decreases of 0.61 and 0.77 pH unit day^{-1} seen between 24-48 and 48-72 h of growth, respectively, consistent with metabolic and growth activities. After 72 h, the rate of acidification was lower than the previous (at a rate of -0.47 pH unit day^{-1}), and virtually no changes in pH were seen between 96 and 120 h.

Hydroxylamine (NH_2OH) was also measured in the course of this experiment. This chemical intermediate in ammonia oxidation was not found in the extracellular compartment, under the experimental conditions applied. However, NH_2OH could be detected intracellularly. The results are shown in Figure 3.4 below.

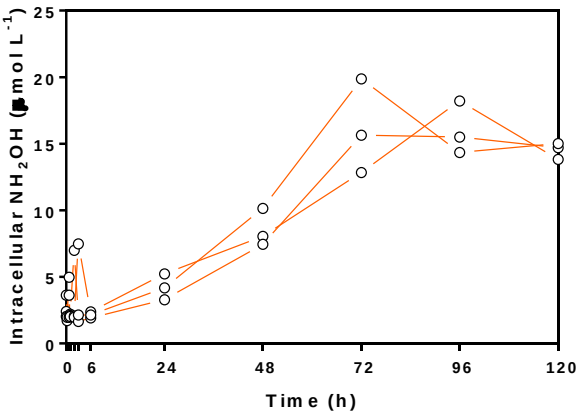

Figure 3.4 Intracellular measurement of NH_2OH, during batch-wise growth of *N. eutropha* D23 (n=3).

As evident, an overall increase in the intracellular levels of NH_2OH was observed, particularly after 6 h of growth. A steady increase in the concentration of NH_2OH is observed up to 72 h of growth in liquid culture, reaching a plateau at around 96 h.

3.3.2 Initial evidence for nitric oxide production

As part of these initial experimental activities, production of NO by *N. eutropha* D23 was primarily evaluated by using two distinct methodologies for NO detection, namely by its

electrochemical and chemiluminescence detection. For assaying production of NO, some experimental modifications were made to enable evaluating production of this metabolite at much lower concentrations of substrate (10 and 5 mmol L^{-1} NH_4^+). Moreover, while previous experiments were carried out in growth medium, initial measurements of NO were conducted in storage medium (pH 7.6).

3.3.2.1 Electrochemical detection of nitric oxide from *N. eutropha* D23

For electrochemical detection of NO, storage medium containing 10 mmol L^{-1} NH_4^+ was placed inside a closed acrylic chamber, kept at a constant temperature of 31 °C, under gentle stirring. Real-time tracings for NO production were recorded immediately after inoculation of *N. eutropha* D23 in the medium. A representative tracing for this short-time incubation is depicted in Figure 3.5 below.

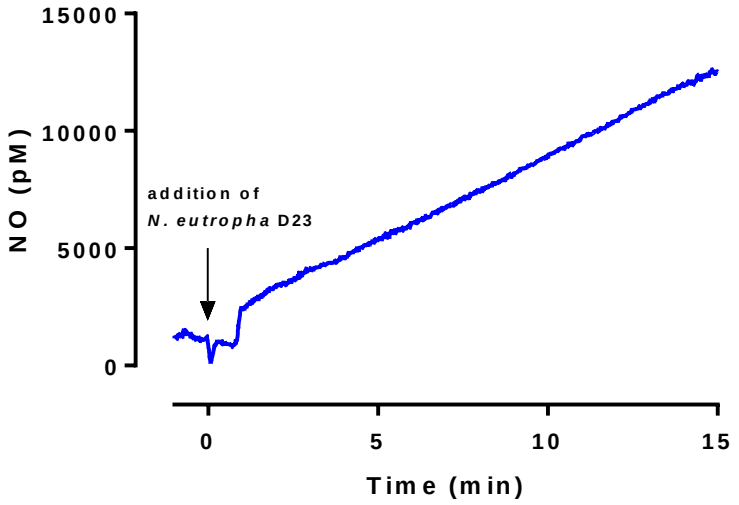

Figure 3.5 Representative tracing of NO produced by *N. eutropha* D23 (~10^7 cells mL^{-1}), in storage medium, at 10 mmol L^{-1} NH_4^+.

Overall, the tracing showed an apparent linear increase in NO concentration over the initial 15 min of incubation. Interestingly, the production of this metabolite was observed shortly after inoculation of the bacteria, within the first minute of recording.

3.3.2.2 Chemiluminescence detection of nitric oxide from *N. eutropha* D23

To assess production of NO through gas-phase chemiluminescence (details described in section 2.3.4.1), *N. eutropha* D23 were inoculated in storage medium containing a final concentration of 5 mmol L^{-1} NH_4^+, and incubated in the reaction vessel of the apparatus

(see Figure 2.5). Real-time tracings for NO production were acquired for *N. eutropha* D23 at two different temperatures (31 and 37 °C). Results are shown in Figure 3.6 below, for a period of 10 min.

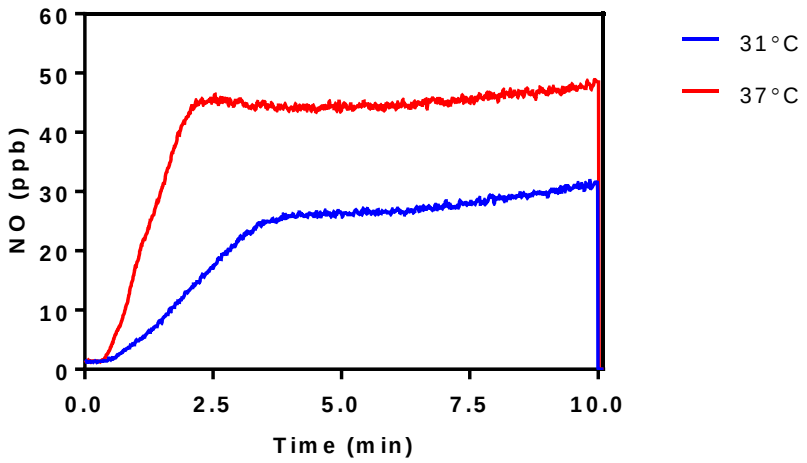

Figure 3.6 Nitric oxide recording from gas-phase chemiluminescence detection during NH_4^+ oxidation (5 mmol L^{-1}) by *N. eutropha* D23 (~10^7 cells mL^{-1}), at 31 and 37±0.2 °C, at pH 7.6. Data presented as mean values of tracings (n=2).

Overall, the production of NO was also observed through gas-phase chemiluminescence, and its production was also observed for a lower concentration of substrate than that used in the previous experiments (2 and 10-fold higher). Furthermore, the overall quantity of NO generated over time seemed dependent on the incubation temperatures. Considering the initial kinetic tracings, a steeper rise in the production of NO was evident at 37 °C, with an apparent steady-state NO production reaching a plateau at around 2.0 min (~45 ppb). On the other hand, at 31 °C, steady-state production of NO occurred at a later stage, at around 3.4 min (~25-30 ppb). Rather than relying on maximal, steady-state concentrations of NO, the online tracings allow a much better comparison of the quantities of NO between the temperatures assayed by computation of the area under the curve (AUC). It can be thus observed that the total production of NO for the entire incubation period at 31 °C was roughly half of that produced at 37 °C, with areas of 235.3 and 419.3, respectively.

Due to the drawbacks of growing *N. eutropha* D23 in laboratory batches (lengthy generation), it was assumed that using chemostat-grown *N. eutropha* D23 would be a good approach, as it allows generation of higher cell densities within a reasonable time. The next experimental steps were done towards the feasibility of using *N. eutropha* D23 collected at different time points from a chemostat culture. In terms of analytical

instrumentation, gas-phase chemiluminescence was chosen as the preferred methodology for evaluating the metabolic efficiency of *N. eutropha* D23 harvested at different time points from a chemostat culture.

3.4 Metabolic comparison among *N. eutropha* D23 harvests grown in chemostat

N. eutropha D23 were grown continuously in a chemostat system and provided by AOBiome in the form of a 10-fold concentrated *N. eutropha* D23 cell density, compared to their commercial product. These cells were harvested at 7, 81, 85, and 90 days of chemostat growth, and will be referred to as harvests A, B, C, and D, respectively. To assess NO production from these harvests, the experimental conditions were as follows: *N. eutropha* D23 were incubated in storage medium (pH 7.6) at a density of ~10^7 cells mL^{-1}, and NO tracings were recorded for a 15-min incubation at 31 °C, at 5, 50, and 200 mmol L^{-1} NH_4^+. Results are shown in Figure 3.7.

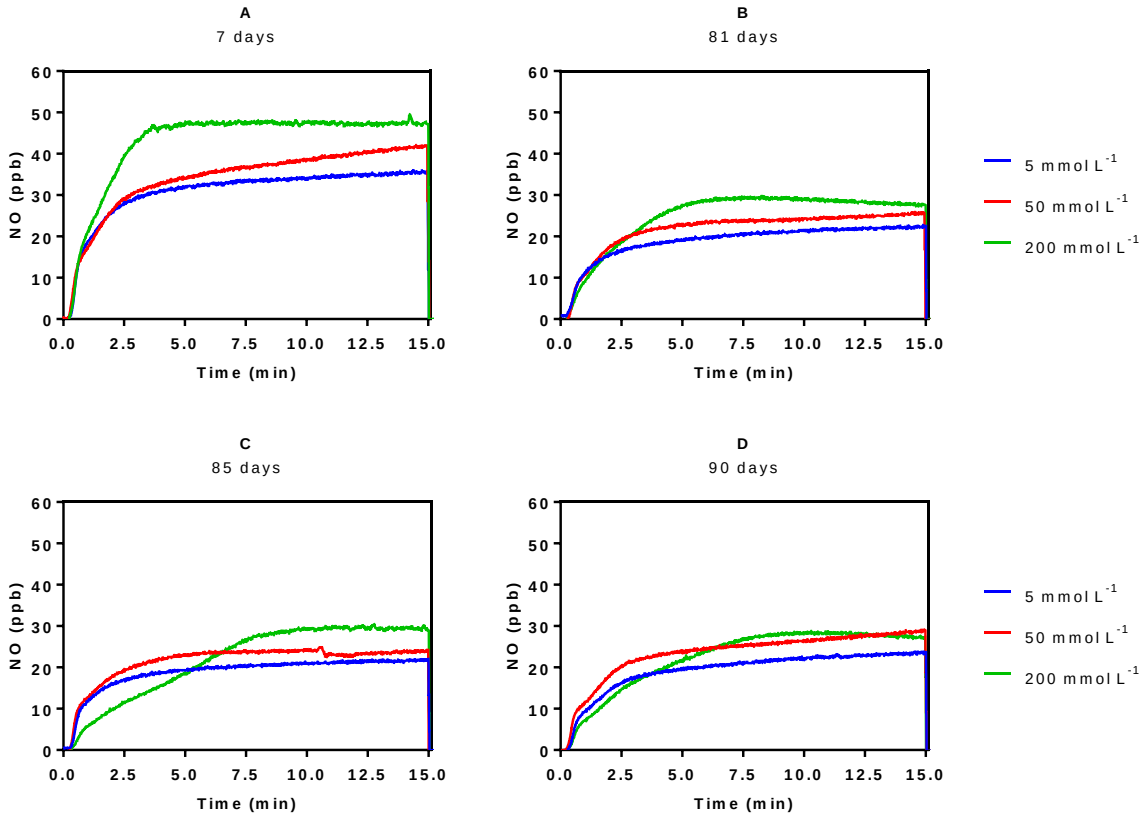

Figure 3.7 Nitric oxide recording by gas-phase chemiluminescence detection for each harvested culture (~10^7 cells mL^{-1}) when treated with 5, 50, and 200 mmol L^{-1} of NH_4^+, during 15 minutes of incubation, at 31±0.2 °C. Data is presented as mean tracings (n=3), in parts per billion (ppb).

In general, *N: eutropha* D23 harvested at 7 days (Figure 3.7, panel A) exhibited the highest production of NO when compared to the other harvests studied, regardless of the concentration of substrate present at the beginning of the experiment. At a kinetic perspective, fast formation of NO was observed with minimal delay, across all harvests. Steady-state production of NO was also observed for all harvests at roughly the same time (> 2.5 min). An exception was seen for harvest C (Figure 3.7, panel C), assayed at 200 mmol L^{-1} NH_4^+, which reached a plateau at around 7.5 min. These observations were consistent with those described in the previous section for studies performed at 5 mmol L^{-1} NH_4^+, regarding the initial and steady-state formation of NO by the bacteria (Figure 3.6).

For harvests C and D, and specifically incubated with 200 mmol L^{-1} NH_4^+, a rapid loss of NO formation was observed, as evidenced by the slope of the initial tracing. A comparison of the plateaus between harvests A, B, and C did not seem to reveal remarkable differences among the NH_4^+ concentrations assayed, as each harvest reached similar concentrations of NO independently of the substrate concentration tested.

Heat-killed *N. eutropha* D23 were also assayed as a negative control for NO formation, and according to the tracings depicted in Figure 3.8 below, no formation of NO was observed.

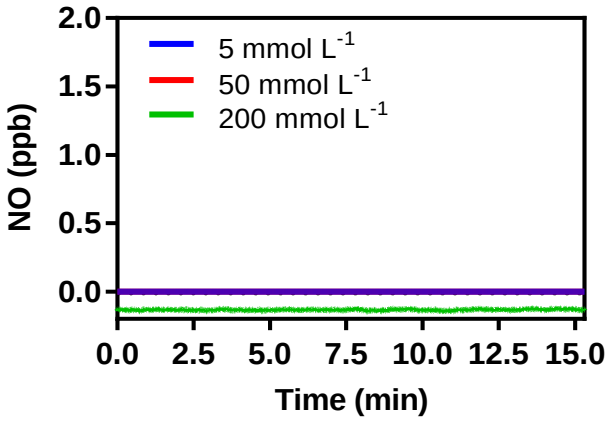

Figure 3.8 Nitric oxide recording by gas-phase chemiluminescence detection for the heat-inactivated cell suspension (7 days) when treated with 5, 50, and 200 mmol L^{-1} of NH_4^+, during 15 minutes of incubation, at 31±0.2 °C (n=1). Data is expressed in parts per billion (ppb).

From the tracings depicted in Figure 3.7, total amounts of NO produced over a 15-min incubation were calculated after integration of the AUC and interpolation from a calibration curve. A quantitative summary is presented in Figure 3.9 below.

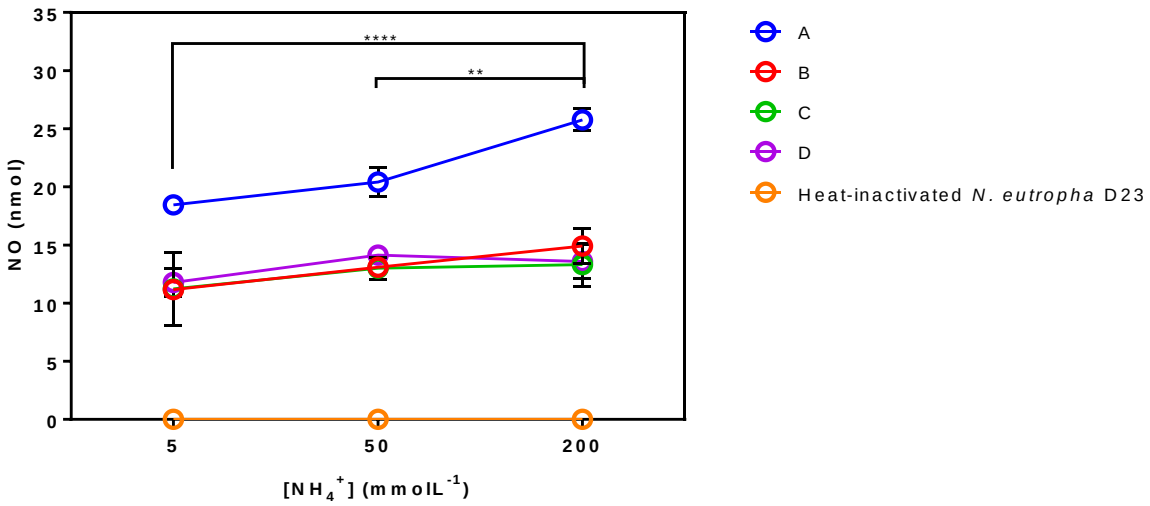

Figure 3.9 Quantitative summary of gas-phase chemiluminescence recordings depicted in figures 3.7 and 3.8. Data presented as mean±SD (n=3). For clarity, statistical comparisons are presented only for harvest A. **p<0.01, ****p<0.0001.

When looking at the mean values for absolute quantities of NO produced, data show that the higher the availability of substrate, the higher the NO formed; an observational trend particularly evident for harvest A, whose cells produced significantly and consistently the highest quantities, regardless of the concentration of NH_4^+ used. Significant differences were seen at 5 and 200 mmol L^{-1} NH_4^+ within harvest A, whereas no major differences were noted when comparing the lowest and the intermediate concentration of NH_4^+ tested. No significant changes were observed for any of the NH_4^+ concentrations between harvests B, C, and D, as also seen from the raw NO tracings in the previous figure.

NO_2^- formation was also assessed from these harvests (n=1, per harvest) in parallel, using experimental conditions as described previously (e.g. temperature, cell density), although only assessing its production at the highest concentration of NH_4^+ (200 mmol L^{-1}). It was assumed that under these conditions, NO_2^- production would be maximal, as judged by the optimal conditions seen for NO production. *N. eutropha* D23 were then incubated in storage medium, containing 200 mmol L^{-1} NH_4^+, and NO_2^- was followed over a period of 1 h. The results are shown in Figure 3.10 below.

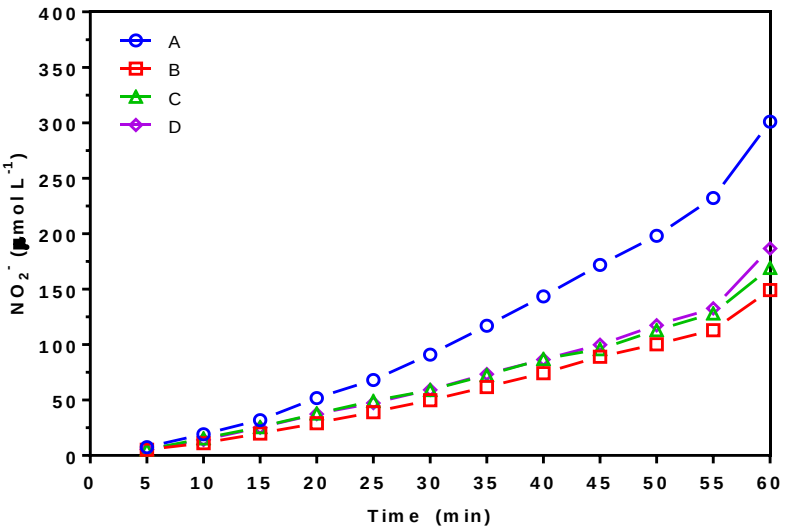

Figure 3.10 NO_2^- production by different harvests of *N. eutropha*, at 200 mmol L^{-1} NH_4^+ in storage medium (31±0.2C, pH 7.6) and measured by ion chromatography. NO_3^- was omitted from the graph, as no changes occurred throughout the incubation period. Data presented from a single experiment (n=1).

An increasing trend in the concentration of NO_2^- in storage medium was noticed for all harvests assayed, with harvests A and B yielding the highest and the lowest concentration of NO_2^-, respectively. The upward trend seen for harvests B, C, and D resemble a linear production of NO_2^- over time, whose rates of production per hour seemed to be fairly constant up to 55 min. On the other hand, the slight changes in the rates of production over time for harvest A suggests an exponential production of NO_2^-. From the data collected from figures 3.9 and 3.10, absolute quantities of NO and NO_2^- from the harvests assayed were compared, for an identical observation period (i.e. 15 min). A ratio of formation of NO and NO_2^- was then established and presented in Figure 3.11 below.

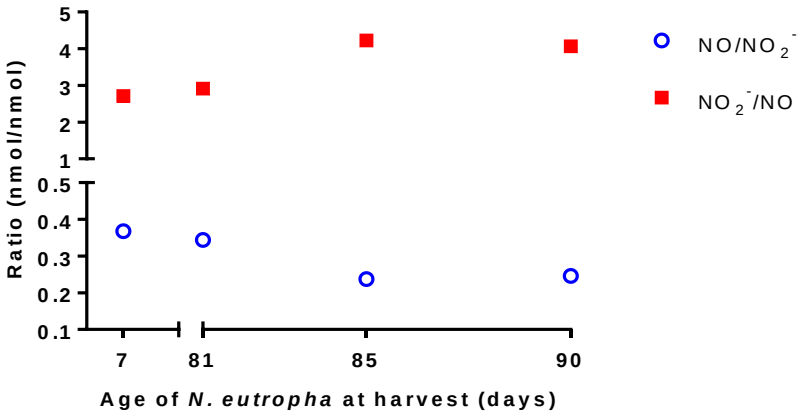

Harvest	NO (nmoles)	NO_2^- (nmoles)	Ratio NO/NO_2^-	Ratio NO_2^-/NO
A	25.77	69.93	0.368	2.714
B	14.92	43.43	0.344	2.911
C	13.31	56.21	0.237	4.223
D	13.59	55.26	0.246	4.066

Figure 3.11 Ratio of NO to NO_2^- formation for different *N. eutropha* harvests. Absolute amounts (nmoles) of both molecules were calculated over 15 minutes of incubation, under similar conditions.

As observed, the ratio NO/NO_2^- was highest for harvest A (7 days), whose cells showed a high ability for NO production (36.8% of that of the corresponding NO_2^-), followed by harvests B, D, and C (34.4, 24.6, and 23.7 % of the corresponding NO_2^-, respectively). When their ratios are expressed as a function of time of harvest, the data suggests that the ability for metabolite production (NO and NO_2^-) decrease for *N. eutropha* D23 harvested at later times from the chemostat, even though other phenomena could explain the decrease in activity for these harvests.

The initial assumption of using continuously-grown *N. eutropha* D23 did not seem ideal, due to the metabolic variation seen in those harvests, namely for NO and NO_2^-. As such, it was decided that further metabolic studies would be carried out with substrate- and energy-starved *N. eutropha* D23 directly collected from the commercial product.

3.5 Impact of factors on nitric oxide production by starved *N. eutropha* D23 using gas-phase chemiluminescence

It was previously observed from gas-phase chemiluminescence that some factors affected production of NO by *N. eutropha* D23, such as temperature and concentration of substrate. As such, this section aims to provide a quantitative assessment of the impact of factors like temperature, concentration of substrate, pH and *N. eutropha* D23 cell density on NO output. For clarity, the results for each factor assayed are presented in separate subsections.

The following characterisation based on gas-phase chemiluminescence was carried out with substrate-starved *N. eutropha* D23 harvested from the commercial source, whose containers were kept at 4 °C according to manufacturer's guidelines, from receipt until the moment of analysis. Storage medium was selected as the medium for this metabolic assessment as *N. eutropha* D23 are conditioned in this vehicle within the commercial product. The results are shown in Figure 3.12; for each condition assayed, gas-phase chemiluminescence tracings (panels A, C, E, and G) and respective quantitative summaries (panels B, D, F. and H) are shown.

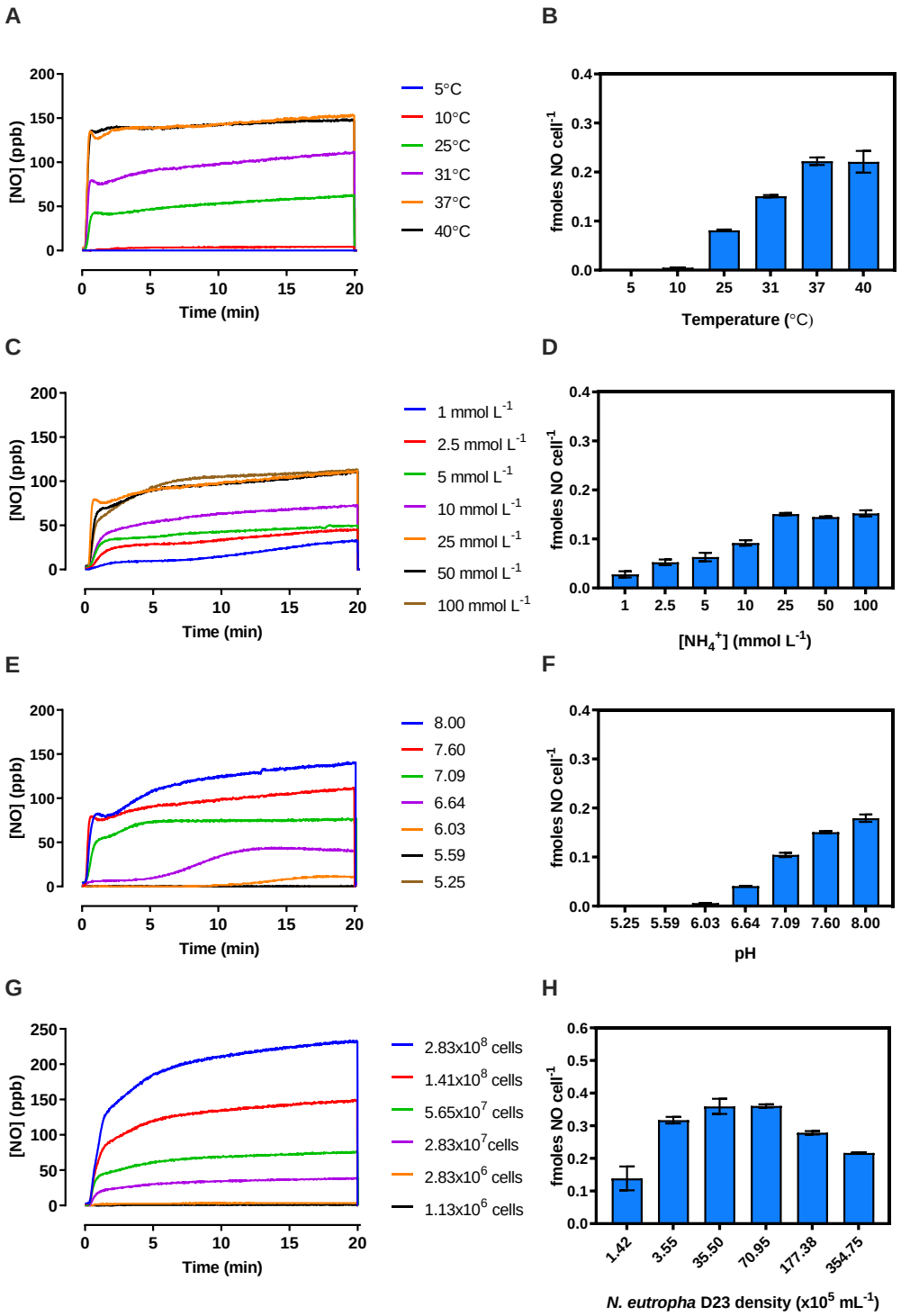

Figure 3.12 Nitric oxide recordings from gas-phase chemiluminescence detection during ammonia oxidation by *N. eutropha* D23, over a 20-min incubation time. Real-time tracings for NO and respective quantitative summaries were acquired at varying temperatures (A, B), NH_4^+ concentration (C, D), pH values (E, F), and *N. eutropha* D23 cell densities (G, H). Each tracing is depicted as a mean of 2-3 tracings. Data is expressed in parts per billion (ppb).

3.5.1 The effect of temperature on the production of nitric oxide

Temperature was varied by means of a water-bath connected to the water-jacketed reaction vessel, where *N. eutropha* D23 were placed at a fixed cell density, in storage medium, and at 25 mmol L^{-1} NH_4^+. From the real-time tracings depicted in panel A, two main conclusions were derived. Firstly, and according to previous observations with batch-grown cells, *N. eutropha* D23 collected from the commercial product retained and showed a striking capacity for NO production, shortly after incubation with NH_4^+. Secondly, gas-phase chemiluminescence tracings also indicated that NO was produced over a wide range of temperatures. Higher levels of NO were formed for substrate oxidation at higher temperatures, in particular at temperatures above 25 °C.

Kinetically, the data showed steep rises in NO detected in the gas-phase for incubations at 25, 31, 37, and 40 °C, with quasi steady-state production of NO plateauing at around 2.0 min, at these range of temperatures. The statistical assessment of those tracings as shown in panel B indicated that the highest amounts of NO per cell were generated at 37 and 40 °C (mean values of 0.222±0.008 and 0.221±0.022 fmoles NO $cell^{-1}$, respectively), with no significant differences in amounts when comparing these two temperatures. Production of NO was observed at 10 °C (0.005±4.42x10^{-4} fmoles NO $cell^{-1}$), albeit at much lower amounts as compared to those at 25 and 31 °C, with production of 0.081±0.001 and 0.151±0.002 fmoles NO $cell^{-1}$, respectively; whereas production of this metabolite was null at 5 °C.

3.5.2 The effect of NH_4^+ availability on the production of nitric oxide

For the remainder of the assessment of NO production by *N. eutropha* D23, further characterisation was carried out at 31 °C, as it closely represents the reported range of temperatures for the surface of the human skin. To study the effect of substrate on NO output, *N. eutropha* D23 were incubated as previously mentioned, but using varying concentrations of NH_4^+, while keeping the reaction vessel kept at 31 °C. As seen in panels C and D, production of NO occurred in an NH_4^+-dependent manner, with increasing levels of NO being generated for increasing concentrations of substrate available in the medium. This trend is evident when looking at the quasi steady-state levels of NO production for incubations up to 25 mmol L^{-1} NH_4^+, with reported mean values for absolute amounts of 0.028±0.006, 0.052±0.006, 0.063±0.009, 0.092±0.005, and 0.151±0.002 fmoles NO $cell^{-1}$ for incubations at 1, 2.5, 5, 10, and 25 mmol L^{-1} NH_4^+, respectively. No major differences could be seen from the kinetic registrations among incubations at 25, 50, and 100 mmol L^{-1} NH_4^+, for which reported NO amounts for the latter two concentrations assayed were 0.145±0.001 and 0.152±0.006 fmoles NO $cell^{-1}$.

3.5.3 The effect of pH on the production of nitric oxide

A concentration of 25 mmol L^{-1} NH_4^+ was chosen for further experiments aimed at the biochemical characterisation of *N. eutropha* D23, based on the previous data where the largest yields of NO were generated. Bacteria were incubated in storage medium prepared at its normal pH (7.60), and the effect of pH on NO output was assessed over a range of acidic (5.25, 5.59, 6.03, 6.64, and 7.09) and alkaline (8.00) values, at 31 °C. As shown in panels E and F, the production of NO by *N. eutropha* D23 was dependent on the pH at which substrate oxidation occurred, with higher levels of NO being generated towards neutral or alkaline pH values. Under these conditions, optimal production of NO was seen at pH 8.00 (0.179±0.007 fmoles NO $cell^{-1}$), whereas no production occurred at pH 5.25 and 5.59. The kinetic tracings also showed that steady-states of NO production were achieved at later stages, especially evident for those incubations at slightly acidic pH values (6.03 and 6.64), with absolute amounts of 0.006±6.60x10^{-5} and 0.041±3.77x10^{-5} fmoles NO $cell^{-1}$.

3.5.4 The effect of cell density on the production of nitric oxide

Even though the production of NO was optimal at pH 8.00, further assessments were carried out using storage medium prepared at 7.60, the pH at which cells are kept and shipped in the commercial product. The density of *N. eutropha* D23 (and therefore absolute numbers) was varied inside the reaction vessel, and the production of NO in storage medium at pH 7.60 was followed at 31 °C, with a substrate concentration of 25 mmol L^{-1} NH_4^+. The results are shown in panels G and H. The production of NO followed a dependence on the number of bacteria present in the reaction vessel, as seen by the higher plateaus in the kinetic tracings. A quantitative summary prepared from integration and interpolation of the AUC for these tracings (data not graphed) was consistent with this visual trend seen in the gas-phase chemiluminescence tracings. However, and interestingly, when normalised for the absolute quantities of *N. eutropha* D23 presented in the reaction vessel, the data showed that the highest amounts of NO were achieved for the 35.50 and 70.95 x10^5 *N. eutropha* D23 mL^{-1}, with mean values of 0.359±0.002 and 0.361±0.005 fmoles NO $cell^{-1}$, whereas ~40% less NO (0.272±0.002 fmoles NO $cell^{-1}$) was produced for the highest cell density.

In summary, the results depicted in Figure 3.12 allowed a more detailed characterisation of the NO-forming abilities by *N. eutropha* D23, and indicated that production of this metabolite is influenced by temperature, pH, and concentration of NH_4^+ available for oxidation by the bacteria. Furthermore, bacterial density may also modulate the overall amounts of NO being generated, with highest amounts of NO $cell^{-1}$ seen for intermediate cell densities, for the same concentration of substrate and fixed experimental conditions.

3.6 Nitrite production by *N. eutropha* D23 under dynamic and static conditions

To complement the information above with results for NO_2^- production, aliquots were taken from the reaction vessel at the end of the incubation period for NO_2^- analysis by HPLC. A parallel system was set up where *N. eutropha* D23 were incubated under comparable conditions, but were not subjected to any purging. By doing so, it was possible to evaluate the effects of a continuous purging system (dynamic) on NO_2^- formation, as compared to a system (static) where no purging was done, and NO was allowed to accumulate in solution. The results for this comparison are shown in Figure 3.13 below, whose quantities of NO_2^- were normalized per million of *N. eutropha* D23 cells, using different temperatures (Figure 3.13, panel A) and concentrations of NH_4^+ (Figure 3.13, panel B).

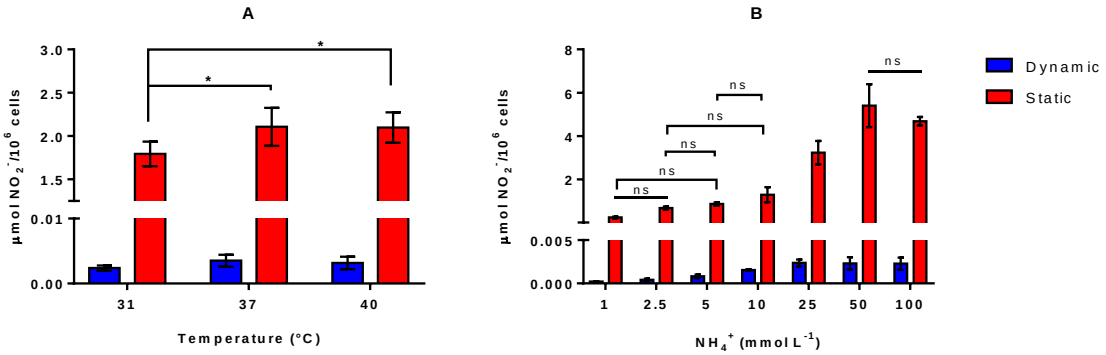

Figure 3.13 Comparison of NO_2^- quantities produced by *N. eutropha* D23 at (A) varying temperatures and (B) NH_4^+ concentrations, between static and dynamic (during NO measurement as in Figure 3.12) conditions. Data is presented as NO_2^- quantities normalised per 10^6 *N. eutropha* D23 cells (mean±SD, n=3). Two-way ANOVA was applied to the dataset for assessing statistical differences (*p<0.05, ns: non-significant). For clarity, only non-significant comparisons are labelled in the graph.

Regardless of the specific conditions chosen (temperature or concentration of substrate), the first observation was that considerably higher NO_2^- levels were produced by cells within the static system. That is, a system which is not subjected to any purging, as opposed to the dynamic system, which continuously removes volatile products such as NO throughout the incubation period.

Two-way ANOVA was applied to these datasets in order to evaluate the differences among the temperatures and the varying concentrations of NH_4^+, as well as the differences in the NO_2^- levels produced between the static and the dynamic system. According to the results, the effect "static/dynamic" was accountable for the majority of the total variance in the NO_2^- levels seen for temperature and concentration of NH_4^+ (97.14 and 42.72 %, respectively, as calculated by the statistical test applied). Significant differences were only seen for incubations under static conditions, for both factors assayed (temperature and NH_4^+ concentrations).

Within the pair temperature/static system, levels of NO_2^- were significantly ($p<0.05$) higher at 37 and 40 °C (2.106±0.220 and 2.098±0.175 µmol $NO_2^-/10^6$ cells, respectively), as compared to those formed at 31 °C (1.794±0.142 µmol $NO_2^-/10^6$ cells). For the varying NH_4^+ concentrations assayed, identical trends in NO_2^- production were observed between incubations occurring under static and dynamic conditions; the only difference being the overall NO_2^- concentrations achieved between the two conditions. As compared to the lowest NH_4^+ concentration assayed (1 mmol L^{-1} NH_4^+), NO_2^- was produced at significantly higher quantities for static incubations occurring above 10 mmol L-1 NH_4^+. No major differences in the production of NO_2^- were found for *N. eutropha* D23 incubated with 50 and 100 mmol L^{-1} NH_4^+.

The afore-mentioned trends for NO_2^- production had already been observed in previous pilot experiments, and characterised in depth for NO formation, whose results also indicated its dependency on temperature and concentration of substrate (Figure 3.12, panels A-B and C-D, respectively). Therefore, to establish a relationship between the production of NO and NO_2^- by *N. eutropha* D23, datasets derived from experiments conducted at different NH_4^+ concentrations (only mean values for NO and NO_2^- were considered) were subjected to a linear regression fitting. The results are shown in Figure 3.14 below.

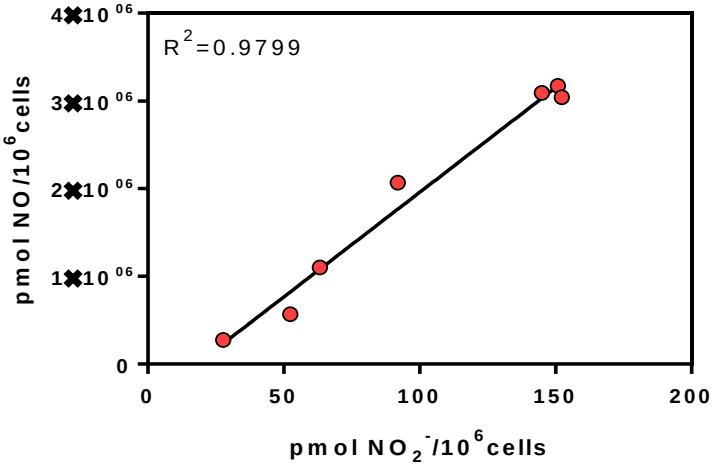

Figure 3.14 Correlation between the mean values of NO and NO_2^-, for each concentration of NH_4^+. Values fit a linear regression curve with a R^2 = 0.9799.

The scatter-dot plot prepared above shows matched amounts of NO and NO_2^- for each concentration of NH_4^+ previously assayed. Data suggest that there is a strong relationship (R^2=0.9799) between the production of these metabolites, which both follow a dependence on NH_4^+. Moreover, Pearson's correlation test was applied to the same dataset, with a correlation factor of 0.99, which is in agreement with the findings from the linear regression fitted curve.

Using the same dataset as above, and to verify how much NO_2^- is generated as compared to NO, the ratios NO/NO_2^- (pmol/10^6 cells) were calculated and expressed in function of the concentration of NH_4^+. The results are shown in Figure 3.15 below.

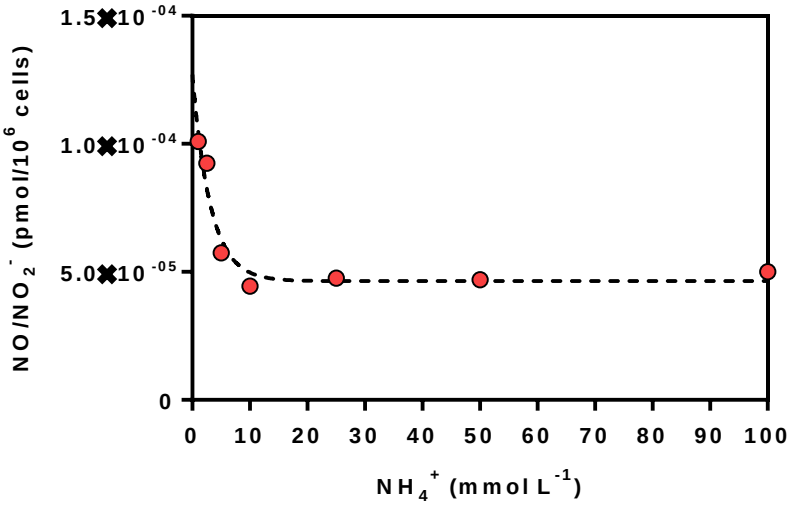

Figure 3.15 Ratio NO/NO_2^- (pmol/10^6 *N. eutropha* D23 cells) expressed in function of the concentration of NH_4^+.

Regardless of the NH_4^+ concentration assayed, *N. eutropha* D23 produced much higher quantities of NO_2^- as compared to NO (0< ratio NO/NO_2^- <1). Interestingly, the ratio NO/NO_2^- was not constant for the varying concentrations of NH_4^+ (1, 2.5, 5, 10, 25, 50, and 100 mmol L^{-1} NH_4^+). The decreasing trend in the ratios is evident for *N. eutropha* D23 incubated at concentrations of substrate up to 10-25 mmol L^{-1} NH_4^+, until reaching a stable value for higher concentrations of substrate.

3.7 Additional methodologies for assessing NO production by starved *N. eutropha* D23

Based on the previous observations that higher levels of metabolites were seen for *N. eutropha* D23 incubated under static conditions, two additional methodologies were used for assessing NO production. These methodologies differ in their principles of detection and, as opposed to gas-phase chemiluminescence, do not require vigorous perturbation of the system for its detection. The nitrosation of the fluorescent probe 4, 5-diaminofluorescein (DAF-2) and the oxyhaemoglobin (oxyHb) capture assays were used.

3.7.1 Fluorimetric detection of nitric oxide by nitrosation of diaminofluorescein-2

For fluorimetric assessments, *N. eutropha* D23 at different cell densities were inoculated in M9 medium, and placed in opaque 96-well microtiter plates, as described in Chapter 2. The kinetic results for NO production are displayed in Figure 3.16 below, which show the concentration of diaminofluorescein triazole derivative (DAF-2T) detected fluorimetrically upon production of NO in solution.

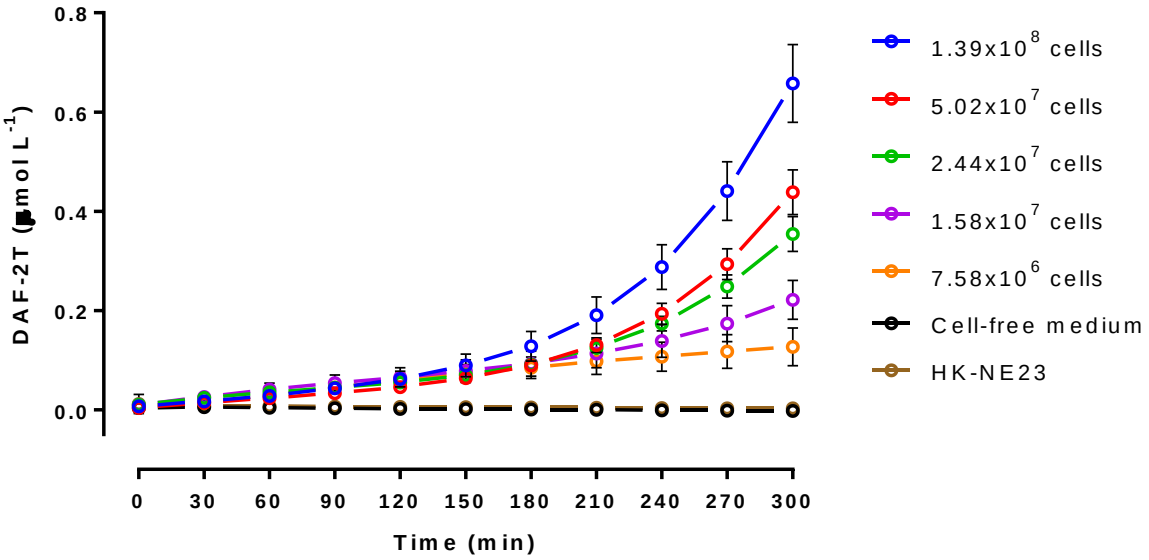

Figure 3.16 Production of NO during ammonia oxidation by *N. eutropha* D23 (varying cell densities), over 5 h of incubation, in M9 medium, at 37 °C. Cell-free medium (M9 medium) and heat-killed *N. eutropha* D23 (HK-NE23, $1.58x10^7$ cells) were incorporated as negative controls. Data is presented as mean±SD (n=27), from 3 technical replicates.

As observed from the data above, NO was only detected for live *N. eutropha* D23 across all cell densities assayed, as no fluorescence signal was found for the negative controls. Besides detection of NO, the data also suggest that its production follow a dependence on the number of *N. eutropha* D23 present in the wells of the microtiter plate, as higher concentrations of DAF-2T were observed for measurements at higher *N. eutropha* D23 cell densities.

The concentration of DAF-2T (and indirectly the concentration of NO) seemed to increase almost in a linear fashion over time, particularly in the first couple of hours of substrate oxidation. After 150-180 min, the rates of production increase every 30 min, and levels of DAF-2T start to be distinguishable among the *N. eutropha* D23 cell densities assayed, with higher yields of nitrosated DAF-2 observed for experiments carried out with higher bacterial counts. Even though bacterial growth was not assumed to occur over the time course of this experiment, the yields of DAF-2T were normalised by the absolute numbers of *N. eutropha* D23 present at the beginning of the 5-h incubation, for each cell density assayed, and as previously done when assessing production of NO using gas-phase chemiluminescence at varying bacterial densities. The results are shown in Figure 3.17 below.

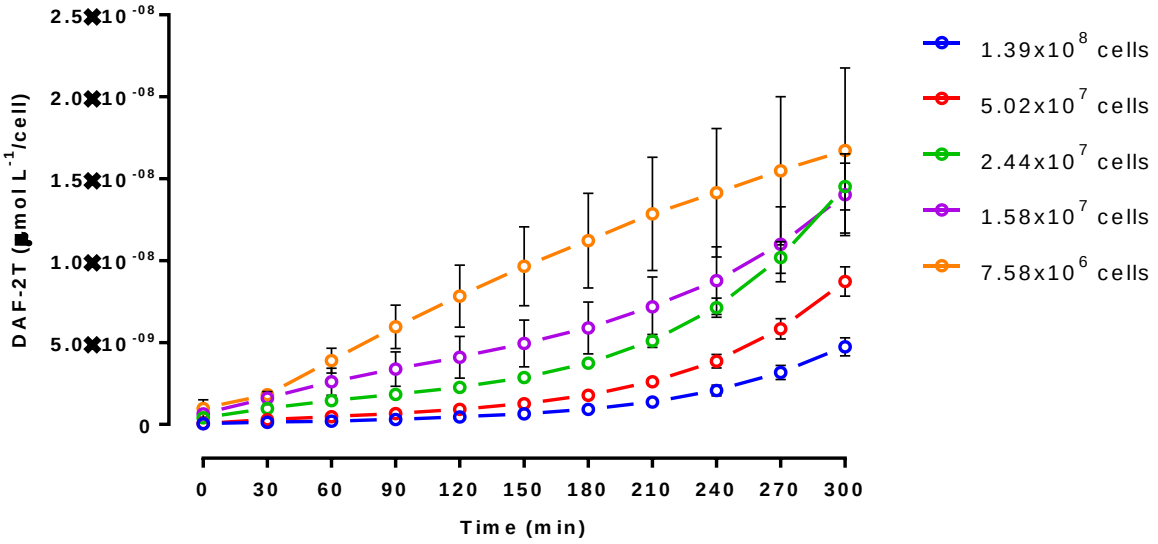

Figure 3.17 Normalised results for the production of NO during ammonia oxidation by *N. eutropha* D23 (varying cell densities), over 5 h of incubation, in M9 medium, at 37 °C. Data presented as mean±SD (n=27), from 3 technical replicas.

The highest levels of nitrosated product detected per *N. eutropha* D23 cell are observed for wells that contained the lowest number of *N. eutropha* D23 cells at the beginning of the experiment; an identical observation as previously seen using gas-phase chemiluminescence. By using an additional method with a different detection principle (i.e. fluorimetric detection), the results from the last two figures further support the findings previously seen in Figure 3.12 (panels G and H), using gas-phase chemiluminescence. In light of these results, a series of control experiments were further carried out, namely the incorporation of CPTIO and an excess of NO_2^- in the presence of *N. eutropha* D23 and DAF-2 as additional controls for assessing specificity of the fluorescence signal to NO and rule out possible contribution of NO_2^- on the signal. The results are shown in Figure 3.18 below.

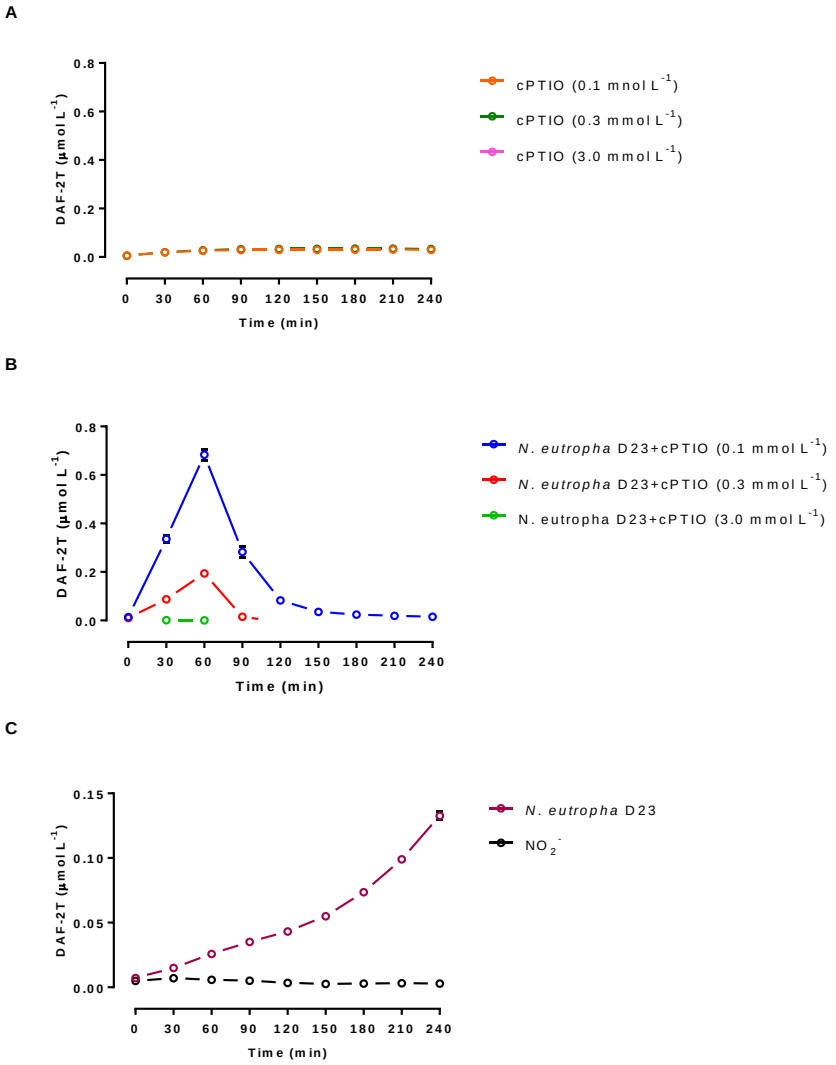

Figure 3.18 Experimental controls carried out to assess specificity of the fluorescence signals to *N. eutropha* D23-derived NO. The effect of CPTIO (0.1, 0.3, and 3.0 mmol L^{-1}) in the absence (A), and in the presence (B) of *N. eutropha* D23. A comparison (C) between the signals obtained from incubation of live *N. eutropha* D23 and abiotic NO_2^- (1 mmol L^{-1}) is also shown in the figure. Data is presented as mean±SD (n=6-9), from a single technical replicate.

As observed in panel A, and in the absence of *N. eutropha* D23, CPTIO itself did not generate any appreciable changes in the fluorescence signal, as virtually no DAF-2T was detected for all three concentration of CPTIO assayed (0.1, 0.3, and 3.0 mmol L^{-1}). However, changes are seen while incubating *N. eutropha* D23 in the presence of CPTIO and DAF-2. As observed from panel B, a transient and quick rise in the concentration of DAF-2T is seen for incubations occurring in the presence of CPTIO during the initial time periods, especially evident at 0.1 and 0.3 mmol L^{-1} CPTIO. The levels of DAF-2T generated seem to follow an inverse dependence on the concentration of CPTIO available. For instance, at 60 min of incubation, the levels of DAF-2T are 0.684±0.022 and 0.194±0.003 µmol L^{-1} for *N. eutropha* D23 incubated at 0.1 and 0.3 mmol L^{-1} CPTIO, representing ~3.5-fold difference in DAF-2T for these concentrations of NO scavenger. After this time point, the concentration of DAF-2T decreases to asymptotic levels around 0 µmol L^{-1} DAF-2T. Abiotic NO_2^- (1 mmol L^{-1}) was assayed due to its production by the bacteria, and results shown in panel C indicated that its presence in the medium did not lead to any rise in DAF-2T, as opposed to metabolically-active *N. eutropha* D23.

3.7.2 Oxyhaemoglobin capture assay

The oxyHb capture assay was used to follow production of NO at different substrate concentrations, whose principle of detection is based on the reactivity of NO towards metal-containing proteins (heme), and, therefore, different from the other methodologies used previously. Prior to any data recording, the quality of oxyHb used in these experiments was verified, by the prominence of common spectral features for this molecule, as opposed to those of ferric-haemoglobin (methaemoglobin, metHb), which is formed during the NO/oxyHb co-oxidation reaction. Figure 3.19 below shows the full spectrum (300-600 nm) for haemoglobin (oxyHb and metHb), and M9 medium, where the following NO measurements took place.

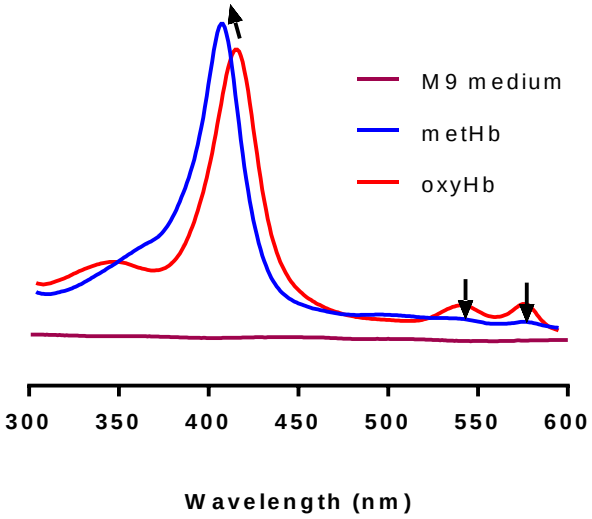

Figure 3.19 Full spectrum (300-600 nm) for oxyhaemoglobin (oxyHb), methaemoglobin (metHb), and M9 medium. Arrows indicate the changes upon oxidation of oxyHb to metHb.

As seen above, the spectrum for haemoglobin is characterised by an intense γ-band (Soret) with absorption maxima at 415 nm (for oxyHb) and 406 (for metHb). Two less pronounced bands are also observed for oxyHb, such as the β- and α-bands (Q-bands), with absorption maxima at 541 and 577 nm, respectively.

For the measurement of NO produced by *N. eutropha* D23, absorbance values between 300 and 600 nm were recorded for 1 h, shortly after incubating the bacteria at a fixed cell density (~10^7 *N. eutropha* D23 cells mL^{-1}) in M9 medium containing oxyHb. The results from this assessment are shown in Figure 3.20 below, which show both full and difference spectra, recorded for production of NO at 1, 10, and 25 mmol L^{-1} NH_4^+.

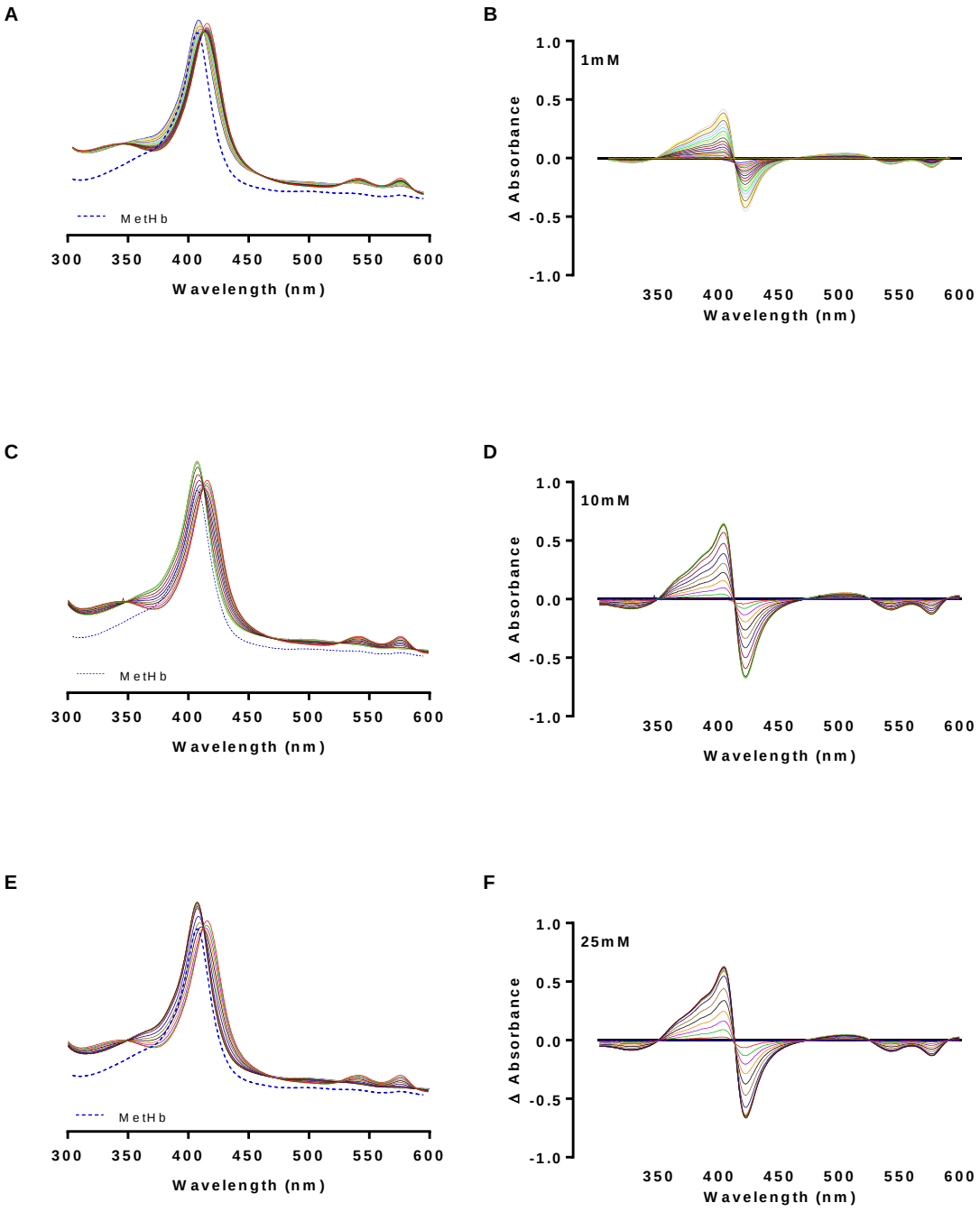

Figure 3.20 Oxyhaemoglobin capture assay for assessment of NO production in solution by *N. eutropha* D23. Absolute (on the left) and difference spectra (on the right) are shown for *N. eutropha* D23 incubated at 1 (panels A and B), 10 (panels C and D), and 25 (panels E and F) mmol L^{-1} NH_4^+. Full spectrum for metHb is superimposed together with the spectra of the conversion of oxyHb to metHb. Data is presented as mean tracing of 2 technical replicates, for each concentration of NH_4^+ assayed.

According to the data shown above, production of NO in solution by *N. eutropha* D23 was observed for all concentrations of substrate. This production is evident by the spectral changes seen in panels A, C, and E for bacteria incubated at 1, 10, and 25 mmol L^{-1} NH_4^+. As compared to the original full spectrum for oxyHb (Figure 3.20), the changes seen in these tracings over time are due to the conversion of ferrous- (oxyHb) to ferric-haemoglobin (metHb), in the presence of NO, with peak maxima gradually shifting from 415 to 406 nm.

The information from these spectra can be better visualised by looking at the difference spectra. These latter are presented in panels B, D, and F, and were acquired by subtracting the initial oxyHb spectrum from all spectra obtained during bacterial production of NO. It can be observed changes (indicated by Δ in absorbance) in the metHb generated over time, indicating production of NO and its trapping in solution, during ammonia oxidation by *N. eutropha* D23. For instance, these changes can be seen more prominently by the difference in absorbance at 401 nm ($\Delta>0$) or at 420 ($\Delta<0$), for all NH_4^+ concentrations.

From the difference spectra, production of NO occurred at a slower rate for *N. eutropha* D23 incubated at 1 mmol L^{-1} NH_4^+ than at the other substrate concentrations assayed. This information is better visualised after plotting the difference in absorbance (which is related to the increase in metHb formation, and hence NO production) over the time course of the experiment (1 h). Figure 3.21 shows the kinetics of NO formation as assayed by the oxyHb capture assay, using the data from the previous figure.

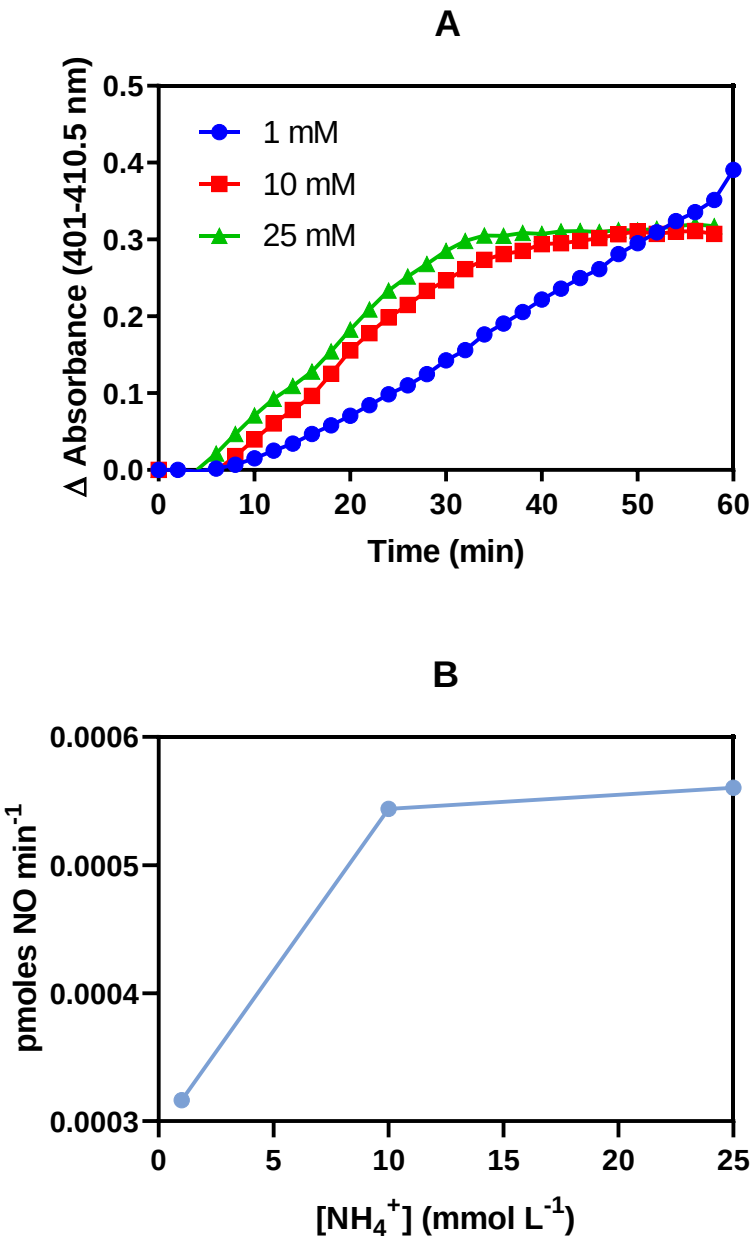

Figure 3.21 Tracing of (A) NO production over one hour and (B) rates of production in function of substrate (NH_4^+) concentration, using the oxyHb capture assay, for *N. eutropha* D23 (~10^7 cells) incubated at 1, 10, and 25 mmol L^{-1} NH_4^+. Data is presented as mean of 2 incubation experiments. Error bars were omitted from the graph to allow better visualisation of the trend in NO production.

Formation of NO over time occurred at earlier times for *N. eutropha* D23 incubated at 10 and 25 mmol L^{-1} NH_4^+, as compared to bacteria incubated at 1 mmol L^{-1} NH_4^+, in a linear fashion over time. The rate of NO production (as judged by the slopes in the linear part of the tracings) was the highest for *N. eutropha* D23 incubated at 25 mmol L^{-1} NH_4^+, as also evident from the rates (calculated for the linear phase of NO production) in panel B. Heat-killed *N. eutropha* D23 were also assayed with this methodology as a negative control. The absolute and differential spectra are shown in Figure 3.22 below.

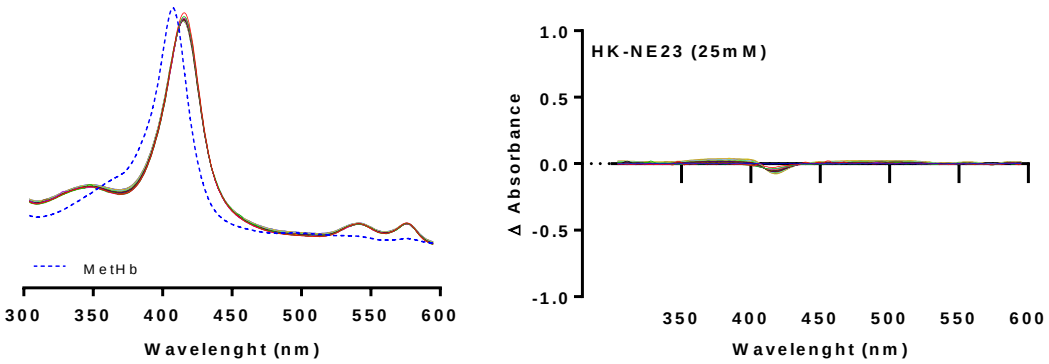

Figure 3.22 Oxyhaemoglobin capture assay for assessment of NO production in solution by heat-killed *N. eutropha* D23, in M9 medium containing 25 mmol L-1 NH_4^+. Full spectrum for metHb is superimposed together with the spectra of the conversion of oxyHb to metHb. Data is presented as mean tracing of 2 technical replicates.

As compared to the spectra shown previously (for live *N. eutropha* D23), no appreciable changes in the absorbance can be seen from the figure above, and therefore, NO is only detected by viable *N. eutropha* D23 using the oxyHb capture assay.

3.8 Stress responses of *N. eutropha* D23

Changes in the metabolic behaviour of *N. eutropha* D23 were evaluated by comparing their metabolism under homeostatic and stress conditions; the latter was chemically achieved by subjecting *N. eutropha* D23 to varying concentrations of stress agents. These included an NO scavenger (CPTIO) and the nitrification inhibitor N-allylthiourea (ATU). Liquid cultures were prepared by inoculating *N. eutropha* D23 in growth medium, as described previously. Stressor agents were added at the beginning of the log/exponential phase of *N. eutropha* D23 (i.e. 48 h, based on previous observations from the growth curves), at varying concentrations. For comparison purposes, vehicle was added to control cultures (i.e. those growing under homeostatic conditions). Aliquots were sampled from the liquid cultures at regular intervals, before and after addition of stressor agent, for analysis of extra- and intra-cellular compartments. Figure 3.23 shows the results obtained by subjecting *N. eutropha* D23 to low (2.5 µmol L^{-1}), intermediate (39.6 µmol L^{-1}) and high (158.5 and 317.0 µmol L^{-1}) concentrations of CPTIO.

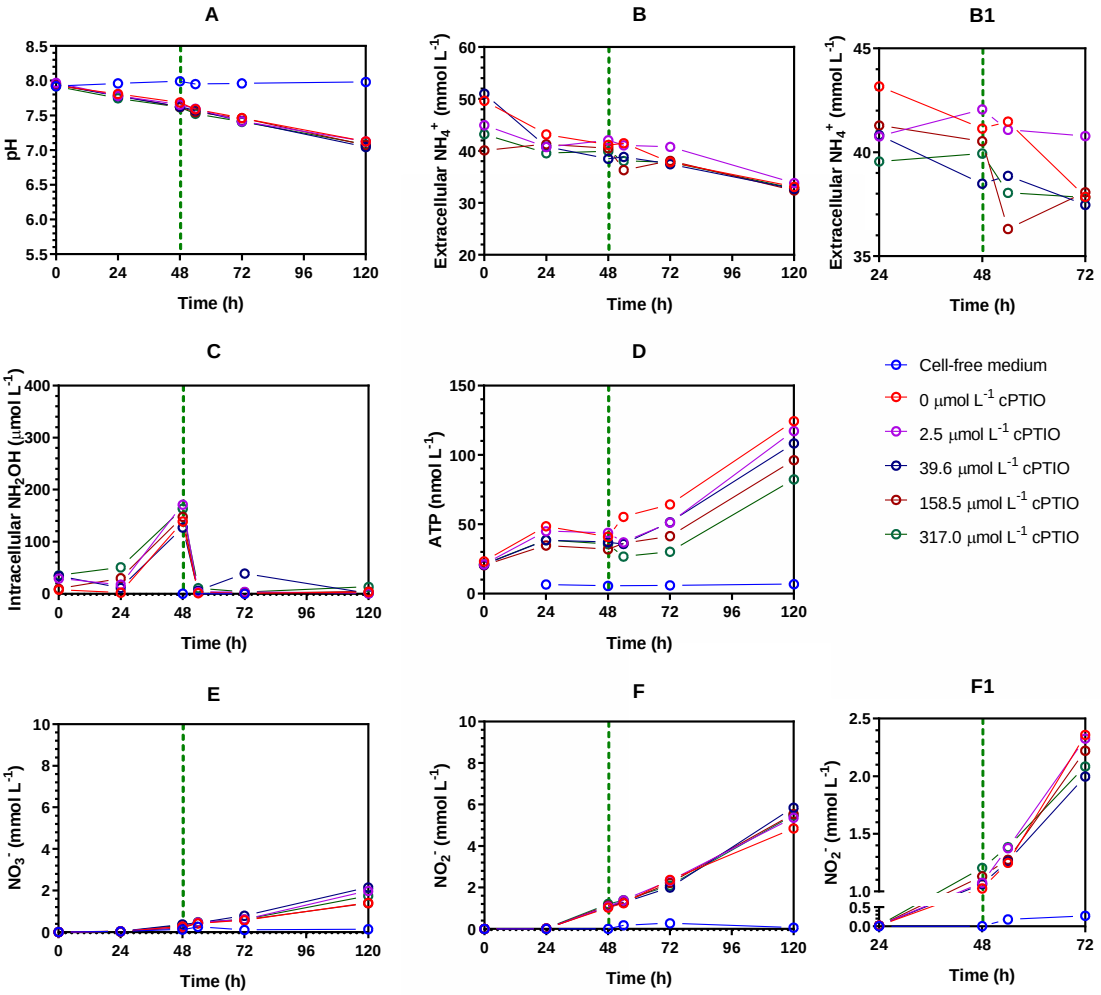

Figure 3.23 Monitoring of growth and metabolic activity of growing cultures of *N. eutropha* D23, under homeostatic (control) and in the presence of varying concentrations of CPTIO. Aliquots were taken from three independent liquid cultures containing *N. eutropha* D23, with aliquots taken for measurement of pH (A), NH_4^+ consumption (B), intracellular levels of NH_2OH (C) and ATP (D), and NOx (E and F). Panels B1 and F1 are zoomed versions of panels B anf F, respectively, for time between 24 and 72 h. For better visualisation, data is presented here as mean (n=3). Dotted line on the X axis (at 48 h) indicates addition of CPTIO. A zoomed in version of Panels B and F are presented for better visualisation of the trends exhibited between 24 and 72 h.

For clarity of overall trends across 5 days of experimental time, error bars are omitted from the graph. As observed, growth and metabolic activity of *N. eutropha* is evident throughout the study period considered, as indicated by the changes in the parameters measured. This is evident by the overall acidification of the growth medium containing actively-growing cells (panel A), as compared to cell-free medium, from 7.93±0.036 to 7.12±0.076 in control cultures. At 120 h, no significant changes in pH between the groups subjected to CPTIO were found. This metabolic activity is accompanied by consumption of NH_4^+ (panel B) from the medium. After addition of CPTIO and the next 6 h (i.e. between 48 and 54 h), the slope of the tracings suggests that the rate of NH_4^+ consumption for *N. eutropha* D23 exposed to 158.5 and 317.0 µmol L^{-1} CPTIO is higher than that of the control (panel B1). Comparing the same time points, no major changes in the rate of NH_4^+ consumption is observed for *N. eutropha* D23 subjected to homeostatic conditions.

Changes in the metabolic activity are also observed for intracellular levels NH_2OH (panel C) and ATP (panel D). While generation of NH_2OH is observed from early time points, its levels reach a maximum at 48 h, i.e. immediately before addition of CPTIO or vehicle, before plummeting down to baseline levels afterwards for both groups. No significant differences in the levels of NH_2OH are observed between both groups at this time point. Similar trend is observed in the generation of intracellular ATP for *N. eutropha* D23 before 48 h. However, while the continuous production of ATP is observed for control cultures further past addition of vehicle, changes in the pool of this metabolite are immediately observed after addition of CPTIO. While generation of ATP is not entirely shutdown, its levels accumulate inside CPTIO-exposed *N. eutropha* D23 cells initially at much lower rates as compared to control cultures. At 120 h, for instance, the mean values of ATP for incubations in the presence of 158.5 and 317.0 µmol L^{-1} CPTIO were significantly lower than control (p-values of 0.0248 and 0.0026, respectively).

In parallel with the metabolic changes above, accumulation of both NO_2^- and NO_3^- (NOx) were observed, whose production seemed to follow a constant production over time. At any time point, NO_3^- (panel E) was produced at much lower concentrations than NO_2^- (panel F). No major changes in the concentration of NO_3^- are observed before 48 h; however, after addition of CPTIO, changes in the rates of NO_3^- generation are seen between the groups. As particularly evident during 72 and 120 h, NO_3^- accumulated in liquid culture at a slightly higher rate with CPTIO-exposed *N. eutropha* D23, as compared to control, although not statistically different. As for NO_2^-, its levels follow a similar trend in production as observed for NO_3^-. While the rate of NO_2^- production seem fairly constant over time for bacteria growing under homeostatic conditions, its value change for cultures exposed to CPTIO in two directions. Firstly, soon after addition of CPTIO (i.e. between 54 and 72 h, panel F1), production of NO_2^- by the bacteria slows down, as seen by the slight

change in the slope of the tracing. However, after 72 h, the rate of NO_2^- production increases, as compared to control cultures, indicating a faster production of this metabolite in solution. At 120 h, mean NO_2^- levels are higher for CPTIO-exposed *N. eutropha* D23, though not significantly distinct from those generated by bacteria under homeostatic conditions.

Besides an NO scavenger, growing cultures of *N. eutropha* D23 were also subjected to a thiourea derivative, such as ATU, which is a known nitrification inhibitor commonly used in functional studies with ammonia-oxidisers. Its mechanism of action entails enzymatic inhibition on the AMO enzyme. The results for the metabolic changes in *N. eutropha* D23 exposed to ATU are shown in Figure 3.24.

Changes in metabolic activity between the groups studied are observed by the acidification of the growth medium over time, as shown by the pH measurement (panel A). These changes are evident from 72 h onwards, particularly for *N. eutropha* D23 exposed to 1, 10, and 100 µmol L^{-1} ATU, as compared to cultures growing under homeostatic conditions. Data suggests that metabolic activity is interrupted immediately after exposing *N. eutropha* D23 to 10 and 100 µmol L^{-1} ATU, which resulted in a significantly less acidification of the growth medium for these cultures, as compared to control, at 120 h.

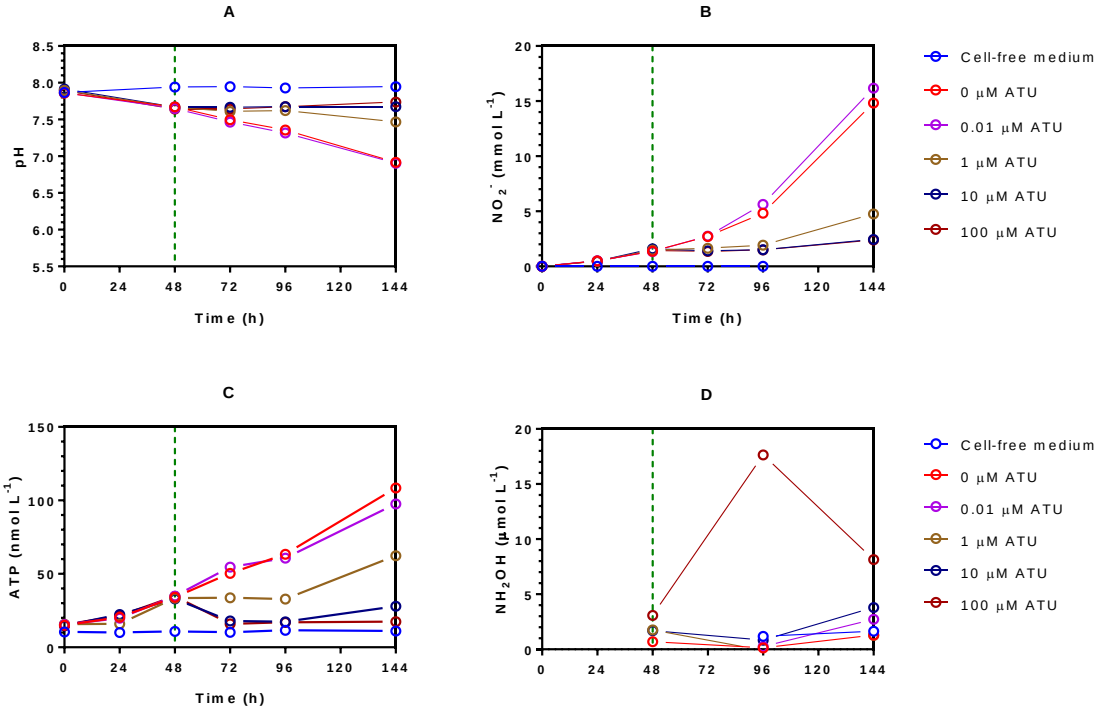

Figure 3.24 Monitoring of growth and metabolic activity of growing cultures of *N. eutropha* D23, under homeostatic (control) and in the presence of varying concentrations of N-allylthiourea (ATU). Aliquots were taken from three independent liquid cultures containing *N. eutropha* D23 for measurement of pH (A), NO_2^- (B), and intracellular levels of ATP (C). Extracellular NH_2OH (D) is here evaluated by plotting absorbance changes over time. Data is presented as mean±SD (n=3).

The trend in NO_2^- production (panel B) is consistent with the information inferred from the pH measurements. Differences in the levels of this metabolite are particularly evident from 72 h onwards, as well, with no further accumulation of NO_2^- seen up to 96 h for cultures exposed to 1-100 µmol L^{-1} ATU. However, as data suggests, production of NO_2^- was restored for *N. eutropha* D23 exposed to 1 µmol L^{-1} ATU, as seen by an increase in the concentration of this metabolite between 96 and 120 h. At 120 h, the levels of NO_2^- accumulated in the cultures growing under homeostatic conditions are significantly higher than those of ATU-exposed cultures (1-100 µmol L^{-1} ATU). The intracellular levels of ATP (panel C) follow identical trends as described for NO_2^-, and data shows that exposure to ATU interferes with generation of energy in *N. eutropha* D23, as particularly seen for cultures incubated in the presence of 1-100 µmol L^{-1} ATU. Even though it is observed that

ATP is affected by the presence of increasing concentrations of ATU, only exposure to 100 µmol L^{-1} ATU led to significantly less production of ATP by *N. eutropha* D23 ($p=0.0209$), as compared to control, at 120 h. Measurement of extracellular NH_2OH (panel D) was also carried out for these conditions, and the results showed its detection in the extracellular compartment for *N. eutropha* D23 exposed to the highest concentration of ATU. Detection of NH_2OH in the extracellular compartment was only achieved under the conditions here applied, and potentially indicate release of this chemical intermediate from the cells.

3.9 Discussion

AOB catalyse a series of oxidative reactions to convert environmental NH_3 (their substrate) into NO_2^- (their main metabolic product), through formation of NH_2OH, as part of their energy-generation metabolic pathway (Figure 3.25).

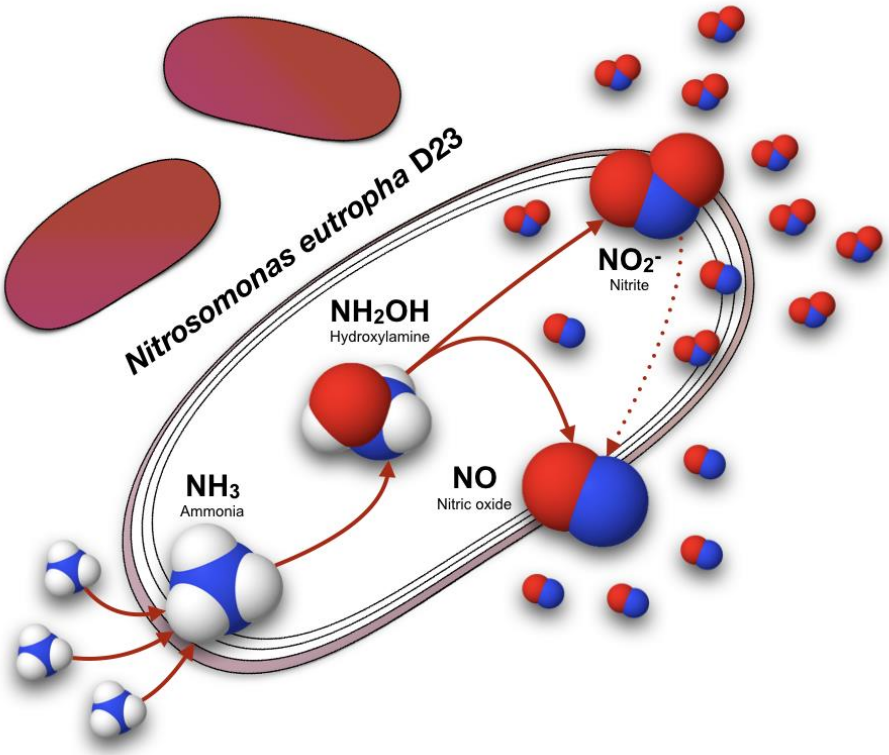

Figure 3.25 Aerobic ammonia oxidation by ammonia-oxidising bacteria, according to the classical pathway.

While the majority of the information available regarding the properties of this group of bacteria derive from research work using *N. europaea* and, to a lesser extent, *N. eutropha*, no information is available in the literature regarding the general biochemical properties of a newly available strain of AOB, *N. eutropha* D23, which is currently in use cosmetically and for biomedical purposes. A limited amount of information is available in the literature for this particular strain, (Gryllos, Ghos*h, et al.*, 2014; Gryllos, Vajrala, *et al.*, 2014). This research thesis is the first to characterise the metabolic properties of *N. eutropha* D23 at a more detailed level, and sets ground for more in-depth characterisation of this strain of ammonia-oxidiser. The strengths of the approach taken here include the study of live, axenic bacterial populations, which are produced at high cell densities under carefully controlled and reproducible manufacturing practices. The initial experimental activities described in this chapter were carried out to confirm the fundamental phenotypic and metabolic properties of *N. eutropha* D23, similar to what has been described in the literature for ammonia-oxidisers (e.g. *Nitrosomonas* sp.). Moreover, these activities explored the applicability of different methodologies for studying the metabolism of this particular strain, with focus on the production of nitrogen oxides, such as NO and NO_2^-. The following paragraphs include an intertwined discussion of figures 3.1 to 3.4, whose results derive from pilot experiments regarding the monitoring of growth and metabolic activities of *N. eutropha* D23 in the laboratory.

3.9.1 Extra- and intracellular changes during growth of *N. eutropha* D23 in batches

From the results shown in figures 3.1 and 3.2, it is observed that *N. eutropha* D23 harvested directly from the commercial product (i.e. sample source) were amenable to growth in a batch-wise fashion. Under the laboratory conditions chosen, *N. eutropha* grew in liquid culture with doubling times of 1-2 days, as commonly reported for other species of ammonia-oxidisers (Koops, Harms and Wehrmann, 1976). Although perhaps not surprising, this confirmed the viability of the cells contained inside the commercial product, and supported the aims of this work to make a more detailed characterisation of this strain. Further to following the growth in liquid culture, the parallel monitoring of consumption and formation of metabolites (i.e. NH_4^+ and NO_2^-, respectively) showed anticipated characteristics one should expect for AOB.

Some interesting features from the pilot data can be pointed out. The initial, slow rate of NO_2^- production seen in both figures (3.1 and 3.2) can likely be explained by the adaptation of the bacteria to the experimental conditions chosen, whose kinetic curve show a lag phase as no appreciable changes are observed from the optical density (OD600, panel B of Figure 3.1) or bacterial biomass measurements (protein, Figure 3.2),

in the first 24 h of study. On the other hand, the consumption of NH_4^+ from the growth medium was more pronounced than the other parameters measured, for the first 24 h, by comparing the slopes (i.e. rates) of consumption and production curves. Lack of energy is here pointed as a possible explanation for this observation, as bacterial biomass is kept in suspension in a buffer (storage medium) devoid of their substrate, within the commercial product, and therefore, with no means for generating energy during storage conditions. This observation is concordant with findings described by Schmidt et al. (2004). In this study, authors report higher rates of NH_4^+/NH_3 uptake for starved *Nitrosomonas* cells (*N. europaea, N. eutropha*, and *N. multiformis*), compared to active cells, with no parallel formation of NO_2^- during uptake and accumulation of substrate.

For *N. eutropha* D23, a rapid consumption of NH_4^+ from the medium, concomitantly with a much slower rate of NO_2^- production seen in this pilot study could also be related to the formation of the NH_2OH intermediate. Production of this chemical intermediate during ammonia oxidation requires a continuous supply of energy (ATP) to the AMO enzyme, via oxidation of NH_2OH to NO_2^-. Generating energy seems required through consumption of high quantities of NH_4^+, before *N. eutropha* D23 are able to achieve a steady-state of NO_2^- production.

The results from Figure 3.1 also show an apparent slowdown in activity. This is particularly obvious by looking at the differences in the rate of consumption of NH_4^+ between days 3 and 4, and those of the previous days. However, as this was a result from *N. eutropha* D23 grown in a single liquid culture (n=1), the experiment was repeated to assess reproducibility and test whether activity slows or shuts down. The results thus shown in Figure 3.2 support the afore-mentioned premise. Besides reproducible, the metabolic activity started to slow down after 72 h of growth, as shown by the decrease in the rates of both NH_4^+ consumption and NO_2^- production. In agreement, the rate of bacterial biomass accumulation in liquid culture also seemed to decrease from 72 h onwards, reaching an asymptotic value at the end of the incubation time, indicating no further appreciable bacterial growth. This observation possibly indicates that the late log phase of growth of *N. eutropha* D23 occurs after 3 days in growth medium.

Two additional parameters measured over the duration of this experiment support the above statement, namely the measurement of the intracellular levels of ATP and the pH of the growth medium. The results shown in Figure 3.3 are in agreement with observations already described (i.e. lag phase during the first 24 h). The peak concentration of intracellular ATP is also concordant with the observations that NH_4^+ is consumed and NO_2^- is produced at much lower rates after 72 h of growth, accompanied by a slowdown in biomass production; acidification of the growth medium also ceases past this point.

Measurement of intracellular NH_2OH (Figure 3.4) revealed its continuous production from early time points, reaching a maximal concentration at 72 h, with sustained levels afterwards. The observable generation of this intermediate inside *N. eutropha* D23 cells during the initial 24 h of growth seemed consistent with the explanation that cells initially uptake high quantities of NH_4^+/NH_3 before any striking metabolism takes place, as previously observed in Figure 4.1, potentially due to the requirement of ATP to support a continuous oxidation process (via the AMO enzyme).

The methodologies used for these initial activities seemed adequate, and were based on simple spectrophotometric methods like indophenol blue and Griess assays, for the measurement of NH_4^+ and NO_2^-, respectively. Even though no sensitivity issues with the microtiter plate-based Griess assay were foreseeable when measuring NO_2^- from *N. eutropha* D23 (as measured in Figure 3.1), with high millimolar concentrations achieved, the purpose of the pilot experiments also included an exploration into using more specific analytical methodologies. Despite sharing identical principle of NO_2^- detection and quantification (based on Griess assay), the measurement of NO_2^- using HPLC (as measured in Figure 3.2) had the advantage of sample automation and high-throughput, was less prone to pipetting error and displayed higher sensitivity, as compared to microtiter plate-based Griess assay. The gain in sensitivity by selecting HPLC as the analytical tool for NO_2^- for further biochemical characterisation of *N. eutropha* D23 was an added benefit.

3.9.2 Initial evidence for NO formation by *N. eutropha* D23

Besides insight on the NO_2^- formation, the initial package for the general characterisation of *N. eutropha* D23 included detection of NO formed during ammonia oxidation, using electrochemical- and chemiluminescence-based methods. The production of NO was evaluated for *N. eutropha* D23 inoculated in a simple, $MgCl_2$-supplemented phosphate buffer containing NH_4^+, as this represents the standard composition of the buffer medium where *N. eutropha* D23 are conditioned under substrate-starved conditions within the commercial product.

Taken together, the results from figures 3.5 and 3.6 indicate an overall ability of energy-starved *N. eutropha* D23 to produce NO during substrate oxidation, over the short incubation period considered. Interestingly, production of NO occurs shortly after the beginning of the registration for each of the methods employed, which indicate that long incubation periods (such as those seen during growth of the bacteria) are not required to measure the production of this molecule, or even others, as starved *N. eutropha* D23 cells respond almost immediately to addition of substrate. Despite not assessing direct production of NO, the findings reported by Wilhelm et al. (1998) support this statement, as

energy-starved *N. europaea* cells (for almost one year) were able to act quickly to addition of a low concentration of substrate to the cultures (as observed due to almost immediate NO_2^- production). In the same line, others have described that the pathway that leads to generation of NO_2^- and ATP production remains stable during substrate starvation in *N. europaea* (Nejidat, Shmuely and Abeliovich, 1997); thus, explaining the quick metabolic activity seen for *N. eutropha* D23 in the presence of substrate.

Furthermore, these initial results indicated that production of NO follows a dependence on the temperature as seen by gas-phase chemiluminescence (Figure 3.6), with higher levels of NO produced at 37 °C. The two temperatures (31 and 37 °C) initially assayed were chosen based on the mesophilic requirements of species of ammonia-oxidisers (Koo*ps et al.*, 1991), whose optimal activity (i.e. metabolic production) has been shown to occur within a range of amenable/moderate temperatures. For instance, while comparing the effect of temperature and feeding patterns in *N. europaea*, Lu et al. (2015) found higher metabolic activity for bacteria incubated at temperatures above ≥ 10 °C, and that temperature exerted a major influence on their overall metabolic behaviour. Optimal conditions for growth of ammonia-oxidisers has also been reported for temperatures between 28 and 35 °C (Skinner and Walker, 1961; Güven and Schmidt, 2009b). As *N. eutropha* D23 are intended for biomedical application, the initial assessment for NO production was thus conducted for the commonly reported human core (37 °C) and external surface/skin (31 °C) temperatures (Liu *et al.*, 2013).

Despite allowing selective detection and quantification of trace levels of NO in real time, the advantages and disadvantages of both methodologies initially used were considered before moving into further metabolic characterisation of *N. eutropha* D23. The selective electrochemical NO probe used for the experiment directly measured concentrations of NO that were produced in small volumes of solution (~3 mL). At an initial glance the detection of NO using probes seemed like an easy method to start characterising the NO output quickly and in real-time from *N. eutropha* D23; upon careful consideration, however, its disadvantages outweighed its advantages. Electrochemical NO probes require relatively long periods of stabilisation, and amperometric signals are often prone to disturbances from the environment that are difficult to control, such as magnetic fields from surrounding equipment, differences in room temperature or vibrations (Csonka *et al*., 2015). These can interfere with the biological measurements and potentially deceive the results obtained.

As opposed to NO probes, gas-phase chemiluminescence requires NO to be purged out from the solution into the gas-phase for its detection, which can potentially exert an impact on the physiology of *N. eutropha* D23 during measurement of NO. However, because of its superior sensitivity, gas-phase chemiluminescence was chosen as the standard

analytical platform to measure NO, and continuing the assessment of the properties of *N. eutropha* D23. Besides its sensitivity, it is less prone to disturbances vs NO probes, it offers more versatility and reproducibility for routine measurements of NO, and it allows real-time recordings of NO production during ammonia oxidation by *N. eutropha* D23.

3.9.3 Metabolic efficiency of chemostat-grown *N. eutropha* D23 harvests

While the first set of experimental activities (entire section 3.3) into the biochemistry of *N. eutropha* D23 were encouraging, they also revealed some drawbacks inherent to the physiology of these bacteria. The quantities of bacteria required for a more detailed characterisation were limiting in relation to the ability to generate *N. eutropha* D23 in batches. This was primarily due to the lengthy generation time and issues related to the maintenance of the growing cultures on-site of analysis. It was assumed that up-scaling the growth of *N. eutropha* D23 to continuous culture in chemostat systems would overcome the above-mentioned drawbacks, as larger cell numbers could be obtained more efficiently. As such, the metabolic properties of *N. eutropha* D23 harvested from chemostat culture were primarily assayed for feasibility purposes and metabolic efficiency, namely by investigating their potential for producing NO and NO_2^-.

Overall, the results from this metabolic assessment show strong physiological similarity between the different *N. eutropha* D23 harvests, although data suggested that harvests exhibited different metabolic efficiencies. As seen by the gas-phase chemiluminescence tracings (Figure 3.7), higher levels of NO were produced by the early harvest A (7 days), regardless of the concentration of NH_4^+. As for the remaining *N. eutropha* D23 harvests (B, C, and D, for 81, 85, and 90 days), no statistically significant differences were found in the amounts of NO generated among these, within the same concentration of NH_4^+. These results indicate that higher levels of NO are produced for higher concentrations of substrate. However, for the three late harvest time points (i.e., 81, 85, and 90 days), this difference was less strikingly observed, as compared to the levels for harvest A. The quantitative summary shown in Figure 3.9 potentially suggests that despite the excess of substrate, cells from harvest B, C, and D do not show an increased performance for NO production, as compared to harvest A. Consistent with these observations, the results shown in Figure 3.10 also indicate that the highest levels of NO_2^- were produced by harvest A, and significantly higher as compared with harvests B, C, and D.

In the interest of investigating whether time of harvest could have an influence on the metabolic efficiency of *N. eutropha* D23, the ratios of metabolite production (i.e. ratio NO/NO_2^-) were calculated, and quantitatively expressed in function of time of cell harvest. In comparative terms, the ratios shown in in Figure 3.11 thus indicate that harvest A demonstrated superior efficiency for metabolite production. When expressing the ratio

NO/NO_2^- of each harvest in function of time (in days), the results suggest that the metabolic capabilities of *N. eutropha* D23 decrease upon prolonged chemostat culture. In terms of NO production, yields from cultures harvested at ≥80 days were 51.6% to 57.9% less than those harvested at 7 days, potentially suggesting that NO production is inversely proportional to the age of culture at harvest. Even though the results may suggest a decreased metabolic efficiency upon prolongued chemostat culture, this interpretation should be taken with caution as important experimental limitations in this study could have exerted an impact on the results obtained, as presented below.

In addition to experimental variables here, it is important to note that an assumption was made that the *N. eutropha* D23 harvests were produced under similar conditions of growth in the chemostat cultures, before being sent out from AOBiome LLC. Despite taking into account the same incubation period (i.e. 15 min) to establish the comparison between the production of the two molecules (NO and NO_2^-) for each harvest, their quantities were biologically generated in somewhat different conditions. For example, NO was detected upon generation by *N. eutropha* D23 during ammonia oxidation inside the reaction vessel which is constantly purged with synthetic air (see sequence of events within the reaction vessel in Figure 3.26 below), whereas for the production of NO_2^-, *N. eutropha* D23 cells were not subjected to any intense aeration during the incubation. This perturbation during NO measurement could have exerted an impact on the overall quantities of NO_2^-. Even though the effect of purging was not evaluated further, it could have been assayed by sampling aliquots directly from the reaction vessel during NO recording for NO_2^- measurements, and establish NO/NO_2^- ratios using amounts produced by *N. eutropha* D23 under these specific and similar experimental conditions. Under these conditions, should the ratios NO/NO_2^- or their trend in function of days of harvest be identical or not significantly affected by purging the cultures, then the results initially obtained are biologically relevant and the initial premise remains true. That is, the metabolic efficiency of *N. eutropha* D23 decreases upon prolonged chemostat growth.

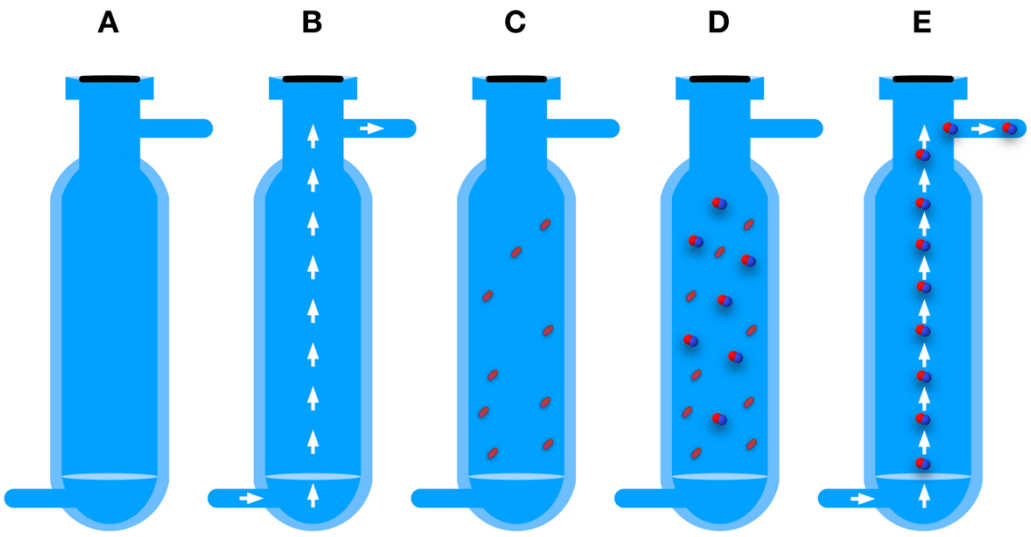

Figure 3.26 Sequence of events occurring within the reaction vessel during real-time measurement of NO produced by *N. eutropha* D23. A reaction vessel (A) is constinously purged (B) with synthetic air, where *N. eutropha* D23 are added (C). During ammonia oxidation, *N. eutropha* D23 generates NO (D) that is transferred to the gas phase (E), due to continuous purging of the reaction vessel.

Besides the unknown effect of purging on the amount of metabolites produced, the viability of the cells could have also had an impact on the results. Despite using the same *N. eutropha* D23 cell density for this experiment, a higher ratio live/dead *N. eutropha* D23 could simply explain the higher amounts of NO and NO_2^- observed for harvest A (7 days) as compared to the other harvests assayed. Viability should have been evaluated (e.g. fluorescence-based microscopy or cell sorting) and used to normalise the amounts of metabolites produced by live *N. eutropha* D23.

Last, but certainly not the least, a full interpretation of these results is hindered by the lack of more representative harvests from the chemostat, due to the large time gap between harvests A (collected on day 7) and the remaining ones (collected on days 81, 85 and 90). Study of the metabolic properties of chemostat-grown *N. eutropha* D23 at more regular time intervals would have been informative. In light of these results, it was decided that further metabolic characterisation of *N. eutropha* D23 would be done using cells collected directly from the commercial product, as the continuous production of axenic cultures in large bioreactors at an industrial scale could conceivably be expected to produce a more

consistent metabolic phenotype, with profiles closer to that what is commercially available for human use.

3.9.4 Factors affecting production of NO by *N. eutropha* D23

Guided by pilot observations, a better picture of the effect of some factors on the NO output was obtained using gas-phase chemiluminescence, including temperature, pH, and concentration of NH_4^+ and cell density. These were chosen based not only on overall physiological requirements described for AOB, but also on properties of the human skin, on which *N. eutropha* D23 is intended to be applied. Overall, the results from Figure 3.12 suggest that production of NO follows a dependence on temperature, pH, and concentration of substrate available for oxidation.

The results obtained for NO measured at varying temperatures (panels A and B, Figure 3.12) are in agreement with pilot data using gas-phase chemiluminescence for initial assessment of NO production (as seen in Figure 3.6), as they also show that higher levels of NO are produced when *N. eutropha* D23 are kept at higher temperatures, during substrate oxidation. As initially expected, production of NO was seen for amenable temperatures ($>$ 20 °C) expected for mesophilic bacteria, though its production was also observed for temperatures as low as 10 °C, indicating therefore a wide range of temperatures where production of this metabolite is expected from *N. eutropha* D23. Production of NO was not observed at 5 °C; temperatures below this value were therefore chosen for storage of *N. eutropha* D23 (e.g. in the fridge) or whenever metabolic quenching was needed. Even though the optimal amounts of NO were produced at 37-40 °C, further assessment of the NO output were conducted at 31 °C, which resembles the temperature on the surface of the human skin (reported ranges of 28-38 °C) (Mehnert *et al*., 2000; Dréno *et al*., 2016).

Gas-phase chemiluminescence tracings also showed that production of NO is dependent on the availability of substrate, and an optimal production of NO was observed for *N. eutropha* D23 incubated at $\geq$ 25 mmol L^{-1} NH_4^+, at 31 °C (panels C and D, Figure 3.12). These results validated previous observations when studying production of NO using chemostat-grown *N. eutropha* D23. The results indicate an ability *N. eutropha* D23 to produce NO at a wide range of NH_4^+ concentrations, with levels detected even at the lowest substrate concentration assayed (i.e. 1 mmol L^{-1} NH_4^+). Even though low concentrations of ammonia have been reported on the human skin (variable levels ~1-5 mmol L^{-1}) (Alvear-Ordenes *et al*., 2005; Meyer *et al*., 2007), further metabolic assessment was conducted with *N. eutropha* D23 incubated at 25 mmol L^{-1} NH_4^+, and kept at 31 °C.

The pH of the storage medium where NO measurements took place also exerted a significant effect on the overall amounts of NO generated by *N. eutropha* D23, whose production is also dependent on the pH (panels E and F, Figure 3.12). As shown in the results, production of NO was observed from bacteria incubated in storage medium incubated at a wide range of pH values, with detectable amounts for bacteria incubated between pH 6.0 and 8.0. Interestingly, detection of NO within this pH range seems consistent with the acidification of the growth medium seen for batch-grown *N. eutropha* D23, whose final pH values of the growth medium were slightly below 7 (Figure 3.1) and around 6 (Figure 3.3).

The absence of NO production at the acidic pH values assayed (i.e. 5.25 and 5.59) can likely be explained based on the NH_3/NH_4^+ chemical equilibrium, as shown in equation 3.1 below, and to the fact that NH_3 is the substrate for oxidation through AMO enzyme (Suzuki, Dular and Kwok, 1974). The extent of the conjugate acid dissociation in solution (i.e. the overall quantity of NH_4^+) is predicted through the acidity constant (K_a) value, according to equation 3.2 below. For instance, at 25 °C, the pK_a for the chemical equilibrium is 9.25 (Nelson, Cox and Lehninger, 2000). That is, at this pH, both base (NH_3) and conjugate acid (NH_4^+) exist in equal proportions. By lowering the pH of the storage medium to the acidic range, the chemical equilibrium is shifted towards increasing the concentration of conjugate acid, rather than its base (NH_3). For instance, for a pH of 5.5, the Henderson-Hasselbalch equation (equation 3.3 below), ascertains that only ~ 0.02% is present as NH_3.

(3.1) $$NH_4{}^+ \rightleftharpoons NH_3 + H^+$$

(3.2) $$K_a = \frac{[NH_3][H^+]}{[NH_4{}^+]}, \qquad pK_a = -\log Ka$$

(3.3) $$pH = 9.25 + \log\left[\frac{[NH_3]}{[NH_4^+]}\right]$$

Based on the above reasoning, the absence of NO production at these acidic pH values is due to the extremely low concentration of NH_3 available for oxidation by *N. eutropha* D23. Low concentrations of NH_3 could also be responsible for the lack of metabolic activity for batch-grown *N. eutropha* D23, as seen for example in figures 3.2 and 3.3, for a pH ~ 6, despite the presence of excess NH_4^+ in growth medium. On the human skin, a wide range of pH values is reported mainly in the acidic range (pH range 4-7) (Lamber*s et al*., 2006; Dréno *et al*., 2016). Inter variability among individuals can be explained by endogenous

and exogenous factors, the latter including the use of cosmetics, soaps and showering, which can raise temporarily the pH of the skin (Lambers *et al.*, 2006).

Ecologically, the influence of pH on nitritation activity by ammonia-oxidisers is known, using NO_2^- as a marker of such influence. Production of NO_2^- by ammonia-oxidisers is affected or ceases completely at the acidic pH range, despite the existence of nitritation activity in acidic soils. However, research has shown that growth and production of NO_2^- by ammonia-oxidisers can occur at low pH values, for instance, by adaptation of the bacteria to acidic conditions. De Boer et al. (1995) describe growth and activity of an acid-sensitive ammonia-oxidiser belonging to *Nitrospira* sp. The authors report activity of aggregates of these bacterial cells at pH 4. Moreover, they also show that suspended cells were able to produce NO_2^- at pH 4, provided that they were previously exposed to pH fluctuations, and at higher cell densities.

Lastly in this series of assessments, it was also observed that higher levels of NO were produced using higher *N. eutropha* D23 cell densities (panel A, Figure 3.12). It is observed that while the total levels of NO generated during the measurement period considered follow a dependence on the density of *N. eutropha* D23, the net amounts of NO generated per single *N. eutropha* D23 cells are observed for the intermediate *N. eutropha* D23 cell densities (i.e. 35.50 – 70.95 $x10^5$ *N. eutropha* cells mL^{-1}). Despite not being evaluated further due to time constraints, this observation could be due to substrate competition phenomena or possible modulation/regulation of NO production by the number of *N. eutropha* D23.

Aliquots were taken from the reaction vessel at the end of NO measurements for assessing the levels of NO_2^- produced under this condition (i.e. under a system subjected to aeration). Moreover, these amounts were compared with those generated when *N. eutropha* D23 were subjected to identical conditions, but not subjected to intense aeration. For clarity and ease of understating, this can be better visualised if one considers two independent systems. Figure 3.27 below shows a static system, which is not subjected to any perturbation, and a dynamic one, where a perturbation is applied during gas-phase chemiluminescence detection of NO. Amounts of NO_2^- were compared between a static and a dynamic system, at varying temperatures and concentration of NH_4^+.

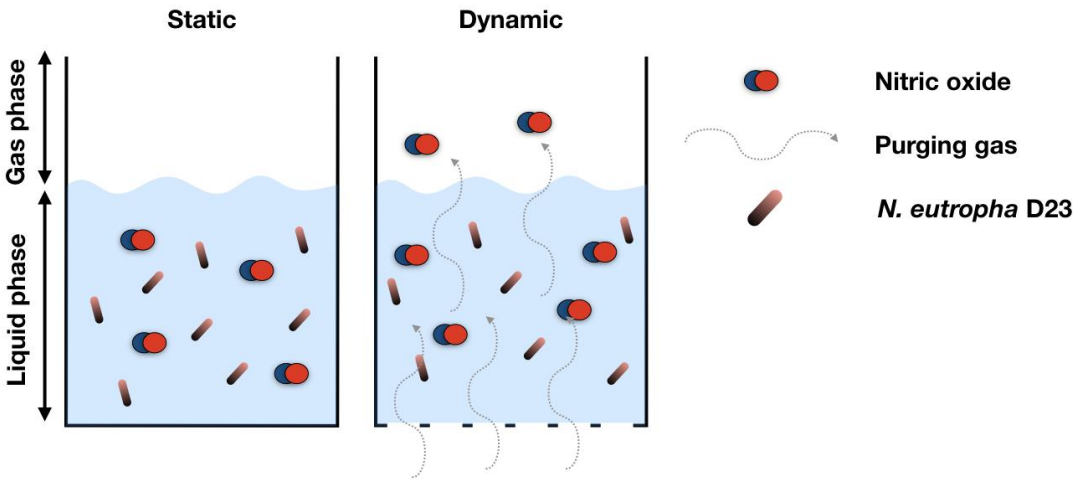

Figure 3.27 Schematic illustration of static and dynamic conditions for assessing NO formation by *N. eutropha* D23.

The results shown in Figure 3.12 indicate that the overall amounts of NO_2^- (main metabolic product) were higher when *N. eutropha* D23 was incubated in the presence of ammonia, under static conditions, i.e. not subjected to perturbations during biotic ammonia oxidation. It is further observed that perturbing the system during ammonia oxidation played a more influential role on the amounts of NO_2^- generated, than the isolated effect of either temperature or concentration of substrate. By establishing a correlation between the amounts of NO and NO_2^- generated under identical conditions (i.e. those generated inside the reaction vessel), the findings presented in Figure 3.14 are particularly relevant. Firstly, they also show that production of NO_2^- follows a dependence on the temperature and concentration of NH_4^+ available for oxidation; similar dependences as seen for the production of NO_2^-. Moreover, and assuming NO and NO_2^- are biologically generated by *N. eutropha* D23, it could be hypothesised that due to the strong relationship between the formation of both metabolites, a perturbation on the formation of one (e.g. NO) will consequently affect the overall levels of the other one (e.g. NO_2^-). While the absolute amounts of these metabolites seemed linearly correlated, for the same concentration of NH_4^+, their ratio NO/NO_2^- changes if expressed as a function of the NH_4^+ concentration. As shown in Figure 3.15, higher NO/NO_2^- ratios are observed for *N. eutropha* D23 incubated at concentrations of $NH_4^+ \leq$ 10-25 mmol L^{-1}. Thus, from this data, it could be inferred that absolute amounts of NO are generated at higher efficiencies for lower concentrations of substrate.

3.9.5 Additional methodologies for evaluating NO production by *N. eutropha* D23

Further to assessing NO production through gas-phase chemiluminescence, two additional and independent techniques were used to confirm production of NO by *N. eutropha* D23. As described in the results section, production of NO by varying *N. eutropha* D23 cell densities were assayed through measurement of a fluorescent probe, whereas OxyHb was applied for studying production of NO according to different concentrations of NH_4^+. Trends in the production of NO were expected using these additional methodologies, based on the previous observations using gas-phase chemiluminescence. Some experimental conditions were changed, namely temperature where production of NO was evaluated at 37 °C, for *N. eutropha* D23 inoculated in M9 medium.

Fluorimetric detection of NO was carried out based on the measurement of DAF-2T, a fluorescent probe generated upon nitrosation of DAF-2. The results presented in Figure 3.16 indicate that production of DAF-2T followed a dependence on the density of *N. eutropha* D23, in agreement with the trend already observed from Figure 3.12 (panel G) for NO. Normalisation of these results by absolute *N. eutropha* D23 numbers as indicated in Figure 3.17 show that the highest efficiency of DAF-2T formation was achieved by the lowest *N. eutropha* D23 cell density assayed; in accordance with previous observations that production of NO could possibly be modulated or regulated by the number of *N. eutropha* D23 cells.

The differences seen in the fluorescence signals between live *N. eutropha* D23 and negative controls over time indicate its applicability to detect and quantify production of biologically-generated NO, in a high-throughput format using a 96-well microtiter plate. However, some aspects related to this methodology are worth-mentioning. As opposed to gas-phase chemiluminescence, DAF-2T is a proxy for evaluating NO production from *N. eutropha* D23, and this not a direct method for detecting NO. Formation of DAF-2T (Figure 3.28 below) relies upon the initial production of a nitrosative intermediate, N_2O_3, which is generated in solution due to the autoxidation reaction of NO with O_2. Nitrosation of DAF-2 by N_2O_3 produces therefore its triazole derivative, which is fluorescent.

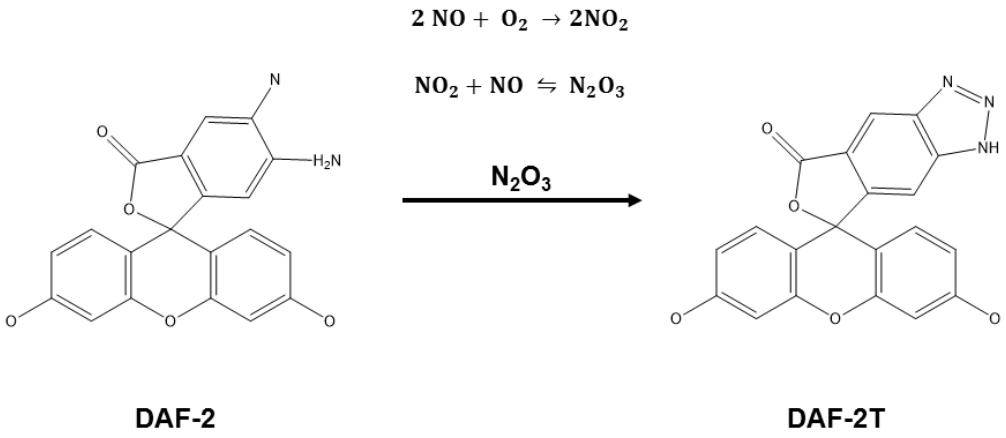

Figure 3.28 Schematic representation of the nitrosation of DAF-2 to DAF-2T. This reaction is possible due to the generation of N_2O_3 derived from the autoxidation of NO in solution, under aerobic conditions.

Due to the dependence on the generation of this nitrosative agent, the concentrations of DAF-2T reported in figures 3.16 and 3.17 may well be underestimated. Despite allowing relatively long kinetic assessments of NO produced by the bacteria, the use of this method for routine measurements of NO is prohibitive, due to the cost of an authentic DAF-2T standard, here used for calibration of the fluorescence signal.

Abiotic NO_2^- and CPTIO were incorporated in a series of control experiments (Figure 3.16), aimed at confirming specificity of *N. eutropha* D23-derived NO on the signals observed for DAF-2T. Although no interference of NO_2^- with NO detected with DAF-2 was expected on chemical grounds, this metabolite was incorporated due to the high concentrations of NO_2^- generated by *N. eutropha* D23 that could potentially influence the fluorescence signal for DAF-2T, as high concentrations of NO_2^- could conceivably generate NO chemically. As expected, NO_2^- did not interfere with the measurement of NO using DAF-2. On the other hand, the results indicated a rise in the concentration of DAF-2T for *N. eutropha* D23 when incubated in the presence of CPTIO, which is particularly evident for the initial time readings (panel B, Figure 3.18). By introducing an NO scavenger in the system, no rise in the concentration of nitrosated product was anticipated; however, the results obtained are in agreement with the nitrosative reaction for the detection of DAF-2T, and the mechanism of action of CPTIO, which generates increased amounts of NO_2 upon scavenging NO from solution (Goldstein, Russo and Samuni, 2003), according to chemical reactions 3.4 and 3.5 below. Despite the increased levels of DAF-2T, these are transient during the first 90-120 min of incubation, although chemistry does not explain the reduction in DAF-2T formation after this period.

(3.4) $\mathrm{NO} + \mathrm{CPTIO} \rightarrow \mathrm{NO_2} + \mathrm{cPTI}$

(3.5) $\mathrm{NO_2} + \mathrm{NO} \leftrightharpoons \mathrm{N_2O_3}$

As opposed to the detection of NO via nitrosation of DAF-2, the OxyHb capture assay allows direct detection of NO generated in solution. Production of NO from *N. eutropha* D23 was evaluated by incubating the bacteria with a fixed concentration of freshly-prepared oxyHb, at three different NH_4^+ concentrations. Fresh stock solutions of oxyHb were prepared and their quality assessed by looking at expected features on its full spectra, as shown in Figure 3.19. As production of NO by *N. eutropha* D23 was found to be continuous during ammonia oxidation, repetitive scans were taken in cycles over an entire period of 1 h, at 37 °C, in M9 medium. The results obtained (figures 3.20 and 3.22) indicate that production of NO occurs with live *N. eutropha* D23, and its dependence on the concentration of NH_4^+ is in agreement with previous observations already made. By looking at the difference spectra for the three concentrations of substrate, it is seen that rates of production of NO are higher for higher concentrations of NH_4^+, i.e., its production is faster at 10 and 25 mmol L^{-1} NH_4^+. Even though slight changes in the absorbance are observed for heat-killed *N. eutropha* D23 assayed in the presence of OxyHb, these are interpreted due to the oxidation of oxyHb to metHb in solution in ambient conditions, rather than a phenomenon caused by the inactive bacterial suspension.

3.9.6 Stress responses in *N. eutropha* D23

An evaluation of the stress responses of *N. eutropha* D23 to two molecules was also carried out. This exploratory study aimed at assessing the effects of an NO scavenger (Figure 3.23) and a nitrification inhibitor (Figure 3.24) on the canonical ammonia oxidation pathway, whose effects have not been determined for this particular strain. This evaluation was guided by the recent interest in better understanding the mechanism of ammonia oxidation, namely the role of NO in this pathway. Caranto & Lancaster (2017) have recently postulated that NO_2^- formation in ammonia-oxidisers occurs via mandatory production of NO, derived from NH_3 oxidation, using purified enzymes. Figure 1.4 (Chapter 1, page 35) already takes this into consideration.

The role of NO in *N. eutropha* D23 was evaluated by exposing live cells to CPTIO. By doing so, some metabolic variances were initially expected, as compared to growing cultures in the absence of CPTIO. If indeed NO is an obligate intermediate in ammonia oxidation, then scavenging it from *N. eutropha* D23 will lead to a decrease in NO_2^-

formation and concomitant accumulation in the growing cultures. According to the results, no major changes in the growth pattern of these cells are evident from the pH of the growing cultures over time. However, at a metabolic perspective, some differences are seen. Contrary to what was initially expected, NO_2^- was found at higher concentrations (mean values) at 120 h for CPTIO-exposed *N. eutropha* D23, as compared to control. A slight decrease in NO_2^- concentration is only seen shortly after addition of CPTIO, although not significant, as compared to control cultures. Accumulation of NO_3^- is visible in the growth medium, and its trend of accumulation is visible after 24 h post-CPTIO addition, reaching higher concentrations in cultures exposed to this molecule as well. It is also observed that incorporation of CPTIO in the growing cultures also led to modification of the intracellular concentration of ATP, whose effects are seen immediately after addition of CPTIO. As suggested by the data, the decrease in the ATP pool is dependent on the concentration of CPTIO. Interruption of intracellular formation of NH_2OH is also observed, whose values abruptly drop after addition of CPTIO to the cultures.

Based on these results, it could be hypothesised that introduction of CPTIO to growing cultures of *N. eutropha* D23 damages their ability to harvest energy from ammonia, by removing NO from the catabolic pathway. As suggested by the intracellular measurement of ATP, this perturbation is only temporary, as *N. eutropha* D23 seem to later overcome the induced stress, by continuing production of ATP at comparable rates as control cultures. Even though a slight decrease in the rate of NO_2^- production occurs during the initial time when CPTIO is introduced into the system, *N. eutropha* D23 increase their rate of NO_2^- production to possibly counteract the damage induced by introducing CPTIO (i.e. by removing NO). Interestingly, the rate of NH_4^+ consumption is higher and evident for cultures exposed to the two highest concentrations of CPTIO assayed, shortly after its introduction in the system; this also supports a strategy to counteract the effects caused by introduction of CPTIO. To verify the above, the experiment in the presence of CPTIO should be repeated at even higher concentrations of CPTIO, and other NO scavengers (e.g. oxyHb) assayed.

Growing cultures of *N. eutropha* D23 were also exposed to varying concentrations of ATU, a chemical agent that acts downstream within the ammonia oxidation pathway, on the AMO enzyme. The results here presented are in agreement with other research (L Y Juliette, Hyman and Arp, 1993*; Shen et al*., 2013). As compared to control, differences in ATU-exposed cultures are observed particularly from 72 h onward, i.e. 24 h upon addition of ATU. According to pH, NO_2^- and intracellular ATP measurements, metabolism of *N. eutropha* D23 is affected by the presence of ≥ 1 µmol L^{-1} ATU, although the effects are clearly more pronounced for cultures exposed to 100 µmol L^{-1} ATU. Intracellular NH_2OH measurements were not conducted due to time constraints, but interestingly it was

detected in the extracellular compartment, as evident by the absorbance change for cultures also exposed to 100 µmol L^{-1} ATU.

3.10 Conclusion

Expected features in the metabolism of ammonia-oxidisers were confirmed for *N. eutropha* D23, an AOB strain currently used for application on the human skin, namely production of NO_2^- via consumption of NH_4^+ in liquid cultures. Energy-starved *N. eutropha* D23 showed a striking and reproducible ability to respond quickly to addition of substrate, and were thus used for the characterisation of the metabolic phenotype of *N. eutropha* D23.

Evidence for NO production by *N. eutropha* D23 was confirmed with gas-phase chemiluminescence, which subsequently was the elected methodology for assessing quantitatively production of NO during aerobic ammonia oxidation. These results were further validated by using independent techniques for NO detection (nitrosation of DAF-2 and OxyHb capture assay). Biotic production of NO is found to be influenced by temperature, pH and concentration of substrate available for oxidation. Under the experimental conditions used, *N. eutropha* D23 exhibited maximal production of NO (0.3-0.4 fmoles NO $cell^{-1}$) at 37-40 °C, in storage medium prepared at pH 8.0, for a concentration of substrate of 25 mmol L^{-1} NH_4^+, with 35.5-70.95x10^5 *N. eutropha* D23 cells mL^{-1}.

Production of NO and NO_2^- are correlated, and a comparison between the levels of NO_2^- produced between purged and non-purged incubations of suspended *N. eutropha* D23 revealed that aeration exerted an impact on the overall amounts of the main metabolic product of these bacteria, in line with earlier reports. An exploratory study on the stress responses of *N. eutropha* D23 to CPTIO and ATU suggests that interference either at initial stages of ammonia oxidation or by removing NO from the bacteria exerted overall a negative impact on the energy-generating pathway in *N. eutropha* D23. While the effects of CPTIO are transitory and discrete under the experimental conditions here chosen, they potentially support the production of NO_2^- via mandatory production of NO, as suggested by Caranto & Lancaster (2017), and (Zart, Schmidt and Bock, 2000). Upon exposure to ATU, NH_2OH was found to be released into the extracellular compartment, even though reproducibility and validation were not further assessed.

Chapter 4

Bioactivity towards Pseudomonas aeruginosa biofilms

Chapter 4: Bioactivity towards *Pseudomonas aeruginosa* biofilms

4.1 Overview

It is widely recognised that bacteria can exist as free-floating, single-cell microorganisms (planktonic phenotype) or form complex, multicellular communities (biofilm phenotype). Biofilms are defined as communities of sessile bacterial cells enclosed together within a self-produced extracellular polymeric substance (EPS), and can be found attached onto surfaces or colonising biotic substrata, i.e., human tissues (Bjarnsholt, 2013; Flemm*ing et al.*, 2016). Even though microbial aggregates were firstly observed by Antonie van Leeuwenhoek in 1684 by studying specimens collected from his mouth, the field of biofilm research only started to grow within the last decades (Hoiby, 2017).

The biofilm cycle (see Figure 4.1) is canonically described as a series of sequential events, which include the initial colonisation by attachment of planktonic cells to a surface or substratum, followed by coalescence and maturation of the communities (or colonies), and finally by active dispersal of the cells from the biofilm (O'Toole, Kaplan and Kolter, 2000; Kaplan, 2010; Römling and Balsalobre, 2012). Dispersal is a pivotal stage in the cycle, as reversal to a planktonic state allow bacteria to colonise new environmental niches and initiate therefore a new cycle.

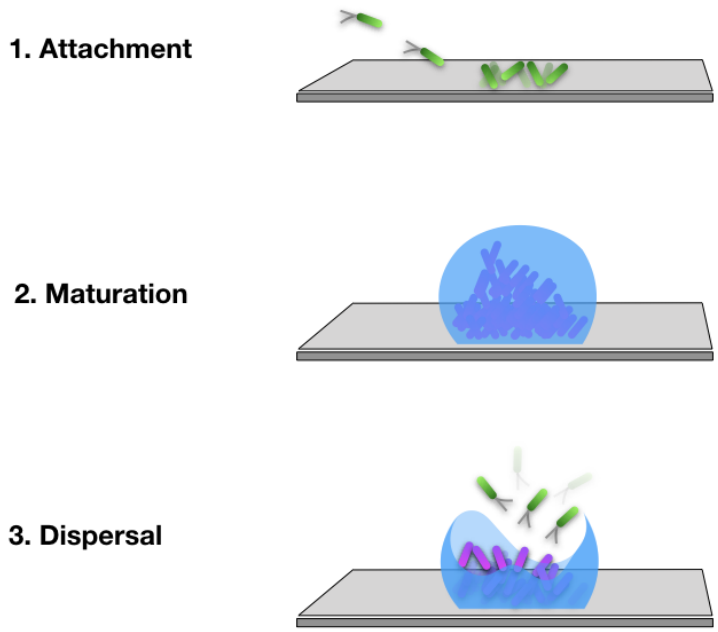

Figure 4.1 Schematic representation of the stages involved in the biofilm cycle. Adapted from O'Toole et al. (2000).

When bacteria coalesce together in biofilms, they exhibit a different phenotype compared to their planktonic counterparts (Donlan and Costerton, 2002). A sessile mode of growth is seen as advantageous to microorganisms, as biofilm growth allow bacteria to thrive by persistent attachment, as well as provide them with enhanced resistance to host-defence mechanisms. Furthermore, it is estimated that bacteria in biofilms exhibit a 1000-fold increase in tolerance to antimicrobials, as compared to the susceptibility of their planktonic counterparts, making biofilms recalcitrant to available antimicrobial therapies (Musk and Hergenrother, 2006; Bar*raud et al*., 2015).

It is estimated that up to 80% of the microbial infections are associated with formation of biofilms (Rasamiravaka *et al*., 2015), thus impacting mortality and morbidity rates with additional economic burden on the global health system for treating biofilm-associated infections. Biofilms have been found in medical devices (e.g. catheters, prosthetic valves, and contact lenses), but have also contributed to the pathogenesis of several human diseases. For instance, biofilms of the opportunist *Pseudomonas aeruginosa* are often collected from lung epithelia of patients suffering from cystic fibrosis, or colonise chronic skin wounds (Bjarnsholt, 2013; Lebeaux *et al.*, 2013; Romling *et al.*, 2014; Tolker-Nielsen, 2014). Strategies to tackle microbial biofilms are a matter of extensive investigation. Due

to their recalcitrance, which renders drug therapies ineffective and unsafe for patients, biofilm regulation-based approaches seem promising (Kaplan, 2010).

For example, predominant research in the field has been based on interfering with intracellular signalling with *P. aeruginosa* biofilms, ultimately leading to enhanced biotic dispersal of *P. aeruginosa* cells from the biofilm to a planktonic state, therefore mimicking the last stage of the biofilm cycle. These biological events are regulated by tightly-controlled molecular signalling and fairly well understood. Some environmental cues have been suggested to trigger the dispersal of *P. aeruginosa* biofilms, including nutritional deficiencies, oxygen depletion and free radicals, second messengers, and quorum sensing (Karatan and Watnick, 2009).

NO functions as a highly conserved signalling molecule across biological systems, and in recent years, it has been implicated in enhancing biofilm dispersal phenomena across a plethora of bacteria (Barraud et al. 2015). Foundational groundwork has been laid by Barraud et al. (2006), whose research has demonstrated enhanced dispersal events in *P. aeruginosa* biofilms upon exposure to low levels of NO, provided through sodium nitroprusside (SNP), as an NO donor. Similar effects have also been demonstrated for multi-species biofilms of gram-negative, gram-positive and fungal microorganisms of clinical and technological relevance, upon exposure to SNP and S-nitrosothiols, and increases in susceptibility to antimicrobials were reported as well (Barraud *et al*., 2009). Different sources for exogenous delivery of NO have been used, ranging from the classical NO donors SNP and NO-releasing NONOates (Barnes *et al.*, 2013), furoxanes (Poh *et al.*, 2017), as well as hybrid molecules containing antimicrobial drugs and NO moieties, such as polymers and nanoparticles (Craven *et al.*, 2016; Nguyen *et al.*, 2016; Adnan *et al.*, 2018).

4.2 Aims

Based on previous evidence linking low levels of NO to dispersal phenomena in *P. aeruginosa* biofilms, along with findings regarding the production of NO by *N. eutropha* D23, it was herein hypothesised that co-culturing established *P. aeruginosa* biofilms with live suspensions of *N. eutropha* D23, as a biological mean to deliver NO, would lead to dispersal of *P. aeruginosa* biofilms. Biofilms are thus regarded as a tool to assess whether the amounts of NO produced by *N. eutropha* D23 are of sufficient quantity to have a meaningful bioactivity. The aims and specific objectives are as follows:

Aim 1 – To evaluate the occurrence of *P. aeruginosa* biofilm dispersal upon co-culture with *N. eutropha* D23.

A.1. To evaluate the occurrence of biofilm dispersal and the feasibility of a microtiter plate-based methodology for its applicability in formation and co-culture of *P. aeruginosa* biofilms;

A.2. To determine the outcome of co-culturing *P. aeruginosa* biofilms with *N. eutropha* D23, using crystal violet (*P. aeruginosa* biofilm biomass) and colony counts (planktonic *P. aeruginosa*) as readout assays;

A.3. To assess biofilm dispersal and to define statistically significant differences between co-cultured *P. aeruginosa*, and control *P. aeruginosa* biofilms;

B. **Aim 2** – To evaluate and distinguish which *N. eutropha* D23-derived metabolite(s) are responsible for the dispersal effect seen in *P. aeruginosa* biofilms.

B.1. To assay a panel of relevant metabolites with *P. aeruginosa* biofilms;

B.2. To confirm the involvement of *N. eutropha* D23-derived NO using NO scavengers, during co-culture with *N. eutropha* D23;

C. **Aim 3** – To translate the effect of co-culturing clinically-relevant *P. aeruginosa* isolates with *N. eutropha* D23.

C.1. To screen clinical isolates for translation effects, and to define dispersal events by assessing statistically significant differences in biomass.

4.3 Biofilm biomass reduction after co-culture with *N. eutropha* D23

The initial experimental activities described in this section were carried out to evaluate the effect of co-culturing two different bacterial species. The methodology herein used allowed the growth of *P. aeruginosa* biofilms in a batch-wise fashion, and the high-throughput assessment of dispersal events derived from the co-incubation of these biofilms with *N. eutropha* D23.

As it was described in the previous chapter, metabolite production by *N. eutropha* D23 is dependent on the availability of substrate. That is, NO and NO_2^- production are dependent on the concentration of ammonium. As such, the effect of NH_4^+ on *P. aeruginosa* biomass was primarily assessed, when in co-culture with *N. eutropha* D23. Biofilms were grown as described, and treated with *N. eutropha* D23 for 4 h, at 37 °C. Co-culture occurred in M9 medium, with and without supplementation with 5 mmol L^{-1} NH_4^+. The results are shown in Figure 4.2 below.

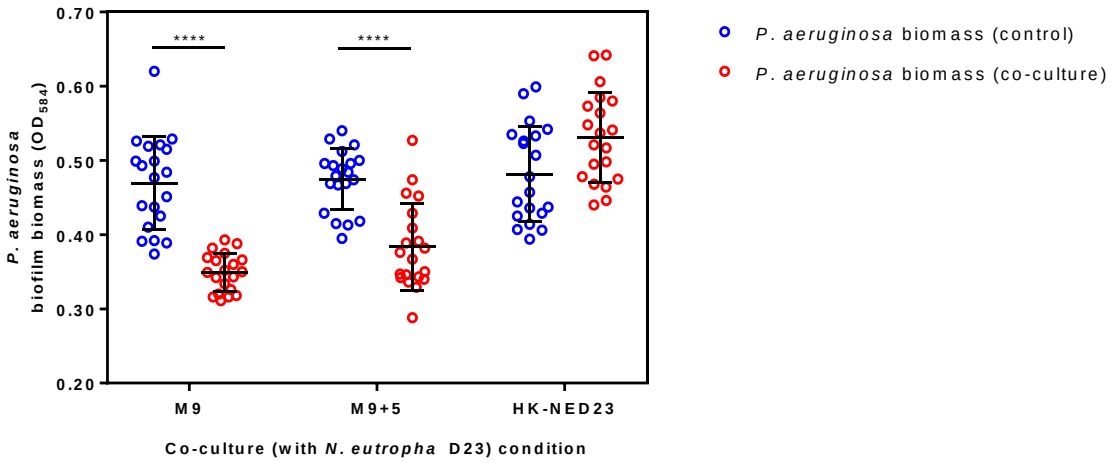

Figure 4.2 Dispersal of *P. aeruginosa* biofilms upon co-culture with *N eutropha* D23, in M9 medium (M9) and its supplementation with 5 mmol L^{-1} NH_4^+ (M9+5). Heat-inactivated *N. eutropha* D23 (HK-NED23) were used as a negative control. Statistical differences were assessed by unpaired *t*-test (****p<0.0001), at 95% confidence level. Numerical dataset is presented in Table C.1 (Appendix C).

Regardless of the experimental condition (NH_4^+ supplementation vs no supplementation), significant reductions ($p<0.0001$) in *P. aeruginosa* biofilm biomass were observed, as determined by the absorbance of crystal violet collected. Moreover, reduction in *P. aeruginosa* biomass was maximal for co-culture conditions occurring under conditions of no NH_4^+ supplementation, with ~26% less biomass after 4 h of co-culture; whereas ~19% in biomass reduction was observed for co-cultures in M9 medium supplemented with 5 mmol L^{-1} NH_4^+. No significant differences were seen for *P. aeruginosa* biofilms treated with heat-killed *N. eutropha* D23. Based on these results, further experiments were conducted in M9 medium, relying solely on the NH_4^+ concentration already present in this medium (7-10 mmol L^{-1} NH_4^+), which was enough to elicit significant changes in *P. aeruginosa* biofilms.

N. eutropha D23 were next inoculated in M9 medium, assessed using the same methodology as before and under similar conditions to follow production of NO_2^- for 8 h, in absence of *P. aeruginosa* biofilms on the surface the immersed pegs. The results are shown in Figure 4.3 below.

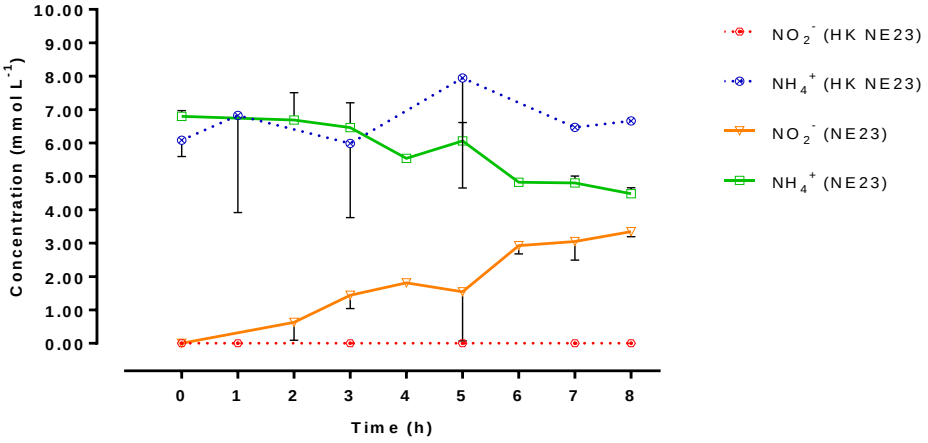

Figure 4.3 NO_2^- formation and NH_4^+ consumption by *N. eutropha* D23 (NE23). Heat-inactivated *N. eutropha* D23 (HK NE23) were used as a negative control. Data presented as mean±SD (for each time point, n=1-2).

As expected, an overall decrease in the concentration of NH_4^+ and increase in NO_2^- in M9 medium were observed, during the entire incubation period. Both formation and consumption of these metabolites resembled a linear trend over time. At 4 h of incubation (standard duration of co-culture, as done before), NO_2^- reached a concentration of 1.81±0.12 mmol L^{-1}. In parallel, nearly 18.4% of the initial concentration of NH_4^+ was

consumed within 4 h of incubation, reaching a concentration of 5.54±0.09 mmol L^{-1} (Δ = -1.25 mmol L^{-1} NH_4^+). Heat-inactivated *N. eutropha* cells neither consumed NH_4^+ nor produced NO_2^-.

The levels of NO_2^- produced by live *N. eutropha* D23 cells during the initial 4 h phase of this study were used as a basis for treating *P. aeruginosa* biofilms with a wide range of concentrations of abiotic NO_2^- (the main metabolite of ammonia oxidation by *N. eutropha* D23), NO_3^- or NO_X (NO_2^- and NO_3^-, the combination as breakdown metabolites of NO). The results from these experiments are shown in Figure 4.4, and were carried out to investigate which metabolite, or combination of metabolites, are responsible for the biomass reduction effect on *P. aeruginosa*, as observed previously.

A

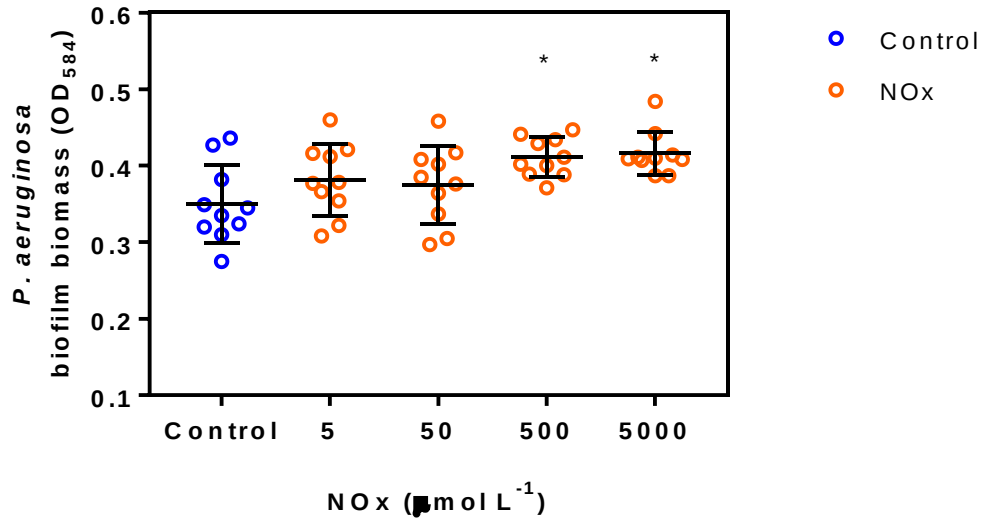

B

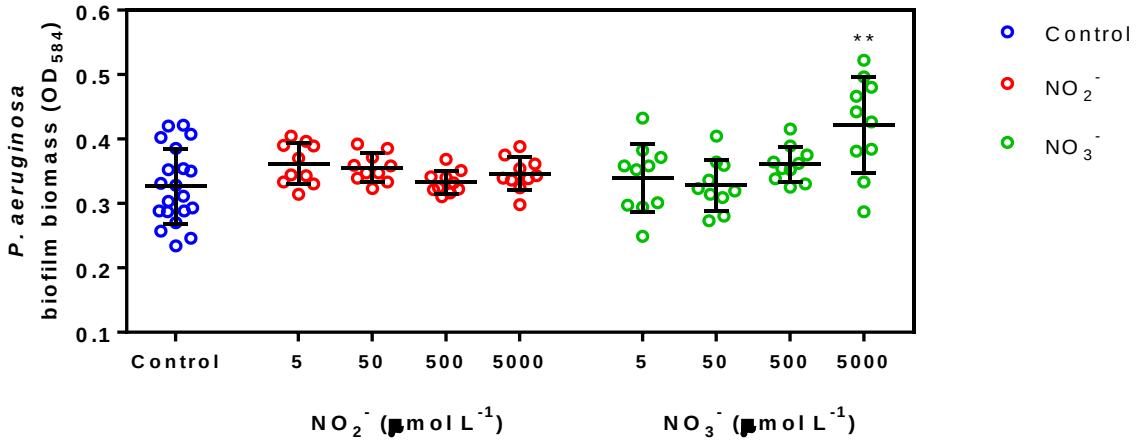

Figure 4.4 The effect of combined NOx (A) and individual NO_2^- or NO_3^- (B) on *P. aeruginosa* biofilm biomass. Data is presented as mean±SD (n=10). Statistical differences were assessed by Kruskal-Wallis (Dunn's correction, *p<0.05, **p<0.005,), at 95% confidence level. Numerical dataset presented in Tables C.2 and C.3 (Appendix C).

No reductions in *P. aeruginosa* biofilm biomass were observed when treating biofilms with an equimolar combination of NO_2^- and NO_3^- (NOx, panel A), from 5 to 500 µmol L^{-1} NOx. However, for higher concentrations of NOx (500 and 5000 µmol L^{-1} NOx), statistically significant increases in *P. aeruginosa* were seen, as compared to control. As such, biofilms were treated with the same concentrations as above, although using either NO_2^-

or NO_3^- alone (panel B) to allow differentiation of the effects seen with the combination (NOx).

According to the data, no appreciable changes in *P. aeruginosa* biofilm biomass were observed for any of the concentrations of abiotic NO_2^- assayed. For NO_3^-, significant differences (p=0.0029) were only seen for *P. aeruginosa* biofilms treated with the highest concentration. This positive difference indicates an increase in biofilm attached on the surface of the immersed peg when high amounts of NO_3^- are present, and this metabolite is likely the responsible for the increase in *P. aeruginosa* biofilm biomass when treated with NOx.

To evaluate the role of biotic *N. eutropha* D23-derived NO on *P. aeruginosa* biofilms, the same methodology was used, and *N. eutropha* D23 were incubated in the presence of an NO scavenger (CPTIO, 0.3 and 1.3 mmol L^{-1}), whose presence in M9 medium allowed scavenging of the NO produced during the co-culture with *N. eutropha* D23. The results are shown in Figure 4.5 below.

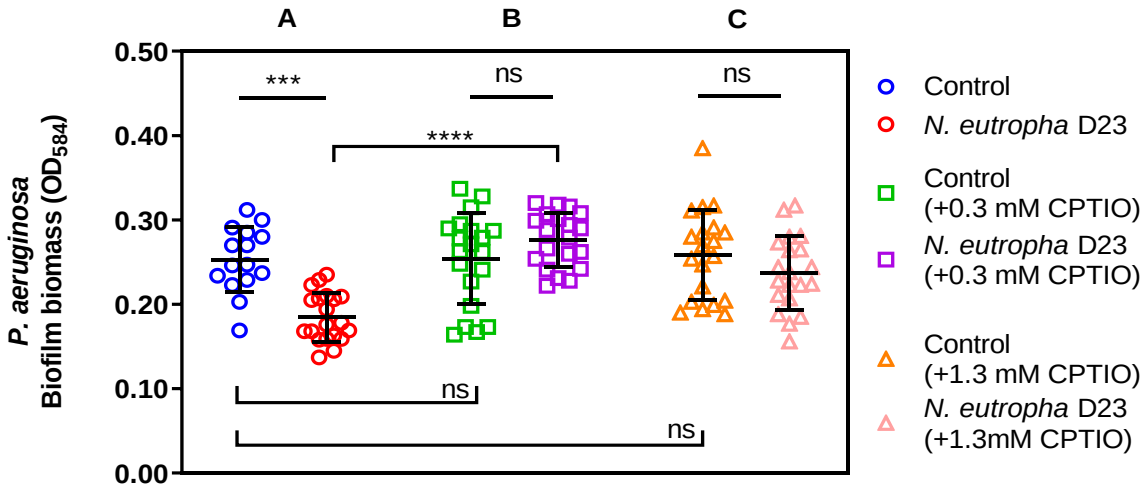

Figure 4.5 The effect of biotic NO on *P.* aeruginosa biofilm dispersal, in the presence and absence of an NO scavenger, CPTIO. Data is presented as mean±SD (n=15-20). Statistical differences were assessed by Kruskal-Wallis (Dunn's correction, (***p=0.0008), at 95% confidence level. Numerical dataset is presented in Table C.4 (Appendix C).

As seen above, co-culture with live *N. eutropha* D23 cells (A) were responsible for a 26.9% reduction in *P. aeruginosa* biofilm biomass, as compared to controls; coincidentally, an identical reduction in percentage is seen in Figure 4.2, for the same *N.*

eutropha D23 and medium. As compared to control biofilms (controls in A, B, and C), CPTIO itself (at both concentrations) did not exert any significant effect on *P. aeruginosa* biofilms. However, when *P. aeruginosa* biofilms were treated with *N. eutropha* D23 in the presence of CPTIO (B and C), no significant changes occurred in *P. aeruginosa* biofilm biomass. This data suggests that NO produced by *N. eutropha* D23 during co-culture was a key metabolite responsible for the reduction in *P. aeruginosa* biofilm biomass. Further mechanistic studies assumed the role of NO on *P. aeruginosa* biofilms, and aimed at a more detailed characterisation of the interaction between both species when in co-culture.

4.4 Establishment of a cell-dependent effect on biofilm biomass reduction

To evaluate the effect of cell density, *P. aeruginosa* biofilms were treated with varying cell densities of *N*. eutropha D23, in M9 medium, using identical conditions as before. Results are shown in Figure 4.6 below.

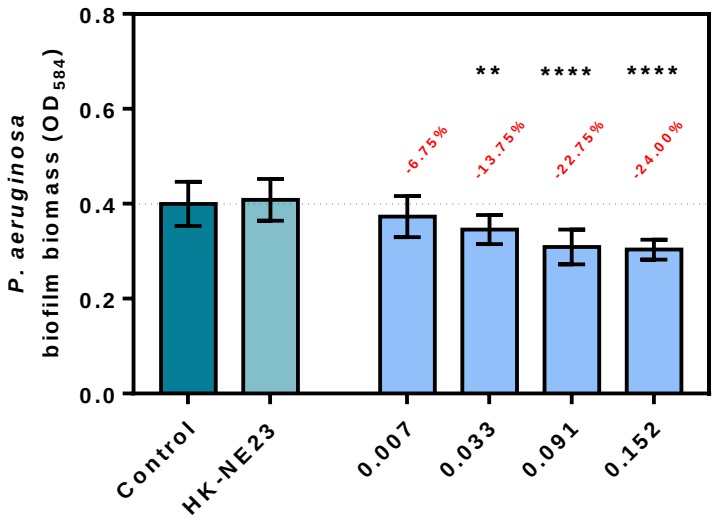

Figure 4.6 Dispersal of *P. aeruginosa* biofilms upon co-culture with *N. eutropha* D23 (varying cell densities, OD_{584}), in M9 medium, for 4 h. Data is reported as mean±SD (n=30), from 3 technical replicates. Statistical differences were assessed by Kruskal-Wallis (Dunn's correction, **p<0.005, ****<0.0001), at 95% confidence level. Numerical dataset is presented in Table C.5 (Appendix C). HK-NE23: heat-killed *N. eutropha* D23.

As seen, and as compared to control, only live and metabolically-active *N. eutropha* D23 exerted effects on *P. aeruginosa* biofilm biomass. No significant effects were seen when treating biofilms with heat-killed *N. eutropha* D23. Such decreases in biomass after co-culture followed a dependence on the density of *N. eutropha* D23 present within the system. Co-culture at the three highest *N. eutropha* D23 cell densities (reported as optical densities in the graph) exhibited maximal and significant effects, with reductions of 15.6% (OD_{600}=0.033, p=0.0015), 24.7% (OD_{600}=0.091, p<0.0001), and 26.1% (OD_{600}=0.152, p<0.0001). Although 8.9% reduction in biofilm biomass was observed for biofilms treated with the lowest density of *N. eutropha* D23 assayed (OD_{600}=0.007), it was not statistically significant (p=0.4577).

4.5 The influence of co-culture duration

Despite the reduction in *P. aeruginosa* biofilm biomass after co-culture, which achieved a maximal reduction of 26.1% with the highest *N. eutropha* D23, further experiments were carried out to evaluate the impact of co-culture duration on improving or enhancing the reduction of *P. aeruginosa* biofilms. It was hypothesised that the longer the co-culture duration, the higher the reduction in *P. aeruginosa* biofilm biomass, possibly due to the production and accumulation of metabolic products (NO and NO_2^-) derived from *N. eutropha* D23's activity. Biofilms were therefore treated with the same *N. eutropha* D23 cell suspensions as above, using two different co-culture durations. The results for an 8 h co-culture are shown in Figure 4.7 below.

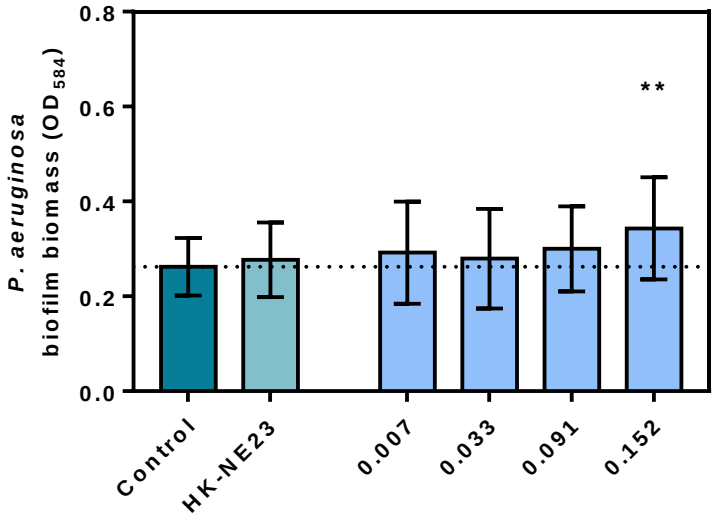

Figure 4.7 Dispersal of *P. aeruginosa* biofilms upon co-culture with *N. eutropha* D23 (varying cell densities, OD_{584}), in M9 medium, for 8 h. Data is reported as mean±SD (n=28-30), from 3 technical replicates. Statistical differences were assessed by Kruskal-Wallis (Dunn's correction, **p=0.0084), at 95% confidence level. Numerical dataset is presented in Table C.6 (Appendix C). HK-NE23: heat-killed *N. eutropha* D23.

Overall, results showed no *P. aeruginosa* biomass reduction after co-culture with *N. eutropha* D23 when increasing the duration of co-culture, from 4 to 8 h. This observation was contrary to what was previously seen and initially hypothesised. That is, no further reduction in biofilm biomass was achieved by increasing the co-culture duration. Compared to control, *P. aeruginosa* biofilm biomass increased across all *N. eutropha* D23 cell densities assayed. The results also suggest an increasing trend in biofilm biomass formation dependent on the *N. eutropha* D23 density, as higher biofilm biomasses were observed for co-cultures with higher *N. eutropha* D23 densities; with a significant change in biomass for *P. aeruginosa* biofilms treated with the highest *N. eutropha* D23 cell density (OD_{600}=0.152, p=0.0084).

From this dataset, it was also observed that *P. aeruginosa* biofilms did not grow at a similar biomass as before, as less biofilm was actually formed on the surface of the pegs as compared to the previous experiment. This is particularly evident when looking at the mean biomass values for control *P. aeruginosa* biofilms between figures 4.6 and 4.7 (0.3997 and 0.2624, respectively).

Even though the effect was lost for longer co-culture durations, the initial assumption was followed, and biofilms were treated for an interim duration of 6 h, an additional 2 h from the standard duration. Results are shown in Figure 4.8 below.

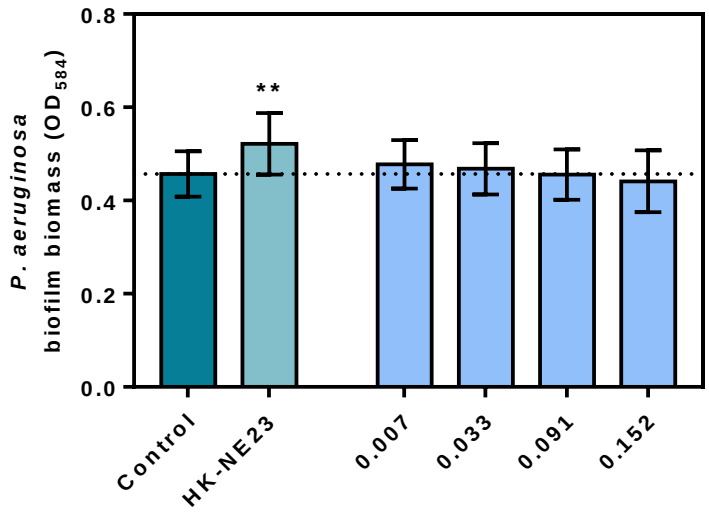

Figure 4.8 Dispersal of *P. aeruginosa* biofilms upon co-culture with *N. eutropha* D23 (varying cell densities, OD_{584}), in M9 medium, for 6 h. Data is reported as mean±SD (n=30), from 3 technical replicates. Statistical differences were assessed by Kruskal-Wallis (Dunn's correction, **p=0.0011), at 95% confidence level. Numerical dataset is presented in Table C.7 (Appendix C). HK-NE23: heat-killed *N. eutropha* D23.

Consistent with previous results (Figure 4.7), co-culturing for 6 h did not lead to any appreciable changes in *P. aeruginosa* biofilm biomass. Even though a downward trend in biofilm biomass was apparent with increasing *N. eutropha* D23, the results failed to provide any statistical differences in treated biofilms, as compared to control. Unexpectedly, a significant increase in *P. aeruginosa* biomass was observed for those biofilms treated with heat-killed *N. eutropha* D23 (p=0.0011). To explain this discrepancy, the lack or loss of biofilm biomass reduction could potentially be due to loss of *N. eutropha* D23 metabolic activity during long incubation periods with *P. aeruginosa*.

P. aeruginosa biofilms were treated in a modified manner. Using the same *N. eutropha* D23 cell densities as above and for a total duration of 6 h. *N. eutropha* D23 were replenished by preparing and changing the co-culture plates with fresh live suspensions every 2 h (3 co-culture plates in total). The results are shown in Figure 4.9 below.

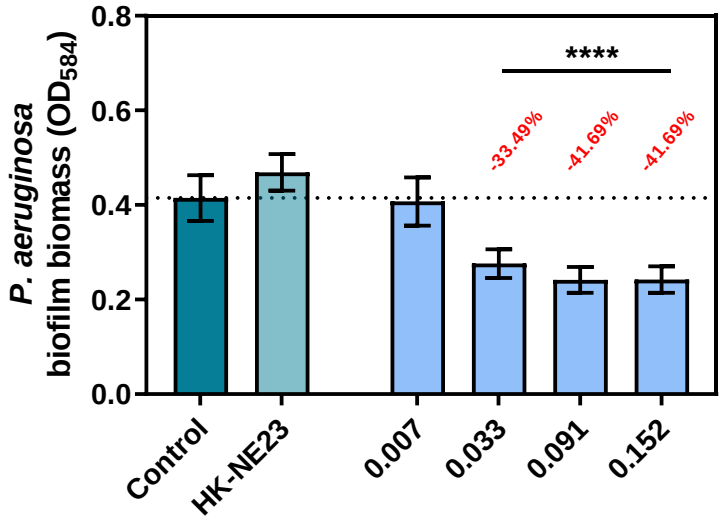

Figure 4.9 Dispersal of *P. aeruginosa* biofilms upon co-culture with *N. eutropha* D23 (varying cell densities, OD_{584}), in M9 medium, for 6 h with co-culture plates replaced every 2 h. Data is reported as mean±SD (n=30), from 3 technical replicates. Statistical differences were assessed by Kruskal-Wallis (Dunn's correction, ****p<0.0001), at 95% confidence level. Numerical dataset is presented in Table C.8 (Appendix C). HK-NE23: heat-killed *N. eutropha* D23.

Under the new conditions, significant reductions in biomass were observed from *P. aeruginosa* biofilms treated with live *N. eutropha* D23; an evident observation for biofilms treated with the highest *N. eutropha* D23 cell densities. By replenishing *N. eutropha* D23 every 2 h, for a total period of 6 h, the reduction effect initially seen for *P. aeruginosa* biofilms was re-established. More interestingly, and compared to the results shown in Figure 4.6 (obtained for a 4 h co-culture), the percentages of biomass reduction were higher, with 32.9% (OD_{600}=0.033), 41.2% (OD_{600}=0.091), and 41.3% (OD_{600}=0.152) less biofilm on the surface of the pegs after co-culture with *N. eutropha* D23. Although the metabolic status of *N. eutropha* D23 has not been directly examined, the results suggest that increased reductions in *P. aeruginosa* biofilm biomass can be achieved with longer co-culture durations, provided that fresh *N. eutropha* D23 are introduced into the system at regular intervals.

In addition to the biomass determinations, colony counts for planktonic *P. aeruginosa* were also determined, as an additional parameter to study the dynamics of biofilm dispersal. At the end of each co-culture experiment, the contents of each co-culture plate were pooled for each *N. eutropha* D23 density assayed, serially diluted and spot-plated on

cetrimide agar plates for colony counts. The results are shown below in figures 4.10 (panels A and B for 4 and 8 h of co-culture, matching results described in figures 4.6 and 4.7, respectively) and Figure 4.11 (6 h of co-culture with regular replenishment, matching results described in Figure 4.9).

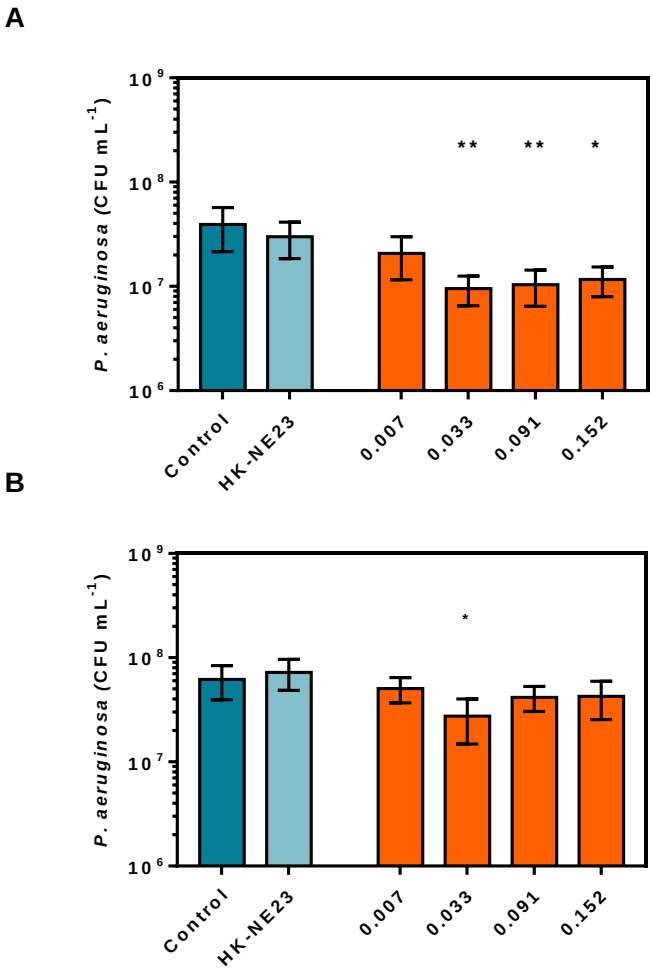

Figure 4.10 Colony counts (CFU mL^{-1}) for planktonic *P. aeruginosa* dispersed upon co-culturing biofilms with *N. eutropha* D23 (varying cell densities, OD_{584}), in M9 medium, for (A) 4 h and (B) 8 h. Data is reported as mean±SD (n=6), from 3 technical replicates. Statistical differences were assessed by Kruskal-Wallis (Dunn's correction, *p<0.05, **p<0.01), at 95% confidence level. Numerical datasets for panels A and B are presented in tables C.9 and C.10, respectively (Appendix C). HK-NE23: heat-killed *N. eutropha* D23.

Overall, no appreciable changes in the numbers of *P. aeruginosa* collected after co-culture with heat-killed *N. eutropha* D23 were seen, as compared to control biofilms.

However, some changes in the number of *P. aeruginosa* colonies were seen for biofilms treated with live *N. eutropha* D23. For a co-culture duration of 4 h (panel A), significant decreases in CFU mL^{-1} as compared to control ($3.93x10^7 \pm 1.78x10^7$ CFU mL^{-1}) were found for biofilms treated with *N. eutropha* D23 at OD_{600}=0.033 ($9.53x10^6 \pm 3.02x10^6$ CFU mL^{-1}, p=0.0015), OD_{600}=0.091 ($1.04x10^7 \pm 3.70x10^6$ CFU mL^{-1}, p=0.0060), and OD_{600}=0.152 ($1.17x10^7 \pm 3.70x10^6$ CFU mL^{-1}, p=0.0122).

The number of colonies collected from the experiments carried out at 8 h of co-culture (panel B) were generally higher than those collected from a 4 h duration. Compared to control *P. aeruginosa* biofilms ($6.17x10^7 \pm 2.21x10^7$ CFU mL^{-1}), significant reductions in the colony numbers were only seen for biofilms treated with *N. eutropha* D23 at OD_{600}=0.033 ($2.75x10^7 \pm 1.26x10^7$ CFU mL^{-1}, p=0.0198); however, for the remaining treated biofilms, data suggest a trend towards a decrease in the number of *P. aeruginosa* colonies after co-culture with *N. eutropha* D23.

For biofilms treated for 6 h, with changes of co-culture plates (Figure 4.11 below), identical numbers of *P. aeruginosa* (controls) were found after 4 and 6 h of co-culture ($5.10x10^6 \pm 1.56x10^6$ and $5.70x10^6 \pm 4.24x10^5$ CFU mL^{-1}). Even though no significant changes were observed across all *N. eutropha* D23 densities, as compared to controls, the mean number of colonies indicated that higher CFU mL^{-1} were only observed after co-culturing for 2 h (first co-culture plate change).

Moreover, after 2 h of co-culture, the number of *P. aeruginosa* collected as planktonic fraction seemed to follow a dependence on the density of *N. eutropha* D23 used for those experiments; consistent with crystal violet results. However, for the remaining plates, CFU seemed to decrease in numbers, which suggests that fewer viable *P. aeruginosa* cells were collected from the wells, after either 4 or 6 h of co-culture.

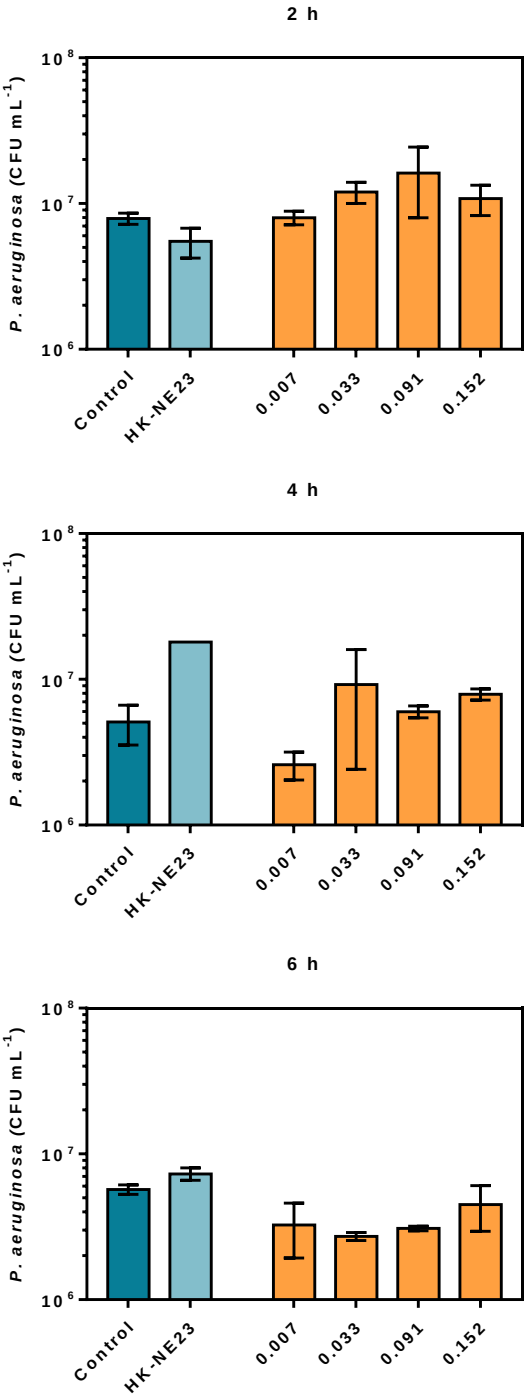

Figure 4.11 Colony counts (CFU mL^{-1}) for planktonic *P. aeruginosa* dispersed upon co-culturing biofilms with *N. eutropha* D23 (varying cell densities, OD_{584}), in M9 medium, for 6 h, with change of the co-culture plates every 2 h. Results are shown at the end of 2, 4, and 6 h. Data is reported as mean±SD (n=1-2). Statistical differences were assessed by Kruskal-Wallis (Dunn's correction), at 95% confidence level. Numerical dataset is presented in Table C.11 (Appendix C). HK-NE23: heat-killed *N. eutropha* D23.

4.6 Screening of *P. aeruginosa* clinical isolates

All previous experimental work in this chapter on *P. aeruginosa* biofilm dispersal using biologically-produced NO was carried out with a laboratory strain (PAO1). The same methodology was used to form and treat 17 different *P. aeruginosa* isolates (Table 2.4, page 61), collected from patients with cystic fibrosis, with the ultimate goal of investigating whether the effect (biomass reduction) could be translated to samples of clinical origin, which exhibit different phenotypes as compared to PAO1.

For that, biofilms were grown as before on the surface of a transfer-peg lid, and treated with a fixed *N. eutropha* D23 cell density, for 4h. For determining the outcome of the co-culture, only measurements based on crystal violet were performed. The results from this screening are shown in Figure 4.12 below.

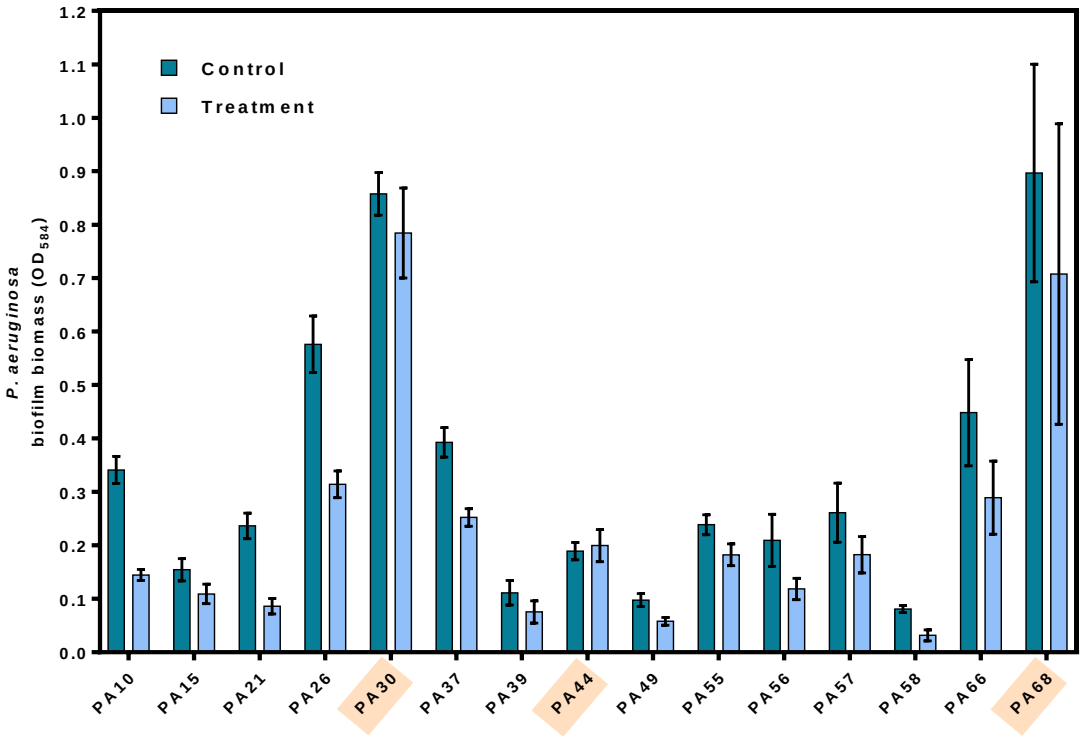

Figure 4.12 Dispersal of *P. aeruginosa* biofilms (clinical isolates, obtained from patients with cystic fibrosis). Data is presented as mean ±SD (n=10), from 2 technical replicates. Statistical differences were assessed by unpaired *t*-test (Holm-Sidak's correction), at 95% confidence level. Non-significant changes in *P. aeruginosa* biofilm biomass (p>0.05) are highlighted at the bottom of the graph. Numerical dataset is presented in Table C.12 (Appendix C).

Ability to form biofilms on the surface of the pegs was observed for 15 out of 17 *P. aeruginosa* isolates, even though at different biomass yields among these and as compared with PAO1. PA08 and PA20 did not seem to form biofilm under the experimental conditions applied, and were therefore omitted from the figure.

The co-culture of these biofilms with *N. eutropha* D23 also revealed that the effect previously seen with PAO1 was translated to different isolates of the same species. Significant reductions in *P. aeruginosa* biofilm biomass were seen for 12 out of 17 clinical isolates assayed, with varying degrees of biomass reduction compared to the respective control biofilms. The clinical isolates and the percentage of biomass reduction are as follows: PA10 (-57.6%), PA15 (-29.3%), PA21 (-63.6%), PA26 (-45.5%), PA37 (-35.8%), PA39 (32.2%), PA49 (-40.7%), PA55 (-23.6%), PA56 (-43.4%), PA57 (-30.2%), PA58 (-61.0%), and PA66 (-35.4%).

4.7 Biofilm dispersal assessment by confocal microscopy (pilot)

P. aeruginosa (PAO1) biofilms were grown on the surface of MatTek plates, and co-cultured with a fixed density of *N. eutropha* D23 for a standard 4-h co-culture duration. For multiple technical replicates (i.e. one MatTek plate), three to four area sections were randomly selected for imaging and further subjected to image processing, using Comstat 2.0 (Heydorn *et al*., 2000; Vorregaard, 2008), for biomass and surface coverage measurements. Figure 4.13 below show maximal projections for control and *P. aeruginosa* biofilms upon co-culture with *N. eutropha* D23. These cells remained attached after co-culturing with *N. eutropha* D23 and successive washing steps.

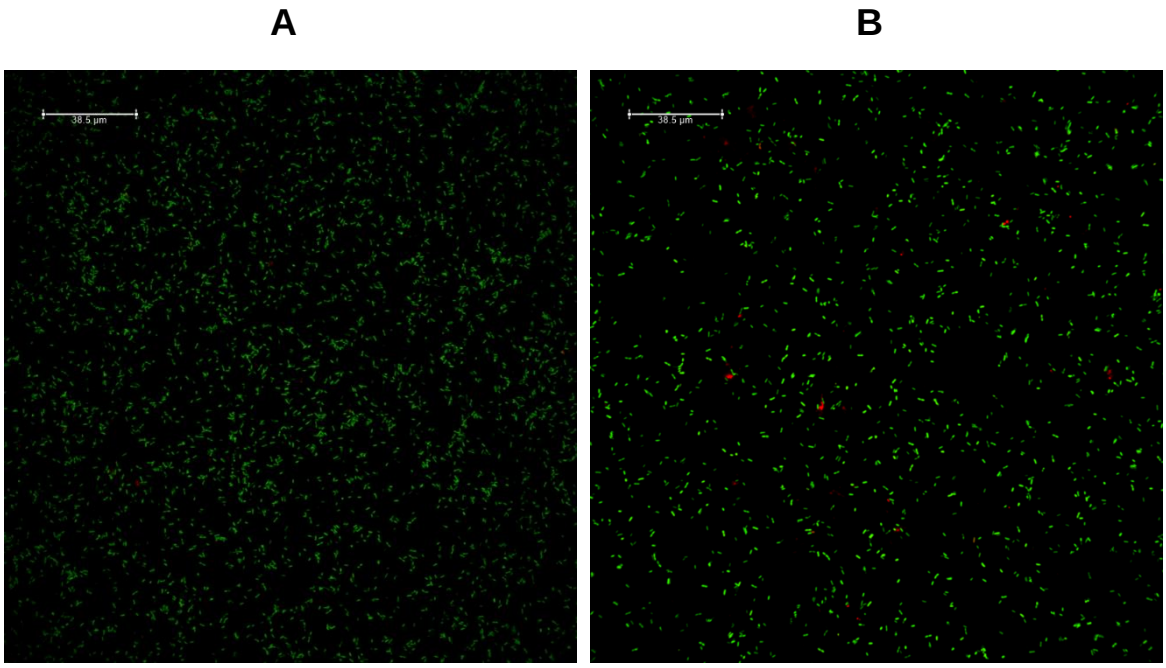

Figure 4.13 Maximal projections (representative) of *P. aeruginosa* biofilm attached on the surface of the MatTek plate, (A) before and (B) after 4 h of co-culture with *N. eutropha* D23.

Overall, as observed from the figure above, confocal microscopy showed formation of *P. aeruginosa* biofilms on the surface of a coated glass slide, placed inside a MatTek plate. The section shown in panel A is a representative of biofilm formed after 3 days of growth, under the experimental conditions chosen. It is observed relatively good confluence of *P. aeruginosa* cells, as seen in the green and red channels related to live and dead *P. aeruginosa* cells, respectively. After co-culturing with *N. eutropha* D23 (panel B), and as

compared to untreated biofilms, *P. aeruginosa* cells remain attached onto the glass slide, even though at a lower density. Comstat 2.0 software was used to analyse a set of stacks of images for measuring biomass and surface attachment of *P. aeruginosa* biofilms, before and after co-culture. The results for this statistical assessment are shown in Figure 4.14 below.

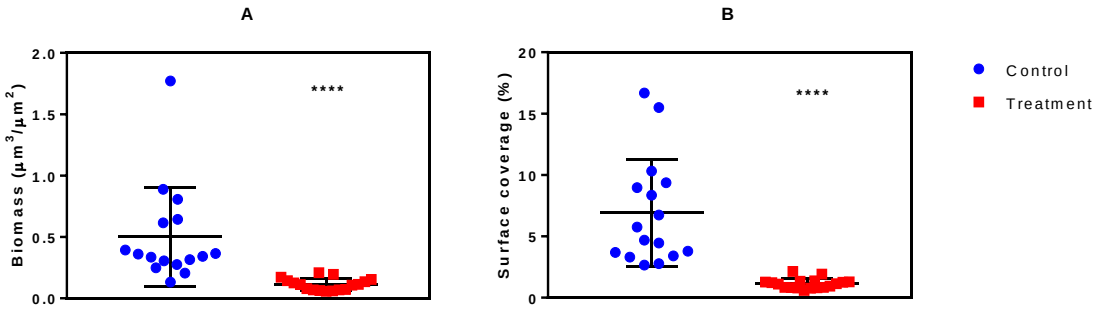

Figure 4.14 Statistical summary from processing the confocal images, using Comstat 2.0 software package (3-4 random areas per plate, for a total of 6 plates). Biomass (A) and surface coverage (B) were two parameters measured for untreated and treated *P. aeruginosa* biofilms.

Variability in the total biomass and surface coverage were observed for the image sections subjected to image processing. Overall, co-culture led to significant decreases in both parameters measured, as compared to untreated biofilms.

4.8 Discussion

A simple methodology was used for high-throughput formation of *P. aeruginosa* biofilms on the surface of a transfer-peg lid, which also provided easy co-culture of these biofilms with suspensions of *N. eutropha* D23. This system is depicted in Figure 4.15 below to help visualising *P. aeruginosa* biofilms grown on the surface of a peg, which protrudes down from the lid and fits a 96-well microtiter plate.

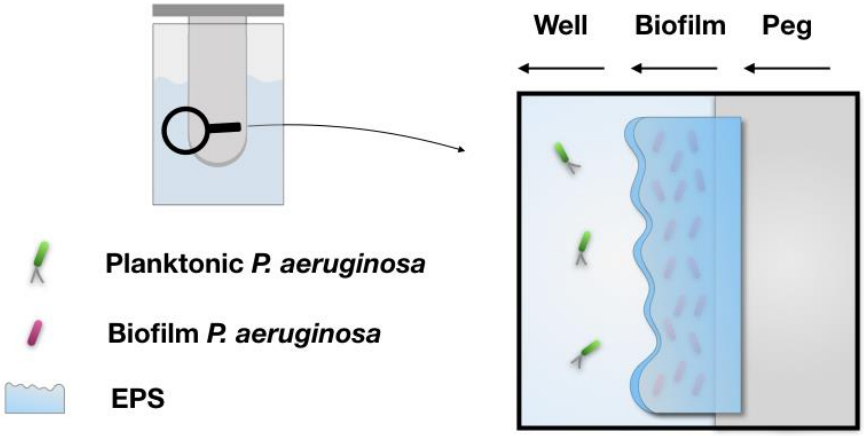

Figure 4.15 Schematic representation of the system used for growth and co-culture of *P. aeruginosa* biofilms with *N. eutropha* D23. Biofilms are formed on the surface of a peg-lid (only one represented). A magnification of the peg shows the compartments for *P. aeruginosa* planktonic (well) and biofilm (peg).

Repeatability and reproducibility across technical replicates could only be ensured by growing and treating a maximum of 60 independent biofilms per batch/peg-lid. Preliminary experiments indicate limitations, which demonstrated that biofilms grown in the outer pegs did not grow at comparable biomass with those grown in the middle of the peg-lid. Therefore, strategies to mitigate this issue were followed (Wenderska *et al.*, 2011) and adaptations to the experimental protocol were applied for growth of *P. aeruginosa* biofilms. These modifications included filling of the outer perimeter wells of the microtiter plate with sterile PBS (standard template according to Figure 4.16 below), and an increase in the number of technical replicates (peg-lid) per experiment.

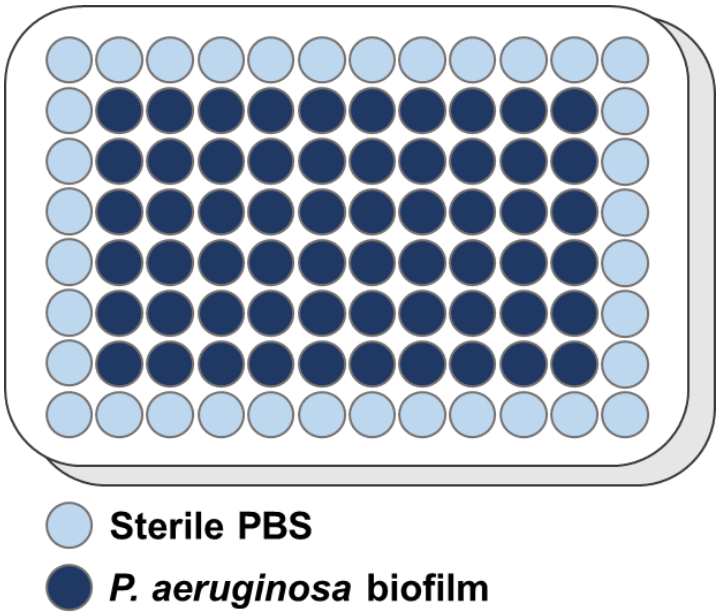

Figure 4.16 Microtiter plate template for *P. aeruginosa* biofilm growth in batches. Peripheral wells of the microtiter plate are filled with sterile PBS to mitigate microtiter plate edge effect.

As seen previously, production of metabolites by *N. eutropha* D23 follow a dependence on certain factors, specifically, the availability or concentration of ammonium for oxidation. Supported by these findings and by evidence that NO is involved in *P. aeruginosa* biofilm dispersal, the next experimental activities were carried out to elucidate the effects of co-culturing both species. At this point, it was initially hypothesised that co-culturing live suspensions of *N. eutropha* D23 with pre-established *P. aeruginosa* biofilms would lead to the dispersal of the latter species, likely due to the production of NO by *N. eutropha* D23. Beyond this assumption, it was also thought that a higher concentration of NH_4^+ in M9 medium would lead to enhanced biofilm dispersal.

To test this, *P. aeruginosa* biofilms were grown as already described, and immersed in live suspensions of *N. eutropha* D23, under conditions of no medium supplementation, and with 5 mmol L^{-1} NH_4^+ supplementation. For this experiment, *N. eutropha* D23 were collected directly from the commercial product, and used in the microtiter plate/peg-lid system at half the cell density as compared to the commercial product. Based on the results shown in Figure 4.2, some considerations can be made. Firstly, it was observed that indeed co-culture with suspensions of *N. eutropha* D23 led to a statistically significant reduction (~26%, $p<0.0001$) in *P. aeruginosa* biomass after 4 h, as indicated by

measurement of the intensity of the crystal violet attached on the peg, that relates to the biomass that remained attached on the peg after co-culture (an example of biofilms stained with crystal violet is presented in Figure D.1, Appendix D).

Furthermore, the results also show that *P. aeruginosa* biofilm dispersal was dependent on the viability of *N. eutropha* D23. Besides confirmation of the expected outcome, it could also be seen that low NH_4^+ supplementation (M9+5) did not lead to increased differences in biofilm biomass, as compared to those biofilms treated under conditions of no supplementation. Therefore, based on these findings, all further biofilm experiments were conducted in M9 medium, whose commercial composition contains 19 mmol L^{-1} NH_4^+. However, due to the experimental conditions chosen, the net concentration of ammonium available as substrate for *N. eutropha* D23 during co-culture was expected to be around two-fold less (i.e. ~ 9.5-10 mmol L-1 NH_4^+), due to the introduction of *N. eutropha* D23 cell suspensions.

The absence of a dispersal effect on *P. aeruginosa* biofilms when treated with heat-killed suspensions of *N. eutropha* D23 suggests that metabolites produced by the latter could be responsible for the effects elicited when treating biofilms with live, metabolically-active *N. eutropha* D23. As such, live suspensions of *N. eutropha* D23 were inoculated in M9 medium to ascertain metabolic activity within the system used and at the specific experimental conditions, in the absence of *P. aeruginosa*. According to the results depicted in Figure 4.3, *N. eutropha* D23 were able to oxidise the available NH_4^+ to millimolar NO_2^- levels, consistent with the findings from the previous chapter. Even though NO was not measured in this system, its production was assumed during co-culture of both species, as previous experiments had shown its production and accumulation in M9 medium, as measured by nitrosation of DAF-2 and oxyHb assay (figures 3.17 and 3.20, respectively).

The levels of NO_2^- accumulated in M9 medium during the first 4 h of incubation (standard co-culture duration) were used as a basis for treating *P. aeruginosa* biofilms with a range of abiotic nitrogen monoxides, in control experiments carried out to elucidate which metabolites could potentially be involved in *P. aeruginosa* biofilm dispersal during co-culture with *N. eutropha* D23. Authentic NO_2^- (the main metabolic product of ammonia oxidation) and NO_3^- (breakdown product of oxidative NO metabolism), as well as their combination ($NOx = NO_2^- + NO_3^-$) were therefore assayed as potential dispersal agents.

The results from Figure 4.4 suggest that neither of the oxyanions tested, individually or in combination, could explain the biotic dispersal effect when biofilms were treated with *N. eutropha* D23, and were therefore ruled out as potential dispersal agents. While addition of abiotic NO_2^- did not exert any changes in biofilm biomass, as compared to untreated

biofilms, NO_3^- led to increased *P. aeruginosa* biomass attached onto the surface of the pegs. In this experiment (Figure 4.4, panel B), the high quantities of NO_3^- in M9 medium could have potentially enhanced denitrification activity, as *P. aeruginosa* can use NO_3^- as a terminal electron acceptor (Yoon *et al*., 2002; Line *et al*., 2014).

Similar findings have been described by other researchers focused on enhancing dispersal of *P. aeruginosa* biofilms upon exposure to abiotic NO sources. For instance, Barraud et al. (2006) provided evidence for enhanced biofilm dispersal when treating pre-established *P. aeruginosa* biofilms with a range of concentrations (25 nmol L^{-1} to 100 mmol L^{-1}) of sodium nitroprusside, an NO donor. While biofilm dispersal was observed for low concentrations of the NO donor, increases in *P. aeruginosa* biofilm biomass were seen for biofilms treated at millimolar concentrations of sodium nitroprusside. The authors suggest that the increase in *P. aeruginosa* biofilm biomass seen in their work could have derived from increased anaerobic respiration, due to the increased generation and accumulation of NO_3^- in the medium.

Finally, a last iteration in this series of control experiments included the incorporation of an NO scavenger in order to scavenge biotic NO produced by *N. eutropha* D23 during co-culture. CPTIO was used as an NO scavenger due to its high solubility in aqueous media (Maeda *et al*., 1994), whose mechanism of action entails the conversion of NO to NO_2 (nitrogen dioxide). In the presence of CPTIO, no change in *P. aeruginosa* biofilm biomass is expected, based on previous literature linking NO to dispersal phenomena in *P. aeruginosa* biofilms, and based on the fact that *N. eutropha* D23 is able to produce NO.

As expected, and according to Figure 4.5, the introduction of CPTIO during co-culture led to a complete abrogation of the dispersal effect that was previously seen for *P. aeruginosa* biofilms treated with metabolically-active *N. eutropha* D23. These results therefore confirm the pivotal role NO plays in modulating dispersal in *P. aeruginosa* biofilms, in agreement with findings described in literature; and provided additional evidence that *N. eutropha* D23-derived NO (rather than its oxidation products) was the metabolite responsible for the dispersal of *P. aeruginosa* biofilms; quantities of which were sufficient to elicit bioactivity. Based on the results obtained, a visual summary is depicted in Figure 4.17 below to show the outcome of co-culture of *P. aeruginosa* biofilms with live *N. eutropha* D23.

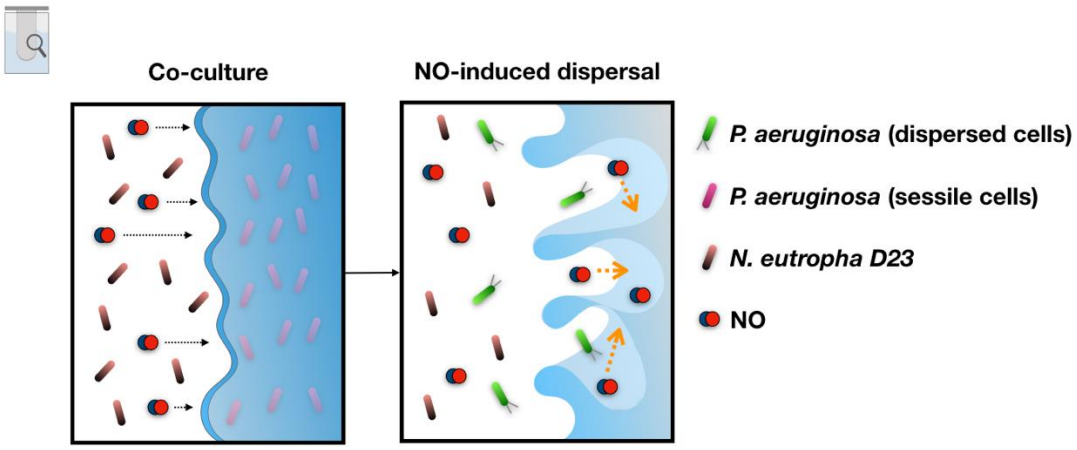

Figure 4.17 Schematic representation of the events suggested to occur within *P. aeruginosa* biofilms during co-culture with *N. eutropha* D23. Production of NO by *N. eutropha* D23 leads to dispersal of *P. aeruginosa* biofilms.

The remaining experimental procedures in this chapter were carried out to characterise in more detail the dispersal phenomena derived from the interaction between both species, when in co-culture. In this series of characterisation experiments, *P. aeruginosa* biofilms were initially treated with a series of *N. eutropha* D23 cell densities (lower densities than used before), for 4 h, in order to establish a cell-dependent dispersal effect.

The results in Figure 4.6 showed that dispersal of *P. aeruginosa* biofilms corresponded to an effect dependent on the density of *N. eutropha* D23 present in the co-culture plate during the incubation period. As seen, increasing densities of *N. eutropha* D23 led to increasing reduction in biofilm biomass, indicative of *P. aeruginosa* biofilm dispersal; an observation likely explained by the increasing amounts of NO generated by higher numbers of *N. eutropha* D23. Even though statistically significant reductions in biofilm biomass were seen for those conditions, means to enhance further biomass reduction were sought, e.g. by increasing the duration of co-culture. By assuming continuous production of NO by *N. eutropha* D23 throughout the co-culture period, it seemed sensible to hypothesise that a longer duration would lead to higher amounts of NO generated and, therefore, enhanced dispersal of *P. aeruginosa* biofilms.

The hypothesis above was examined by treating *P. aeruginosa* biofilms for 8 and 6 h, and the results are depicted in figures 4.7 and 4.8, respectively. Overall, and contrary to the initial expectations, no reductions in biofilm biomass were seen, as compared to those for a standard 4 h of co-culture. In fact, increases in *P. aeruginosa* biofilm biomass were observed for a duration of 8 h; an effect that seemed dependent on the number of *N.*

eutropha D23. For a 6 h of co-culture, no major changes in biofilm biomass were found for those treated with *N. eutropha* D23, even though an apparent trend in biomass reduction was observed for biofilms treated with higher densities of *N. eutropha* D23.

If production of NO by *N. eutropha* D23 was continuous over the entire co-culture period, then higher amounts of NO should have been produced over 6 and 8 h, as compared to those generated over a standard 4 h of co-culture. Although contrary to what was expected initially, these results reinforced the previous suggestion that an increase in *P. aeruginosa* biofilm biomass could potentially be related to the accumulation of breakdown products of NO during co-culture (NO_3^-) that would then favour growth of biofilm through anaerobic respiration. If indeed growth of *P. aeruginosa* biofilm was enhanced by breakdown metabolites of NO, it was then presumed that an opposite effect would happen by replacing the co-culture plate for extended experimental periods.

The results presented in Figure 4.9 shed some light on this matter. *P. aeruginosa* biofilms were treated again for 6 h, but introducing fresh *N. eutropha* D23 in the system at regular intervals, every 2 h. This time period was chosen to allow enough time for plate processing between changes of the co-culture plates. In doing so, at the end of each 2 h, the wells of the co-culture plate were replaced with fresh M9 medium, and hence any metabolic products generated from previous co-culture would be discarded. Overall, the results showed that for the three highest *N. eutropha* D23 cell densities assayed, significant reductions in *P. aeruginosa* biofilm biomass were seen. By replacing the co-culture plate during an extended period of time, the effect (biofilm dispersal) that was seen previously was also recovered for a 6 h of co-culture. Furthermore, biomass reductions were even higher than those seen for a standard 4 h of co-culture.

Dispersal of *P. aeruginosa* biofilms upon co-culture with *N. eutropha* D23 was primarily evaluated according to the intensity of crystal violet, whose determination indicates the biomass that was left on the peg after co-culture. In addition to this parameter, that looked at the *P. aeruginosa* fraction on the peg (biofilm biomass), colony counts (CFU mL^{-1}) were determined for the *P. aeruginosa* planktonic fraction (i.e. *P. aeruginosa* cells that shed from the biofilm/peg to the microtiter plate), in order to evaluate dispersal phenomena after co-culture. This was carried out based on the assumption that higher numbers of planktonic *P. aeruginosa* cells would be present in the co-culture wells, compared to control wells (*P. aeruginosa* and PBS), due to the higher numbers of *P. aeruginosa* that shed off from the biofilm into the microtiter plate.

To verify further this, *P. aeruginosa* colony counts were performed after co-culture with *N. eutropha* D23, for 4 and 8 h of duration, by collecting the volumes from the co-culture plate and plate them on agar. Cetrimide agar was herein chosen for colony counting, as it

is a selective medium for *P. aeruginosa*. The results in Figure 4.10 indicate the CFU mL^{-1} specifically for the planktonic fraction of *P. aeruginosa*. As observed, the number of *P. aeruginosa* cells recovered after co-culture with *N. eutropha* D23 were less than the respective controls; an opposite observation as to what was initially expected. Significant decreases in CFU counts were found for both co-culture durations (4 and 8 h), which were more pronounced for a 4-h period, across the three highest *N. eutropha* D23 cell densities.

Planktonic *P. aeruginosa* CFU mL^{-1} were also evaluated for biofilms treated for 6 h, with changes of the co-culture plate. Interestingly, higher *P. aeruginosa* colony counts were only found after the first 2 h of co-culture, with decreasing colonies seen for the remaining time-points measured throughout the experiment. Despite this observation, it allowed verification of the initial assumption that higher numbers of *P. aeruginosa* cells would be collected after co-culture remained true, at least during its early duration. By looking at the colony counts at 2, 4, and 6 h, the results potentially suggest disruption of the biofilm occurs during initial times of co-culture, as higher *P. aeruginosa* cells were collected after shedding off the biofilm. As a possible response, further reorganisation of the biofilm may have occurred, potentially explaining the decrease in colony counts of the *P. aeruginosa* planktonic fraction. To match both fractions, that is, biofilm and planktonic *P. aeruginosa* cells, biomass measurements at the end of 2 and 4 h could have been conducted.

Even though no statistically significant differences were found, the downward trend in colony counts for *P. aeruginosa* could have derived from either of the following reasons. Poor sample homogeneity could have introduced error in measurement, influencing the results obtained. Despite recognising this possibility, samples were thoroughly vortexed before being spot-plated on cetrimide agar. As colony counting is sensitive to viable bacteria, the decrease in CFU mL^{-1} could have resulted from bactericidal phenomena to planktonic *P. aeruginosa* cells, as a consequence of co-culturing with *N. eutropha* D23; or co-culture could have induced phenotypic changes that rendered *P. aeruginosa* less prone to grow. Due to time constrains, viability of *P. aeruginosa* cells could not be evaluated further.

Although direct comparisons are difficult to make, the results herein described are not in agreement with past evidence in the literature, as different methodologies for *P. aeruginosa* biofilm growth and treatment were used, as well as different NO sources. For example, when looking at the planktonic fraction upon exposure of *P. aeruginosa* biofilms to 500 nmol L^{-1} sodium nitroprusside, Barraud et al. (2006) described no significant changes or a decreasing trend in CFU mL^{-1}, as compared to untreated biofilms, and have also showed total viability of *P. aeruginosa* cells within the biofilm. Even though their study does not provide the exact biologically effective concentrations or amounts of NO that

induced *in* vivo dispersal of *P. aeruginosa* biofilms, the authors suggest that amounts of NO delivered to biofilms were 1000-fold less than the concentration of sodium nitroprusside used, and that viability of *P. aeruginosa* was not compromised upon treatment with 500 nmol L^{-1} sodium nitroprusside.

Finally, clinical isolates of *P. aeruginosa* isolated from sputa of patients suffering with cystic fibrosis were screened for dispersal phenomena upon co-culture with *N. eutropha* D23. These clinical strains were collected elsewhere and assayed for dispersal phenomena *ex vivo* using sodium nitroprusside. In a proof-of-concept clinical trial, Howlin et al. (2018) demonstrate *ex vivo* dispersal of biofilms formed by 12 of these strains upon exposure to NO, in concentrations as low as 450 nmol L^{-1} NO. As observed from the data presented in this thesis, 12 of the 17 clinical strains co-cultured with *N. eutropha* D23 led to reductions in biofilm biomass, as expected from the studies with PAO1. However, no information is available to compare whether this effect occurred for the same strains used by Howlin et al. (2018).

While co-culturing with *N. eutropha* D23 led to biomass reductions of 20-40 %, some clinical isolates exhibited a remarkable ability to disperse upon co-culture with *N. eutropha* D23, for instance, isolates PA10 (-57.61%) and PA21 (-63.55%). Even though PA58 exhibited a reduction of 61.04% as compared to the respective untreated biofilm, the initial biomass formed after growth of the biofilm was extremely low as compared to other clinical isolates, and to PAO1. The differences in biofilm-forming ability observed for *in vitro* experiments using clinical and laboratory strains could be putatively explained by differences in the phenotypic characteristics of *P. aeruginosa* strains, and have been described before (Varga *et al.*, 2015). It was envisaged to study the susceptibility of these clinical strains to antimicrobials upon co-culture with *N. eutropha* D23; however, due to time constrains, no further experimental activities were conducted.

Lastly, confocal microscopy was used in an attempt to confirm and validate the observations previously seen based on biomass determinations (i.e. measurement of crystal violet). The results from this pilot set of experiments (shown in figures 4.13 and 4.14) indicated that co-culture with *N. eutropha* D23 leads to dispersal of pre-established *P. aeruginosa* biofilms. However, some strong drawbacks are recognised in this set of experiments. Due to time constrains, only a few number of technical replicates were analysed and subjected to image processing, with very limited time for protocol optimisation. As observed from the statistical summary presented in Figure 4.14, *P. aeruginosa* biofilms were formed at very low biomasses. Despite allowing growth for 3 days, and following standard protocols available in the laboratory, biofilms here were formed at considerably lower biomasses than those formed by other researchers in the same laboratory, for the same experimental conditions. Experience with confocal

microscopy is also imperative to obtain high-quality images without deceiving the information shown in the images obtained, either by generation of artefacts or deletion of potentially important information. Despite the expected outcome upon co-culture with *N. eutropha* D23, the results based on confocal microscopy should thus be interpreted with caution.

4.9 Conclusion

An *in vitro* methodology was used to allow reproducible growth of *P. aeruginosa* biofilms on the surface of peg lids, and the outcome assessment (dispersal) upon co-culture with *N. eutropha* D23, an ammonia-oxidising bacterium that produces NO as part of its metabolic activity. Dispersal phenomena were observed as biofilm biomass reductions upon co-culture of both species, and overall, less than 30% reductions ($p<0.0001$) in *P. aeruginosa* biofilm biomass were observed for *P. aeruginosa* biofilms in co-culture with *N. eutropha* D23, for periods of 4 hours.

Such dispersal events seemed dependent on the number of live *N. eutropha* D23 present at the moment of co-culture, with maximal effects observed at higher *N. eutropha* D23 cell densities, which corresponded to an overall lower cell density as compared to that found within the commercial product. Enhanced *P. aeruginosa* biomass reductions (~41 %, $p<0.0001$) were observed for longer co-culture durations, albeit only when replacing the contents of the co-culture plate, mimicking repeated applications of *N. eutropha* D23 to established *P. aeruginosa* biofilms.

Experimental activities aimed at identifying the effect of three nitrogen oxides (NO, NO_2^- and NO_3^-) elucidated that *N. eutropha* D23-derived NO is the principal agent underpinning the effects observed, as this phenomenon was not seen in co-culture in the presence of an NO scavenger.

These findings ultimately demonstrate that the amounts of NO generated by *N. eutropha* D23 during ammonia oxidation and in co-culture with *P. aeruginosa* biofilms are of sufficient quantities to elicit a meaningful bioactivity, as seen for a laboratory strain and 12 clinical isolates of *P. aeruginosa*. Hence, biotic biofilm dispersal can be triggered using a natural, biological NO-generating system, such as *N. eutropha* D23.

Chapter 5

Signature profile of Nitrosomonas eutropha D23 at a human systemic level

Chapter 5: Signature profile of *Nitrosomonas eutropha* D23 at a human systemic level

5.1 Study overview

The following chapter considers the results obtained from a short and timed application of *N. eutropha* D23 (AO+ Mist™, MotherDirt™, AOBiome LLC) on the skin of disease-free volunteers, in terms of local and systemic changes in a panel of readouts for *in vivo* bioactivity.

This study was conducted as an integrative part of a parallel PhD research project led by Rfeef Yousif Alyami ("Investigation into NO emanations from adult human skin – assessing the impact of AOBiome AO+Mist application and sweating on NO emanation", IRAS ID 185688, reference 15/NI/0180, ERGO ID14838, amendment 23883), aimed at evaluating different skin sampling methods for 16S ribosomal ribonucleic acid (16S rRNA) analysis and NO emanations from the skin of healthy individuals upon addition of *N. eutropha* D23

For this particular PhD research project, further analysis of plasma samples collected from the volunteers enrolled in the aforementioned clinical study were conducted independently. In order to illustrate a more complete profile of the systemic effect of cutaneous application of *N. eutropha* D23 over 14 days, clinical parameters and circulatory biomarkers used herein have been combined from both PhD research projects.

5.2 Aims

Overall, this chapter aims to explore potential local and systemic effects following application of *N. eutropha* D23 on the skin of healthy adult volunteers. The specific aims and objectives are as follows:

Aim 1 – To evaluate changes in local skin physiology upon intervention with *N. eutropha* D23

A.1. To measure changes in skin pH and trans-epidermal water loss after application of *N. eutropha* D23 for 14 days, in specific body areas, namely foot, hand, head, and arm (inner elbow); by comparing the results with baseline assessments.

Aim 2 – To evaluate hemodynamic changes upon intervention with *N. eutropha* D23

A.2. To measure systolic and diastolic blood pressure before and after application of *N. eutropha* D23 for 14 days.

Aim 3 – To explore a potential metabolic biosignature of the application of *N. eutropha* D23 on the skin

A.3. To evaluate and to measure a panel of circulatory biomarkers related to NO status and metabolism, as well as oxidative stress and redox thiol metabolome, using the plasma samples collected from the volunteers; and to assess changes in their circulating concentrations upon intervention with *N. eutropha* D23.

5.3 Methodology

5.3.1 Ethics

Permission to proceed with the main study was given by the Northern Ireland Ethics Committee (Project IRAS ID 185688, reference 15/NI/0180) and locally by the University of Southampton (ERGO ID14838, amendment 23883), University Hospital Southampton NHS Foundation Trust (R&D CRI 0320), and Southampton Centre for Biomedical Research Facility.

5.3.2 Enrolment of participants

For this study, exclusion criteria included (a) diagnosed and active/ongoing skin disease at the time of recruitment, (b) antibiotic course (topical or oral), (c) pregnancy, and (d) cardiovascular problems. Participants were enrolled upon receiving written and informed consent to participate willingly in this study, following guidelines of the Helsinki Declaration.

5.3.3 Assessment visits

Data collection occurred in two visits, with a total time of 3 hours per visit: at recruitment (day 0, “baseline assessment” visit) and after regular application of *N. eutropha* D23 for 2 weeks (day 14, “post-AOB application” visit). Since none of the participants used AO+ Mist (MotherDirt™, AOBiome LLC) previous to this study, a test application was performed on the surface of the hand, as a safety measure to check possible local inflammatory reactions. Anthropometric data (height, weight) were collected, as well as surface skin pH and trans-epidermal water loss (TEWL). The skin phenotype and history of skin diseases and allergies were collected during baseline assessment.

5.3.3.1 pH

The skin pH of each volunteer was measured (pH 905, Courage-Khazaka Electronic, Germany) in four body areas of interest. These included foot, hand, head, and arm (inner elbow); with three measurements done per area considered. The pH electrode was stored in KCl buffer when not in use. After calibration, the pH probe was rinsed with saline and dried using low-lint tissues (Kimberly-Clark Kimtech Kimwipes ®).

5.3.3.2 Trans-epidermal water loss

Measurement of TEWL was carried out using Tewameter® TM300 (Courage-Khazaka Electronic, Germany), according to manufacturer’s instructions. This parameter was also

evaluated in the four considered areas (i.e. foot, hand, head, and arm), with 10-12 recordings per body area.

5.3.3.3 Blood collection and processing

From each volunteer, 10 mL of peripheral venous blood were collected into EDTA-containing vacutainers (BD Vacutainer®, BD). For each collection, an aliquot of whole blood was immediately treated with 10% (v/v) N-ethylmaleimide (NEM), while the remaining was left untreated. Whole blood samples were centrifuged on site at 800g for 15 min, and plasma placed into pre-rinsed cryovials. Plasma samples (NEM- and non-NEM treated) were snap frozen in liquid nitrogen, and stored at -20 °C until further analysis.

5.3.4 Plasma biomarker analysis

5.3.4.1 Plasma protein

Plasma protein (µg mL^{-1}) was measured using the Bradford assay (Pierce™ Coomassie Protein Assay Kit), according to the manufacturer's instructions, in a 96-well microtiter plate format, using a dilution factor of 80 before incubation with coomassie reagent. Protein concentration was calculated by interpolation from a calibration curve (0-2000 µg mL^{-1}, working range: 100-1500 µg mL^{-1}), using BSA as standard. The calibration curve is presented in Figure B11 (panel B), in Appendix B.

5.3.4.2 NO metabolism markers

The analysis of plasma NOx and total nitroso species were performed by Rfeef Alyami (data not published), and used herein solely as complementary data for integrated discussion with the analysis of other biomarker analysis carried out for this thesis.

5.3.4.2.1 Guanosine 3, 5-cyclic monophosphate

Plasma levels of cGMP were quantified using an enzyme-linked immunosorbent assay (ELISA, cGMP Parameter Assay Kit, R&D Systems®, Biotechne®), according to the manufacturer's guidelines for the analysis of human plasma samples. The concentration of cGMP in plasma samples was obtained from interpolation of the calibration curve (0-500 pmol mL^{-1}), using cGMP as standard, and a four parameter logistic curve-fit (SoftMax® Pro, Molecular Devices). The calibration curve is presented in Figure B8, in Appendix B.

5.3.4.2.2 NOx

NOx (i.e. NO_2^- and NO_3^-) were quantified in non-NEM treated plasma samples, using HPLC for its measurement according to local standard operating procedures, and as essentially described in sections 2.4.2.2 and 2.4.3, with minor modifications. Aliquots of plasma samples were pre-treated with methanol (1:1 ratio), immediately vortexed and allowed to stand for 15 min at room temperature, in order to precipitate plasma protein. Samples were then centrifuged at 16,100 *g*, for 20 min, at 4 °C and placed in plastic vials for measurement through HPLC (ENO-20, Eicom, Japan). NOx concentrations were calculated by interpolation of a calibration curve (0-30 µmol L^{-1} NOx), using $NaNO_2$ and $NaNO_3$ as standards. Representative examples of calibration curves for NO2- and NO3- using HPLC and the analytical platform are presented in Figures B2 and B3 (panels A and B), in Appendix B.

5.3.4.2.3 Plasma total nitroso species

The levels of RXNO were quantified in NEM-treated plasma using a methodology based on the chemiluminescence measurement of NO released upon reductive cleavage of nitroso species, in an acidic environment, and in the presence of a mixture of KI/I_2, as described elsewhere (Benzie and Strain, 1996; Feelisch *et al*., 2002). The calibration procedure followed is as described in section 2.4.4.1. A representative calibration curve is presented in Figure B4, Appendix B.

5.3.4.3 Oxidative stress markers

5.3.4.3.1 Antioxidant capacity

The ferric-reducing ability of plasma (FRAP, also known as “ferric-reducing antioxidant power) assay was used for evaluating the total antioxidant capacity of the human plasma samples. This assay (Benzie and Strain, 1996) entails the reduction of ferric (Fe^{3+}) to ferrous (Fe^{2+}) iron, and is based on the colorimetric detection (λ = 593 nm) of a Fe^{2+}-tripyridyltriazine blue complex, which is formed upon reduction from its ferric form by antioxidants present in plasma, at pH 3.6. The antioxidant capacity of plasma samples was calculated by interpolation of a calibration curve, using $FeSO_4.7H_2O$ (0-700 µmol L-1 Fe^{2+}) as standard. The calibration curve is presented in Figure B9, in Appendix B.

5.3.4.3.2 Lipid peroxidation

Three distinct parameters were measured in plasma for evaluating oxidative damage of lipid components, and used as markers of lipid peroxidation, which include the determination of malondialdehyde (MDA), 4-hydroxynonenal (4-HNE), and 8-isoprostane. The levels of 4-HNE and 8-isoprostane in plasma samples were quantified using ELISA-

based commercial kits (4-HNE Elisa Kit by Elabscience® and 8-Isoprostane Express ELISA kit by Cayman Chemical, respectively), and performed according to manufacturer's guidelines and protocols. Calibration curves (R^2 of 0.99 and 1.00 for 4-HNE and 8-isoprostane, respectively) were obtained using standards provided in the kits, and sample concentrations were interpolated from a four parameter logistic curve. Calibration curve for 4-HNE is presented in Figure B10, in Appendix B.

The thiobarbituric acid reactive species (TBARS) in a group-specific assay that mainly detects and quantifies MDA in samples, a marker for oxidative stress and a final product of oxidation of polyunsaturated fatty acids (Janero, 1990; Uchida, 2003). This assay is based on the colourimetric detection of a chromophore formed upon reaction of thiobarbituric acid (TB) and MDA, under acidic conditions and at high temperatures. Plasma samples were subjected to pre-treatment for protein precipitation, as described in section 5.3.4.2.2. After centrifugation, a supernatant aliquot was placed in 0.5-mL microtubes, and mixed with TBARS colour reagent (0.52 g TB in 100 mL of 20% CH_3COOH) immediately, in a 2:1 sample-to-reagent ratio. Microtubes were placed in a pre-heated block, and incubated for 30 min, at 90 °C. After incubation, tubes were cooled down for 10 min at room temperature, and a 50-µL aliquot was placed in a 96-well microtiter plate for measuring absorbance at 532 and 750 nm (for background correction). The concentration of MDA in samples was calculated by interpolation of a calibration curve, using a freshly-prepared MDA solution as a standard, and assayed in parallel with samples. Calibration curve for TBARS is presented in Figure B11, in Appendix B.

5.3.5 Thiol analysis

5.3.5.1.1 Total free thiols

The concentration (µmol L^{-1}) of plasma total free thiols (TFT) was determined using Ellman's reagent, according to the experimental protocol described by Koning et al. (2016). The calibration curve is presented in Figure B12, in Appendix B.

5.3.5.1.2 Redox thiol metabolome

Several circulating metabolites were considered for the analysis of the redox thiol metabolome for this cohort of participants. This panel included the analysis of free and bound metabolites such as cysteine (Cys), cysteine (CysSS), homocysteine (HCys), homocystine (HCysSS), N-acetylcysteine (NAC), oxidised (GSSG) and reduced glutathione (GSH), glutamylcysteine (GluCys), cysteinylglycine (CysGly), and sulfide. These were measured using ultrahigh-performance liquid chromatography in combination with electrospray-ionisation tandem mass spectrometry (UPLC-ESI-MS/MS), according to

details described by Sutton et al. (2018). In addition to the above-mentioned metabolites, sulphate and thiosulfate were also analysed, using ion chromatography coupled to MS (IC-MS, Dionex ICS-5000+ system, Thermo Scientific), as described by Cumpstey et al. (2019).

5.4 Data presentation and data analysis

Data sets and statistical analysis were generated using GraphPad Prism® (v7, GraphPad Software, Inc., La Jolla, CA, USA) and MetaboAnalyst 4.0 *(*Chong *et al.*, 2018). Statistical significance was assessed using paired *t*-test*.* Results were considered significant for $p<0.05$.

5.5 Participant profile

Demographic, anthropometric and participant history were collected during baseline assessment from the volunteers enrolled in this study. This information is summarised in Table 5.1.

Table 5.1 Demographic and anthropometric data for the subjects enrolled in this study. Volunteers that completed both visits, with matching plasma samples are highlighted in green. NR – not reported.
[a] Blood pressure is presented as mean of three measurements, for both systolic and diastolic pressures.

	Volunteer						
	V1	**V2**	**V3**	**V4**	**V5**	**V6**	**V7**
Age	36	25	24	29	25	27	28
Gender	Male	Female	Female	Female	Female	Female	Female
Ethnicity	Asian	White	White	White	White	White	Mixed
Weight (kg)	74.7	72.4	65.7	93.4	58.2	81.8	54.4
Height (cm)	171.6	168.6	155	162.5	173.2	172.2	154.8
Blood Pressure (Systolic/Diastolic, mmHg)[a]	105/63	114/61	131/78	109/74	113/67	126/76	104/56
Fitzpatrick skin type	4	2	1	2	1	2	1
History of skin disease	Acne	NR	NR	NR	NR	Eczema	Eczema
Allergy	No	No	Hay fever	No	Hay Fever	Asthma Hay fever	Hay fever Food allergy

A total of 7 young adult (6 female) volunteers (V1-V7) were recruited to this study (>18 years old, 24-36 year old). One volunteer (V2) withdrew before the final assessment visit, and was excluded from the analysis of circulating biomarkers. Racial backgrounds were predominantly white British (5 out of 7), the others from Asian and Mixed backgrounds and correspondingly Fitzpatrick's skin types were mainly 1-2 (Table 5.1 above). Three volunteers reported previous skin inflammatory conditions, and four had a history of airborne or food allergies.

After initial assessment, peripheral venous blood samples were processed on site (as described in 5.3.3.3) and stored for later analysis. Volunteers were given a bottle of commercial product (AO+ Mist™, MotherDirt™, AOBiome LLC), containing a live, axenic suspension of *N. eutropha* D23. Volunteers were asked to apply the bacteria twice daily for 14 days. Application was advised after morning shower and before sleeping, on specific body areas, such as hand, arm, head, and foot. Additionally, volunteers were also advised not to use regular soaps and detergent products. Instead, they were given a skin cleanser and shampoo (MotherDirt™, AOBiome LLC) to use during intervention with *N. eutropha* D23. After 14 days of application, peripheral venous blood samples were again collected at day 14 (post AOB application assessment visit). For this project, only plasma samples were analysed for a set of parameters to explore potential systemic metabolic signatures of the application of *N. eutropha* D23 on the skin of healthy human volunteers.

5.6 Effect of the intervention on the skin – pH and trans-epidermal water loss

For both visits, measurement of the pH of the surface of the skin of the volunteers was carried out in specific body areas (hand, head, arm, and foot). The results are shown in Figure 5.1 below.

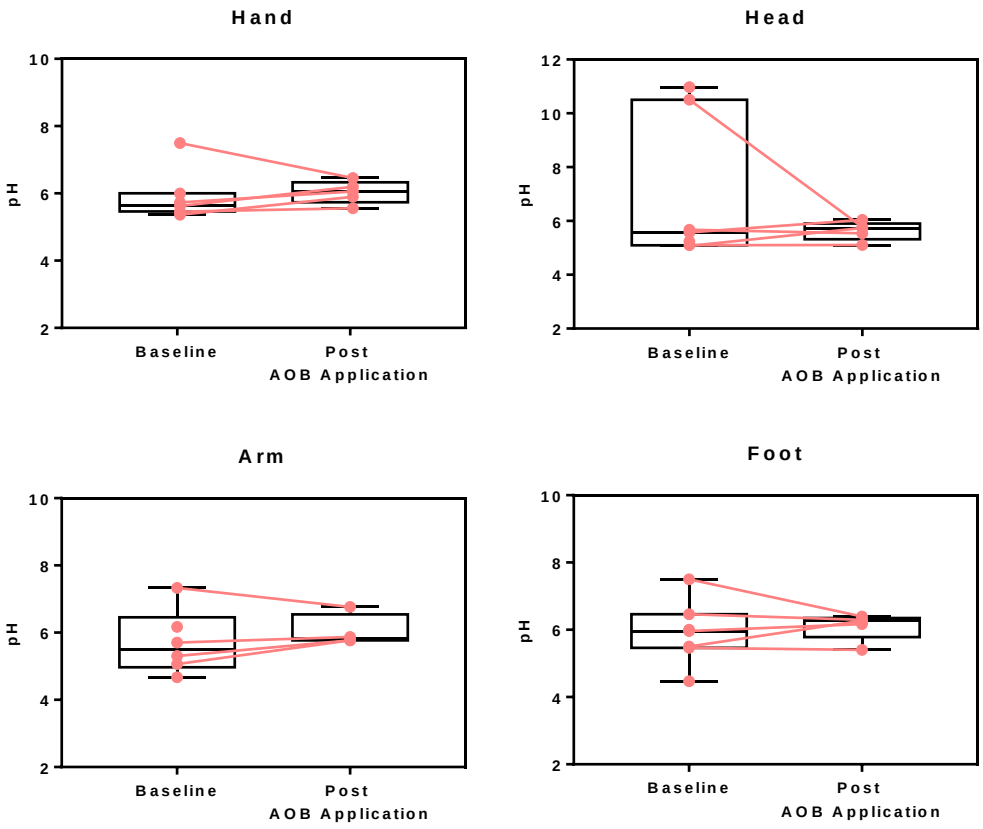

Figure 5.1 Measurement of pH on various surface skin surfaces, namely hand, head, arm, and foot. Data for each individual is superimposed on top of the box-plot representation (Tukey). Values were measured at days 0 (baseline) and 14 (post-AOB application). Each data point represents the mean values of 3 pH measurements.

According to the results, a wide range of pH values is observed, as measured at the different skin sites of the individuals enrolled for this study. Overall, and regardless of the body area, the pH values were mainly measured within its acidic range (pH 4-7), with no major differences across the body regions studied. At baseline, the most inter-individual variability in pH values is observed primarily within the arm and foot regions, whereas the measured pH of hand and head regions exhibited less variability in the values. Baseline assessments in all four body areas were consistently higher for one individual assessed (V1). After intervention (i.e. topical administration of *N. eutropha* D23 for 14 days), the pH of the body regions studied increased slightly.

The highest change in median pH values are observed within body extremities, such as hand and foot, with an increase to pH of 6.01 and 6.27, respectively, as compared to the baseline values of 5.63 and 5.97. An increase in the median values is also observed for

the remaining two body areas assessed, with an increase to 5.73 and 5.87 for head and arm, respectively, as compared to the baseline values of 5.57 and 5.70. Despite the observation, the increase in pH occurring after intervention is not statistically significant in any of the body parts evaluated, as assessed by paired *t*-test on these regions.

Besides pH, TEWL was also evaluated in this study, as a proxy for evaluating the integrity of the skin barrier. The results for these measurements are presented in Figure 5.2 below.

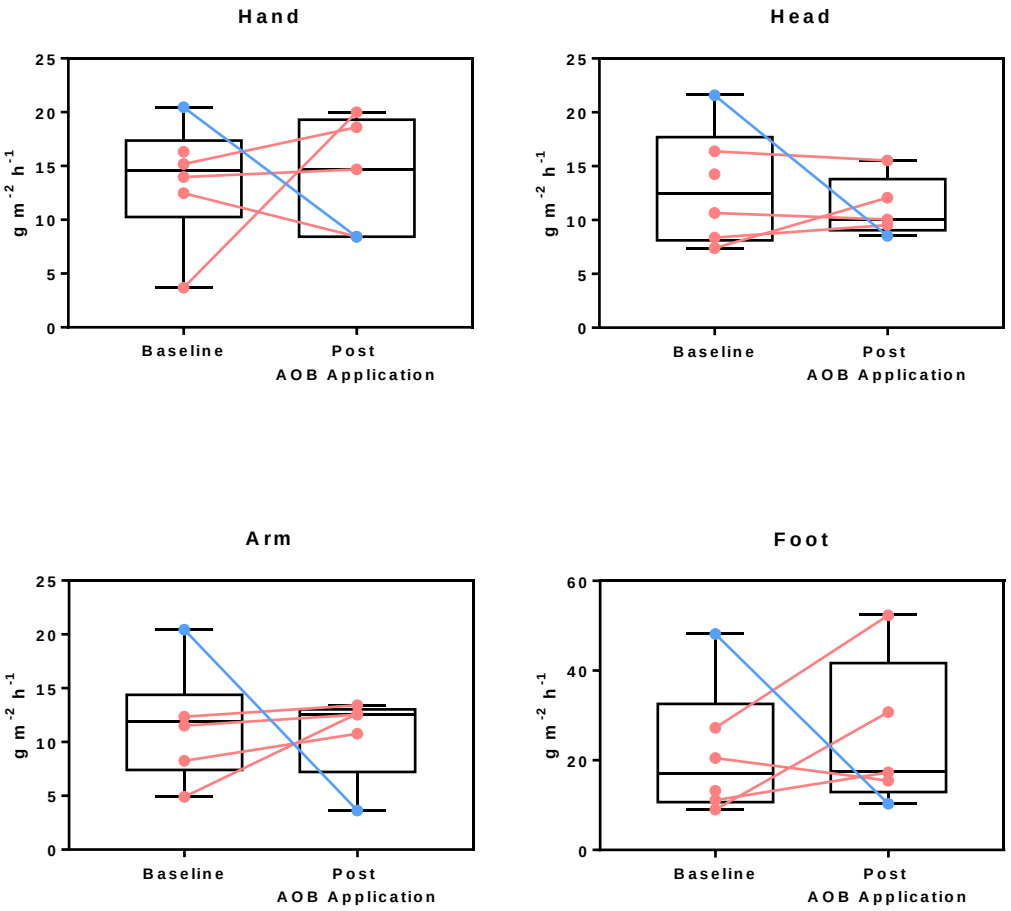

Figure 5.2 Measurement of trans-epidermal water loss (TEWL) in four different body areas, namely hand, arm, head, and foot. Data for each individual is superimposed on top of the box-plot representation (Tukey). Values were measured at days 0 (baseline) and 14 (post-AOB application). Data is presented as median values of 10-12 TEWL measurements. Volunteer 6 (V6) is highlighted in light blue due to the different pattern exhibited compared to the remaining participants.

Values for measured TEWL are more variable among the volunteers than those of pH, and trends are more difficult to observe at an individual level. An analysis of the median values for TEWL suggest that foot is the region with the highest value for TEWL (median at baseline of 16.98 g m^{-2} h^{-1}). Overall, intervention with *N. eutropha* D23 led to the highest changes in TEWL for the head region, with a slight decrease in median value to 10.06 g m^{-2} h^{-1}, as compared to the baseline value of 12.45 g m^{-2} h^{-1}. For the remaining body areas evaluated, intervention led to a decrease in the median values of TEWL, with medians of 14.68, 12.55, and 17.45 g m^{-2} h^{-1} for hand, arm, and foot, respectively, as compared to the baseline levels of 14.58, 11.94, and 16.98 g m^{-2} h^{-1}. Despite the changes in TEWL between both visits, these were not statistically significant. Interestingly, for one volunteer (V6, highlighted in light blue in Figure 5.2), a consistent large decrease in TEWL is observed among the volunteers, occurring as a result of the intervention, and across all body areas studied.

5.7 Effect of the intervention on blood pressure

Besides the local measurements on the skin (i.e. pH and TEWL), blood pressure measurements were also monitored in these individuals, at both visits, as an exploratory parameter to evaluate a potential systemic response derived from the application of *N. eutropha* D23 on the skin. The results are shown in Figure 5.3 below.

Systolic and diastolic pressures were measured within a homeostatic range, at baseline. It is observed that intervention led to a slight decrease in the systolic blood pressure (panel A), as evident by the decrease in the median value for this parameter. On the other hand, diastolic pressure (panel B) increases after 14 days of application of *N. eutropha* D23. Despite the changes, these are not statistically significant. At an individual level (panel C), only V1 showed an increase in both blood pressures, whereas an overall decrease is observed for the remaining volunteers. A maximal reduction in the diastolic blood pressure (~20%) is evident for V6 (highlighted in light blue in panels A and B), although not accompanied by a similar degree for the respective systolic blood pressure.

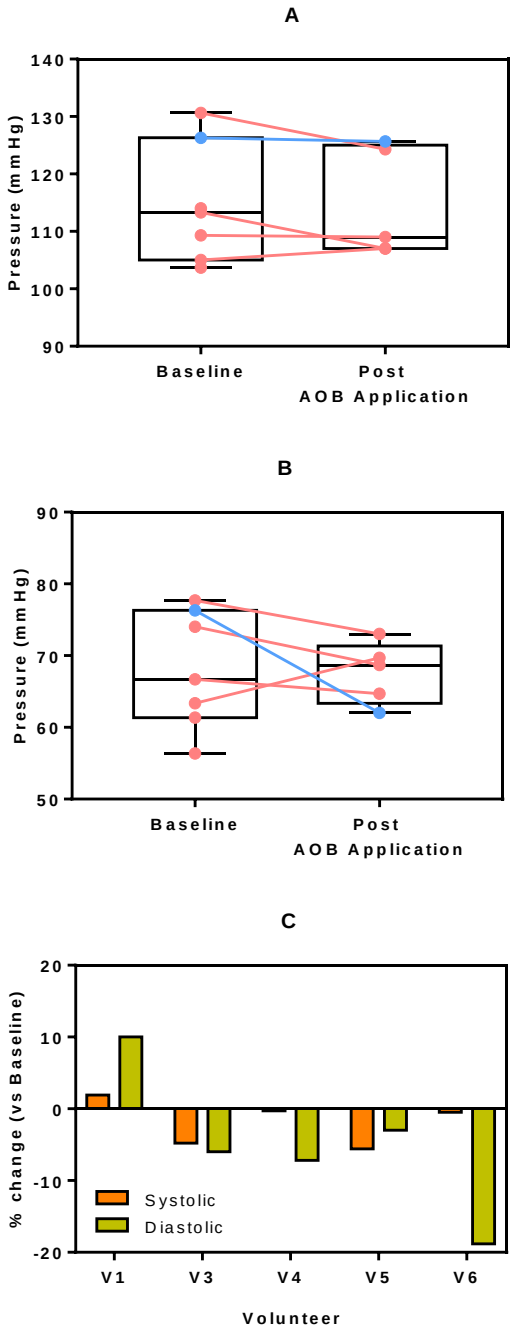

Figure 5.3 Measurement of the blood pressure of the volunteers, separated in (A) systolic and (B) diastolic blood pressures, at days 0 (baseline) and 14 (post-AOB application). Data for each individual is superimposed on top of the box-plot (Tukey) representation (panels A and B). Blood pressure is presented as mean systolic and diastolic (n=3 measurements) pressure measurements. For each volunteer, a percentage of the change in the mean blood pressure (C) as compared to baseline values is also presented.

5.8 Systemic biosignature of *N. eutropha* D23

A potential systemic signature in these individuals derived from the application of *N. eutropha* D23 via skin was evaluated by analysing plasma collected during the visits from volunteers with paired plasma samples (5 to 6 volunteers) for varying parameters. For better clarification, Table 5.2 below congregates these parameters into their respective panels related to NO status and metabolism, oxidative stress markers, and redox thiol metabolome.

Table 5.2 Overview of the markers evaluated in plasma samples from 4 to 5 volunteers who completed both assessment visits.

NO Metabolism	**Oxidative Stress**	**Redox Thiol Metabolome**
cGMP	FRAP	HCysSS
RXNO	8-Isoprostane	NAC
NOx	TBARS	GSSG
	4-HNE	GSH
		Cys
		HCys
		GluCys
		CysSS
		CysGly
		Sulfide
		Thiosulfate
		Sulfate
		TFT

5.8.1 Nitric oxide metabolism

Four plasmatic biomarkers related to NO status and metabolism were evaluated, namely circulating NOx (NO_2^- and NO_3^-), total nitroso species (RXNO), and guanosine 3, 5-cyclic monophosphate (cGMP). The results are shown in Figure 5.4 below.

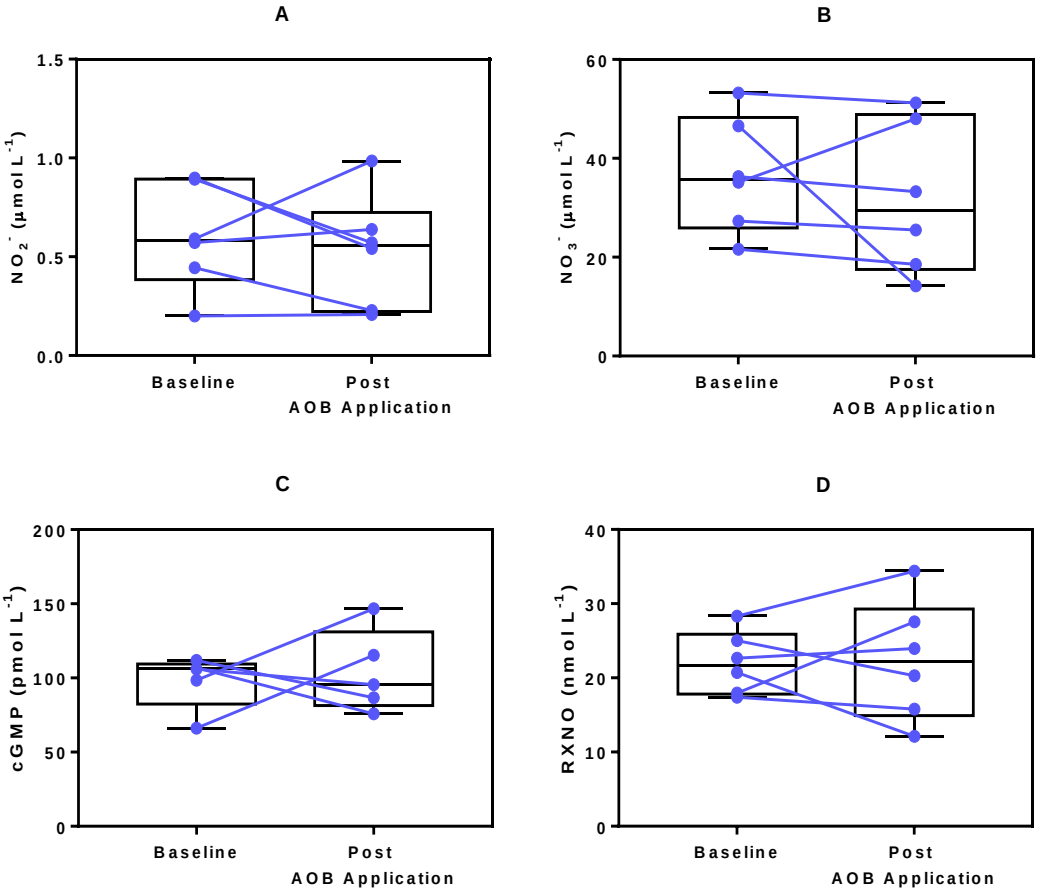

Figure 5.4 Plasma biomarkers for NO status and metabolism: NO_2^- (A), NO_3^- (B), cGMP (C), and RXNO (D). Only paired plasma samples were considered (5 volunteers). Data for each individual is superimposed on top of the box-plot (Tukey) representation.

NOx is a marker used as a proxy to evaluate the production and metabolism of NO in a biological sample. At individual levels, some decreases in the median concentration value of circulating NOx (panels A and B) are observed. Even though no statistical differences were found for NOx concentration between visits for this cohort, intervention with *N. eutropha* D23 led to a very discrete decrease in the median concentration of NO_2^-, and a

more pronounced decrease in the median concentration of NO_3^-, with a drop in the median baseline concentration of 36.36 to 29.45 µmol L^{-1} NO_3^-. The range of plasma NOx concentrations measured for this cohort is identical to that described by Lundberg & Govoni (2004), for a group of fasted healthy human volunteers of similar age range.

The cGMP levels (panel C) measured indicate a decreasing trend after intervention with *N. eutropha* D23 for some individuals (3 out of 5 paired individuals), and an insignificant increase in the median concentration of this parameter, from baseline 103 to 105.4 pmol L^{-1} cGMP. No major changes in the concentration of RXNO for this cohort are observed, as evident by the median concentration for this parameter upon intervention.

5.8.2 Oxidative stress

The oxidative stress biomarkers evaluated in this cohort included the measurement of the specific metabolites 4-hydroxynonenal (4-HNE) and 8-isoprostane, the group-specific thiobarbituric-acid reactive species (TBARS) and the ferric-reducing ability of plasma (FRAP) as a measurement of the total antioxidant capacity. The results are presented in Figure 5.5.

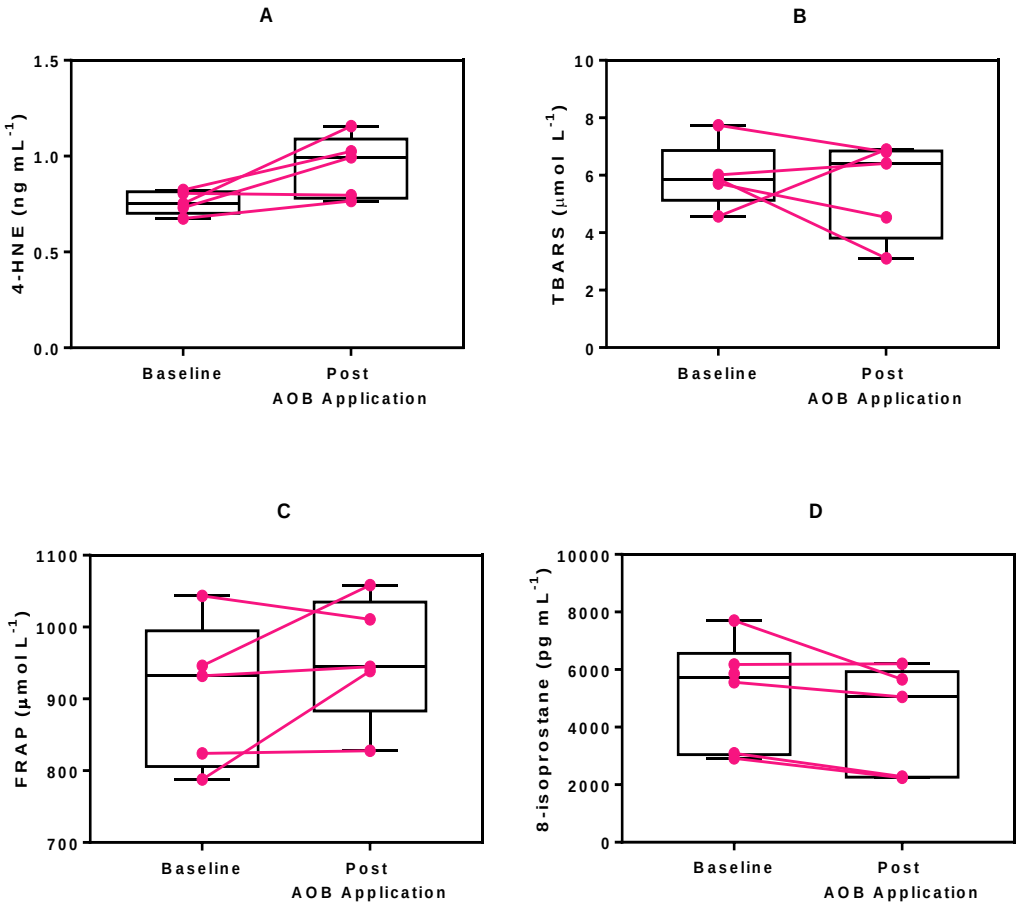

Figure 5.5 Oxidative stress biomarkers: 4-HNE (A), TBARS (B), FRAP (C), and 8-isoprostane (D). Only paired plasma samples were considered (5 volunteers). Data for each individual is superimposed on top of the box-plot (Tukey) representation.

An overall increase in the concentration of 4-HNE (panel A) is observed at the post-AOB application visit, across individual trends. After 14 days, intervention led to an increase in the median concentration from the baseline level of 0.78 to 0.89 ng mL^{-1} 4-HNE. Although not statistically significant (p=0.055), as assessed by paired *t*-test, the increasing trend suggest that application of *N. eutropha* D23 may potentially lead to an increase in this biomarker of lipid peroxidation. TBARS (panel B) was also measured as a marker of lipid peroxidation, and according to the results a slight increase in the median values for this marker is observed (from baseline 5.93 to 6.28 µmol L^{-1} TBARS). Individual trends for this marker seem more variable than those seen with 4-HNE. A slight increase in the median values for FRAP (panel C) is seen after 14 days of application of *N. eutropha* D23, i.e. from baseline 883.7 to 941.8 µmol L^{-1}. Lastly, according to the results from panel D related to the measurement of 8-isoprostane, an overall decreasing trend is observed in the

concentration of this metabolite upon application of *N. eutropha* D23 on the skin, with a decrease in the median value (i.e. from baseline 5711 to 4084 pg mL^{-1} 8-isoprostane).

To better visualise the metabolite changes upon application of *N. eutropha* D23, fold changes (FC) compared to baseline values are presented as a summary in Figure 5.6 below. The metabolites are grouped for each volunteer studied, and include the metabolites evaluated previously, such as NO_2^-, NO_3^-, cGMP, RXNO, 4-HNE, TBARS, FRAP, and 8-isoprostane.

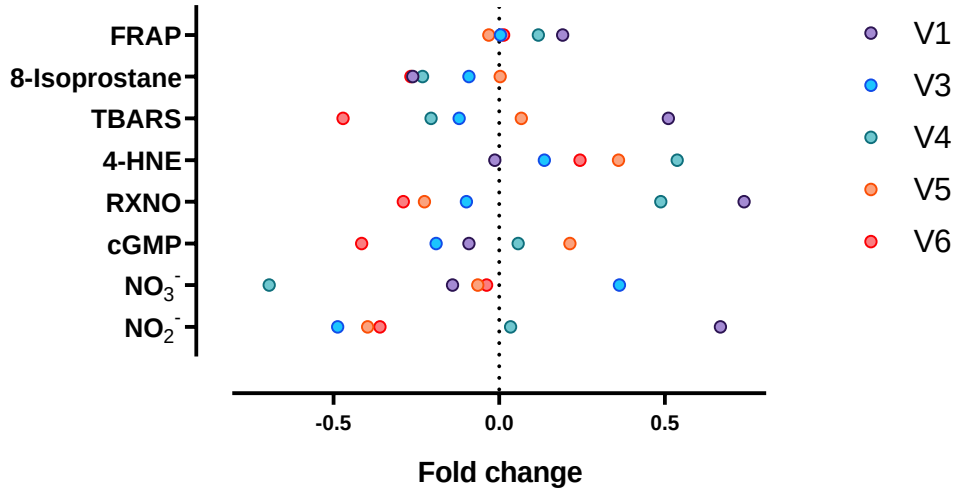

Figure 5.6 Fold change (compared to baseline levels) of 8 metabolites measured in plasma samples for 5 individuals, namely NO_2^-, NO_3^-, cGMP, RXNO, 4-HNE, TBARS, FRAP, and 8-isoprostane.

As observed, intervention with *N. eutropha* D23 led to a higher number of metabolites whose concentration decreased upon 14 days of topical administration of *N. eutropha* D23. For instance, from the 8 metabolites considered, V6 exhibited the highest number of metabolites found with decreasing concentrations (namely NO_2^-, NO_3^-, cGMP, RXNO, TBARS, and 8-isoprostane), compared to their respective baseline levels, and followed by V3, with 5 out of 8 metabolites decreasing in concentration. On the other hand, V4 exhibited the highest number of metabolites found at higher concentrations upon intervention, namely NO_2^-, RXNO, cGMP, 4-HNE, and FRAP.

5.8.3 Redox thiol metabolome

Plasma total free thiols (TFT) were initially assessed, and the results are presented in Figure 5.7 below. The concentration of TFT are normalised by the plasma protein content from each volunteer studied.

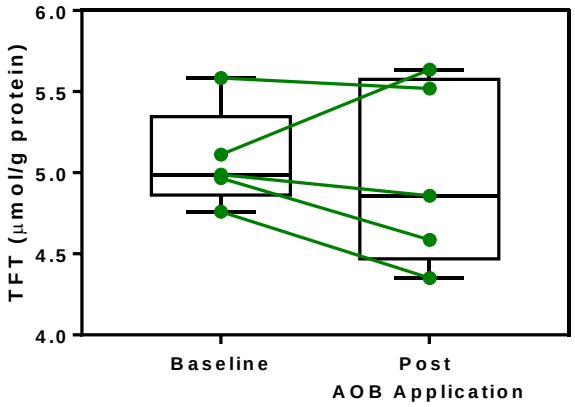

Figure 5.7 Plasma total free thiols (TFT). Only paired plasma samples were considered (5 volunteers). Data for each individual is superimposed on top of the box-plot (Tukey) representation.

Intervention with *N. eutropha* D23 led to a decrease in the concentration of this marker for the majority of the individuals studied, as evident by the individual trends, and a decrease in the overall median concentration from baseline 4.98 to 4.73 µmol g protein^{-1} for this cohort, even though not statistically significant.

The remaining thiol-related metabolites (total of 19) were analysed as part of the targeted redox thiol metabolome in these individuals, using mass spectrometry-based methods. This analysis included the measurement of free and bound thiol-related metabolites, namely cysteine (Cys), cystine (CysSS), homocysteine (HCys), homocystine (HCysSS), N-acetylcysteine (NAC), oxidised (GSSG) and reduced glutathione (GSH), glutamylcysteine (GluCys), cysteinylglycine (CysGly), sulfide, sulfate, and thiosulfate. The initial assessment of the metabolite changes within the redox thiol metabolome was done by evaluating overall trends (individual trends for each metabolite are presented in Appendix E). The results are shown in figures 5.7 and 5.8 below. These figures indicate a visual fold change in the concentration of these metabolites (overall), and for a specific metabolite (in a form of a heatmap), respectively.

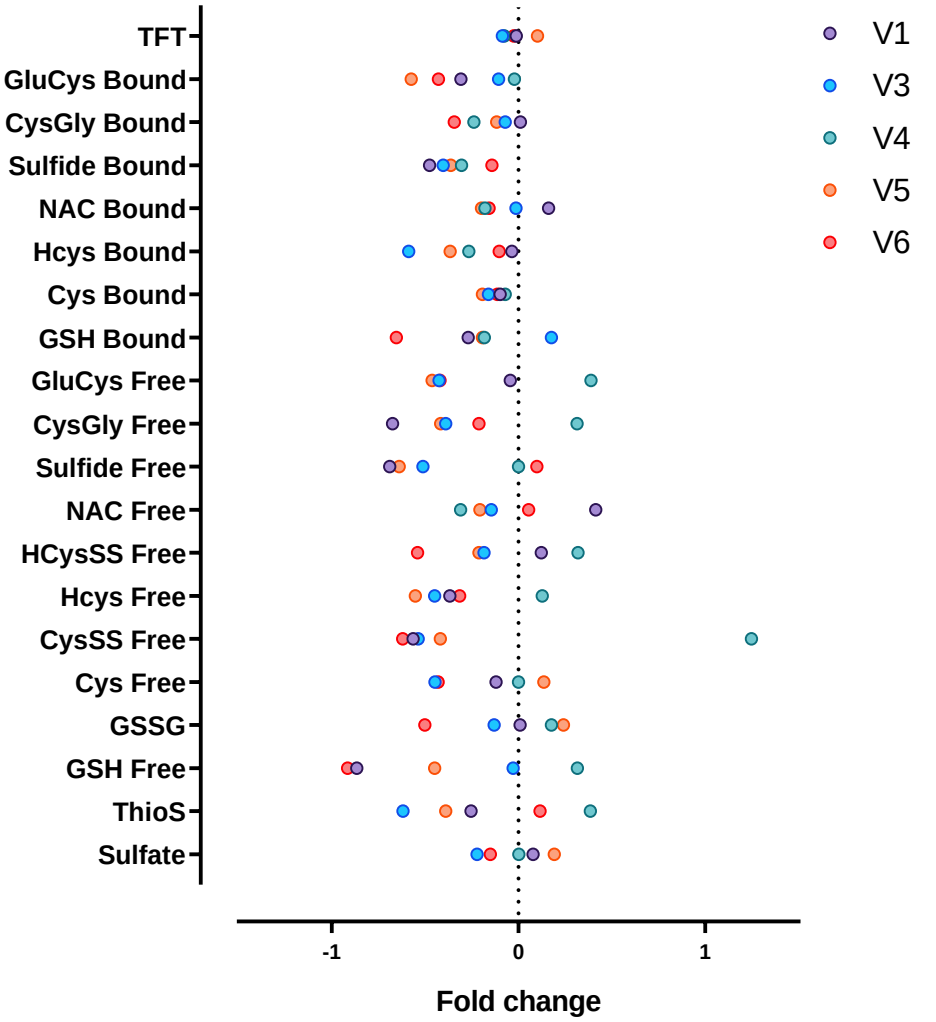

Figure 5.8 Fold change analysis (compared to baseline levels) of 20 thiol-related metabolites measured in plasma samples of 5 individuals, namely sulfate, thiosulfate, free and bound GSH, free GSSG, free and bound Cys, free CysSS, free and bound HCys, free HCysSS, free and bound NAC, free and bound sulfide, free and bound CysGly, free and bound GluCys, and TFT.

A generalised systemic decrease of circulating thiol metabolites is evident from Figure 5.8, as seen after application of *N. eutropha* D23 to the skin for 14 days. Interestingly, some heterogeneity was noticed amongst the volunteers, with V3 and V6 exhibiting the highest number of these changes (19 and 17 metabolites out of 20, respectively). The information above can be seen for individual metabolites per participant, as presented in the heatmap of Figure 5.9, which shows colour-coded, normalised concentrations of several thiol-related metabolites, and other analysed parameters (above).

All metabolites followed the same trend (i.e. decrease in their concentration after intervention), except bound GSH (>FC in V3), thiosulfate, free NAC and sulfide (>FC in V6). The highest FC was found for free GSH, for V6 (FC=-0.92). On the other hand, and as similarly identified in the previous fold change analysis, V4 exhibited a higher number of metabolites (total of 9) found at higher concentrations upon intervention, including the highest positive FC seen for free CysSS (FC=1.25).

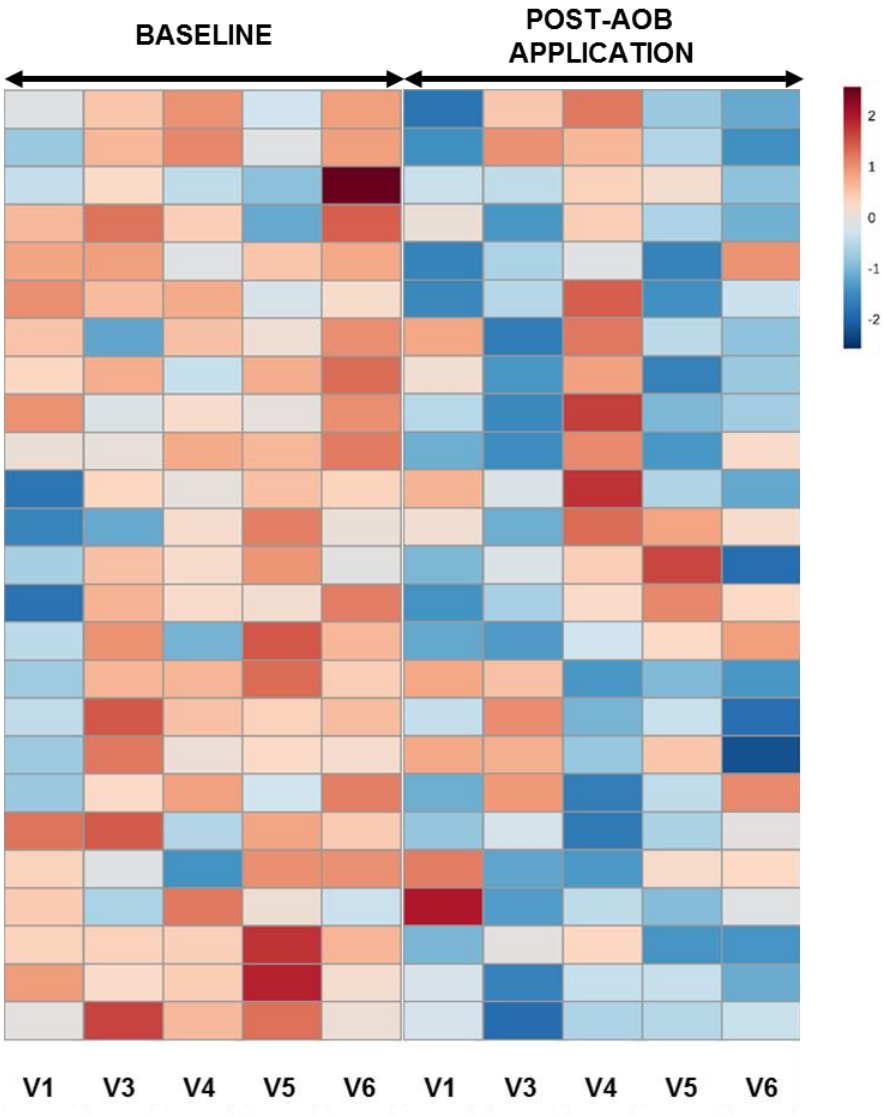

Figure 5.9 Heatmap representation of normalised concentration of several thiol-related metabolites and other parameters, upon intervention with *N. eutropha* D23. Colours are displayed by using normalised concentrations (darker red and blue colours indicate higher and lower concentrations, respectively). Difference in marker analyte are compared between baseline (right panel) and post-AOB assessment (left panel) visits. Prepared using MetaboAnalyst 4.0 (Cho*ng et al*., 2018).

5.9 Discussion

A number of healthy individuals were enrolled in this cohort to explore the effects of the application of *N. eutropha* D23 on their skin, and to evaluate the potential local and systemic biosignature of the bacteria on human hosts. Even though there were other outcomes included in this study, such as the evaluation of the NO emanations on the skin, and the collection of samples for 16S rRNA analysis by different sampling methods (carried out by another researcher), the results presented in this research thesis focused on the analysis of plasma samples collected from these individuals during the study, including parameters related to NO status and metabolism, oxidative stress markers and redox thiol metabolome as proxy parameters to evaluate systemic changes of the cutaneous application of *N. eutropha* D23.

A total of 7 volunteers were enrolled for this study, but only 6 completed successfully baseline and post-AOB application assessments, for an intervention of 14 days of application of *N. eutropha* D23 on their skin. As indicated by Table 5.1, healthy, young adults participated in this study, mostly British females. At the time of recruitment, individuals were normotensive and did not display signs of ongoing inflammatory skin conditions.

The initial baseline assessment in these individuals included collection of data regarding the pH of the skin, TEWL, and blood pressure. The first two parameters were chosen to provide information of possible local processes occurring as an effect to the application of *N. eutropha* D23 on a human interface. A decrease in the pH value of the skin was initially assumed to occur upon application of *N. eutropha* D23 due to their metabolism. However, the results for this marker show slight increases in the median pH values after application of *N. eutropha* D23 across all body areas measured (i.e. hand, head, arm, and foot), although not significantly different from baseline values. This effect can also be observed per subject, as individual trends show an increase in pH for the majority of the subjects enrolled.

Two individuals (V1 and V2) showed high pH values measured at baseline, on the head region (pH of 10.5±1.9 and 10.9±1.1 for V1 and V2, respectively). However, V1 consistently showed high pH values measured across all body areas, compared to other subjects at baseline assessment (pH of 7.5±2.3, 7.33±0.25 and 7.5±2.9 for hand, arm, and foot, respectively). Endogenous and exogenous factors can be responsible for this observation in V1 (e.g. age, anatomical site, hydration, ethnicity, cosmetic use, washing, for instance) (Schmid-Wendtner and Korting, 2006; Bíró *et al.*, 2018; Farage *et al.*, 2018), and thus contributing for the variability among subjects. An alternative possible cause for the high pH values measured at baseline was an artefact of the measurement technique

applied (e.g. deficient instrument measurement), as suggested by the larger spread of the triplicate measurements per each area.

The increasing trend in pH seen in this cohort upon application of *N. eutropha* D23 for 14 days is contrary to what I initially expected, even though the nexus of causality is difficult to establish, due to several limitations in this study. Such limitations include a very small number of volunteers (total of 5 analysed in this study); application of *N. eutropha* D23 for a short period of time (14 days, with only one outcome assessment at day 14); and absence of a control group. Despite attempting to control for hygienic routine (individuals were given a set of personal hygienic products), full compliance could not entirely be guaranteed. To overcome these limitations, the design of the study should be reviewed to include a higher number of healthy volunteers, using the product for a longer period of time; the latter allowing an increase in the time point for assessments. Moreover, it would have been important to establish survival or carriage of *N. eutropha* D23 on the skin (e.g. 16S rRNA approaches) throughout the study period, which could also correlate with the results.

Another local parameter measured in these individuals included the measurement of TEWL, as an assessment of the integrity (damage) of the barrier of the skin, by measuring the rate of water loss through the surface of the skin. A higher rate of water loss (i.e. higher TEWL) potentially indicates problems with the integrity of the surface of the skin. The results indicate a much higher variability in the TEWL rates among the subjects enrolled. Overall, application of *N. eutropha* D23 did not lead to any significant changes in this physiological parameter, despite the discrete decreasing trend in the cohort, as compared to baseline levels. In this cohort, and based on this observation, it was concluded that cutaneous application of *N. eutropha* D23 may be considered safe.

One individual (V6) exhibited the highest change in individual TEWL rate between the baseline and outcome assessment visits; whose decreasing trend is consistently observed in all body areas studied. Interestingly, V6 is highlighted among the cohort as this volunteer required greater quantities of *N. eutropha* D23 to complete the study and may have inadvertently been exposed to a “higher dose” of bacteria. While pH was not as strikingly affected as TEWL for this individual, the highest change in the latter parameter observed for V6 could be potentially related to a higher number of application of *N. eutropha* D23 on the skin, assuming its use *ad libitum* by the volunteer. Based on this observation, it could be postulated that application of *N. eutropha* D23, either by an increase in the frequency of application or an increase in the number of *N. eutropha* D23 delivered per application may lead to a decrease in skin permeation. This hypothesis could be tested by reviewing the research protocol to accommodate the suggestions made to overcome the limitations of the current study.

Blood pressure measurements in these individuals were also carried out as an exploratory hemodynamic parameter to evaluate a potential effect of the application of *N. eutropha* D23 on the skin. According to the results, systolic and diastolic blood pressures decreased for the majority of the individuals who completed both assessment visits upon intervention with *N. eutropha* D23, though at varying degrees. Only V1 showed an opposite trend, i.e. higher blood pressure. The greatest decrease in diastolic blood pressure is observed for V6, which is not accompanied by a similar decrease in its respective systolic blood pressure. The decrease in diastolic blood pressure observed for V6 could potentially be linked to an increase in the frequency of application of *N. eutropha* D23 on the skin.

Despite the fact that no significant changes in blood pressure were observed for the entire cohort, the median values for systolic and diastolic indicate opposite trends: while systolic pressure seemed to decrease, diastolic pressure increased upon intervention with *N. eutropha* D23. As mentioned earlier, a major limitation of this study is the small size of the cohort studied. Regarding the results of the diastolic blood pressure in these 5 participants (mean difference of 0.4 and 8.2 of standard deviation), the calculated power is only 5%, for a 95% significance, making it underpowered compared to previous clinical trials using *N. eutropha* D23. This is important to take into consideration, as a decrease in blood pressure would be expected according to the findings described by Peter et al. (2017) (n=9 per group) and mentioned earlier in Chapter 3. In this study, the authors reported significant decreases in both blood pressures after two weeks of cutaneous application of *N. eutropha* D23 on the skin of acne patients. Based on their results, their study has a calculated power of >50 and >70% for systolic and diastolic blood pressures, respectively.

The different blood pressure outcomes from previous work (Peter et al. 2017) may also derive from the fact that the authors used a much higher density of *N. eutropha* D23 cells (100-fold more concentrated than the one used for the cohort studied in Southampton) leading to a concentration-dependent decrease in the blood pressure. Based on this information, it could be hypothesised that the highest changes observed for V6 in this cohort (e.g. diastolic blood pressure, TEWL) could derive from a higher frequency in application or higher overall number of *N. eutropha* D23 cells on the skin.

Despite being exploratory and prone to limitations, these results suggest a systemic effect of a cutaneous application of *N. eutropha* D23. Should the hypothesis above be tested, the design of the study must be reviewed to accommodate not only the already-mentioned suggestions (e.g. increase in number of outcome assessment points), but also an increase in sample size, a higher frequency of cutaneous application of *N. eutropha* D23 and a control group. Regarding the sample size, for instance, it is estimated that for a meaningful decrease of 3.5 mmHg in diastolic blood pressure, and an estimated 4.5

mmHg of standard deviation, a total of 15 individuals should be recruited, for a power of 80% and a p-value of <0.05 for statistical significance, which demonstrates its feasibility.

Here, plasma samples collected at both assessment visits were also subjected to a more detailed analysis for a panel of metabolites, including NO status and metabolism markers, oxidative stress (including lipid peroxidation) markers and a snapshot of the redox thiol metabolome in these individuals. Due to the limitations already mentioned (i.e. very small cohort and one outcome assessment point), this study should be regarded as exploratory. The rationale for this analysis and the selection of the biomarkers relies on the initial expectation that potential effects derived from the intervention would be likely mediated by NO and NO_2^-, which are generated by *N. eutropha* D23 at the surface of the human skin, where substrate is expected to be present (Czarnows*ki et al*., 1992; Alvear-Ordenes *et al*., 2005; Nose *et al*., 2005; Schmidt *et al*., 2013). Production of these molecules at the integumentary interface could have the potential to induce visible changes at a systemic level, by percutaneous action (Shabani *et al.*, 1996; Mowbray *et al.*, 2008; Garcia-Saura *et al.*, 2010).

According to the results from the markers analysed within the NO metabolism panel (NO_2^-, NO_3^-, cGMP, and RXNO), no significant differences in the median concentration of the metabolites for the cohort were observed. However, some interesting features are worth-mentioning. Bioavailability of NO was herein assessed via measuring the levels of cGMP, a second messenger generated upon interaction of NO with guanylate cyclase enzymes (Murad, 1994). A higher bioavailability of NO in these individuals would be reflected by an increase in cGMP levels and higher circulating levels of NOx, especially NO_3^-. The individual trends in cGMP indicate a steep increase in this marker for two volunteers, who had the lowest concentration of cGMP at baseline assessment, despite no changes in the median value for this parameter in this cohort. The NO_3^- levels measured are not consistent with a higher bioavailability of NO, and a decrease was observed in the median value for this parameter, though not at a statistical significant level. Even though the results indicate an opposite trend as to what I initially expected to see for these individuals upon intervention, they may indicate a physiological regulation of the NO levels, rather than an effect derived from the application of *N. eutropha* D23. A full interpretation of these results and a distinction of effect and response is hindered by the small number of patients and the existence of a single outcome assessment time point.

An array of oxidative stress markers were also evaluated for these individuals (4-HNE, TBARS, FRAP, and 8-isoprostane), including markers for lipid peroxidation. Under oxidative/inflammatory conditions, reactive species lead to oxidative breakdown of polyunsaturated fatty acids, resulting in damage to cell membranes. Two major end

products of this process were measured for these individuals, namely 4-HNE and malondialdehyde (major component measured via TBARS assay).

Overall increases in the median values of 4-HNE and TBARS were observed after skin spraying with *N. eutropha* D23, whereas the median levels of 8-isoprostane tend to decrease upon intervention. The increase seen in the levels of 4-HNE is particularly evident at an individual scale, almost reaching a statistically significant result ($p=0.055$), as compared to its baseline value for the cohort. While individual trends for TBARS are more scattered, the majority of the individuals exhibited higher values upon intervention, at varying degrees. For example, the higher increases were observed for V1 and V6, with the latter exhibiting the highest increase in TBARS value upon intervention. Identically, V6 also exhibited the highest decrease in 8-isoprostane levels, followed by V1 and V4.

FRAP is a measure of total antioxidant capacity of samples, in this case, plasma samples from the individuals enrolled in the study. No significant changes in its median value were observed, despite individual trends indicating a slight increase in this parameter. Interestingly, a decrease in this parameter would be expected upon observing an increase in lipid peroxidation makers (i.e. 4-HNE, TBARS). Whether the results seen are an effect of a biological counter-regulation is yet to be determined.

These samples were also subjected to a targeted analysis of their redox thiol metabolome. Although not statistically significant, the minor decrease in TFT observed in this cohort, and for the majority of the individuals (3 out of 5), could potentially indicate an ongoing oxidative process upon intervention with *N. eutropha* D23, which is supported by the observed increase in lipid peroxidation markers. An exploratory assessment at the targeted thiol metabolome in these individuals also revealed a generalised decrease in the concentration of a higher number of thiol-containing metabolites (figures 5.8 and 5.9) upon intervention with *N. eutropha* D23. Only V4 exhibited a higher number of metabolites at higher concentrations. Some of these changes are consistent with oxidation phenomena seen upon application of *N. eutropha* D23. For instance, free and bound GSH decrease for the majority of the individuals, with V6 exhibiting the highest decrease in the concentration of free GSH upon intervention. According to this finding, an increase in the concentration of oxidised glutathione (GSSG) was speculated, even though the results show a decrease in the GSSG levels after intervention. For V6, the change in RXNO levels after intervention is highlighted as one of the metabolites that mostly changed, among the other volunteers.

5.10 Conclusion

Local and systemic changes derived from the cutaneous application of *N. eutropha* D23 were investigated in a small cohort of human volunteers. Intervention with *N. eutropha* D23 occurred for a short period of time and was considered to be safe and well tolerated by the participants.

The results here described should be regarded as exploratory due to the inherent limitations of the study, which include the small number of participants, the lack of control group and the existence of only one point for outcome assessment. Notwithstanding, local and systemic changes were observed after skin spraying with *N. eutropha* D23. Although no significant changes were found in TEWL and blood pressure, the large reductions in these parameters for one particular participant may be linked to increased quantities of *N. eutropha* D23 on the skin.

Additional evidence of systemic changes were provided by plasma biomarker analysis. Although no significant changes were found, data suggested that an oxidative mechanism may take place, as seen by the increasing trend in the concentration of biomarkers related to oxidative stress (e.g. 4-HNE, TBARS), upon topical administration of *N. eutropha* D23. This was consistent with a decrease in TFT levels, as observed for the majority of the participants. Furthermore, an evaluation of the redox thiol metabolome revealed a general decrease in sulfhydryl-containing molecules (e.g. GSH and Cys), consistent with the decrease in TFT, and an overall oxidative process.

As a systemic signature was observed after topical application of *N. eutropha* D23, further investigations are needed to characterise its mechanism of action, and the overall effects for the human host. Clarifying the hemodynamic changes upon intervention with *N. eutropha* D23, for example, may create opportunities for its targeted biomedical and therapeutic use.

Chapter 6

Conclusions

Chapter 6: Conclusions

6.1 Summary and reflection

The overall purpose set for this research project was to evaluate whether the metabolites generated by *N. eutropha* D23 (i.e. NO and/or NO_2^-) exert meaningful bioactivity. For that, a better characterisation of the metabolic properties of *N. eutropha* D23 was of particular importance and required for this project, as the available scientific background for this particular strain was limited.

A key strength of the current PhD project is the use of pure and live cultures of *N. eutropha* D23, available in the form of a cosmetic product (AO+ Mist™, MotherDirt™, AOBiome LLC). This allowed an in-depth evaluation of their phenotype within a reasonable time, in a consistent and reproducible manner. The following paragraphs summaries the major findings and conclusions from this research thesis as well as provide my overall reflection.

The results from the biochemical assessment demonstrated that *N. eutropha* exhibits the fundamental metabolic properties as one may expect for an ammonia-oxidising bacterium, namely consumption of NH_3 with concomitant production of NO_2^-, the main metabolite produced by *N. eutropha* D23. The ability to generate millimolar concentrations of NO_2^- was noteworthy, as well as the fact that energy-starved *N. eutropha* D23 cells retain high metabolic efficiencies; as observed immediately upon addition of substrate. At a microbial ecology perspective, it would have been quite informative to compare side-by-side the metabolic phenotype of *N. eutropha* D23 with other AOB, such as the phylogenetically-related *N. europaea*. Due to time restrictions, this remains to be determined and warrants further dedication.

Providing clear evidence for generation of NO by *N. eutropha* D23 was set as a major aim of this research project. In the past, production of NO was often inferred, but thus far, no evidence for its generation by this strain has been made available. To my best knowledge, this research thesis is the first to describe and quantify production of NO by *N. eutropha* D23, using four independent methodologies with different principles of detection: gas-phase chemiluminescence, amperometric detection, the nitrosation of DAF-2, and the oxyHb capture assay; the former allowed for quantitative characterisation of production of NO in real time, as well as elucidation of factors affecting its production. The factors chosen were based on physiological requirements described for ammonia-oxidisers (e.g. the model organism *N. europaea*), and on physicochemical properties of the skin interface.

As *N. eutropha* D23 are meant to be applied on the skin, selecting conditions that resemble the cutaneous environment was logical for studying the *in vitro* metabolic properties of *N. eutropha* D23. Major findings indicate that formation of NO during NH_3 oxidation by *N. eutropha* D23 follows a dependence on temperature, pH, and concentration of substrate. Maximal *in vitro* production of NO was observed for bacteria incubated with 25 mmol L^{-1} NH_4^+, at 37 °C and at pH 8.00; conditions which led to generation of fentomoles of NO per *N. eutropha* D23 cell, for a 20-min study window. Maximal NO production was also seen for an intermediate number of *N. eutropha* D23 cells (36-71x10^5 *N. eutropha* D23), suggesting potential modulation of NO production according to the *N. eutropha* D23 cell density. The dependence on cell density and concentration of substrate was also observed using the nitrosation of DAF-2 as an indirect approach for measuring and quantifying NO production, and the oxyHb capture assay, respectively, in M9 medium.

A decrease in the amounts of NO can be assumed by decreasing the concentration of substrate, temperature and pH; based on the findings herein. This is particularly relevant if one contextualises the application of *N. eutropha* D23 on the human skin. While metabolic activity (e.g. NO production) is observed at temperatures and concentrations of NH_3/NH_4 reported for the surface of the human skin (ranges of 28-38 °C, and 1-5 mmol L^{-1}, respectively), it could be argued that the acidic pH of the surface of the skin (pH range: 4-7) may render the metabolism of these bacteria ineffective, as *in vitro* activity of *N. eutropha* D23 was only demonstrated between pH 6 and pH 8. The skin is not a sterile interface as it harbours a plethora of microorganisms. Evidence has suggested that instead of thriving solely on the surface of the skin, microbes (e.g. commensal bacteria) can indeed occupy and spread further into deeper viable layers of the skin (Nakatsuji et al. 2013), for which a pH gradient towards neutrality (pH 7.4-8) has been also described (Wagn*er et al*., 2003). Thus, bioactivity of *N. eutropha* D23 on the skin cannot be entirely ruled out based on the acidic range of the surface of the skin, as it remains to be identified or pinpointed the exact location of *N. eutropha* D23 when applied on the human skin, as well as its local activity remains to be described. In fact, local and systemic changes are demonstrated in a small cohort of healthy human volunteers as part of this research project.

Perturbation of *N. eutropha* D23 during NH_3 oxidation by means of intense aeration (as required for gas-phase chemiluminescence) or by removing NO from solution by its scavenging (e.g. using CPTIO) led to decreased yields of NO_2^- and ATP, as compared to controls. These findings suggest that production of NO and NO_2^- are dependent on each other, and suggest that NO has a pivotal function for this bacteria, rather than just a by-product of the ammonia oxidation pathway in nitrifying bacteria. This is concordant with

current research that place NO as an obligatory intermediate for NO_2^- formation. As the renewed interest in this pathway has led to a rethinking of the microbial and chemical processes driving the biogeochemical N cycle, further investigations on this matter are needed to fully understand the role of NO, which could potentially be carried out by using *N. eutropha* D23 as a biological tool.

Bioactivity was primarily demonstrated towards the dispersal of pre-formed *P. aeruginosa* biofilms. These were used as a tool to assess whether the amounts of metabolites produced by *N. eutropha* D23 were sufficient to elicit any biological activity. The rationale for using *P. aeruginosa* biofilms derived from research using NO donors (e.g. SNP, NONOates) (Nicolas Barraud *et al*., 2006; Cai, 2018) to trigger biotic dispersal of *P. aeruginosa*. Results demonstrated that significant reductions in *P. aeruginosa* biofilm biomass were achieved, upon co-culture with live suspensions of *N. eutropha* D23, in M9 medium. Dispersal of *P. aeruginosa* biofilms was dependent on the cell density of *N. eutropha* D23 present in the co-culture system. It was also demonstrated that *N. eutropha* D23-derived NO was the metabolite responsible for the effects observed in *P. aeruginosa* biofilms, as introduction of an NO scavenger (CPTIO) during co-culture abrogated dispersal of *P. aeruginosa* biofilms, as compared to control (no CPTIO). Thus, it was concluded that the amounts of NO generated by *N. eutropha* D23 were sufficient to disperse *P. aeruginosa* biofilms, and hence, bioactivity was demonstrated. Furthermore, biofilm dispersal was also confirmed to occur clinical isolates, collected from infected lung epithelia of patients suffering from cystic fibrosis.

In this work, bioactivity of *N. eutropha* D23 as a biological tool to generate and deliver NO is limited to a single biofilm-producing species (i.e. *P. aeruginosa*). Bearing in mind the conserved action of NO across species and the economic and clinical importance of microbial biofilms, it would have been complementary to investigate whether dispersal effects also occur with other relevant microbial species, upon co-culture with *N. eutropha* D23. It is recognised that the methodology used for assessing *in vitro* bioactivity of *N. eutropha* D23 may not reflect the *in vivo* reality, considering that biofilms often colonise biotic substrata, such as lung epithelia or wound beds. It would have been an added benefit to study dispersal events in biofilms attached to biotic surfaces, either *in vivo* or *ex vivo*; with the limited duration of this research project, such studies could not be carried out.

The final results Chapter ultimately demonstrates biological activity of *N. eutropha* D23 when applied on the skin of healthy human participants. Although a small number of samples were analysed, local and systemic effects were still clearly evident. While no major changes in the parameters related to local skin's physiology (i.e. TEWL and pH) were seen, across the four body areas measured, the major findings include the

distinguishable changes for one particular participant, for TEWL and blood pressure. This participant exhibited the highest decrease in TEWL values after topical application of *N. eutropha* D23, albeit not significantly different from baseline assessment. As TEWL indicates transcutaneous loss of water, this finding may suggest an increase in skin's barrier function; thus, further research is needed on this matter. While blood pressure was found to decrease for the majority of the participants, the aforementioned volunteer also exhibited the highest percent change (~ 20% decrease) in diastolic blood pressure after skin application with *N. eutropha* D23, among the cohort of volunteers. These anomalous observations (i.e. TEWL and hemodynamic changes) were attributed to the notion that this participant requested an extra supply of *N. eutropha* D23 (AO Mist™, MotherDirt™, AOBiome LLC), potentially loading the skin surface with *N. eutropha* D23.

The difficulty in establishing a causality for the hemodynamic changes observed is due to the limitations of the study. The changes observed were speculated to derive from the topical application of a higher number of bacteria or from an increase in the frequency of skin spraying; as significant reductions in blood pressure have been previously demonstrated previously by Peter et al. (2017), using higher densities of *N. eutropha* D23.

Plasma samples were analysed for a panel of additional biomarkers (NO status and metabolism, oxidative stress and redox thiol metabolome), as readouts for systemic bioactivity of *N. eutropha* D23. Due to the potential metabolic activity of *N. eutropha* D23 on the skin (i.e. production of NO and NO_2^-), and the possibility of transdermal absorption of NO_2^- to the bloodstream (Garcia-Saura *et al*., 2010), I thus expected to observe changes in the NO status and metabolism panel. However, no major observations or changes were found in NOx, cGMP, and RXNO for this cohort. The results from the oxidative stress panel suggested that a potential oxidation process derives from the cutaneous application of *N. eutropha* D23, as indicated by the nearly significant change in 4-HNE concentration, and TBARS. An increase in oxidative stress would likely be reflected by a decrease in the antioxidant capacity of plasma; however, no major changes in FRAP were actually observed. Major findings from the analysis of the redox thiol metabolome revealed an overall decrease in the concentration of some circulatory thiols, for instance, reduced glutathione and free cysteine, suggesting an increase in oxidative stress. Besides showing decreased concentrations of thiol-containing metabolites, the results also indicated that the changes were uniformly found across the majority of the participants enrolled.

To conclude, the results presented in this research thesis led to the validation of my initial hypothesis. That is, *N. eutropha* D23 exerts biological activity, as demonstrated by the ability of *N. eutropha* D23-derived NO to disperse *P. aeruginosa* biofilms; and when

applied on the human skin, local and systemic changes can be observed in a small cohort of human volunteers.

6.2 Future work and direction

The overall scope of this PhD project was to characterise the metabolic phenotype of *N. eutropha* D23, and to investigate whether the metabolites produced by the bacteria exert meaningful biological activity. While the findings herein described allow answering the fundamental essence of the research hypothesis, some topics are worth of further dedication. Among others, these include extending the knowledge in the role of NO within the ammonia metabolism pathway, as well as the factors and/or mechanisms driving local and systemic effects upon exposure of humans to *N. eutropha* D23. Regardless of the activities carried out in the near future, this project can be further developed to fit research niches in biomedical sciences, soil and environmental microbiology, and redox biology.

As part of a doctoral research plan, a more complete picture of the metabolic phenotype of *N. eutropha* D23 is envisaged to accommodate other N-containing metabolites known to be generated during ammonia oxidation by AOB species, with the ultimate goal of establishing a mass balance. These include the chemical intermediate NH_2OH, but also the gaseous products N_2O and N_2. Even though insights on the production of NH_2OH were gathered in this doctoral project, future tasks should include development and optimisation of mass spectrometry-based methodologies to achieve better sensitivity, as compared to the colourimetric method used for this thesis. I consider that a better understanding how substrate is quantitatively converted to different products with demonstrated or potential biological activity may provide industrial/commercial applications, for example, by exploring drivers of metabolism that can enhance of inhibit the production of specific *N. eutropha* D23-derived products. Publication-wise, a metabolic comparison with the model organism *N. europaea* is needed, and the application of the methodologies herein used will be an added benefit in the field of soil microbiology and bacterial metabolism.

Mass-balance studies will also allow a better understanding of the role and place of NO within the ammonia metabolism pathway, which has received recent and renewed interest by Caranto and Lancaster (2017). Development and optimisation of methodologies based on mass spectrometry and stable isotopes are thus required and envisaged to drive this study to fruition. Whether bacterial density can play a role in modulating the overall flux of NO production is a question worth following in the future, with possible microbial ecology implications, if one thinks in a broader context (e.g. multispecies biofilm and AOB natural

habitats). Depending on funding, and human resources and access to appropriate facilities, these activities are feasible and able to be completed in a short term.

The observation that *N. eutropha* D23-derived NO stimulates biotic dispersal of *P. aeruginosa* biofilms demonstrated first insights into the bioactivity of *N. eutropha* D23, and are concordant with other research using chemically-produced NO for studying the mechanisms of biofilm dispersal, and the development of targeted antimicrobial therapies (e.g. prodrugs) (Soren *et al.*, 2019). Within this topic, further dedication should focus on the interaction between the two species (i.e. *N. eutropha* D23 and *P. aeruginosa*) at a mechanistic/biochemical signalling, using more appropriate methodologies in biofilm research for assessing co-culture treatment outcomes. Internal and external expertise/collaborations should be sought to drive this arm of research towards more realistic, biologically-relevant scenarios using, for example, infection models on epithelial layers and/or human explants.

Lastly, this doctoral project provided insights into the effects of the application of *N. eutropha* D23 on the skin of a small cohort of healthy, human volunteers. I consider that future developments in this research area are worth of an individual doctoral project, due to the time required to overcome the limitations already discussed before, together with tasks allocated for volunteer recruiting, sample and complex data analysis. More dedicated and mechanistic approaches should be applied to fully explain some of the findings observed (e.g. hemodynamic changes, thiol changes) that will contribute for establishing a possible mechanism of action of these bacteria when applied on the human skin. While research into the metabolomics of redox active thiol-containing molecules is in its infancy, its incorporation in this area is pivotal. Shotgun metabolomics, bioinformatics tools and multivariate data analysis could be applied to better understand the qualitative changes that occur in the human thiol metabolome, and more important, provide information regarding which metabolites (reduced and/or oxidised thiols) are modified upon intervention with *N. eutropha* D23. These analysis could not be carried out in this doctoral project due to the small size of the cohort, and due to the targeted metabolomics approach applied.

Appendices

Appendix A: Pictures from the commercial products used in this thesis.

Appendix B: Calibration curves

B1: Ammonium (NH_4^+)

B2: Nitrite (NO_2^-)

B3: Nitrate (NO_3^-)

B4: Nitric Oxide (NO)

B5: Hydroxylamine (NH_2OH)

B6: Guanosine 3, 5-cyclic monophosphate (cGMP)

B7: Ferric-reducing ability of plasma (FRAP)

B8: 4-hydroxynonenal (4-HNE)

B9: Thiobarbituric acid reactive species (TBARS)

B10: Total free thiols (TFT)

B11: Protein

B12: Adenosine 5'-triphosphate (ATP)

Appendix C: Numerical datasets used to prepare the figures displayed in the main text.

Appendix D: Pictures related to biofilm dispersal studies.

Appendix E: Figures related to the analysis or each metabolite within the redox thiol metabolome, at assessment and post-AOB assessment visits

Appendix A

Figure A.1 AO+ Mist™ (MotherDirt™, AOBiome LLC). *N. eutropha* D23 cell agglomerates are visible at the bottom of the commercial product depicted on the left.

Appendix B

B1: Ammonium (NH_4^+)

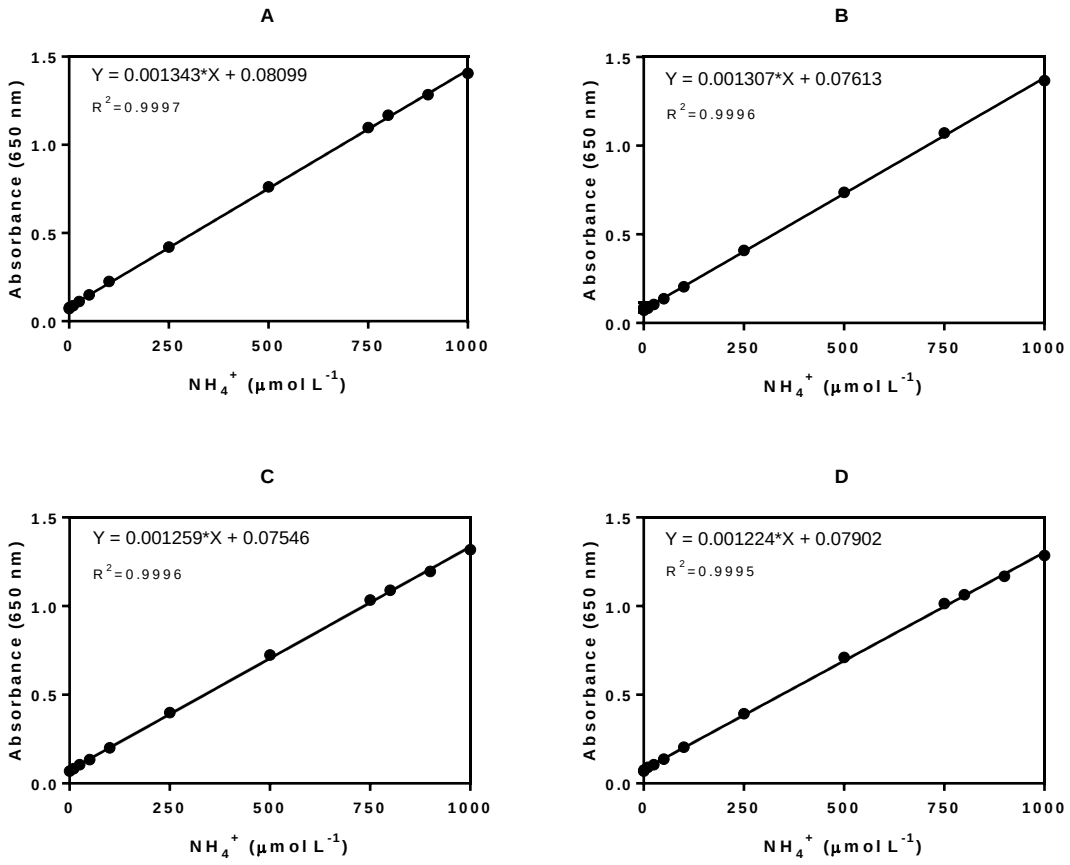

Figure B.1 Examples of calibration curves for NH_4^+ (A-D), using the Berthelot's assay and $(NH_4)_2SO_4$ as standards, in different days.

B2: Nitrite (NO_2^-)

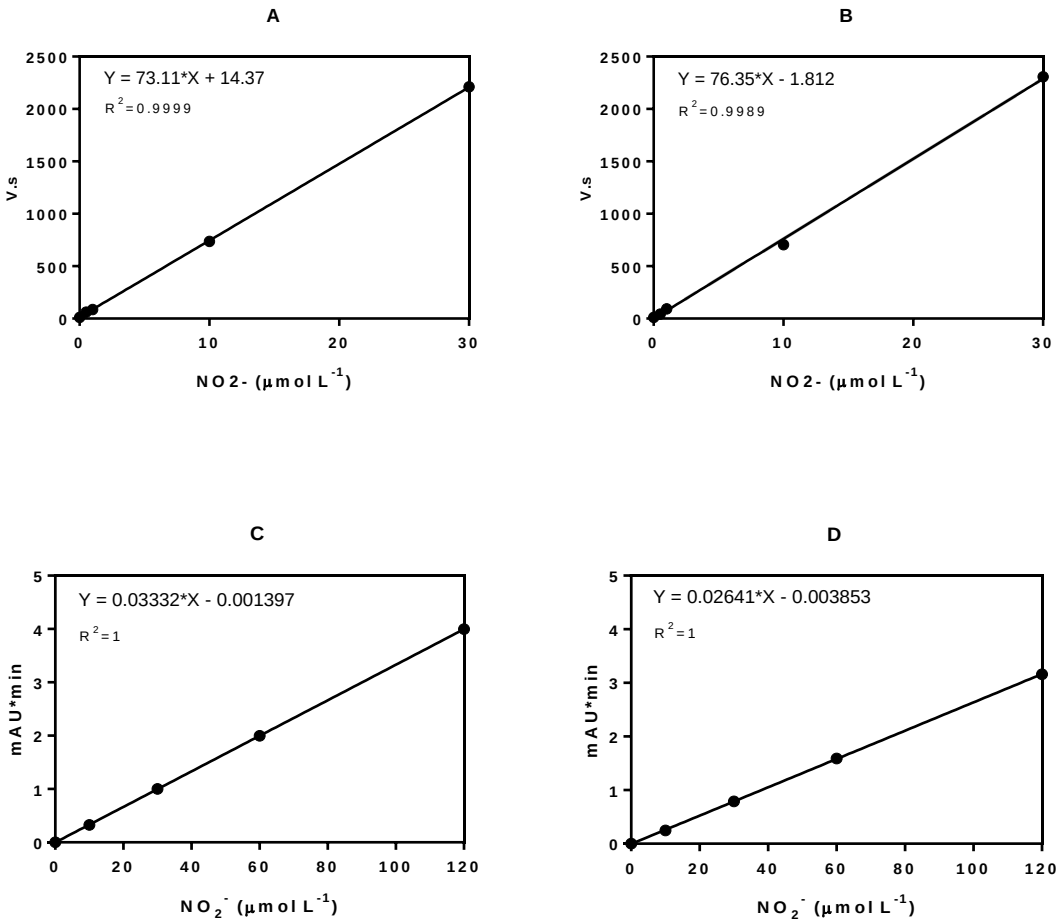

Figure B.2 Examples of calibration curves for NO_2^-, using high-performance liquid chromatography (ENO-20, panels A and B) and ion chromatography (Dionex ICS-5000$^+$, panels C and D), using $NaNO_2$ as standard, and obtained in different days.

B3: Nitrate (NO_3^-)

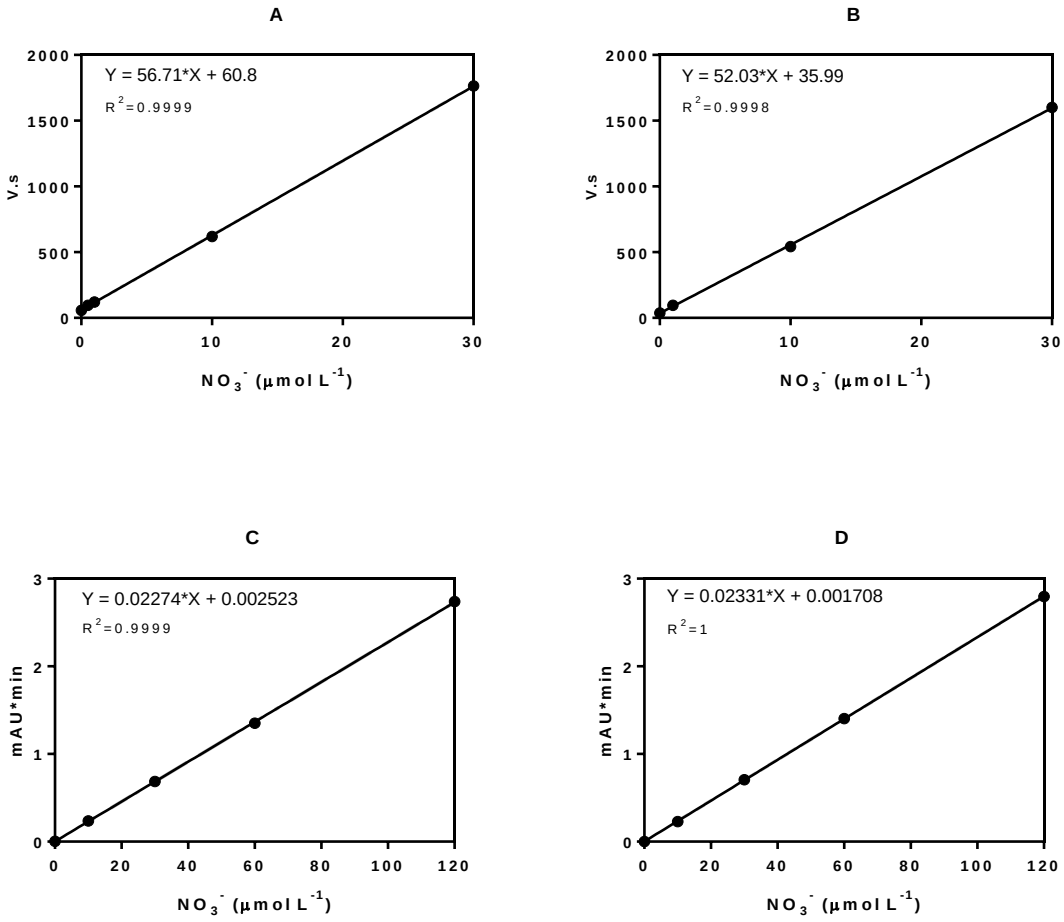

Figure B.3 Examples of calibration curves for NO_3^-, using high-performance liquid chromatography (ENO-20, panels A and B) and ion chromatography (Dionex ICS-5000$^+$, panels C and D), using $NaNO_3$ as standard, and obtained in different days.

B4: Nitric Oxide (NO)

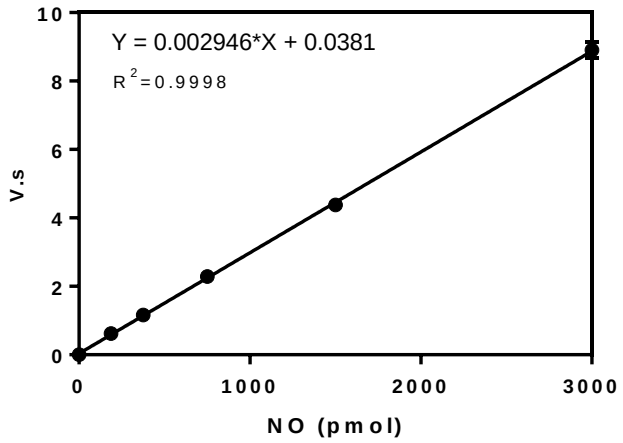

Figure B.4 Example of a calibration curve for chemiluminescence detection and quantification of NO, obtained after reductive denitrosation of NO_2^- standards in tri-iodide mixture solution, under acidic conditions.

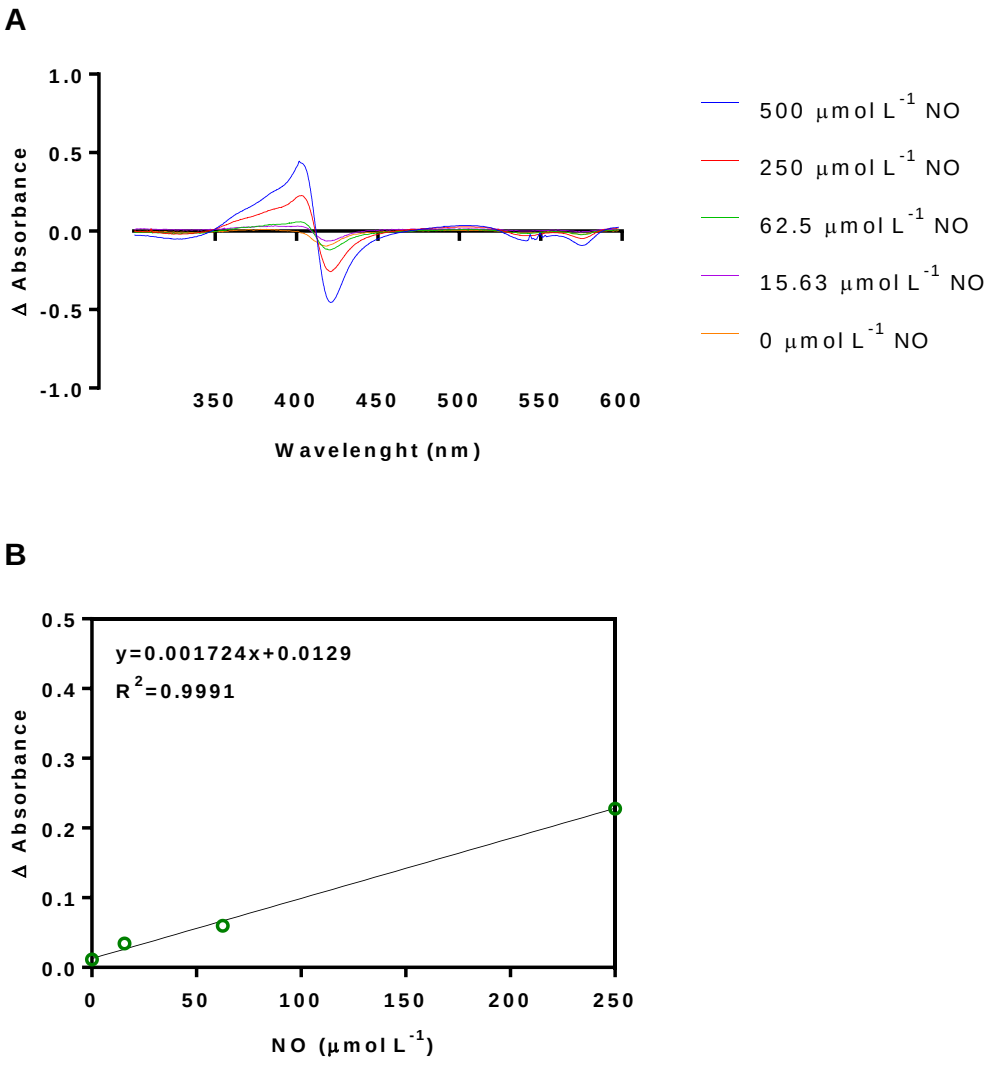

Figure B.5 Example of a calibration curve used for measurement of NO using the oxyHb capture assay, and dethylamine NONOate as an NO-donor.

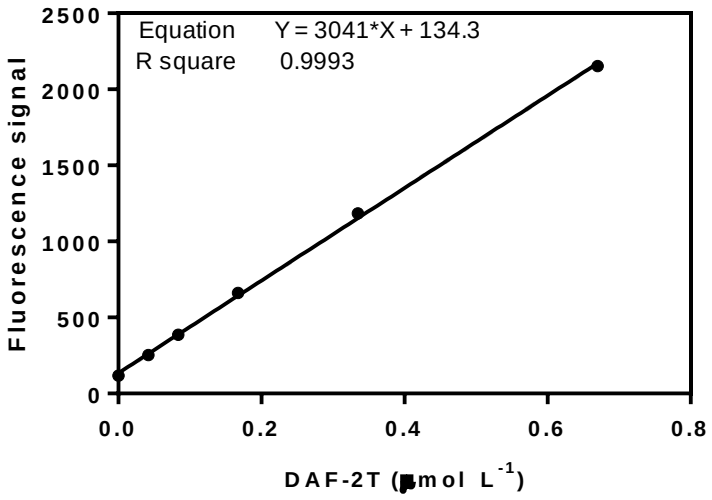

Figure B.6 Calibration curve used for measurement of DAF-2T, as an indirect method for detection and measurement of NO in solution. Calibration performed using authentic DAF-2T standard (Abcam).

B5: Hydroxylamine (NH_2OH)

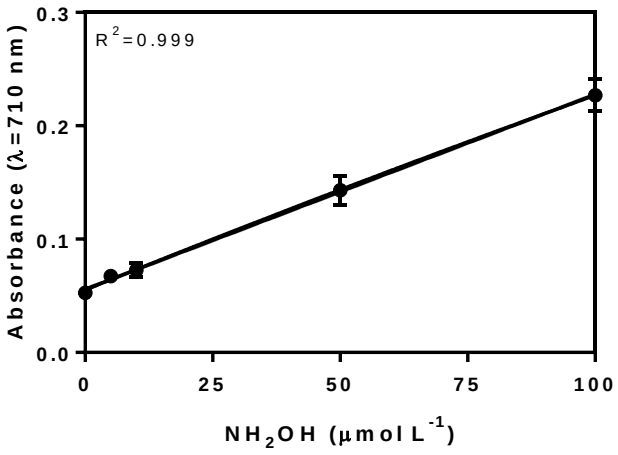

Figure B.7 Example of a calibration curve for NH_2OH. Interpolation of sample concentrations from a quadratic-fit curve.

B6: Guanosine 3, 5-cyclic monophosphate (cGMP)

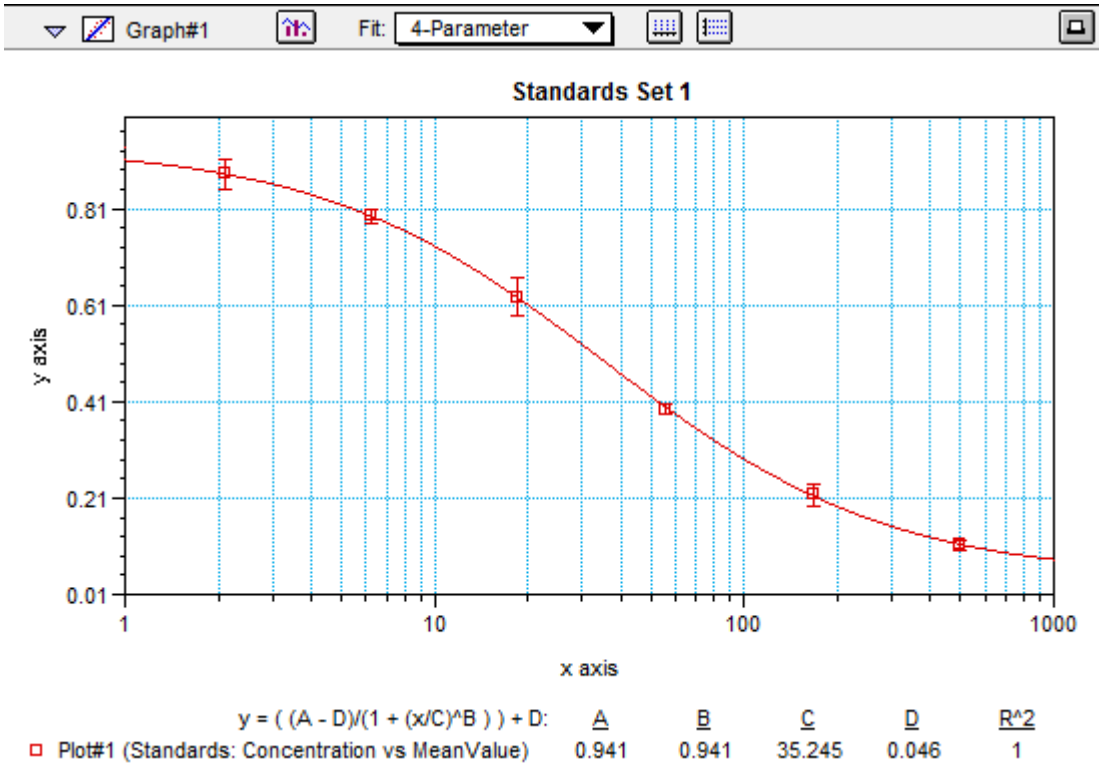

Figure B.8 Calibration curve for the measurement of cGMP in plasma samples.

B7: Ferric-reducing ability of plasma (FRAP)

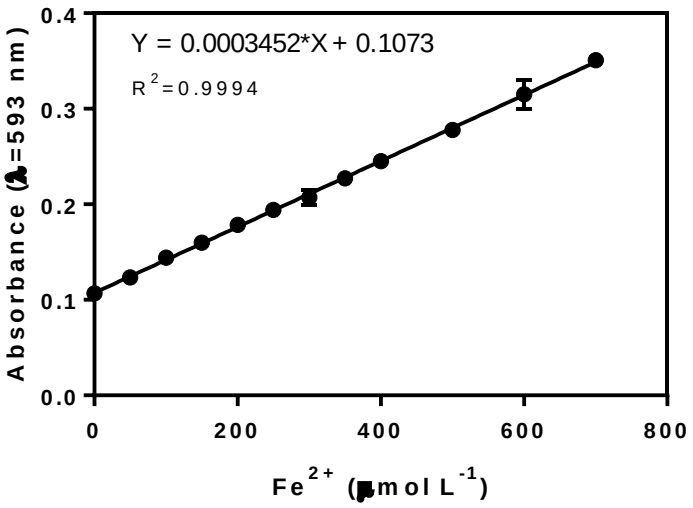

Figure B.9 Calibration curve for the measurement of FRAP in plasma samples.

B8: 4-hydroxynonenal (4-HNE)

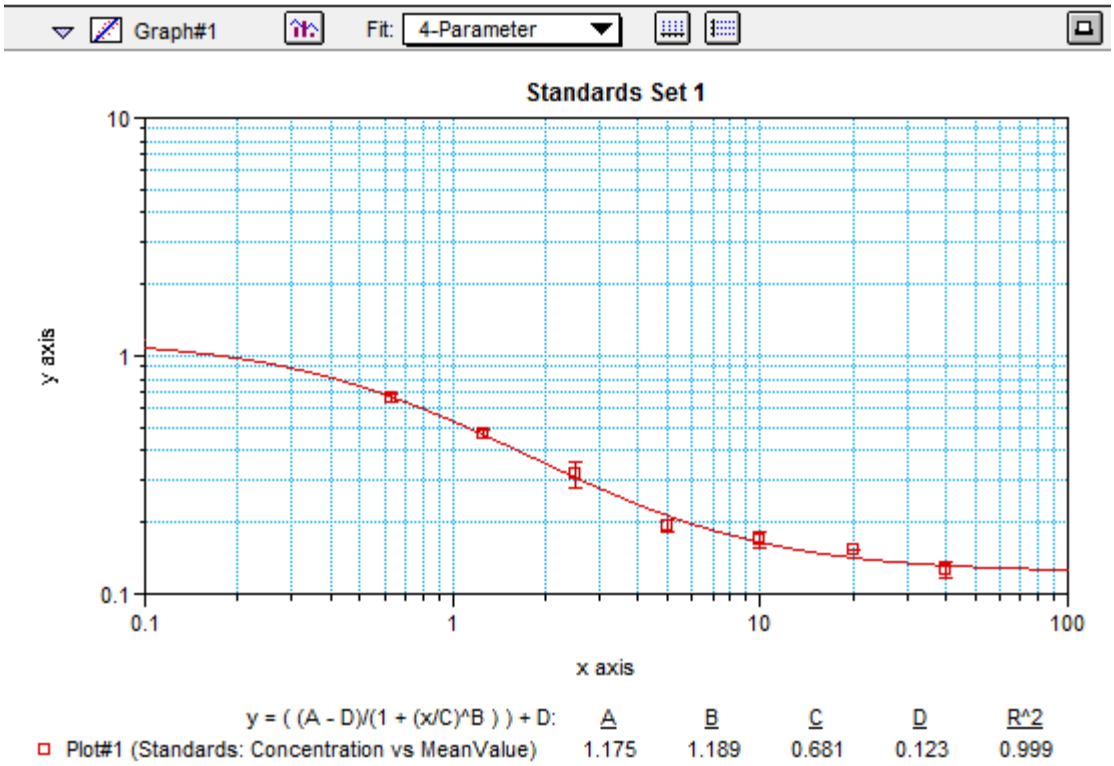

Figure B.10 Calibration curve for the measurement of 4-HNE in plasma samples.

B9: Thiobarbituric acid reactive species (TBARS)

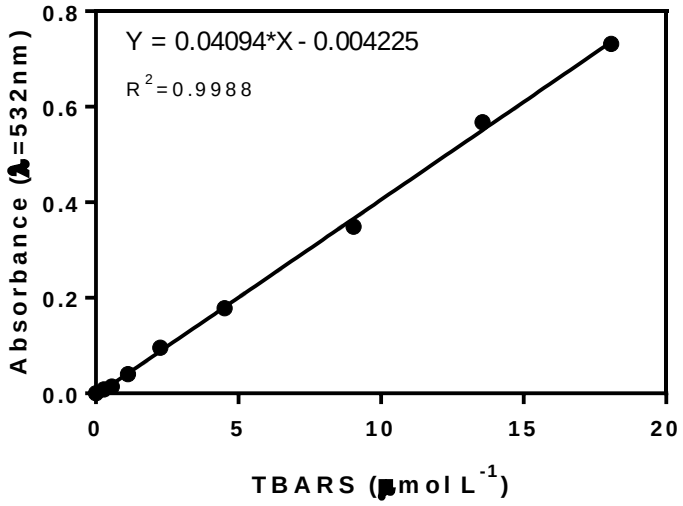

Figure B.11 Calibration curve for the measurement of TBARS in plasma samples.

B10: Total free thiols (TFT)

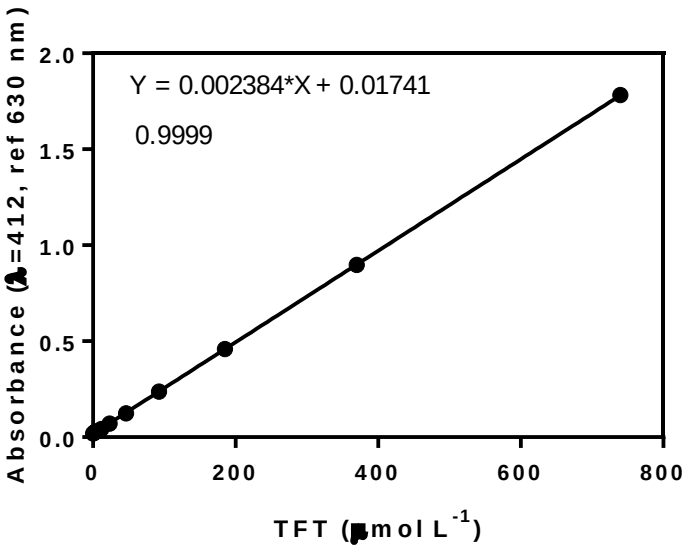

Figure B.12 Calibration curve used for the measurement of TFT in plasma samples.

B11: Protein

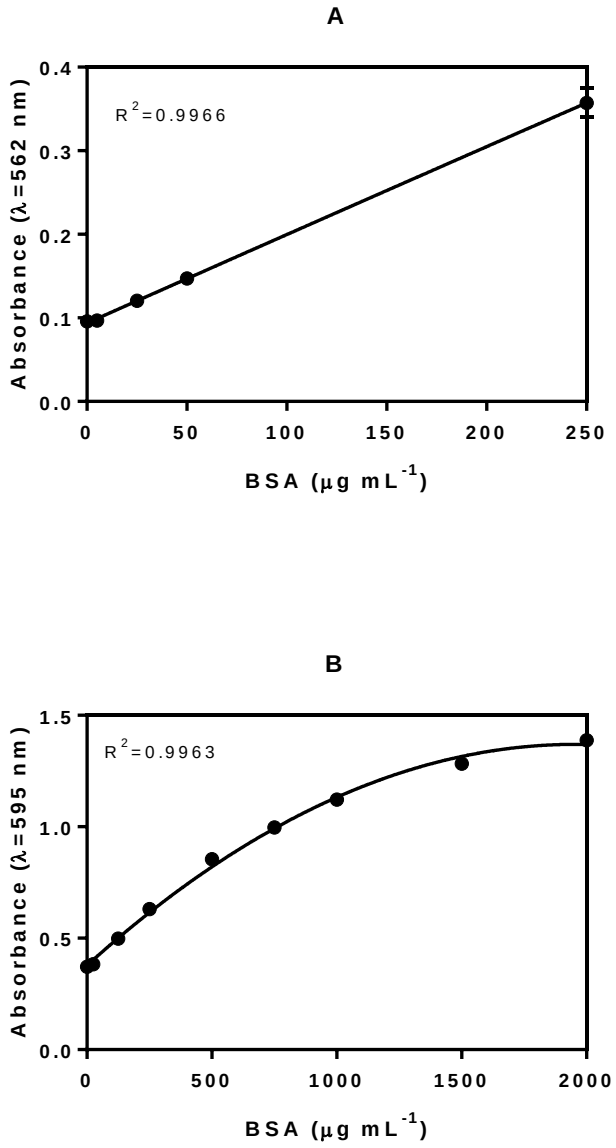

Figure B.13 Example of calibration curves used for the measurement of protein in microbial (panel A, BCA assay) and human (panel B, Coomassie assay) samples.

B12: Adenosine 5-triphosphate (ATP)

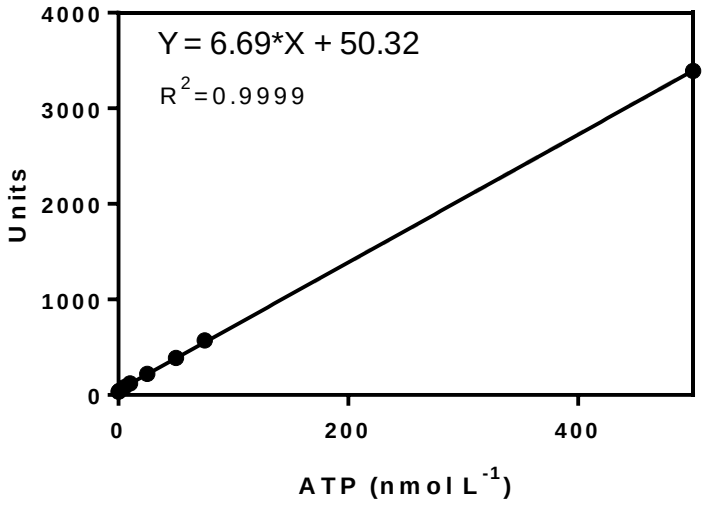

Figure B.14 Example of a calibration curve used for the measurement of adenosine 5'-triphosphate in bacterial lysate samples.

Appendix C

Table C.1 Numerical dataset used for the preparation of Figure 4.2. Statistical significance determined using unpaired *t*-test, with alpha=0.05.

	OD (584nm) Control		OD (584nm) Treatment		Reduction		
	Mean±SD	**n**	**Mean±SD**	**n**	**Difference**	**%**	**P-value**
N. eutropha (M9)	0.470±0.063	20	0.349±0.026	20	-0.121	-25.7	<0.0001
N. eutropha (M9+5)	0.474±0.041	20	0.384±0.059	20	-0.090	-18.9	<0.0001
HK *N. eutropha*	0.482±0.065	20	0.531±0.061	20	0.049	10.2	0.0182

Table C.2 Numerical dataset used for the preparation of Figure 4.4 (panel A). Statistical significance determined using Kruskal-Wallis (Dunn's correction), with alpha=0.05.

	OD (584nm)		Dispersal (vs control)		
	Mean±SD	**n**			
Control	0.350±0.051	10	**Difference**	**%**	**P-value**
5 µM NOx	0.381±0.047	10	0.031	+8.9	0.8336
50 µM NOx	0.375±0.051	10	0.025	+7.1	>0.9999
500 µM NOx	0.411±0.026	10	0.061	+17.4	0.0318
5000 µM NOx	0.416±0.028	10	0.066	+18.9	0.0230

Table C.3 Numerical dataset used for the preparation of Figure 4.4 (panel B). Statistical significance determined Kruskal-Wallis (Dunn's correction), with alpha=0.05.

	OD (584nm)		Dispersal (vs control)		
	Mean±SD	**n**			
Control	0.326±0.058	20	**Difference**	**%**	**P-value**
5 µM NO_2^-	0.361±0.032	10	+0.035	+10.7	0.4017
50 µM NO_2^-	0.355±0.022	10	+0.029	+8.9	0.6866
500 µM NO_2^-	0.333±0.018	10	+0.006	+1.8	>0.9999
5000 µM NO_2^-	0.346±0.026	10	+0.019	+5.8	>0.9999
5 µM NO_3^-	0.339±0.053	10	+0.013	+4.0	>0.9999
50 µM NO_3^-	0.328±0.039	10	+0.002	+0.6	>0.9999
500 µM NO_3^-	0.360±0.028	10	+0.034	+10.4	0.3853
5000 µM NO_3^-	0.422±0.075	10	+0.096	+29.4	0.0029

Table C.4 Numerical dataset used for the preparation of Figure 4.5. Statistical significance determined using Kruskal-Walis (Dunn's correction), with alpha=0.05.

	OD (584nm)		Dispersal		
	Mean±SD	**n**			
(A) Control	0.253±0.039	15	**Difference**	**%**	**P-value**
(B) Control (+0.3mM CPTIO)	0.254±0.054	20	-	-	>0.9999 (vs A)
(C) Control (+1.3mM CPTIO)	0.259±0.053	20	-	-	>0.9999 (vs A)
(D) *N. eutropha*	0.185±0.029	20	-0.068	-26.9	0.0008 (vs A)
(E) *N. eutropha* (+0.3mM CPTIO)	0.276±0.032	20	+0.022	+8.6	0.9412 (vs B)
(F) *N. eutropha* (+1.3mM CPTIO)	0.237±0.044	20	-0.021	-8.1	>0.9999 (vs C)

Table C.5 Numerical dataset used for the preparation of Figure 4.6. Statistical significance determined Kruskal-Wallis (Dunn's correction), with alpha=0.05.

	OD (584nm)		Dispersal (vs control)		
	Mean±SD	**n**			
Control	0.400±0.047	30	**Difference**	**%**	**P-value**
HK-NE23	0.408±0.044	30	+0.008	+2.00	>0.9999
OD_{600}=0.007	0.373±0.043	30	-0.027	-6.75	0.4577
OD_{600}=0.033	0.345±0.031	30	-0.055	-13.75	0.0015
OD_{600}=0.091	0.309±0.037	30	-0.091	-22.75	<0.0001
OD_{600}=0.152	0.304±0.021	30	-0.096	-24.00	<0.0001

Table C.6 Numerical dataset used for the preparation of Figure 4.7. Statistical significance determined Kruskal-Wallis (Dunn's correction), with alpha=0.05.

	OD (584nm)		Dispersal (vs control)		
	Mean±SD	**n**			
Control	0.262±0.061	28	**Difference**	**%**	**P-value**
HK-NE23	0.277±0.079	30	+0.015	+5.73	>0.9999
OD_{600}=0.007	0.292±0.107	30	+0.030	+11.45	>0.9999
OD_{600}=0.033	0.279±0.105	30	+0.017	+6.49	>0.9999
OD_{600}=0.091	0.300±0.090	30	+0.038	+14.50	0.5512
OD_{600}=0.152	0.343±0.108	30	+0.081	+30.92	0.0084

Table C.7 Numerical dataset used for the preparation of Figure 4.8. Statistical significance determined Kruskal-Wallis (Dunn's correction), with alpha=0.05.

	OD (584nm)		Dispersal (vs control)		
	Mean±SD	**n**			
Control	0.457±0.049	30	**Difference**	**%**	**P-value**
HK-NE23	0.522±0.066	30	+0.065	+14.22	0.0011
OD_{600}=0.007	0.478±0.052	30	+0.021	+4.60	0.4758
OD_{600}=0.033	0.468±0.055	30	+0.011	+2.41	>0.9999
OD_{600}=0.091	0.456±0.054	30	-0.001	-0.22	>0.9999
OD_{600}=0.152	0.441±0.066	30	-0.016	-3.50	>0.9999

Table C.8 Numerical dataset used for the preparation of Figure 4.9. Statistical significance determined Kruskal-Wallis (Dunn's correction), with alpha=0.05.

	OD (584nm)		Dispersal (vs control)		
	Mean±SD	**n**			
Control	0.415±0.048	30	**Difference**	**%**	**P-value**
HK-NE23	0.469±0.039	30	+0.054	+13.01	0.2522
OD_{600}=0.007	0.408±0.051	30	-0.007	-1.69	>0.9999
OD_{600}=0.033	0.276±0.031	30	-0.139	-33.49	<0.0001
OD_{600}=0.091	0.242±0.027	30	-0.173	-41.69	<0.0001
OD_{600}=0.152	0.242±0.028	30	-0.173	-41.69	<0.0001

Table C.9 Numerical dataset used for the preparation of Figure 4.10 (panel A). Statistical significance determined Kruskal-Wallis (Dunn's correction), with alpha=0.05.

	CFU mL^{-1}		Dispersal	
	Mean±SD	**n**	**(vs control)**	
Control	$3.93x10^7±1.78x10^7$	6	**Difference**	**P-value**
HK-NE23	$3.00x10^7±1.15x10^7$	5	$-9.37x10^6$	>0.9999
OD_{600}=0.007	$2.07x10^7±6.16x10^6$	6	$-1.86x10^7$	>0.9999
OD_{600}=0.033	$9.53x10^6±3.02x10^6$	6	$-2.98x10^7$	0.0015
OD_{600}=0.091	$1.04x10^7±3.95x10^6$	6	$-2.89x10^7$	0.0060
OD_{600}=0.152	$1.17x10^7±3.70x10^6$	6	$-2.77x10^7$	0.0122

Table C.10 Numerical dataset used for the preparation of Figure 4.10 (panel B). Statistical significance determined Kruskal-Wallis (Dunn's correction), with alpha=0.05.

	CFU mL^{-1}		Dispersal	
	Mean±SD	**n**	**(vs control)**	
Control	$6.17x10^7±2.21x10^7$	6	**Difference**	**P-value**
HK-NE23	$7.23x10^7±2.38x10^7$	6	$-1.91x10^7$	>0.9999
OD_{600}=0.007	$5.07x10^7±1.38x10^6$	6	$-2.00x10^7$	>0.9999
OD_{600}=0.033	$2.75x10^6±1.26x10^6$	6	$-3.42x10^7$	0.0198
OD_{600}=0.091	$4.17x10^7±1.12x10^6$	6	$-1.10x10^7$	0.4844
OD_{600}=0.152	$4.25x10^7±1.70x10^6$	6	$-1.07x10^7$	0.7293

Table C.11 Numerical dataset used for the preparation of Figure 4.11. Statistical significance determined Kruskal-Wallis (Dunn's correction), with alpha=0.05.

	CFU mL^{-1}		Dispersal	
2h	**Mean±SD**	**n**	**(vs control)**	
Control	$7.90x10^6±7.07x10^5$	2	**Difference**	**P-value**
HK-NE23	$5.50x10^6±1.27x10^6$	2	$-2.40x10^6$	>0.9999
OD_{600}=0.007	$8.00x10^6±8.49x10^5$	2	$+1.00x10^5$	>0.9999
OD_{600}=0.033	$1.20x10^7±1.98x10^6$	2	$+4.10x10^6$	0.5507
OD_{600}=0.091	$1.62x10^7±8.20x10^6$	2	$+8.30x10^6$	0.5507
OD_{600}=0.152	$1.08x10^7±2.55x10^6$	2	$+2.90x10^6$	>0.9999

	CFU mL^{-1}		Dispersal	
4h	**Mean±SD**	**n**	**(vs control)**	
Control	$5.10x10^6±1.56x10^6$	2	**Difference**	**P-value**
HK-NE23	$1.80x10^7$	1	$+1.29x10^7$	-
OD_{600}=0.007	$2.60x10^6±5.66x10^5$	2	$-2.50x10^6$	>0.9999
OD_{600}=0.033	$9.20x10^6±6.79x10^6$	2	$+4.10x10^6$	>0.9999
OD_{600}=0.091	$6.00x10^6±5.66x10^5$	2	$+9.00x10^5$	>0.9999
OD_{600}=0.152	$7.90x10^6±7.07x10^5$	2	$2.80x10^6$	0.7458

	CFU mL^{-1}		Dispersal	
6h	**Mean±SD**	**n**	**(vs control)**	
Control	$5.70x10^6±4.24x10^5$	2	**Difference**	**P-value**
HK-NE23	$7.30x10^6±7.07x10^5$	2	$+1.60x10^6$	>0.9999
OD_{600}=0.007	$3.26x10^6±1.33x10^6$	2	$-2.44x10^6$	0.8276
OD_{600}=0.033	$2.72x10^6±1.70x10^5$	2	$-2.98x10^6$	0.3574
OD_{600}=0.091	$3.08x10^6±1.13x10^5$	2	$-2.62x10^6$	>0.9999
OD_{600}=0.152	$4.50x10^6±1.56x10^6$	2	$-1.20x10^6$	>0.9999

Table C.12 Numerical dataset used for the preparation of Figure 4.12. Statistical significance determined using unpaired *t*-test, with alpha=0.05.

	OD (584nm) Control		OD (584nm) Treatment		Dispersal (vs control)		
	Mean±SD	**n**	**Mean±SD**	**n**	**Difference**	**%**	**P-value**
PA10	0.341±0.025	10	0.145±0.010	10	-0.1965	-57.61	<0.0001
PA15	0.154±0.021	10	0.109±0.018	10	-0.0453	-29.34	0.0004
PA21	0.237±0.024	10	0.086±0.014	10	-0.1503	-63.55	<0.0001
PA26	0.576±0.053	10	0.314±0.025	10	-0.2621	-45.48	<0.0001
PA30	0.858±0.040	10	0.784±0.084	10	-0.0733	-8.55	0.0667
PA37	0.393±0.028	10	0.252±0.017	10	-0.1406	-35.79	<0.0001
PA39	0.111±0.023	10	0.076±0.021	10	-0.0359	-32.23	0.0069
PA44	0.189±0.016	10	0.200±0.030	10	+0.0103	+5.44	0.3543
PA49	0.098±0.012	10	0.058±0.007	10	-0.0398	-40.70	<0.0001
PA55	0.239±0.019	10	0.182±0.020	10	-0.0562	-23.55	<0.0001
PA56	0.210±0.049	10	0.119±0.020	10	-0.091	-43.44	0.0002
PA57	0.261±0.055	10	0.183±0.034	10	-0.0788	-30.16	0.0060
PA58	0.081±0.007	10	0.032±0.010	10	-0.0495	-61.04	<0.0001
PA66	0.448±0.099	10	0.289±0.068	10	-0.1589	-35.45	0.0034
PA68	0.897±0.204	10	0.708±0.0281	10	-0.1889	-21.07	0.1945

Appendix D

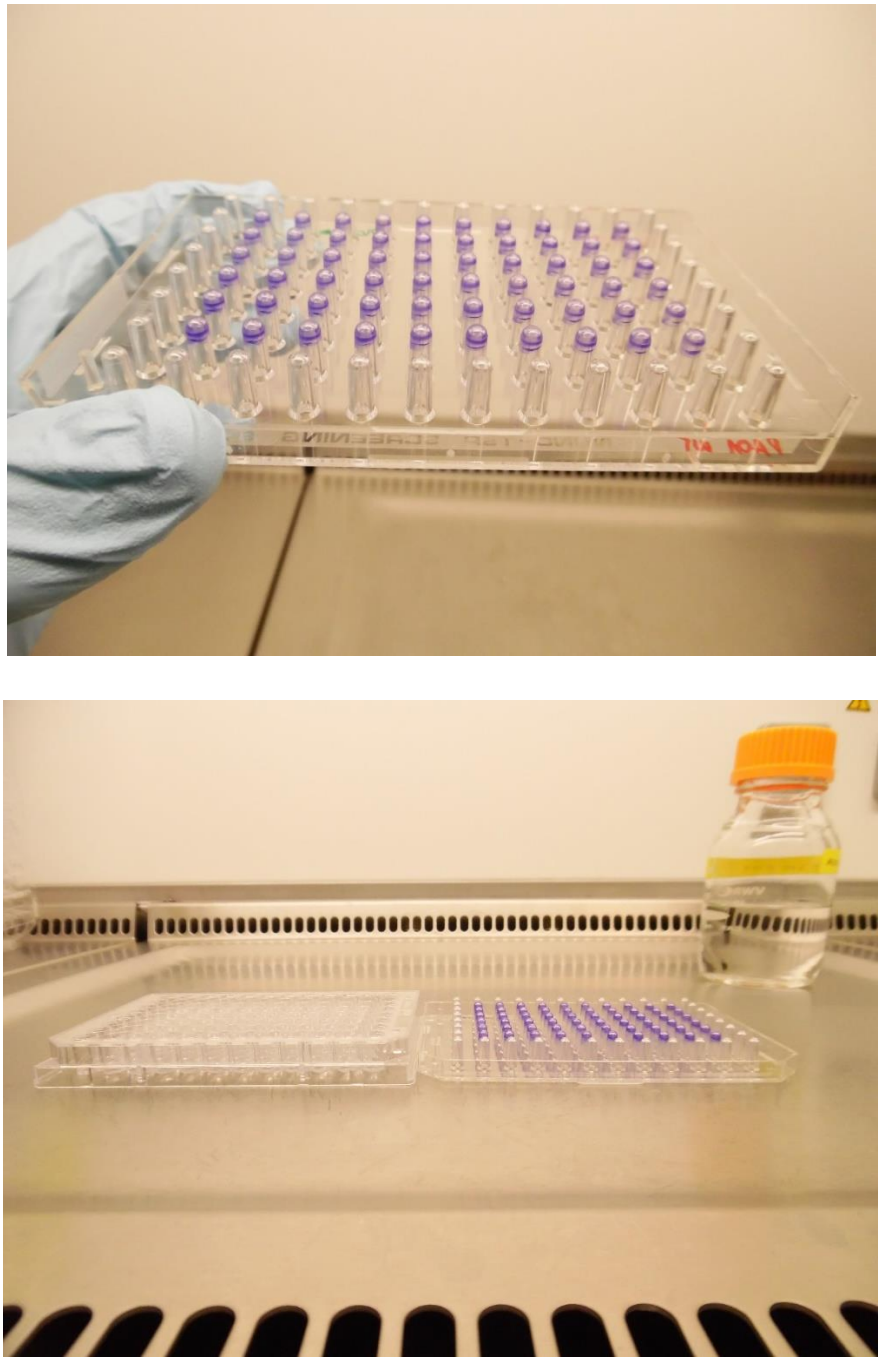

Figure D.1 *P. aeruginosa* biofilms stained with 0.1% crystal violet, before dissolution in glacial acetic acid – transfer-peg lid examples.

Appendix E

E1: Sulfate

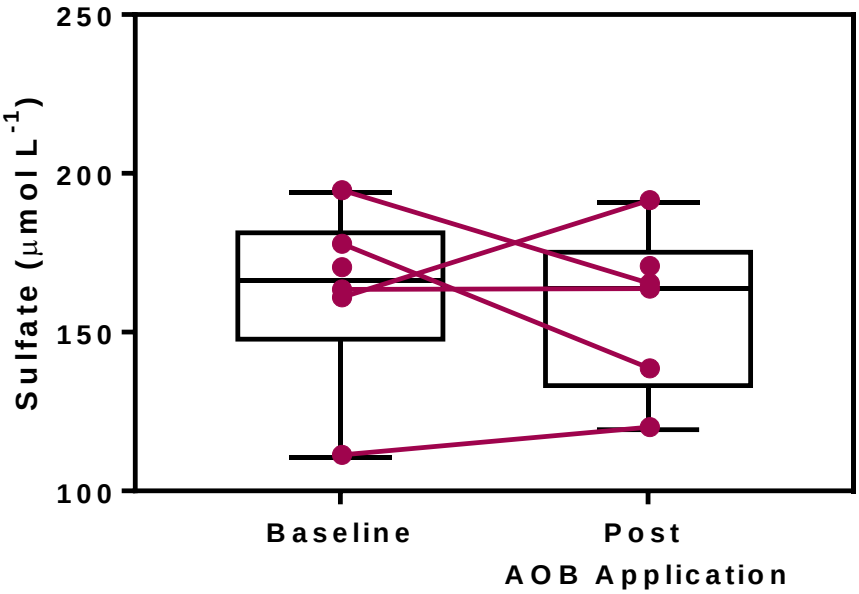

E2: Thiosulfate

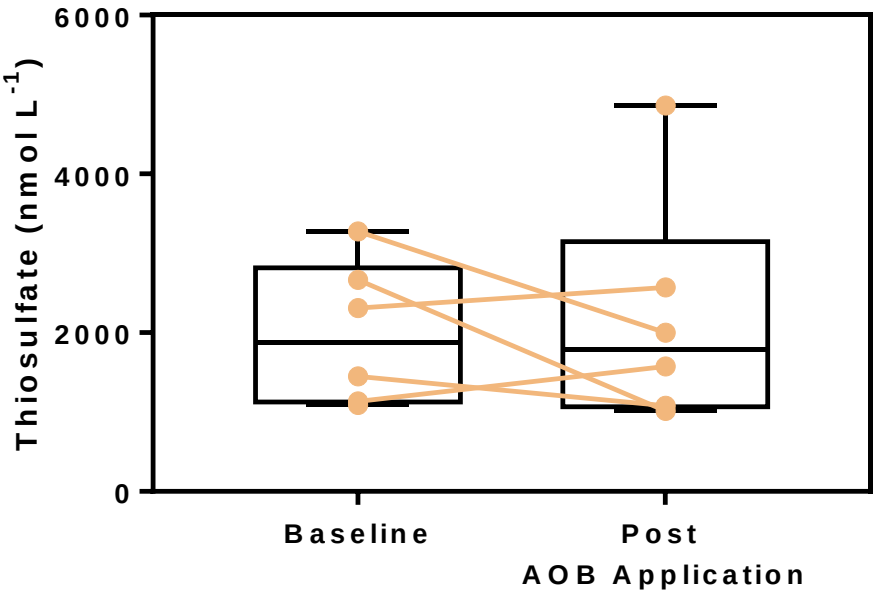

E3: Reduced glutathione (GSH)

- **Free**

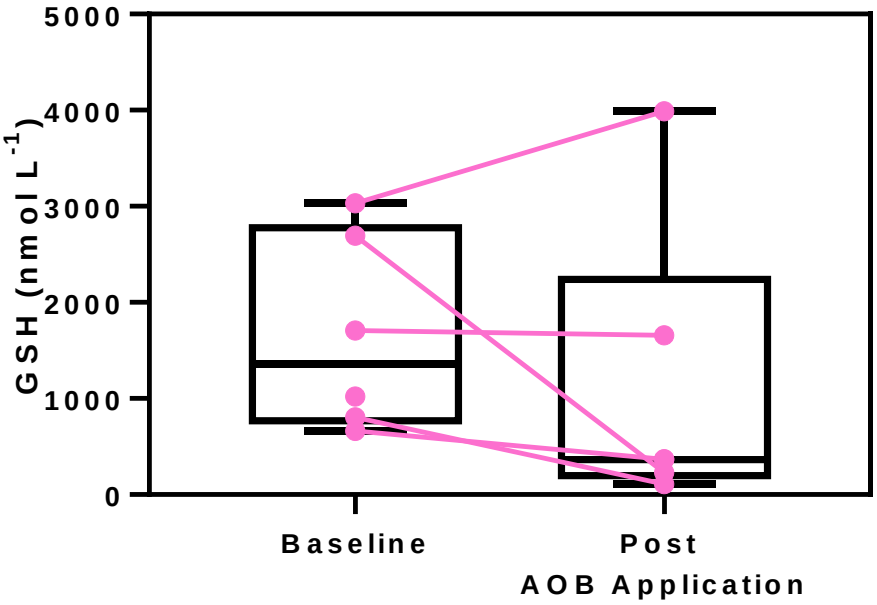

- **Bound**

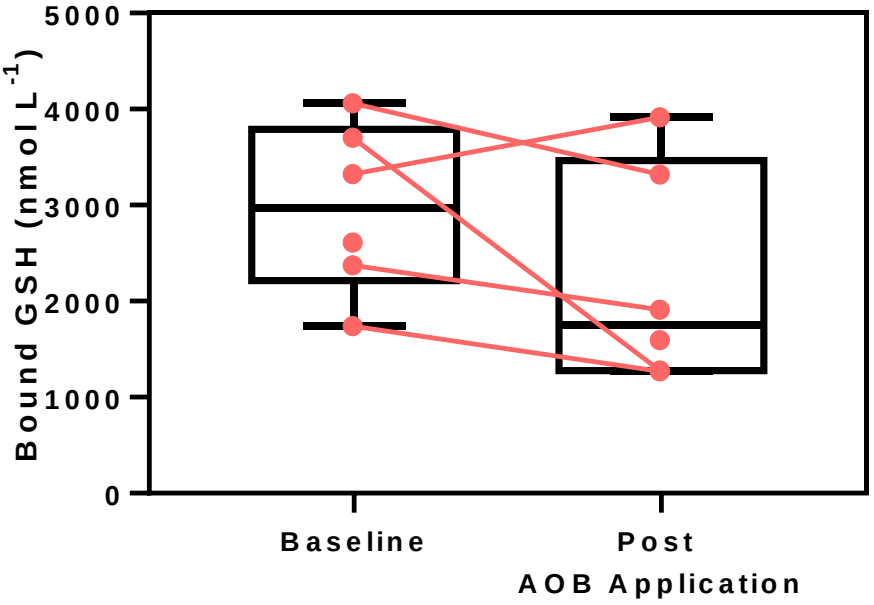

E4: Oxidised glutathione (GSSG)

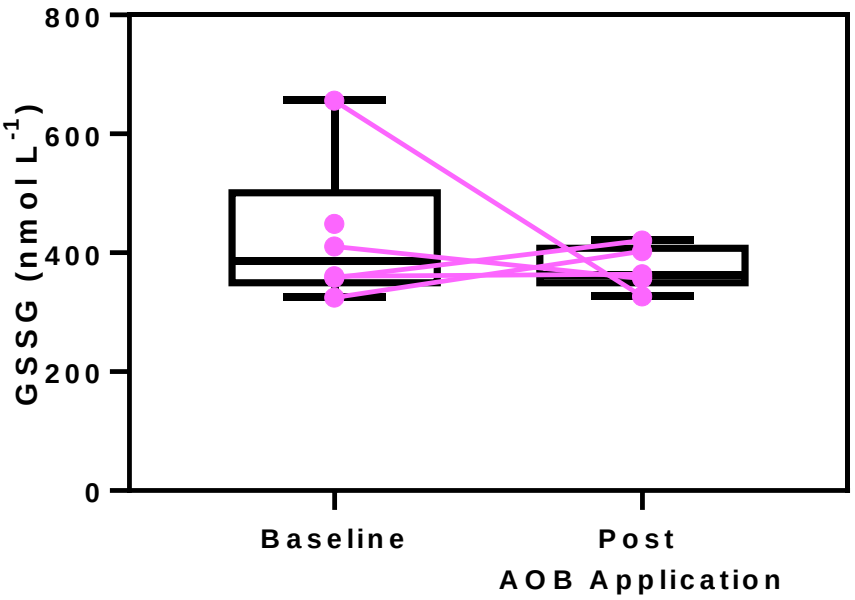

E5: Cysteine (Cys)

- **Free**

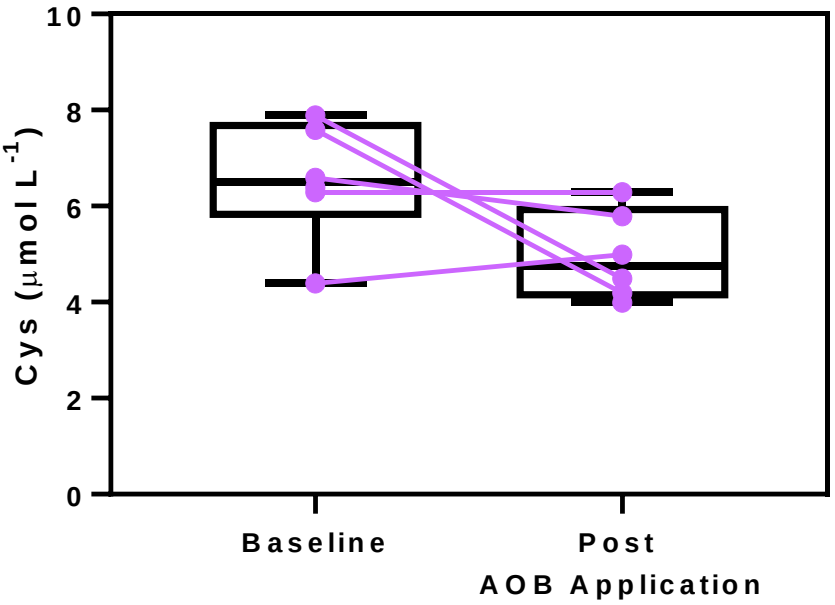

- **Bound**

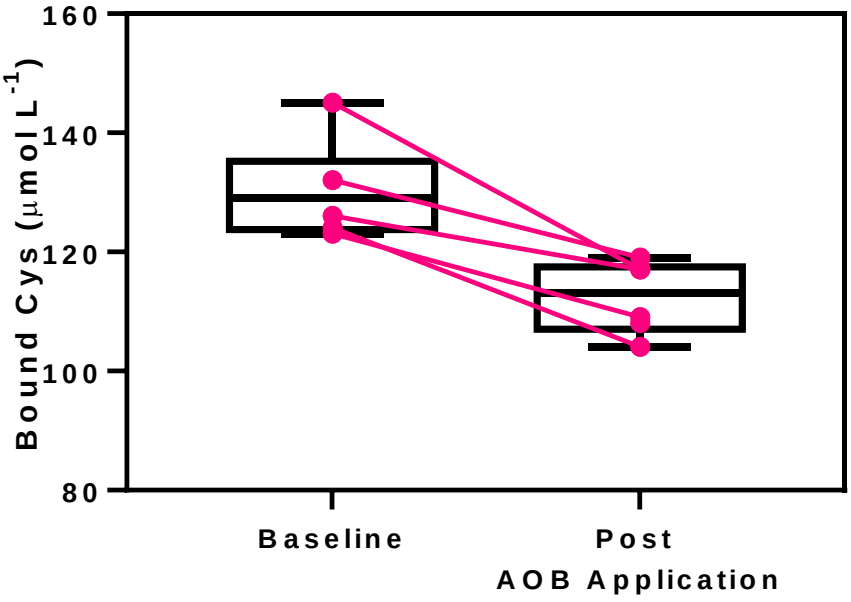

E6: Cystine (CysSS)

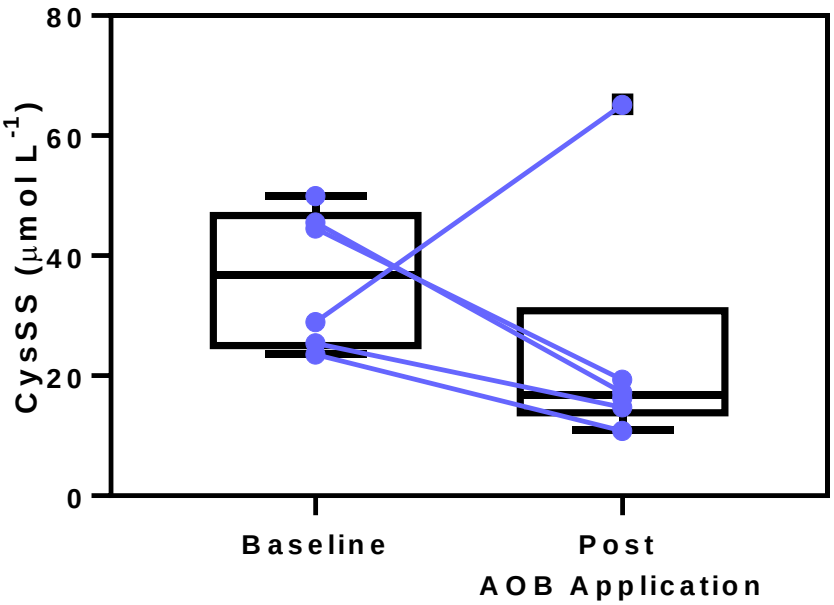

E7: Homocysteine (HCys)

- **Free**

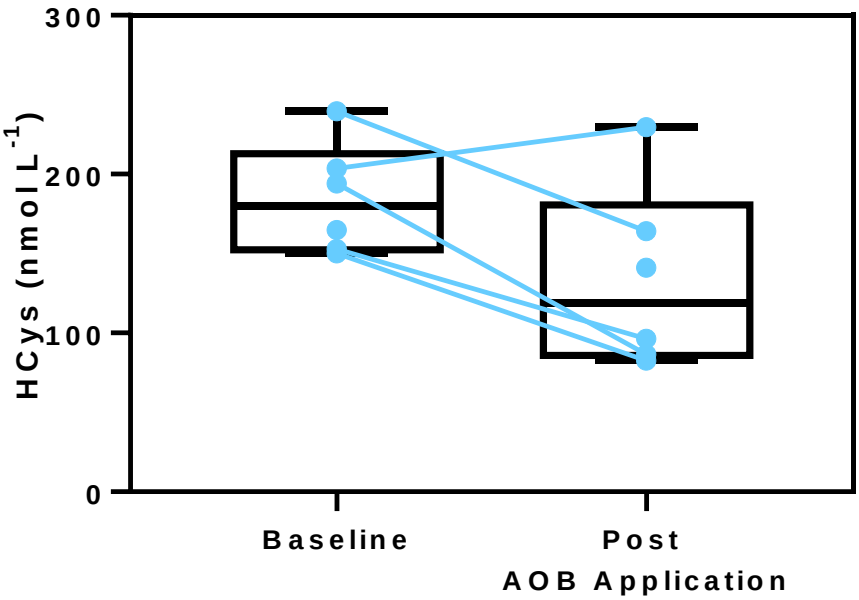

- **Bound**

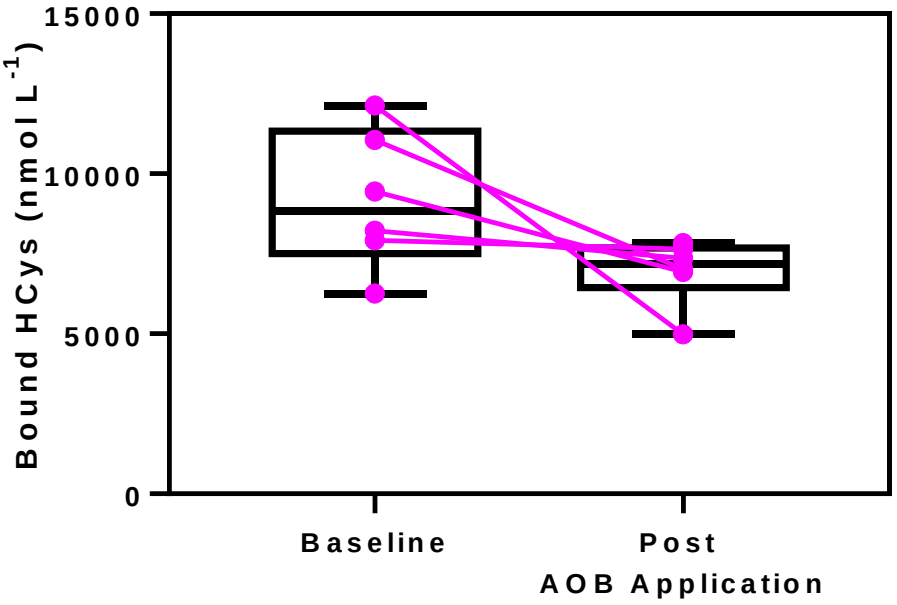

E8: Homocystine (HCysSS)

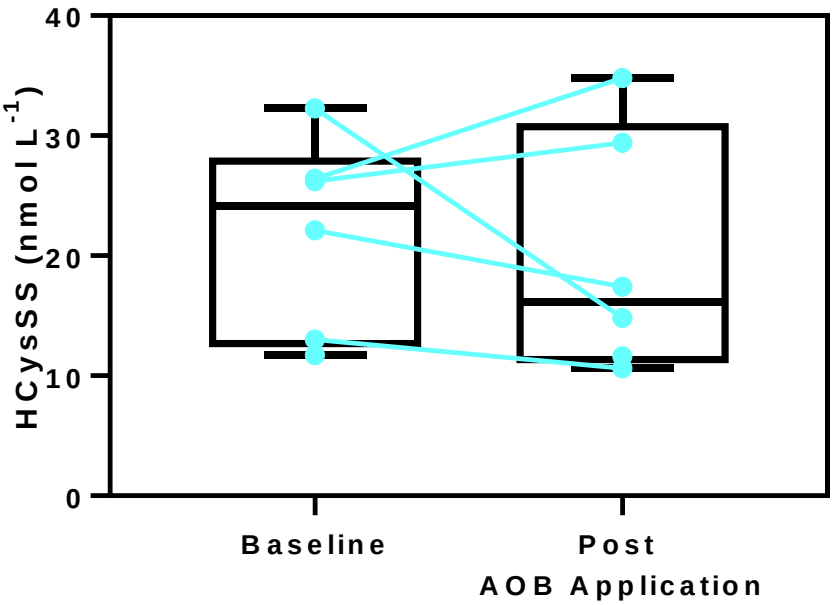

E9: N-acetilcysteine (NAC)

- **Free**

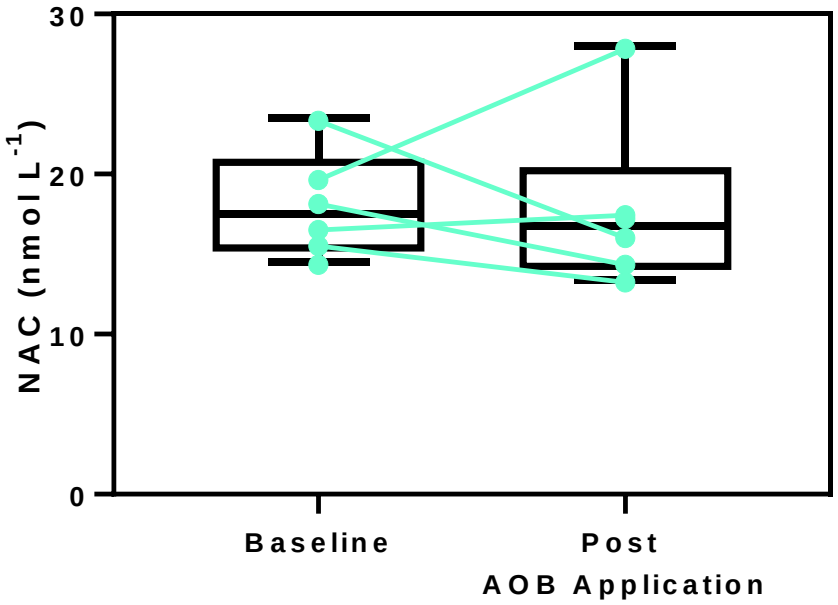

- **Bound**

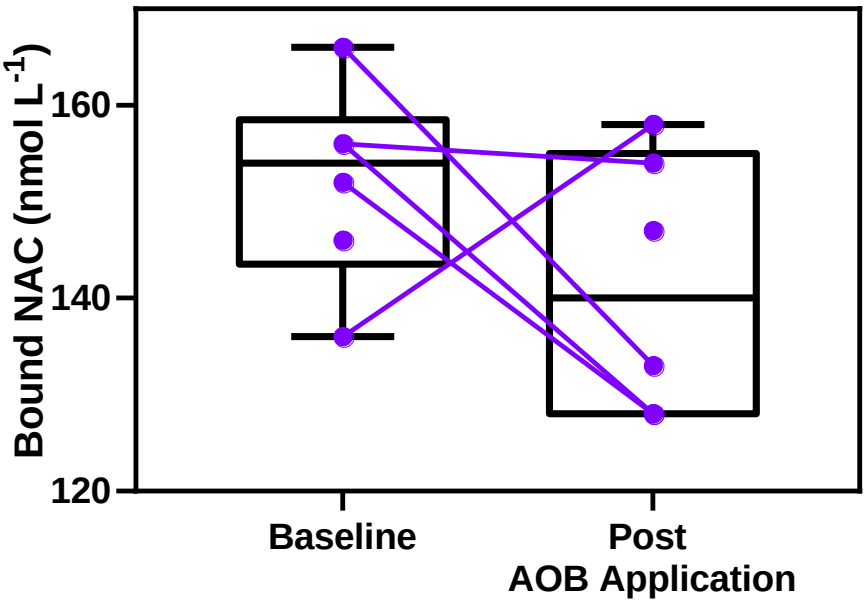

E10: Sulfide

- **Free**

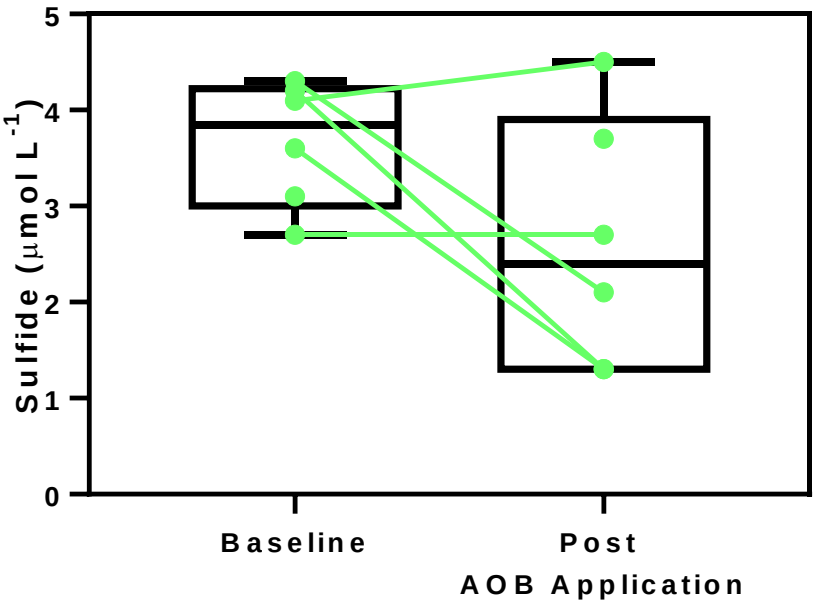

- **Bound**

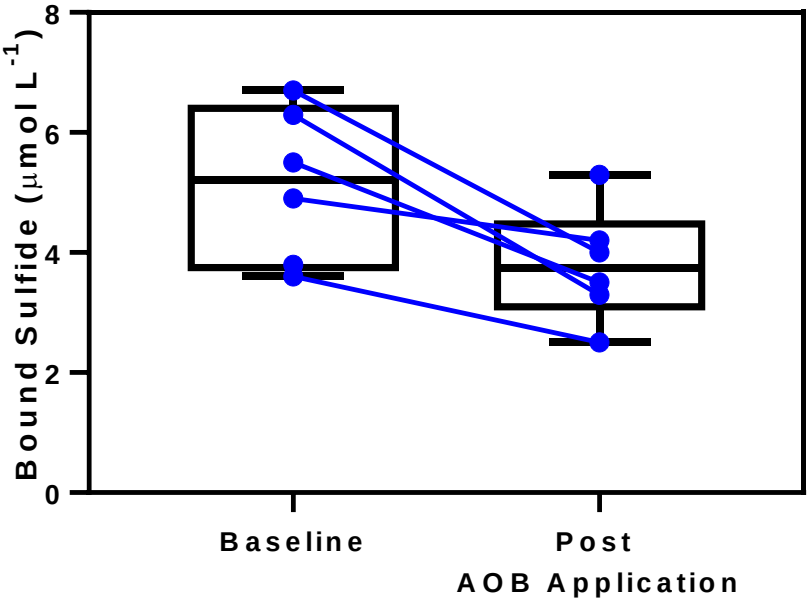

E11: Cysteinylglycine (CysGly)

- **Free**

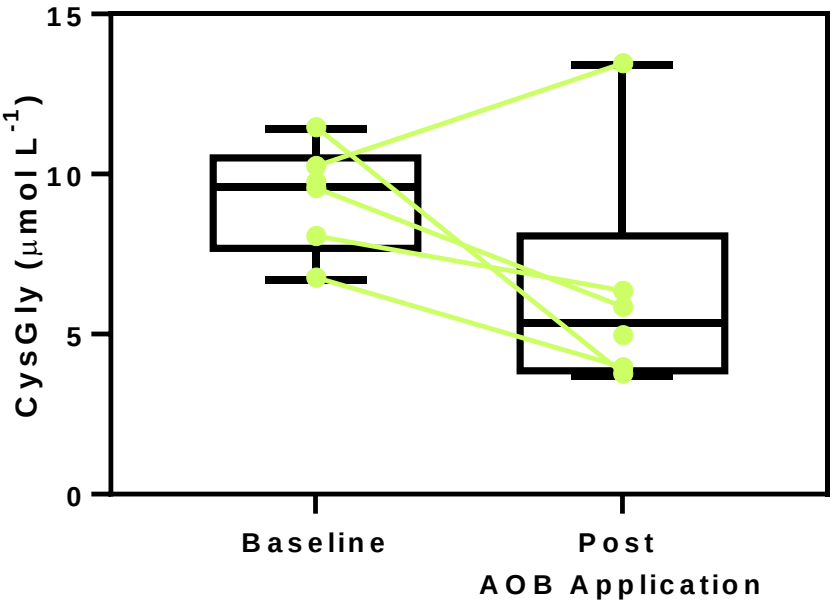

- **Bound**

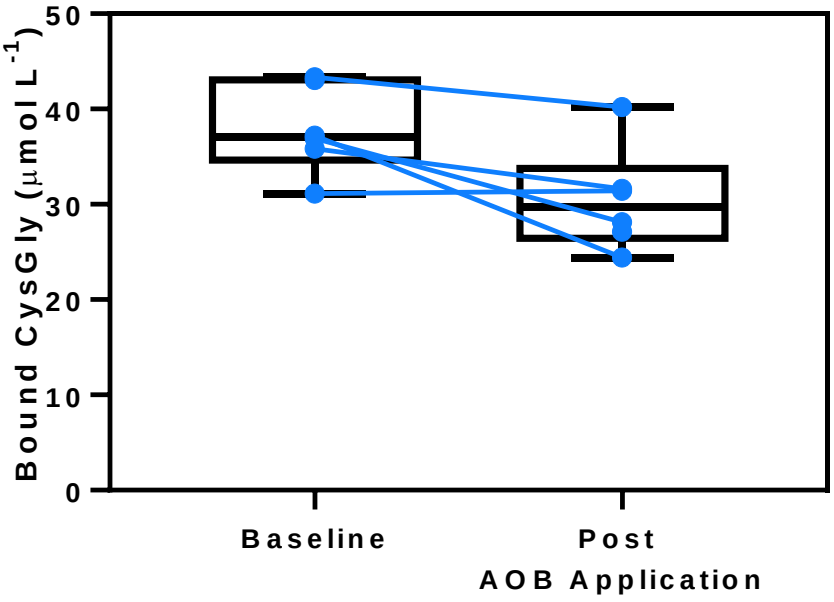

E12: Glutamylcysteine (GluCys)

- **Free**

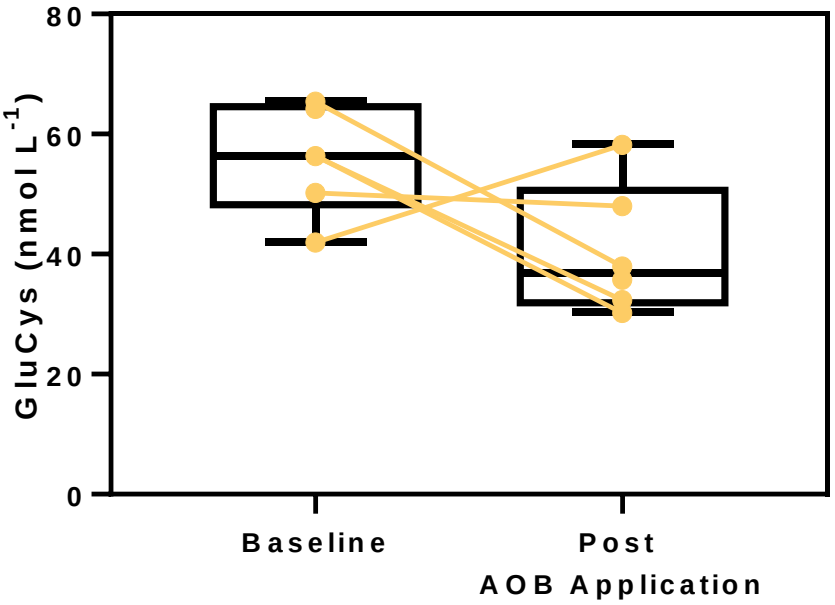

- **Bound**

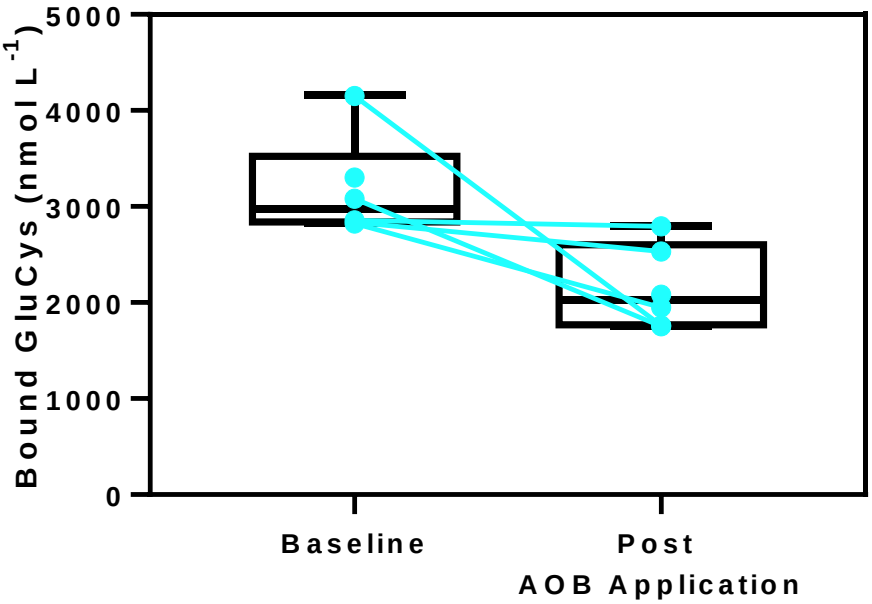

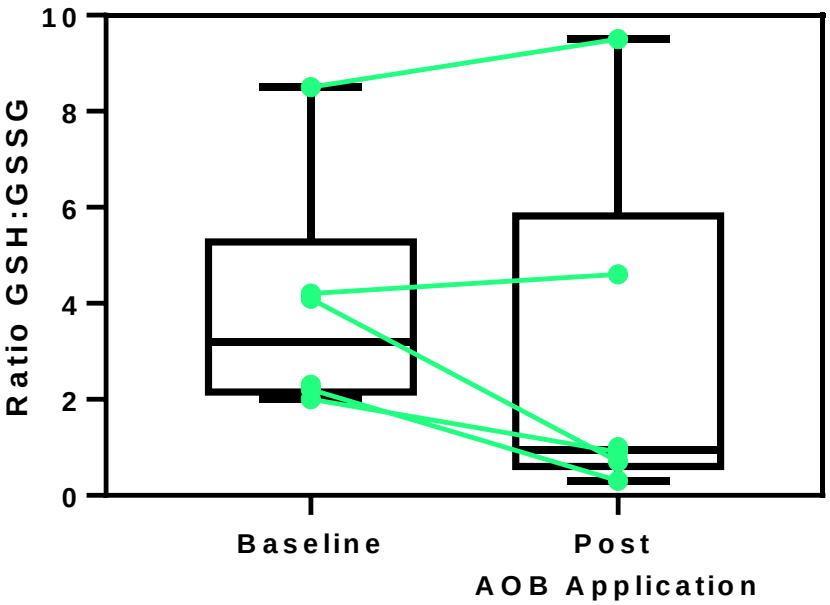
10
8
6
4
2
0
Ratio GSH:GSSG
Baseline
Post
AOB Application

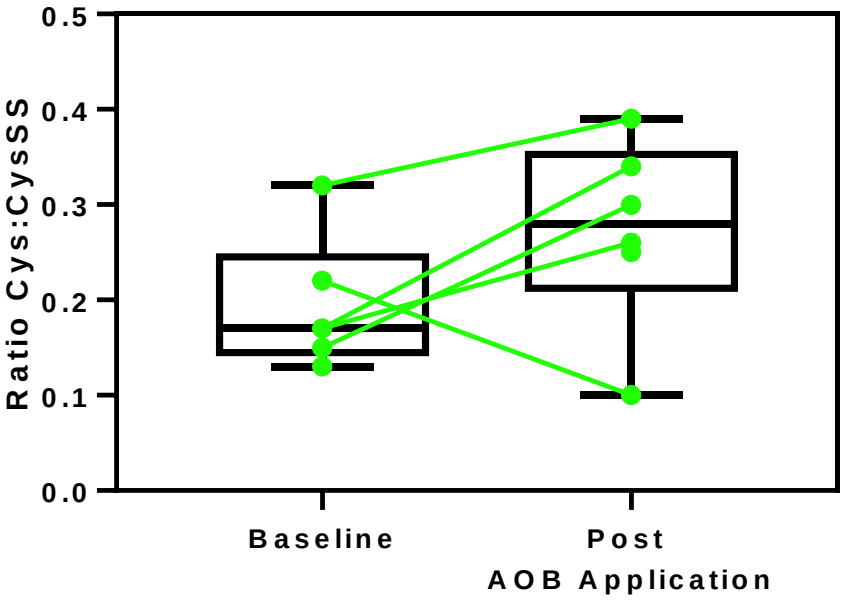
0.5
0.4
0.3
0.2
0.1
0.0
Ratio Cys:CysSS
Baseline
Post
AOB Application

Appendix E

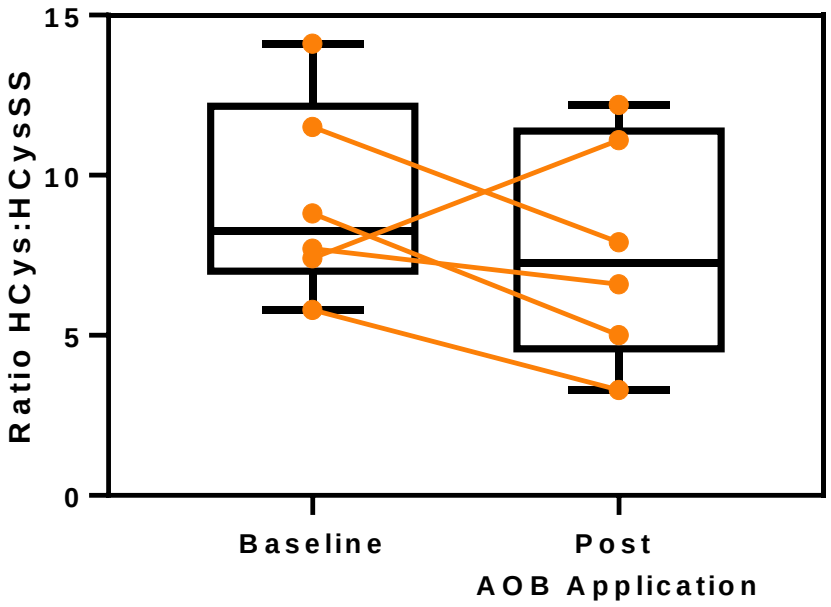

List of References

Adnan, N. N. M. *et al.* (2018) 'Exploiting the Versatility of Polydopamine-Coated Nanoparticles to Deliver Nitric Oxide and Combat Bacterial Biofilm', *Macromolecular Rapid Communications*, 39(13), pp. 1–8.

Alvear-Ordenes, I. *et al.* (2005) 'Sweat Lactate, Ammonia, and Urea in Rugby Players', *Int J Sports Med*. 22.02.2005, 26(08), pp. 632–637.

Aneja, V. P., Schlesinger, W. H. and Erisman, J. W. (2008) 'Farming pollution', *Nature Geoscience*. Nature Publishing Group, 1, p. 409.

Arnelle, D. R. and Stamler, J. S. (1995) 'NO+, NO., and NO− Donation by S-Nitrosothiols: Implications for Regulation of Physiological Functions by S-Nitrosylation and Acceleration of Disulfide Formation', *Archives of Biochemistry and Biophysics*, 318(2), pp. 279–285.

Arp, D. J. and Bottomley, P. J. (2006) 'Nitrifiers: More than 100 years from isolation to genome sequences ', *Microbe*, 1(5), pp. 229–234.

Arp, D. J. and Stein, L. Y. (2003) 'Metabolism of Inorganic N Compounds by Ammonia-Oxidizing Bacteria', *Critical Reviews in Biochemistry and Molecular Biology*. Taylor & Francis, 38(6), pp. 471–495.

Baethgen, W. E. and Alley, M. M. (1989) 'A manual colorimetric procedure for measuring ammonium nitrogen in soil and plant Kjeldahl digests', *Communications in Soil Science and Plant Analysis*. Taylor & Francis, 20(9–10), pp. 961–969.

Barin, J. G., Tobias, L. D. and Peterson, D. A. (2015) 'The microbiome and autoimmune disease: Report from a Noel R. Rose Colloquium', *Clinical Immunology*, 159(2), pp. 183–188.

Barnes, R. J. *et al.* (2013) 'Optimal dosing regimen of nitric oxide donor compounds for the reduction of Pseudomonas aeruginosa biofilm and isolates from wastewater membranes.', *Biofouling*, 29(2), pp. 203–12.

Barraud, Nicolas *et al.* (2006) 'Involvement of nitric oxide in biofilm dispersal of Pseudomonas aeruginosa', *Journal of Bacteriology*, 188(21), pp. 7344–7353.

Barraud, Nicolas *et al.* (2006) 'Involvement of Nitric Oxide in Biofilm Dispersal of Pseudomonas aeruginosa', *Journal of Bacteriology* , 188(21), pp. 7344–7353.

Barraud, N. *et al.* (2009) 'Nitric oxide-mediated dispersal in single- and multi-species biofilms of clinically and industrially relevant microorganisms', *Microbial Biotechnology*,

2(3), pp. 370–378.

Barraud, N. *et al.* (2015) ‘Nitric oxide: a key mediator of biofilm dispersal with applications in infectious diseases.’, *Current pharmaceutical design*. Netherlands, 21(1), pp. 31–42.

Benzie, I. F. and Strain, J. J. (1996) ‘The ferric reducing ability of plasma (FRAP) as a measure of “antioxidant power”: the FRAP assay.’, *Analytical biochemistry*. United States, 239(1), pp. 70–76.

Bíró, T. *et al.* (2018) ‘Endogenous Factors That Can Influence Skin pH’, in *Current Problems in Dermatology*, pp. 54–63.

Bjarnsholt, T. (2013) ‘The role of bacterial biofilms in chronic infections.’, *APMIS. Supplementum*. Denmark, (136), pp. 1–51.

De Boer, W., Klein Gunnewiek, P. A. and Laanbroek, H. J. (1995) ‘Ammonium-oxidation at low pH by a chemolithotrophic bacterium belonging to the genus Nitrosospira’, *Soil Biology and Biochemistry*, 27(2), pp. 127–132.

Bogdan, C. (2001) ‘Nitric oxide and the immune response.’, *Nature immunology*. United States, 2(10), pp. 907–916.

Bonner, F. T. and Stedman, G. (1996) ‘The Chemistry of Nitric Oxide and Redox-related Species’, in *Methods in Nitric Oxide Research*, pp. 3–18.

Bouslimani, A. *et al.* (2015) ‘Molecular cartography of the human skin surface in 3D’, *Proc Natl Acad Sci U S A*, 112(17), pp. E2120-9.

Bruch-Gerharz, D., Ruzicka, T. and Kolb-Bachofen, V. (1998) ‘Nitric oxide and its implications in skin homeostasis and disease - a review.’, *Archives of dermatological research*. Germany, 290(12), pp. 643–651.

Brüne, B., Messmer, U. K. and Sandau, K. (1995) ‘The role of nitric oxide in cell injury.’, *Toxicology letters*, 82–83, pp. 233–237.

Bryan, N. S. *et al.* (2004) ‘Cellular targets and mechanisms of nitros(yl)ation: an insight into their nature and kinetics in vivo.’, *Proceedings of the National Academy of Sciences of the United States of America*, 101(12), pp. 4308–4313.

Bryan, N. S. and Grisham, M. B. (2007) ‘Methods to Detect Nitric Oxide and its Metabolites in Biological Samples’, *Free radical biology & medicine*, 43(5), pp. 645–657. doi: 10.1016/j.freeradbiomed.2007.04.026.

Burnett, A. L. (2005) ‘Phosphodiesterase 5 mechanisms and therapeutic applications.’,

The American journal of cardiology. United States, 96(12B), pp. 29M-31M.

Cai, Y. (2018) *Molecular mechanism of nitric oxide-mediated regulation of intracellular cyclic-di-GMP in Pseudomonas aeruginosa biofilms*. University of Southampton.

Cals-Grierson, M.-M. and Ormerod, A. D. (2004) 'Nitric oxide function in the skin', *Nitric Oxide*, 10(4), pp. 179–193.

Caranto, J. D. and Lancaster, K. M. (2017) 'Nitric oxide is an obligate bacterial nitrification intermediate produced by hydroxylamine oxidoreductase.', *Proceedings of the National Academy of Sciences of the United States of America*. United States, 114(31), pp. 8217–8222.

Carpenter, A. W. and Schoenfisch, M. H. (2012) 'Nitric oxide release: part II. Therapeutic applications', *Chemical Society reviews*. 2012/02/24, 41(10), pp. 3742–3752.

Chain, P. *et al.* (2003) 'Complete genome sequence of the ammonia-oxidizing bacterium and obligate chemolithoautotroph Nitrosomonas europaea.', *Journal of bacteriology*, 185(9), pp. 2759–73.

Chong, J. *et al.* (2018) 'MetaboAnalyst 4.0: towards more transparent and integrative metabolomics analysis', *Nucleic Acids Research*, 46(W1), pp. W486–W494.

Clemente, J. C. *et al.* (2015) 'The microbiome of uncontacted Amerindians', *Science Advances*, 1, e1500183.

Cogan, D. *et al.* (2014) 'The development of an autonomous sensing platform for the monitoring of ammonia in water using a simplified Berthelot method', *Analytical Methods*. The Royal Society of Chemistry, 6(19), pp. 7606–7614.

Conrad, R. (1996) 'Soil microorganisms as controllers of atmospheric trace gases (H_2, CO, CH_4, OCS, N_2O, and NO).', *Microbiological reviews*. United States, 60(4), pp. 609–640.

Craven, M. *et al.* (2016) 'Nitric Oxide-Releasing Polyacrylonitrile Disperses Biofilms Formed by Wound-Relevant Pathogenic Bacteria', *Journal of Applied Microbiology*, 120(4), pp. 1085–99.

Csonka, C. *et al.* (2015) 'Measurement of NO in biological samples.', *British journal of pharmacology*. England, 172(6), pp. 1620–1632.

Cumpstey, A. F. *et al.* (2019) 'Pushing arterial-venous plasma biomarkers to new heights: A model for personalised redox metabolomics?', *Redox biology*. Netherlands, 21, p. 101113.

Czarnowski, D. *et al.* (1992) ‘Plasma ammonia is the principal source of ammonia in sweat’, *European Journal of Applied Physiology and Occupational Physiology*, 65(2), pp. 135–137.

Dai, Y. *et al.* (2015) ‘Activity, abundance and structure of ammonia-oxidizing microorganisms in plateau soils’, *Research in Microbiology*, 166(8), pp. 655–663.

Daims, H. *et al.* (2015) ‘Complete nitrification by Nitrospira bacteria’, *Nature*. Nature Publishing Group, a division of Macmillan Publishers Limited. All Rights Reserved., 528, p. 504.

Daniela, B.-G., Thomas, R. and Kolb-Bachofen, V. (1998) ‘Nitric Oxide in Human Skin: Current Status and Future Prospects’, *Journal of Investigative Dermatology*, 110(1), pp. 1–7.

Davies, K. P. (2015) ‘Development and therapeutic applications of nitric oxide releasing materials to treat erectile dysfunction’, *Future Science OA*. Future Science, 1(1).

Donlan, R. M. and Costerton, J. W. (2002) ‘Biofilms: Survival mechanisms of clinically relevant microorganisms’, *Clinical Microbiology Reviews*, pp. 167–193.

Dréno, B. *et al.* (2016) ‘Microbiome in healthy skin, update for dermatologists’, *Journal of the European Academy of Dermatology and Venereology*, 30(12), pp. 2038–2047.

Duncan, C. *et al.* (1995) ‘Chemical generation of nitric oxide in the mouth from the enterosalivary circulation of dietary nitrate.’, *Nature medicine*. United States, 1(6), pp. 546–551.

Dworkin, M. (2012) ‘Sergei Winogradsky: a founder of modern microbiology and the first microbial ecologist’, *FEMS Microbiology Reviews*. John Wiley & Sons, Ltd (10.1111), 36(2), pp. 364–379.

Fang, F. C. (1997) ‘Perspectives series: host/pathogen interactions. Mechanisms of nitric oxide-related antimicrobial activity.’, *Journal of Clinical Investigation*, 99(12), pp. 2818–2825.

Farage, M. A. *et al.* (2018) ‘Intrinsic and Extrinsic Factors Affecting Skin Surface pH’, in *Current Problems in Dermatology*, pp. 33–47.

Farges, B. *et al.* (2012) ‘Axenic cultures of Nitrosomonas europaea and Nitrobacter winogradskyi in autotrophic conditions: a new protocol for kinetic studies.’, *Applied biochemistry and biotechnology*. United States, 167(5), pp. 1076–1091..

Feelisch, M. *et al.* (2002) ‘Concomitant S-, N-, and heme-nitros(yl)ation in biological

tissues and fluids: implications for the fate of NO in vivo.', *FASEB journal : official publication of the Federation of American Societies for Experimental Biology*. United States, 16(13), pp. 1775–1785.

Feelisch, M. (2008) 'The chemical biology of nitric oxide--an outsider's reflections about its role in osteoarthritis.', *Osteoarthritis and cartilage / OARS, Osteoarthritis Research Society*. England, 16 Suppl 2, pp. S3–S13.

Feelisch, M. *et al.* (2008) 'Tissue Processing of Nitrite in Hypoxia: an intricate interplay of nitric oxide-generating and –scavenging systems', *Journal of Biological Chemistry* , 283(49), pp. 33927–33934.

Feelisch, M., Kubitzek, D. and Werringloer, J. (1996) 'The oxyhemoglobin assay', in Feelisch, M. and Stambler, J. S. (eds) *Methods in nitric oxide research*. Chichester: Wiley, pp. 455–478.

Feelisch, M. and Martin, J. F. (1995) 'The early role of nitric oxide in evolution.', *Trends in ecology & evolution*. England, 10(12), pp. 496–499.

Feelisch, M. and Stamler, J. S. (1996) *Methods in nitric oxide research*. Chichester: Wiley.

Flemming, H.-C. *et al.* (2016) 'Biofilms: an emergent form of bacterial life.', *Nature reviews. Microbiology*. England, 14(9), pp. 563–575.

Förstermann, U. and Sessa, W. C. (2012) 'Nitric oxide synthases: Regulation and function', *European Heart Journal*.

Fukuto, J. M. *et al.* (2012) 'Small Molecule Signaling Agents: The Integrated Chemistry and Biochemistry of Nitrogen Oxides, Oxides of Carbon, Dioxygen, Hydrogen Sulfide, and Their Derived Species', *Chemical Research in Toxicology*. American Chemical Society, 25(4), pp. 769–793.

Garcia-Saura, M. F. *et al.* (2010) 'Dermal nitrite application enhances global nitric oxide availability: new therapeutic potential for immunomodulation?', *The Journal of investigative dermatology*. United States, pp. 608–611.

Gaston, B. *et al.* (1993) 'Endogenous nitrogen oxides and bronchodilator S-nitrosothiols in human airways', *Proceedings of the National Academy of Sciences of the United States of America*, 90(23), pp. 10957–10961.

Ghaffari, A. *et al.* (2007) 'Efficacy of gaseous nitric oxide in the treatment of skin and soft tissue infections.', *Wound repair and regeneration : official publication of the Wound Healing Society [and] the European Tissue Repair Society*. United States, 15(3), pp. 368–

377.

Goldstein, S., Russo, A. and Samuni, A. (2003) ‘Reactions of PTIO and Carboxy-PTIO with ·NO, ·NO2, and ’, *Journal of Biological Chemistry* , 278(51), pp. 50949–50955.

Gryllos, I., Ghosh, S., *et al.* (2014) ‘Oral 2011-2 - Ammonia-oxidizing bacteria accelerate wound closure in diabetic mice’, *Nitric Oxide*, 42, pp. 111–112.

Gryllos, I., Vajrala, N., *et al.* (2014) ‘P129 - Ammonia-oxidizing bacteria for the generation and delivery of acidified nitrite and nitric oxide in vivo’, *Nitric Oxide*, 42, p. 124.

Gupta, K. J. *et al.* (2011) ‘On the origins of nitric oxide.’, *Trends in plant science*. England, 16(3), pp. 160–168.

Güven, D. and Schmidt, I. (2009a) ‘Specific activity and viability of Nitrosomonas europaea during discontinuous and continuous fermentation’, *Process Biochemistry*, 44(5), pp. 516–520.

Güven, D. and Schmidt, I. (2009b) ‘Specific activity and viability of Nitrosomonas europaea during discontinuous and continuous fermentation’, *Process Biochemistry*, 44(2), pp. 516–520.

Hatzenpichler, R. (2012) ‘Diversity, Physiology, and Niche Differentiation of Ammonia-Oxidizing Archaea’, *Applied and Environmental Microbiology* , 78(21), pp. 7501–7510.

Hawkins, R. D. (1996) ‘NO Honey, I Don’t Remember’, *Neuron*, 16(3), pp. 465–467.

Haynes, W. G. *et al.* (1993) ‘Inhibition of nitric oxide synthesis increases blood pressure in healthy humans.’, *Journal of hypertension*. England, 11(12), pp. 1375–1380.

Head, I. M. *et al.* (1993) ‘The phylogeny of autotrophic ammonia-oxidizing bacteria as determined by analysis of 16S ribosomal RNA gene sequences.’, *Journal of general microbiology*. ENGLAND, 139 Pt 6, pp. 1147–1153.

Heinrich, T. A. *et al.* (2013) ‘Biological nitric oxide signalling: chemistry and terminology’, *British Journal of Pharmacology*, 169(7), pp. 1417–1429.

Heller, A. (2009) ‘The need for monitoring the actual nitric oxide concentration in tumors.’, *Bioanalytical reviews*, 1(1), pp. 3–6.

Hendrickx, L. *et al.* (2006) ‘Microbial ecology of the closed artificial ecosystem MELiSSA (Micro-Ecological Life Support System Alternative): Reinventing and compartmentalizing the Earth’s food and oxygen regeneration system for long-haul space exploration missions’, *Research in Microbiology*, 157(1), pp. 77–86.

Hetrick, E. M. *et al.* (2008) ‘Bactericidal efficacy of nitric oxide-releasing silica nanoparticles.’, *ACS nano*. United States, 2(2), pp. 235–246.

Hetrick, E. M. and Schoenfisch, M. H. (2009) ‘Analytical chemistry of nitric oxide.’, *Annual review of analytical chemistry (Palo Alto, Calif.)*. United States, 2, pp. 409–433

Heydorn, A. *et al.* (2000) ‘Quantification of biofilm structures by the novel computer program COMSTAT.’, *Microbiology (Reading, England)*. England, 146 (1), pp. 2395–2407.

Hirsch, P. R. and Mauchline, T. H. (2015) ‘Chapter Two - The Importance of the Microbial N-Cycle in Soil for Crop Plant Nutrition’, in Sariaslani, S. and Gadd, G. M. B. T.-A. in A. M. (eds). Academic Press, pp. 45–71.

Hofman, T. and Lees, H. (1953) ‘The biochemistry of the nitrifying organisms. 4. The respiration and intermediary metabolism of Nitrosomonas’, *Biochemical Journal*, 54(4), pp. 579–583.

Hoiby, N. (2017) ‘A short history of microbial biofilms and biofilm infections.’, *APMIS : acta pathologica, microbiologica, et immunologica Scandinavica*. Denmark, 125(4), pp. 272–275.

Hommes, N. G., Sayavedra-Soto, L. A. and Arp, D. J. (2003) ‘Chemolithoorganotrophic Growth of Nitrosomonas europaea on Fructose’, *Journal of Bacteriology* , 185(23), pp. 6809–6814.

Hooper, A. B. and Terry, K. R. (1979) ‘Hydroxylamine oxidoreductase of Nitrosomonas: Production of nitric oxide from hydroxylamine’, *Biochimica et Biophysica Acta (BBA) - Enzymology*, 571(1), pp. 12–20.

Howlin, R. P. *et al.* (2018) ‘Low-Dose Nitric Oxide as Targeted Anti-biofilm Adjunctive Therapy to Treat Chronic *Pseudomonas aeruginosa* Infection in Cystic Fibrosis’, *Molecular Therapy*. Elsevier, 25(9), pp. 2104–2116.

Janero, D. R. (1990) ‘Malondialdehyde and thiobarbituric acid-reactivity as diagnostic indices of lipid peroxidation and peroxidative tissue injury’, *Free Radical Biology and Medicine*, 9(6), pp. 515–540.

Jones, M. *et al.* (2012) ‘Novel nitric oxide producing probiotic wound healing patch: preparation and in vivo analysis in a New Zealand white rabbit model of ischaemic and infected wounds.’, *International wound journal*. England, 9(3), pp. 330–343.

Jones, M. L. *et al.* (2010) ‘A novel nitric oxide producing probiotic patch and its antimicrobial efficacy: preparation and in vitro analysis.’, *Applied microbiology and*

biotechnology. Germany, 87(2), pp. 509–516.

Juliette, Lisa Y, Hyman, M. R. and Arp, D. J. (1993) ‘Inhibition of Ammonia Oxidation in Nitrosomonas europaea by Sulfur Compounds: Thioethers Are Oxidized to Sulfoxides by Ammonia Monooxygenase’, *Applied and Environmental Microbiology*, 59(11), pp. 3718–3727.

Juliette, L Y, Hyman, M. R. and Arp, D. J. (1993) ‘Mechanism-Based Inactivation of Ammonia Monooxygenase in Nitrosomonas europaea by Allylsulfide.’, *Applied and environmental microbiology*. United States, 59(11), pp. 3728–3735.

Kaplan, J. B. (2010) ‘Biofilm Dispersal: Mechanisms, Clinical Implications, and Potential Therapeutic Uses’, *Journal of Dental Research*. SAGE Publications Inc, 89(3), pp. 205–218.

Karatan, E. and Watnick, P. (2009) ‘Signals, regulatory networks, and materials that build and break bacterial biofilms.’, *Microbiology and molecular biology reviews : MMBR*. United States, 73(2), pp. 310–347.

van Kessel, M. A. H. J. *et al.* (2015) ‘Complete nitrification by a single microorganism.’, *Nature*. England, 528(7583), pp. 555–559.

Kiechle, F. L. and Malinski, T. (1993) ‘Nitric oxide: Biochemistry, pathophysiology, and detection’, *American Journal of Clinical Pathology*, pp. 567–575.

Koning, A. M. *et al.* (2016) ‘Serum free thiols in chronic heart failure’, *Pharmacological Research*, 111, pp. 452–458.

Könneke, M. *et al.* (2005) ‘Isolation of an autotrophic ammonia-oxidizing marine archaeon’, *Nature*, 437(7058), pp. 543–546.

Koops, H.-P. *et al.* (1991) ‘Classification of eight new species of ammonia-oxidizing bacteria’, *Journal of General Microbiology*, 137(7), pp. 1689–1699.

Koops, H.-P., Harms, H. and Wehrmann, H. (1976) ‘Isolation of a moderate halophilic ammonia-oxidizing bacterium, *Nitrosococcus mobilis* nov. sp.’, *Archives of Microbiology*, 107(3), pp. 277–282.

Koops, H.-P. and Pommerening-Röser, A. (2001) ‘Distribution and ecophysiology of the nitrifying bacteria emphasizing cultured species’, *FEMS Microbiology Ecology*, 37(1), pp. 1–9.

Koops, H. P. *et al.* (1991) ‘Classification of eight new species of ammonia-oxidizing bacteria: *Nitrosomonas communis* sp. nov., *Nitrosomonas ureae* sp. nov., *Nitrosomonas*

aestuarii sp. nov., *Nitrosomonas marina* sp. nov., *Nitrosomonas nitrosa* sp. nov., *Nitrosomonas eutropha* sp. nov.', *Journal of General Microbiology*. Microbiology Society, 137(7), pp. 1689–1699.

Koshland, D. E. (1992) 'The molecule of the year', *Science*, 258(5090), pp. 1861 LP – 1861.

Kowalchuk, G. A. and Stephen, J. R. (2001) 'Ammonia-oxidizing bacteria: a model for molecular microbial ecology.', *Annual review of microbiology*. United States, 55, pp. 485–529.

Kozlowski, J. A., Kits, K. D. and Stein, L. Y. (2016a) 'Complete Genome Sequence of *Nitrosomonas ureae* Strain Nm10, an Oligotrophic Group 6a Nitrosomonad.', *Genome announcements*. United States, 4(2).

Kozlowski, J. A., Kits, K. D. and Stein, L. Y. (2016b) 'Genome Sequence of *Nitrosomonas communis* Strain Nm2, a Mesophilic Ammonia-Oxidizing Bacterium Isolated from Mediterranean Soil.', *Genome announcements*. United States, 4(1).

Krasuski, R. A. *et al.* (2000) 'Inhaled nitric oxide selectively dilates pulmonary vasculature in adult patients with pulmonary hypertension, irrespective of etiology', *Journal of the American College of Cardiology*, 36(7), pp. 2204 LP – 2211.

LaBauve, A. E. and Wargo, M. J. (2012) 'Growth and Laboratory Maintenance of *Pseudomonas aeruginosa*', in *Current Protocols in Microbiology*. Hoboken, NJ, USA: John Wiley & Sons, Inc., p. Unit 6E.1.

Lambers, H. *et al.* (2006) 'Natural skin surface pH is on average below 5, which is beneficial for its resident flora', *International Journal of Cosmetic Science*. John Wiley & Sons, Ltd (10.1111), 28(5), pp. 359–370.

Lancaster, J. (1994) 'Simulation of the diffusion and reaction of endogenously produced nitric oxide', *Proceedings of the National Academy of Sciences of the United States of America*, 91(17), pp. 8137–8141.

Law, Y. *et al.* (2012) 'Nitrous oxide emissions from wastewater treatment processes.', *Philosophical transactions of the Royal Society of London. Series B, Biological sciences*. England, 367(1593), pp. 1265–1277.

Lebeaux, D. *et al.* (2013) 'From in vitro to in vivo Models of Bacterial Biofilm-Related Infections', *Pathogens*. Multidisciplinary Digital Publishing Institute, 2(2), pp. 288–356.

van de Leemput, I. A. *et al.* (2011) 'Predicting microbial nitrogen pathways from basic

principles', *Environmental Microbiology*. John Wiley & Sons, Ltd (10.1111), 13(6), pp. 1477–1487.

Lees, H. (1952) 'The biochemistry of the nitrifying organisms. 1. The ammonia-oxidizing systems of Nitrosomonas', *Biochemical Journal*, 52(1), pp. 134–139.

Lewis, R. F. and Pramer, D. (1958) 'Isolation of *Nitrosomonas* in pure culture', *Journal of Bacteriology* , 76(5), pp. 524–528.

Li, H. *et al.* (2008) 'Nitric oxide production from nitrite occurs primarily in tissues not in the blood: critical role of xanthine oxidase and aldehyde oxidase.', *The Journal of biological chemistry*. United States, 283(26), pp. 17855–17863.

Li, Y. and Lee, P. I. (2010) 'Controlled nitric oxide delivery platform based on S-nitrosothiol conjugated interpolymer complexes for diabetic wound healing.', *Molecular pharmaceutics*. United States, 7(1), pp. 254–266.

Line, L. *et al.* (2014) 'Physiological levels of nitrate support anoxic growth by denitrification of *Pseudomonas aeruginosa* at growth rates reported in cystic fibrosis lungs and sputum', *Frontiers in Microbiology*, p. 554.

Liu, D. *et al.* (2014) 'UVA Irradiation of Human Skin Vasodilates Arterial Vasculature and Lowers Blood Pressure Independently of Nitric Oxide Synthase', *Journal of Investigative Dermatology*. Nature Publishing Group, 134(7), pp. 1839–1846.

Liu, Y. *et al.* (2013) 'A study of human skin and surface temperatures in stable and unstable thermal environments', *Journal of Thermal Biology*, 38(7), pp. 440–448.

Loscalzo, J. and Welch, G. (1995) 'Nitric oxide and its role in the cardiovascular system.', *Progress in cardiovascular diseases*. United States, 38(2), pp. 87–104.

Lu, H. *et al.* (2015) 'Global metabolomic responses of Nitrosomonas europaea 19718 to cold stress and altered ammonia feeding patterns', *Applied Microbiology and Biotechnology*.

Lugli, G. A. *et al.* (2017) 'Ancient bacteria of the Ötzi's microbiome: a genomic tale from the Copper Age', *Microbiome*, 5(1), p. 5.

Lundberg, J. O. *et al.* (2009) 'Nitrate and nitrite in biology, nutrition and therapeutics', *Nature Chemical Biology*. Nature Publishing Group, 5, p. 865.

Lundberg, J. O., Gladwin, M. T. and Weitzberg, E. (2015) 'Strategies to increase nitric oxide signalling in cardiovascular disease', *Nature Reviews Drug Discovery*. Nature Publishing Group, 14, p. 623.

Lundberg, J. O. and Govoni, M. (2004) ‘Inorganic nitrate is a possible source for systemic generation of nitric oxide’, *Free Radical Biology and Medicine*, 37(3), pp. 395–400.

Lundberg, J. O., Weitzberg, E. and Gladwin, M. T. (2008) ‘The nitrate-nitrite-nitric oxide pathway in physiology and therapeutics.’, *Nature reviews. Drug discovery*. England, 7(2), pp. 156–167.

Luo, J. and Chen, A. F. (2005) ‘Nitric oxide: a newly discovered function on wound healing.’, *Acta pharmacologica Sinica*. United States, 26(3), pp. 259–264.

Maeda, H. *et al.* (1994) ‘Multiple functions of nitric oxide in pathophysiology and microbiology: analysis by a new nitric oxide scavenger’, *Journal of leukocyte biology*, 56(5), pp. 588–92.

McCoy, K. D. and Köller, Y. (2015) ‘New developments providing mechanistic insight into the impact of the microbiota on allergic disease’, *Clinical Immunology*, 159(2), pp. 170–176.

Medinets, S. *et al.* (2015) ‘A review of soil NO transformation: Associated processes and possible physiological significance on organisms’, *Soil Biology and Biochemistry*, 80, pp. 92–117.

Mehnert, P. *et al.* (2000) ‘Prediction of the average skin temperature in warm and hot environments.’, *European journal of applied physiology*. Germany, 82(1–2), pp. 52–60.

Mendum, T. A., Sockett, R. E. and Hirsch, P. R. (1999) ‘Use of molecular and isotopic techniques to monitor the response of autotrophic ammonia-oxidizing populations of the beta subdivision of the class proteobacteria in arable soils to nitrogen fertilizer’, *Applied and environmental microbiology*. American Society for Microbiology, 65(9), pp. 4155–4162.

Meyer, F. *et al.* (2007) ‘Effect of age and gender on sweat lactate and ammonia concentrations during exercise in the heat’, *Brazilian Journal of Medical and Biological Research*, 40(1), pp. 135–143.

Miranda, K. M., Espey, M. G. and Wink, D. A. (2001) ‘A Rapid, Simple Spectrophotometric Method for Simultaneous Detection of Nitrate and Nitrite’, *Nitric Oxide*, 5(1), pp. 62–71.

Monaghan, C. *et al.* (2018) ‘The effects of two different doses of ultraviolet-A light exposure on nitric oxide metabolites and cardiorespiratory outcomes.’, *European journal of applied physiology*. Germany, 118(5), pp. 1043–1052.

Moncada, S. and Higgs, A. (1993) ‘The L-Arginine-Nitric Oxide Pathway’, *New England Journal of Medicine*. Massachusetts Medical Society, 329(27), pp. 2002–2012.

Moncada, S. and Higgs, E. A. (1995) ‘Molecular mechanisms and therapeutic strategies related to nitric oxide.’, *The FASEB Journal* , 9(13), pp. 1319–1330.

Moncada, S., Palmer, R. M. and Higgs, E. A. (1991) ‘Nitric oxide: physiology, pathophysiology, and pharmacology.’, *Pharmacological Reviews* , 43(2), pp. 109–142.

Monteiro, M., Séneca, J. and Magalhães, C. (2014) ‘The history of aerobic ammonia oxidizers: from the first discoveries to today.’, *Journal of microbiology (Seoul, Korea)*, 52(7), pp. 537–47.

Monteny, G.-J., Bannink, A. and Chadwick, D. (2006) ‘Greenhouse gas abatement strategies for animal husbandry’, *Agriculture, Ecosystems & Environment*, 112(2), pp. 163–170.

Mowbray, M. *et al.* (2008) ‘Topically Applied Nitric Oxide Induces T-Lymphocyte Infiltration in Human Skin, but Minimal Inflammation’, *Journal of Investigative Dermatology*, 128(2), pp. 352–360.

Mowbray, M. *et al.* (2009) ‘Enzyme-Independent NO Stores in Human Skin: Quantification and Influence of UV Radiation’, *Journal of Investigative Dermatology*, 129(4), pp. 834–842.

Murad, F. (1994) ‘The nitric oxide-cyclic GMP signal transduction system for intracellular and intercellular communication.’, *Recent progress in hormone research*. United States, 49, pp. 239–248.

Musk, D. J. J. and Hergenrother, P. J. (2006) ‘Chemical countermeasures for the control of bacterial biofilms: effective compounds and promising targets.’, *Current medicinal chemistry*. United Arab Emirates, 13(18), pp. 2163–2177.

Nakatsuji, T. *et al.* (2013) ‘The microbiome extends to subepidermal compartments of normal skin’, *Nat Commun*, 4.

Nejidat, A., Shmuely, H. and Abeliovich, A. (1997) ‘Effect of ammonia starvation on hydroxylamine oxidoreductase activity of *Nitrosomonas europaea*.’, *Journal of biochemistry*. England, 121(5), pp. 957–960.

Nelson, D. L., Cox, M. M. and Lehninger, A. L. (2000) *Lehninger principles of biochemistry*. New York: Worth Publ.

Nguyen, T. K. *et al.* (2016) ‘Co-delivery of nitric oxide and antibiotic using polymeric

nanoparticles', *Chemical Science*. Royal Society of Chemistry, 7(2), pp. 1016–1027.

Norton, J. M. *et al.* (2008) 'Complete genome sequence of Nitrosospira multiformis, an ammonia-oxidizing bacterium from the soil environment', *Applied and environmental microbiology*. 2008/04/04. American Society for Microbiology (ASM), 74(11), pp. 3559–3572.

Nose, K. *et al.* (2005) 'Identification of ammonia in gas emanated from human skin and its correlation with that in blood.', *Analytical sciences : the international journal of the Japan Society for Analytical Chemistry*. Japan, 21(12), pp. 1471–1474.

O'Toole, G., Kaplan, H. B. and Kolter, R. (2000) 'Biofilm Formation as Microbial Development', *Annual Review of Microbiology*, 54(1), pp. 49–79.

Oplander, C. *et al.* (2009) 'Whole body UVA irradiation lowers systemic blood pressure by release of nitric oxide from intracutaneous photolabile nitric oxide derivates.', *Circulation research*. United States, 105(10), pp. 1031–1040.

Oplander, C. *et al.* (2012) 'Dermal application of nitric oxide releasing acidified nitrite-containing liniments significantly reduces blood pressure in humans.', *Nitric oxide : biology and chemistry*. United States, 26(2), pp. 132–140.

Orman, M. A. and Brynildsen, M. P. (2016) 'Persister formation in Escherichia coli can be inhibited by treatment with nitric oxide.', *Free radical biology & medicine*. United States, 93, pp. 145–154.

Palmer, R. M., Ashton, D. S. and Moncada, S. (1988) 'Vascular endothelial cells synthesize nitric oxide from L-arginine.', *Nature*. England, 333(6174), pp. 664–666.

Peng, L. *et al.* (2014) 'The effect of dissolved oxygen on N2O production by ammonia-oxidizing bacteria in an enriched nitrifying sludge', *Water Research*, 66, pp. 12–21.

Peter, H. *et al.* (2017) 'Abstract P496: Effects of Nitrosomonas Eutropha D23 Topical Spray on Blood Pressure: Results From a Randomized, Double-blind, Vehicle Controlled, Dose-ranging Study in Normotensive Adults', *Hypertension*. American Heart Association, 70(suppl_1), pp. AP496–AP496.

Pinder, A. G. *et al.* (2008) 'The measurement of nitric oxide and its metabolites in biological samples by ozone-based chemiluminescence', *Methods in Molecular Biology*, 476, pp. 11–28.

Poh, W. H. *et al.* (2017) 'Furoxan Nitric Oxide Donors Disperse Pseudomonas aeruginosa Biofilms, Accelerate Growth, and Repress Pyoverdine Production', *ACS Chemical*

Biology, 12(8), pp. 2097–2106.

Prosser, J. I. and Nicol, G. W. (2012) 'Archaeal and bacterial ammonia-oxidisers in soil: the quest for niche specialisation and differentiation', *Trends in Microbiology*. Elsevier Ltd, 20(11), pp. 523–531.

Rasamiravaka, T. *et al.* (2015) ' The Formation of Biofilms by Pseudomonas aeruginosa : A Review of the Natural and Synthetic Compounds Interfering with Control Mechanisms ', *BioMed Research International*, 2015, pp. 1–17.

Rockström, J. *et al.* (2009) 'A safe operating space for humanity', *Nature*. Nature Publishing Group, 461, p. 472.

Romling, U. *et al.* (2014) 'Microbial biofilm formation: a need to act.', *Journal of internal medicine*. England, 276(2), pp. 98–110.

Römling, U. and Balsalobre, C. (2012) 'Biofilm infections, their resilience to therapy and innovative treatment strategies', *Journal of Internal Medicine*. John Wiley & Sons, Ltd (10.1111), 272(6), pp. 541–561.

Sato, C. *et al.* (1985) 'Test Medium for the Growth of Nitrosomonas europaea', *Applied and Environmental Microbiology*, 49(5), pp. 1101–1107.

Schairer, D. O. *et al.* (2012) 'The potential of nitric oxide releasing therapies as antimicrobial agents.', *Virulence*, 3(3), pp. 271–9.

Scharschmidt, T. C. and Fischbach, M. A. (2013) 'What lives on our skin: ecology, genomics and therapeutic opportunities of the skin microbiome', *Drug Discovery Today: Disease Mechanisms*, 10(3–4), pp. e83–e89.

Schleper, C. and Nicol, G. W. (2010) 'Ammonia-oxidising archaea--physiology, ecology and evolution.', *Advances in microbial physiology*. England, 57, pp. 1–41.

Schmid-Wendtner, M.-H. and Korting, H. C. (2006) 'The pH of the skin surface and its impact on the barrier function.', *Skin pharmacology and physiology*. Switzerland, 19(6), pp. 296–302.

Schmidt, F. M. *et al.* (2013) 'Ammonia in breath and emitted from skin.', *Journal of breath research*. England, 7(1), p. 17109.

Schmidt, I. *et al.* (2004) 'Ammonium and hydroxylamine uptake and accumulation in Nitrosomonas.', *Microbiology (Reading, England)*. England, 150(Pt 5), pp. 1405–1412.

Seabra, A. B. *et al.* (2004) 'Topically applied S-nitrosothiol-containing hydrogels as

experimental and pharmacological nitric oxide donors in human skin.', *The British journal of dermatology*. England, 151(5), pp. 977–983.

Shabani, M. *et al.* (1996) 'Enhancement of wound repair with a topically applied nitric oxide-releasing polymer.', *Wound repair and regeneration : official publication of the Wound Healing Society and the European Tissue Repair Society*. United States, 4(3), pp. 353–362.

Shabeeh, H. *et al.* (2013) 'Differential role of endothelial versus neuronal nitric oxide synthase in the regulation of coronary blood flow during pacing-induced increases in cardiac workload.', *American journal of physiology. Heart and circulatory physiology*. United States, 304(9), pp. H1277-82.

Shabeeh, H. *et al.* (2017) 'Blood Pressure in Healthy Humans Is Regulated by Neuronal NO Synthase.', *Hypertension (Dallas, Tex. : 1979)*. United States, 69(5), pp. 970–976. d

Shen, T. *et al.* (2013) 'Responses of the terrestrial ammonia-oxidizing archaeon Ca. Nitrososphaera viennensis and the ammonia-oxidizing bacterium Nitrosospira multiformis to nitrification inhibitors', *FEMS Microbiology Letters*, 344(2), pp. 121–129.

Shiva, S. (2013) 'Nitrite: A physiological store of nitric oxide and modulator of mitochondrial function', *Redox Biology*, 1(1), pp. 40–44.

Skinner, F. A. and Walker, N. (1961) 'Growth of Nitrosomonas europaea in batch and continuous culture', *Archiv für Mikrobiologie*, 38(4), pp. 339–349.

Soren, O. *et al.* (2019) 'Cephalosporin nitric oxide-donor prodrug DEA-C3D disperses biofilms formed by clinical cystic fibrosis isolates of Pseudomonas aeruginosa (in press)', *Journal of Antimicrobial Chemotherapy*.

Spiertz, J. H. J. (2010) 'Nitrogen, sustainable agriculture and food security. A review', *Agronomy for Sustainable Development*, 30(1), pp. 43–55.

Stamler, J. S., Jaraki, O., *et al.* (1992) 'Nitric oxide circulates in mammalian plasma primarily as an S-nitroso adduct of serum albumin.', *Proceedings of the National Academy of Sciences of the United States of America*. United States, 89(16), pp. 7674–7677.

Stamler, J. S., Simon, D. I., *et al.* (1992) 'S-nitrosylation of proteins with nitric oxide: synthesis and characterization of biologically active compounds.', *Proceedings of the National Academy of Sciences of the United States of America*. United States, 89(1), pp. 444–448.

Stein, L. Y. *et al.* (2007) 'Whole-genome analysis of the ammonia-oxidizing bacterium,

Nitrosomonas eutropha C91: implications for niche adaptation.', *Environmental microbiology*. England, 9(12), pp. 2993–3007.

Stein, L. Y. (2019) 'Insights into the physiology of ammonia-oxidizing microorganisms.', *Current opinion in chemical biology*. England, 49, pp. 9–15.

Stein, L. Y. and Klotz, M. G. (2016) 'The nitrogen cycle', *Current Biology*, pp. R94–R98.

Stieglmeier, M. *et al.* (2014) 'Aerobic nitrous oxide production through N-nitrosating hybrid formation in ammonia-oxidizing archaea.', *The ISME journal*. England, 8(5), pp. 1135–1146.

Sulemankhil, I. *et al.* (2012) 'Prevention and treatment of virulent bacterial biofilms with an enzymatic nitric oxide-releasing dressing.', *Antimicrobial agents and chemotherapy*. United States, 56(12), pp. 6095–6103.

Susswein, A. J. *et al.* (2004) 'Nitric Oxide and Memory', *The Neuroscientist*. SAGE Publications Inc STM, 10(2), pp. 153–162.

Sutton, T. R. *et al.* (2018) 'A robust and versatile mass spectrometry platform for comprehensive assessment of the thiol redox metabolome.', *Redox biology*. Netherlands, 16, pp. 359–380.

Suzuki, I., Dular, U. and Kwok, S. C. (1974) 'Ammonia or Ammonium Ion as Substrate for Oxidation by Nitrosomonas europaea Cells and Extracts', *Journal of Bacteriology*, 120(1), pp. 556–558.

Szaciłowski, K., Chmura, A. and Stasicka, Z. (2005) 'Interplay between iron complexes, nitric oxide and sulfur ligands: Structure, (photo)reactivity and biological importance', *Coordination Chemistry Reviews*, 249(21–22), pp. 2408–2436.

Thomas, D. D. *et al.* (2008) 'The chemical biology of nitric oxide: Implications in cellular signaling', *Free Radical Biology and Medicine*, 45(1), pp. 18–31.

Tolker-Nielsen, T. (2014) 'Pseudomonas aeruginosa biofilm infections: From molecular biofilm biology to new treatment possibilities', *APMIS*. John Wiley & Sons, Ltd (10.1111), 122(s138), pp. 1–51.

Uchida, K. (2003) '4-Hydroxy-2-nonenal: a product and mediator of oxidative stress', *Progress in Lipid Research*, 42(4), pp. 318–343.

Vajrala, N. *et al.* (2010) 'Role of Nitrosomonas europaea NitABC iron transporter in the uptake of Fe3+-siderophore complexes', *Archives of Microbiology*, 192(11), pp. 899–908.

Varga, J. J. *et al.* (2015) ‘Genotypic and phenotypic analyses of a Pseudomonas aeruginosa chronic bronchiectasis isolate reveal differences from cystic fibrosis and laboratory strains’, *BMC genomics*. BioMed Central, 16, p. 883.

Vorregaard, M. (2008) *Comstat2 - a modern 3D image analysis environment for biofilms*, *Mathematical Modelling*.

Wagner, H. *et al.* (2003) ‘pH profiles in human skin: influence of two in vitro test systems for drug delivery testing’, *European Journal of Pharmaceutics and Biopharmaceutics*, 55(1), pp. 57–65.

Wallace, W. and Nicholas, D. J. D. (1969) ‘The biochemistry of nitrifying microorganisms’, *Biological Reviews*. Blackwell Publishing Ltd, 44(3), pp. 359–389.

Wang, X. *et al.* (2014) ‘Abundance and community structure of ammonia-oxidizing microorganisms in reservoir sediment and adjacent soils’, *Applied Microbiology and Biotechnology*, 98(4), pp. 1883–1892.

Weinberger, B. *et al.* (2001) ‘The Toxicology of Inhaled Nitric Oxide’, *Toxicological Sciences*, 59(1), pp. 5–16.

Weitzberg, E., Hezel, M. and Lundberg, J. O. (2010) ‘Nitrate-nitrite-nitric oxide pathway: implications for anesthesiology and intensive care.’, *Anesthesiology*. United States, 113(6), pp. 1460–1475.

Weller, R. *et al.* (1996) ‘Nitric oxide is generated on the skin surface by reduction of sweat nitrate’, *Journal of Investigative Dermatology*, 107(3), pp. 327–331.

Weller, R. *et al.* (1998) ‘A randomized trial of acidified nitrite cream in the treatment of tinea pedis.’, *Journal of the American Academy of Dermatology*. United States, 38(4), pp. 559–563.

Weller, R. B. (2009) ‘Nitric Oxide–Containing Nanoparticles as an Antimicrobial Agent and Enhancer of Wound Healing’, *Journal of Investigative Dermatology*, 129(10), pp. 2335–2337.

Weller, R. B. (2017) ‘The health benefits of UV radiation exposure through vitamin D production or non-vitamin D pathways. Blood pressure and cardiovascular disease’, *Photochemical & Photobiological Sciences*. The Royal Society of Chemistry, 16(3), pp. 374–380.

Weller, R. and Finnen, M. J. (2006) ‘The effects of topical treatment with acidified nitrite on wound healing in normal and diabetic mice’, *Nitric Oxide*, 15(4), pp. 395–399.

Wenderska, I. B. *et al.* (2011) ‘Palmitoyl-DL-carnitine is a multitarget inhibitor of Pseudomonas aeruginosa biofilm development.’, *Chembiochem : a European journal of chemical biology*. Germany, 12(18), pp. 2759–2766.

Whitlock, D. R. *et al.* (2015) ‘Ammonia-oxidizing *Nitrosomonas eutropha* strain D23’. Available at:ttps://patentscope.wipo.int/search/en/detail.jsf?docId=WO2015160911 (Accessed: 5 January 2018).

Whitlock, D. R. and Feelisch, M. (2009) ‘Soil bacteria, nitrite and the skin - The Hygiene Hypothesis and Darwinian Medicine’, in Rook, G. A. W. (ed.) *The Hygiene Hypothesis and Darwinian Medicine*. Basel: Birkhäuser Basel, pp. 103–115.

Wierer, U. *et al.* (2018) ‘The Iceman’s lithic toolkit: Raw material, technology, typology and use’, *PLOS ONE*. Public Library of Science, 13(6), p. e0198292.

Wilhelm, R., Abeliovich, A. and Nejidat, A. (1998) ‘Effect of long-term ammonia starvation on the oxidation of ammonia and hydroxylamine by Nitrosomonas europaea.’, *Journal of biochemistry*. England, 124(4), pp. 811–815.

Wink, D. A. *et al.* (2002) ‘The Chemical Biology of Nitric Oxide BT - Reactive Oxygen Species in Biological Systems: An Interdisciplinary Approach’, in Gilbert, D. L. and Colton, C. A. (eds). Boston, MA: Springer US, pp. 245–291.

Wink, D. A., Beckman, J. S. and Ford, P. C. (1996) ‘Kinetics of Nitric Oxide Reaction in Liquid and Gas Phase’, in *Methods in Nitric Oxide Research*, pp. 29–37.

Wink, D. A. and Mitchell, J. B. (1998) ‘Chemical biology of nitric oxide: insights into regulatory, cytotoxic, and cytoprotective mechanisms of nitric oxide’, *Free Radical Biology and Medicine*, 25(4–5), pp. 434–456.

Yetik-Anacak, G. and Catravas, J. D. (2006) ‘Nitric oxide and the endothelium: History and impact on cardiovascular disease’, *Vascular Pharmacology*, 45(5), pp. 268–276.

Yoon, S. S. *et al.* (2002) ‘Pseudomonas aeruginosa Anaerobic Respiration in Biofilms: Relationships to Cystic Fibrosis Pathogenesis’, *Developmental Cell*, 3(4), pp. 593–603.

Zart, D., Schmidt, I. and Bock, E. (2000) ‘Significance of gaseous NO for ammonia oxidation by Nitrosomonas eutropha’, *Antonie van Leeuwenhoek*, 77(1), pp. 49–55.

Zhao, C. *et al.* (2013) ‘Rapid Screening of Ammonia Oxidizing Bacteria in the Sewage’, *International Journal of Bioscience, Biochemistry and Bioinformatics*, 3(2), pp. 93–97.